PACIFIC EARTHQUAKE ENGINEERING
RESEARCH CENTER

Building Vulnerability Studies: Modeling and Evaluation of Tilt-up and Steel Reinforced Concrete Buildings

Editors:
John W. Wallace
Jonathan P. Stewart
Department of Civil and Environmental Engineering
University of California, Los Angeles

Andrew S. Whittaker
Department of Civil and Environmental Engineering
University of California, Berkeley

PEER 1999/13
DECEMBER 1999

Building Vulnerability Studies: Modeling and Evaluation of Tilt-up and Steel Reinforced Concrete Buildings

EDITORS:

John W. Wallace
Jonathan P. Stewart
University of California, Los Angeles

Andrew S. Whittaker
University of California, Berkeley

CONTRIBUTORS:

Ayse O. Kulahci, Graduate Research Assistant
Sandrine Lermite, Graduate Research Assistant
Seunghyun Kim, Graduate Research Assistant
Frances Yang, Undergraduate PEER Summer Intern
University of California, Los Angeles

PEER Report 1999/13
Pacific Earthquake Engineering Research Center
College of Engineering
University of California, Berkeley

December 1999

ABSTRACT

The California building inventory includes many different building types. Two common building types in this inventory are tilt-up buildings and reinforced concrete buildings with embedded steel frames (sometimes referred to as steel reinforced concrete, or SRC, buildings). Many of these buildings were built before the implementation of modern provisions for seismic design and may be susceptible to significant damage in moderate-to-strong earthquake ground motions. Given this potential vulnerability, a study was undertaken to assess modeling and evaluation approaches for each building type.

For tilt-up buildings, a nonlinear analysis methodology was developed using a series of simple 2-D models to evaluate connection forces and deformations, as well as demand in the roof diaphragm, for a given ground motion. Data from the response of an instrumented building (CSMIP Station 47391) were used to validate the model. The correlation studies showed that the model was capable of representing the overall measured response of the building reasonably well. Sensitivity studies were performed to assess the influence of various parameters on tilt-up response, including soil-foundation-structure interaction (SFSI). The sensitivity studies indicate that diaphragm stiffness has a considerable impact on response and behavior and that near-field earthquakes with forward directivity increased connection and diaphragm forces from 10 to 25%. Soil-foundation-structure interaction did not have a significant impact on building response.

Due to the nature of the dynamic response of SRC buildings, which is dominated by out-of-plane “breathing” of the walls and roof, linear dynamic analysis methods were employed. The Linear Dynamic Procedure (LDP) described in FEMA 273 was used to assess critical structural elements of the lateral and gravity force-resisting systems. The evaluation indicated that the system was both strong and stiff, and thus, remained essentially elastic for the spectrum provided (10%/50 yr). Soil-foundation-structure interaction did not have a significant impact due to the dynamic response characteristics of the building.

ACKNOWLEDGMENTS

The work presented in this report was supported by funds from Phase I of the Pacific Earthquake Engineering Research (PEER) Center and Pacific Gas and Electric (PG&E) cooperative research program for Building Vulnerability Studies. Mr. Kent Ferre served as the PG&E technical monitor for this project and his assistance with all aspects of the project is acknowledged. The comments provided by Mr. Ron Hamburger of EQE and Mr. Chris Poland of Degenkolb Engineers, as well as other Phase I researchers, are greatly appreciated. We would also like to thank Jack Yee of the Bay Area Rapid Transit District for providing boring logs near the SRC building in Berkeley.

This work was supported in part by the Pacific Earthquake Engineering Research Center through the Earthquake Engineering Research Centers Program of the National Science Foundation under Award number EEC-9701568.

CONTENTS

LIST OF FIGURES

LIST OF TABLES

1 Introduction and Report Organization

1.1 INTRODUCTION

Two common building types in the California inventory of buildings are tilt-up buildings and reinforced concrete buildings with embedded steel frames (sometimes referred to as steel reinforced concrete, or SRC, buildings). Many of these buildings were built prior to the implementation of modern provisions for seismic design and are susceptible to significant damage in moderate-to-strong ground motions. Given this potential vulnerability, a study was undertaken to assess modeling and evaluation approaches for each building type. Representative buildings were selected to establish typical building configurations and structural details. An electrical repair facility located in Fremont, California, provided the basis for evaluation of the tilt-up buildings and an electrical substation in Berkeley, California was used as a representative SRC building. Modeling approaches and analysis tools were selected for the evaluation of each building type. The influence of soil-foundation-structure interaction (SFSI) was also considered.

1.2 BUILDING TYPES

1.2.1 Tilt-up Buildings

Tilt-up buildings are common in California because they offer a large, open floor space and are economical to construct. However, the poor performance of tilt-up buildings in previous California earthquakes indicates that they are susceptible to damage. Although code requirements have been improved over the past 25 years based on observed damage, significant damage was reported in the Northridge earthquake. Typical damage included failure of connections between the roof and walls and failures between individual wall panels, often resulting in partial collapse of the roof and wall panels. Nonlinear modeling is likely needed to best predict the connection forces and deformations to improve evaluation techniques for tilt-up buildings. Given these general observations, this report emphasizes the use of simple nonlinear modeling and analysis methods. Although soil-foundation-structure interaction is not expected to play a significant role in the dynamic response of a tilt-up building, relatively simple studies were undertaken to quantitatively assess the impact of such interaction.

Calibration of the modeling approach developed in this study for tilt-up buildings was an essential component of the study. To address this need, a tilt-up building in Hollister, California, instrumented by the California Strong Motion Instrumentation Program (CSMIP) and subjected to moderate ground shaking in the Loma Prieta earthquake, was used to study building response. The structural systems for the Hollister and Fremont buildings are similar; therefore, conclusions derived from the study of the Hollister building can be applied to other similar buildings in the California building inventory. No specific studies of the Fremont building were undertaken.

1.2.2 Steel Reinforced Concrete Buildings

The Berkeley substation building was used as an example of an older, box-like steel and reinforced concrete building. The structural system for the low-rise building consists of steel trusses and columns with perimeter concrete walls and a concrete roof. The steel members are either fully or partially embedded in the concrete roof and walls. Relatively little information on the seismic performance of this type of building is available. Given the large number of stiff reinforced concrete walls in this type of building, there is an expectation that the collapse prevention performance level can be achieved with little or no modification. Although the concrete wall panels were likely neglected in the original lateral load analysis of the building, the stiff low-rise walls provide substantial lateral-force resistance. The role of out-of-plane response on the behavior of the thin wall panels and the deformations that the wall panels impose on the structural steel components in the building may substantially impact building response. As well, given the stiff structural system, soil-foundation-structure interaction may play a significant role in the response of such buildings. The primary objectives of the SRC building study are (1) to study the dynamic response of a typical SRC building and (2) to identify appropriate modeling and evaluation techniques.

1.3 REPORT ORGANIZATION

The report is organized into four chapters. The first chapter provides an overview of the project. Soil-foundation-structure interaction is the focus of Chapter 2. Modeling and evaluation of tilt-up and SRC buildings are addressed in Chapters 3 and 4, respectively. The approach developed in Chapter 2 is used in Chapters 3 and 4 to assess the importance of soil-foundation-structure interaction on building response. A brief study is also undertaken in Chapter 3 to assess the impact of near-field ground motion characteristics on the response of tilt-up buildings. Conclusions for each building type are summarized at the end of Chapters 3 and 4.

2 Modeling of Soil-Structure Interaction Effects

2.1 INTRODUCTION

2.1.1 Background

The seismic excitation experienced by structures is a function of the earthquake source, travel-path effects, local site effects, and soil-foundation-structure interaction (SFSI) effects. The product of the first three of these factors is a free-field ground motion. Structural response to free-field motion is influenced by SFSI. In particular, accelerations within structures are affected by the flexibility of foundation support and variations between foundation and free-field motions. Consequently, an accurate assessment of inertial forces and displacements in structures requires a rational treatment of SFSI effects.

SFSI analysis procedures include direct approaches in which the soil and structure are modeled together in a single analysis, and substructure approaches where the analysis is broken down into several steps. The emphasis here is on the relatively straightforward and more commonly used substructure approach, illustrated in Fig. 2.1. The substructure approach separately evaluates the following two principal mechanisms of interaction between soil and foundation:

- *Kinematic Interaction*: The presence of stiff foundation elements on or in soil cause foundation motions to deviate from free-field motions as a result of ground motion incoherence, wave inclination, or foundation embedment. Kinematic effects are described by a frequency dependent transfer function relating the free-field motion to the motion that would occur on the base slab if the slab and structure were massless.
- *Inertial Interaction*: Inertia developed in the structure due to its own vibrations gives rise to base shear and moment, which in turn cause displacements of the foundation relative to the free field. Frequency-dependent foundation impedance functions describe the flexibility of the foundation support as well as the damping associated with foundation-soil interaction.

The focus here is on inertial interaction, which is the more important effect for foundations without large rigid base slabs or deep embedment. When kinematic interaction is ignored, it is equivalent to assuming a transfer function of unity.

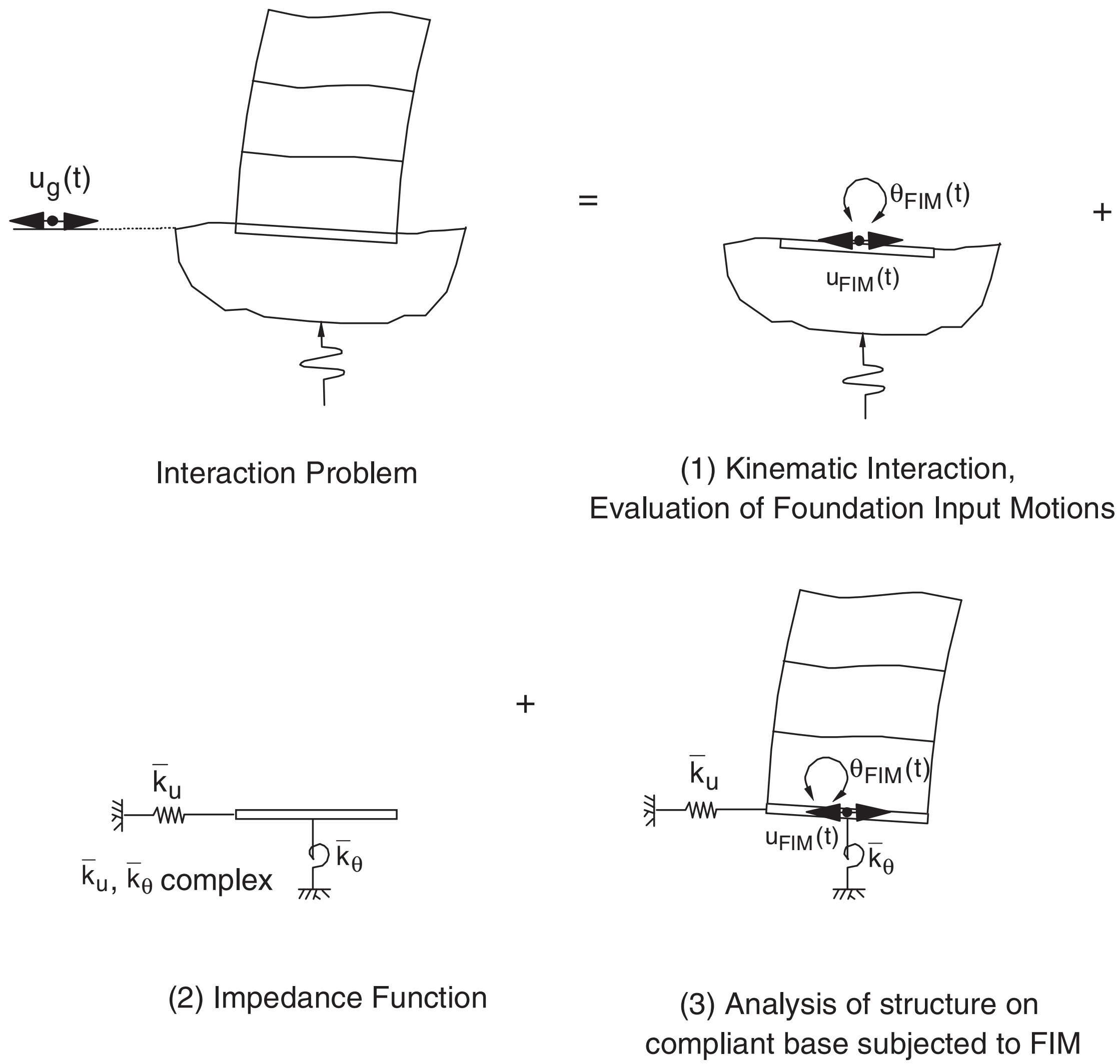

Fig. 2.1: Substructure approach to analysis of the SSI problem

The effects of inertial interaction can be readily visualized using the model shown in Fig. 2.2. The figure consists of a single-degree-of-freedom structure of height h on a flexible foundation medium represented by the frequency-dependent and complex-valued impedance terms $\bar{k}_u$ and $\bar{k}_\theta$. Using this model, Veletsos and Meek (1974) found that the seismic response of a flexible-base structure can be represented with an equivalent fixed-base single-degree-of-freedom structure with vibration period and damping ratio $\tilde{T}$ and $\tilde{\zeta}$, respectively. The corresponding fundamental-mode parameters for a structure on a rigid soil/foundation system (i.e., a fixed-base structure) are T and ζ. Hence, the effects of SFSI can be expressed through a comparison of the fixed- and flexible-base vibration parameters as follows:

$$\tilde{T}/T = \text{Period lengthening ratio}$$

$$\tilde{\zeta}_0 = \tilde{\zeta} - \frac{\zeta}{\left(\tilde{T}/T\right)^3} = \text{Foundation damping factor}$$

These factors are a useful quantification of inertial SFSI effects for structures modeled with lumped masses, because they can be combined with fixed-base parameters (assumed to be "known") to evaluate flexible-base parameters. In turn, they can be used in simple response-spectrum-based analyses of seismic structural response (e.g., Fig. 2.3). This framework is the basis of SFSI provisions in the NEHRP *Recommended Provisions for Seismic Regulations for New Buildings and Other Structures* (BSSC, 1998). However, for reasons discussed in Section 2.3, this framework is not readily applicable to the subject structures in this study, and a different approach is adopted in which impedance functions are directly included in structural response analyses.

Impedance functions ($\bar{k}_u$ and $\bar{k}_\theta$) generally represent the single greatest source of uncertainty in SFSI analyses. Hence, the primary focus of this chapter, presented in Section 2.2, is on simplified procedures for evaluating impedance functions. Key issues addressed include the selection of representative shear wave velocities for nonuniform soil profiles, and the evaluation of impedance for arbitrary foundation shapes and flexible foundations. These procedures improve the basic formulation in the NEHRP *Provisions* as well as the procedures adopted by Stewart et al. (1998). Section 2.3 and the Appendix for this Chapter discuss the application of these procedures for the buildings discussed in detail in Chapters 3 and 4.

2.2 IMPEDANCE FUNCTION

2.2.1 Mathematical Representation

The impedance function is represented in Fig. 2.2 by $\bar{k}_u$ and $\bar{k}_\theta$. For surface or lightly embedded foundations, neglecting the coupling between the translational and rocking deformation modes

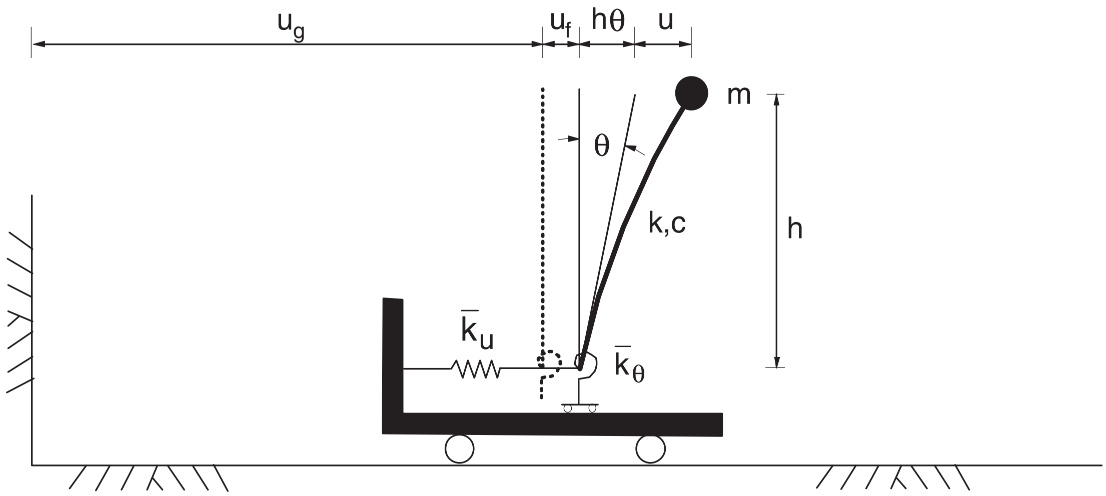

Fig. 2.2: Simplified model for analysis of inertial interaction

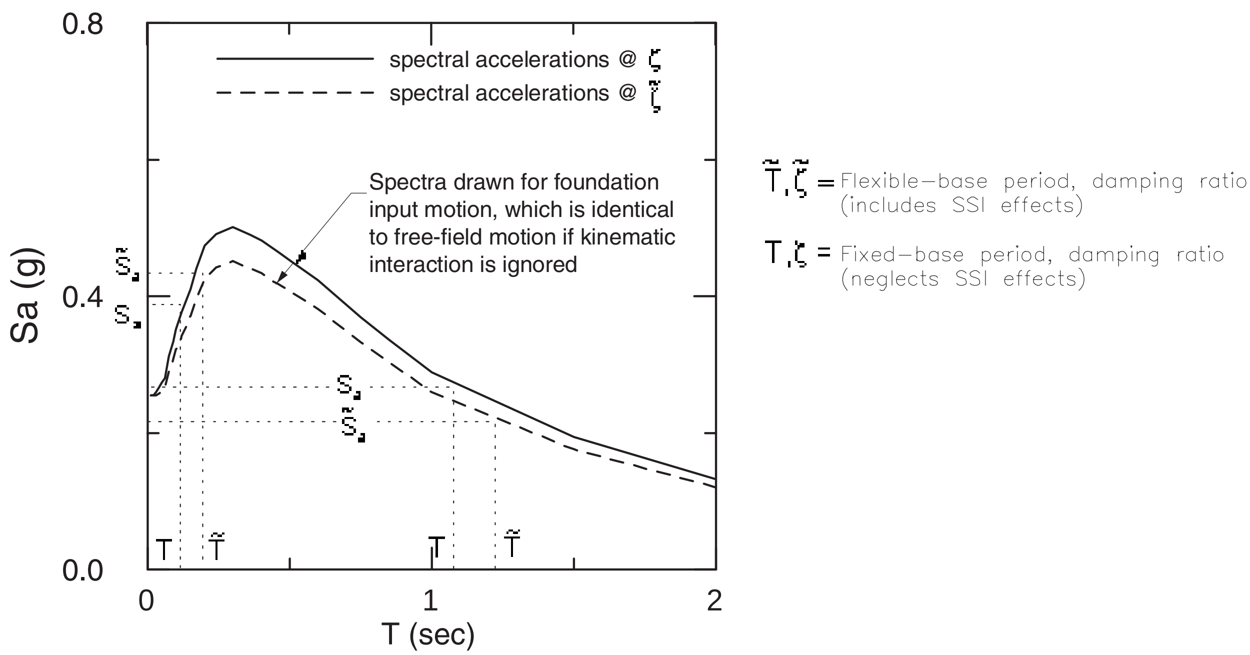

Fig. 2.3: Schematic showing effects of period lengthening and foundation damping on design spectral acceleration using smoothed spectral shape. Sa can increase or decrease due to SSI.

introduces negligible errors. Simplified impedance function solutions for translation and rocking are available for rigid circular disk foundations located on the ground surface or embedded into a uniform, visco-elastic halfspace. Terms in the impedance function are expressed in the form

$$\bar{k}_j = k_j(a_0,\upsilon) + i\omega c_j(a_0,\upsilon) \tag{2.1}$$

where j denotes either deformation mode u or θ, ω is angular frequency (radians/sec.), a_0 is a dimensionless frequency defined by $a_0 = \omega r/V_S$, r = equivalent foundation radius, V_S = soil shear wave velocity, and υ = soil Poisson ratio. Foundation radii are computed separately for translational and rocking deformation modes to match the area (A_f) and moment of inertia (I_f) of the actual foundation (i.e. $r_u = \sqrt{A_f/\pi}$, $r_\theta = \sqrt[4]{4I_f/\pi}$). There are corresponding $(a_0)_u$ and $(a_0)_\theta$ values as well.

The real stiffness and damping of the translational and rocking springs and dashpots are expressed, respectively, by

$$k_u = \alpha_u K_u \qquad c_u = \beta_u \frac{K_u r_u}{V_S} \tag{2.2a}$$

$$k_\theta = \alpha_\theta K_\theta \qquad c_\theta = \beta_\theta \frac{K_\theta r_\theta}{V_S} \tag{2.2b}$$

where α_u, β_u, α_θ, and β_θ express the frequency dependence of the impedance terms, and K_u and K_θ represent the static stiffness of the foundation. The following sections outline procedures for evaluating the static stiffness terms and the dynamic modifiers for stiffness and damping (α and β terms).

2.2.2 Static Stiffness

The static stiffness of surface foundations can often be adequately represented by the solution for a rigid disk founded on a halfspace,

$$K_u = \frac{8}{2-\upsilon} G r_u \qquad K_\theta = \frac{8}{3(1-\upsilon)} G r_\theta^3 \tag{2.3}$$

where G = soil dynamic shear modulus. Poisson's ratios recommended for use with Eq. 2.3 in the NEHRP recommended provisions are indicated in Table 2.1. For foundations embedded to depth e, the solution in Eq. 2.3 can be modified as suggested by Kausel (1974):

$$(K_U)_E = K_U\left(1+\frac{2}{3}\frac{e}{r}\right) \qquad (K_\theta)_E = K_\theta\left(1+2\frac{e}{r}\right) \tag{2.4a}$$

For foundations embedded to depth e within a finite soil layer of depth H that overlies a rigid base, the solution by Kausel (1974) is

$$\begin{aligned}(K_u)_{FL/E} &= K_u\left(1+\frac{2}{3}\frac{e}{r}\right)\left(1+\frac{5}{4}\frac{e}{H}\right)\left(1+\frac{1}{2}\frac{r}{H}\right)\\ (K_\theta)_{FL/E} &= K_\theta\left(1+2\frac{e}{r}\right)\left(1+0.7\frac{e}{H}\right)\left(1+\frac{1}{6}\frac{r}{H}\right)\end{aligned} \tag{2.4b}$$

Eqs. 2.4 are approximate expressions that apply for $r/H < 0.5$ and $e/r < 1$. The conditions for which the finite soil layer over rigid base site characterization may be applied are discussed below.

Three key issues associated with the use of Eqs. 2.3 and 2.4 are (1) the selection of a soil shear modulus that represents a strain-degraded, nonuniform stratum, (2) limitations of the circular foundation formulation for noncircular foundation shapes, and (3) applicability of the rigid foundation model to discontinuous foundation systems.

Table 2.1: NEHRP-prescribed values of Poisson's Ratio (BSSC, 1998)

Soil Type	Poisson's Ratio (υ)
Clean sands, gravels	0.33
Stiff clays, cohesive soils	0.40
Soft Clays	0.45

Representative Soil Shear Modulus

The selection of a representative shear modulus must account for the nonuniformity of the profile and the reduction of modulus associated with increasing shear strain.

The small strain shear modulus is evaluated from shear wave velocity as $V_S^2 \rho = G$, where ρ = mass density. For nonuniform soil deposits, representative halfspace shear wave velocities, $(V_S)_H$, can be calculated as the ratio of effective profile depth (Z_p) to shear wave travel time through the profile. Effective profile depths in the NEHRP recommended provisions are $Z_p = 4 \times r_u$ for translations and $Z_p = 1.5 \times r_\theta$ for rocking. Alternatively, Roesset (1980) has suggested for circular foundations the use of soil properties from a depth of $1/2 \times r$, while Gazetas (1991) recommends for square foundations (side dimension $2a$) that soil properties be selected for a depth of $1/2 \times a$ for translations and $1/3 \times a$ for rocking. While the Roesset and Gazetas recommendations are similar, the NEHRP recommendations are quite different, so further investigation of this matter is undertaken.

The evaluation of optimal profile depth (Z_p) is investigated by comparing rigorously defined static impedance solutions for square foundations on various nonuniform soil profiles (Wong and Luco, 1985) with static stiffnesses calculated for an "equivalent" halfspace using the following closed form expressions for a square foundation on a halfspace (Gazetas, 1991)

$$K_u = \frac{9}{2-\upsilon} G_H a \qquad K_\theta = \frac{3.6}{1-\upsilon} G_H a^3 \tag{2.5}$$

where G_H is the effective halfspace shear modulus. The objective is to evaluate the effective profile depths for which the halfspace solution represents the actual static stiffness in translation and rocking with acceptably small errors. These analyses are performed for a rigid square foundation of side dimension *2a* resting on two different profile configurations: (1) a stepped halfspace and (2) a linearly increasing velocity profile overlying a halfspace. These configurations are drawn in the upper right-hand corners of Figs. 2.4. For both the halfspace and nonuniform profiles, the mass densities of the surface layer and underlying halfspace are assumed to form a ratio of ρ_1/ρ_2=1.13 by Wong and Luco (1985). In the case of the nonuniform layer, mass density increases from ρ_1 at the top of the layer to ρ_2 at the bottom of the layer. The effective halfspace density (ρ_H) is taken as a weighted average across the profile depth.

Plotted in Fig. 2.4 are normalized residuals of the static translational and rocking stiffness, calculated as follows:

$$\text{Residual (u)} = (K_{U,Half} - K_U)/K_U$$
$$\text{Residual } (\theta) = (K_{\theta,Half} - K_\theta)/ K_\theta \qquad (2.6)$$

where K_U and K_θ are the actual static stiffnesses for the profiles computed from Wong and Luco (1985). As shown in Figs. 2.4(a) and (b), the code recommends values of $Z_p/r_u = 4$ for translation and $Z_p/r_\theta = 1.5$ for rocking lead to significant overestimates of foundation stiffness for strongly nonuniform profiles. As expected, residuals decrease with increasing profile uniformity (V_{S1}/V_{S2} approaching unity and $H/a \to \infty$). The largest errors occur for the profiles having the shallowest depth range across which V_S varies (Fig. 2.4(a), $H/a = 0.5$, Fig. 2.4(b), $H/a = 2$).

Figs. 2.4 (c) and (d) show residuals for normalized profile depths of $Z_p/r_{u\ or\ \theta} \leq 1.0$. From these figures, $Z_p/r_u = Z_p/r_\theta = 0.75$ are seen to provide nearly optimal solutions for the stepped halfspace and linearly varying profiles. With these profile depths, equivalent halfspace solutions for most H/a values fall within 25% of the actual solution, with the exception of stepped halfspace profiles with $V_{S1}/V_{S2} < 0.5$ – a circumstance addressed in the following paragraph. The residuals do not trend to exactly zero as V_{S1}/V_{S2} approaches unity because of the nonuniform density profile used by Wong and Luco (1985). It may be noted that if ρ_H was taken as ρ_2, the residuals at V_{S1}/V_{S2} =0.8 would effectively be eliminated.

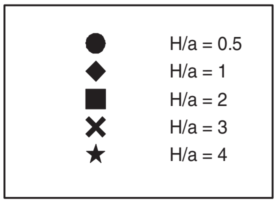

$$\text{Residual}\quad (u) = \frac{K_{u,\,Half} - K_u}{K_u}$$

$$\text{Residual}\quad (\theta) = \frac{K_{\theta,\ Half} - K_\theta}{K_\theta}$$

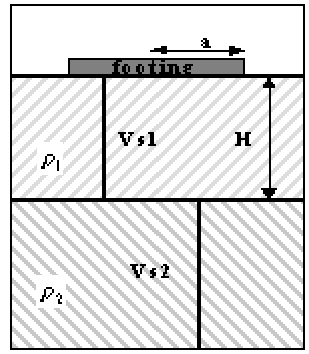

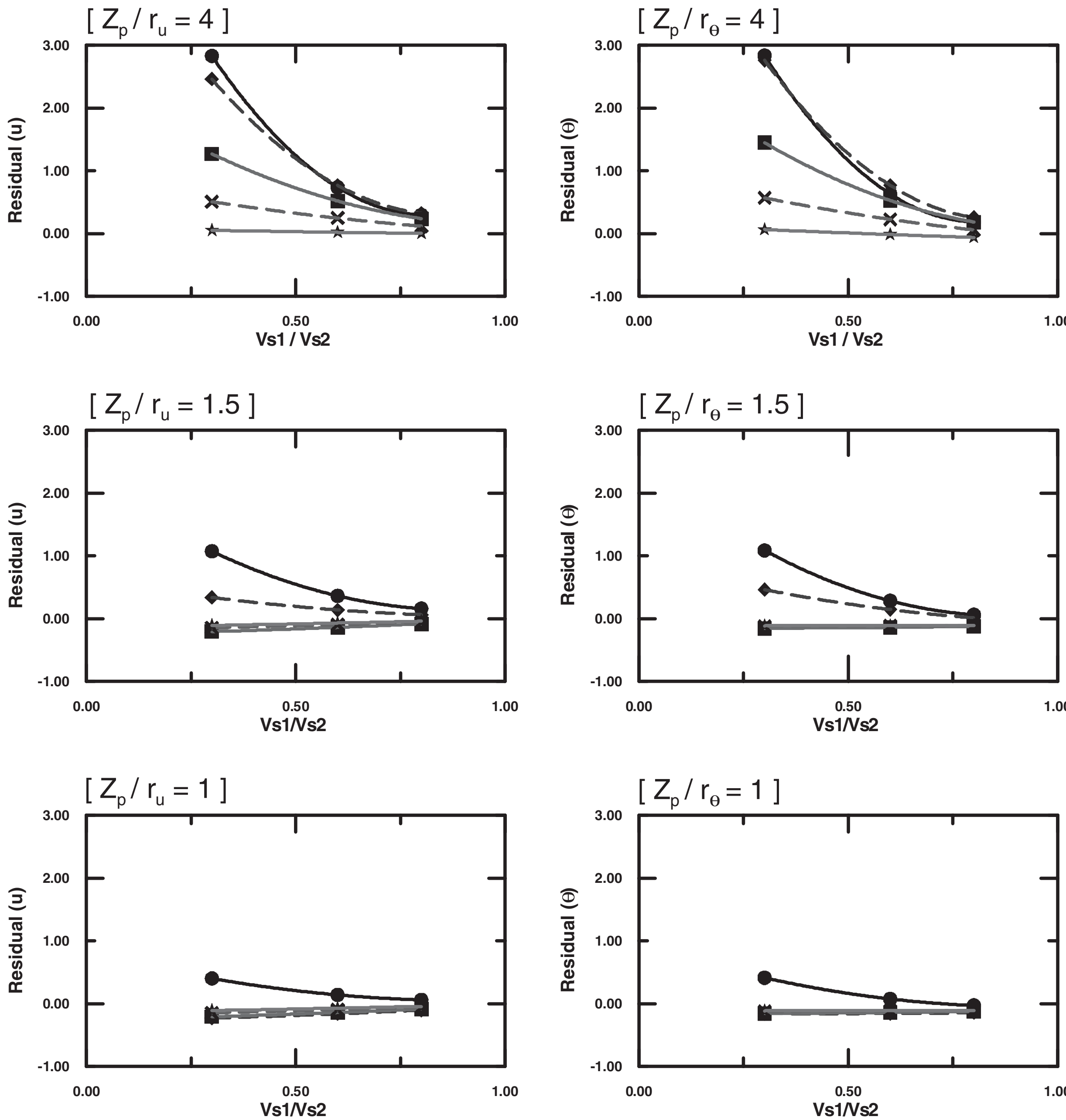

Fig. 2.4 (a) : Static stiffness residuals for finite soil layer over halfspace
(Normalized Profile Depth, Z_p/r = 4.0, 1.5, 1.0)

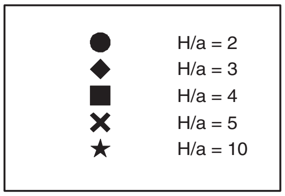

$$\text{Residual}\ (u) = \frac{K_{u,\mathrm{Half}} - K_u}{K_u}$$

$$\text{Residual}\ (\theta) = \frac{K_{\theta,\ \mathrm{Half}} - K_\theta}{K_\theta}$$

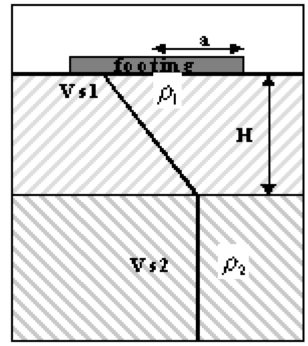

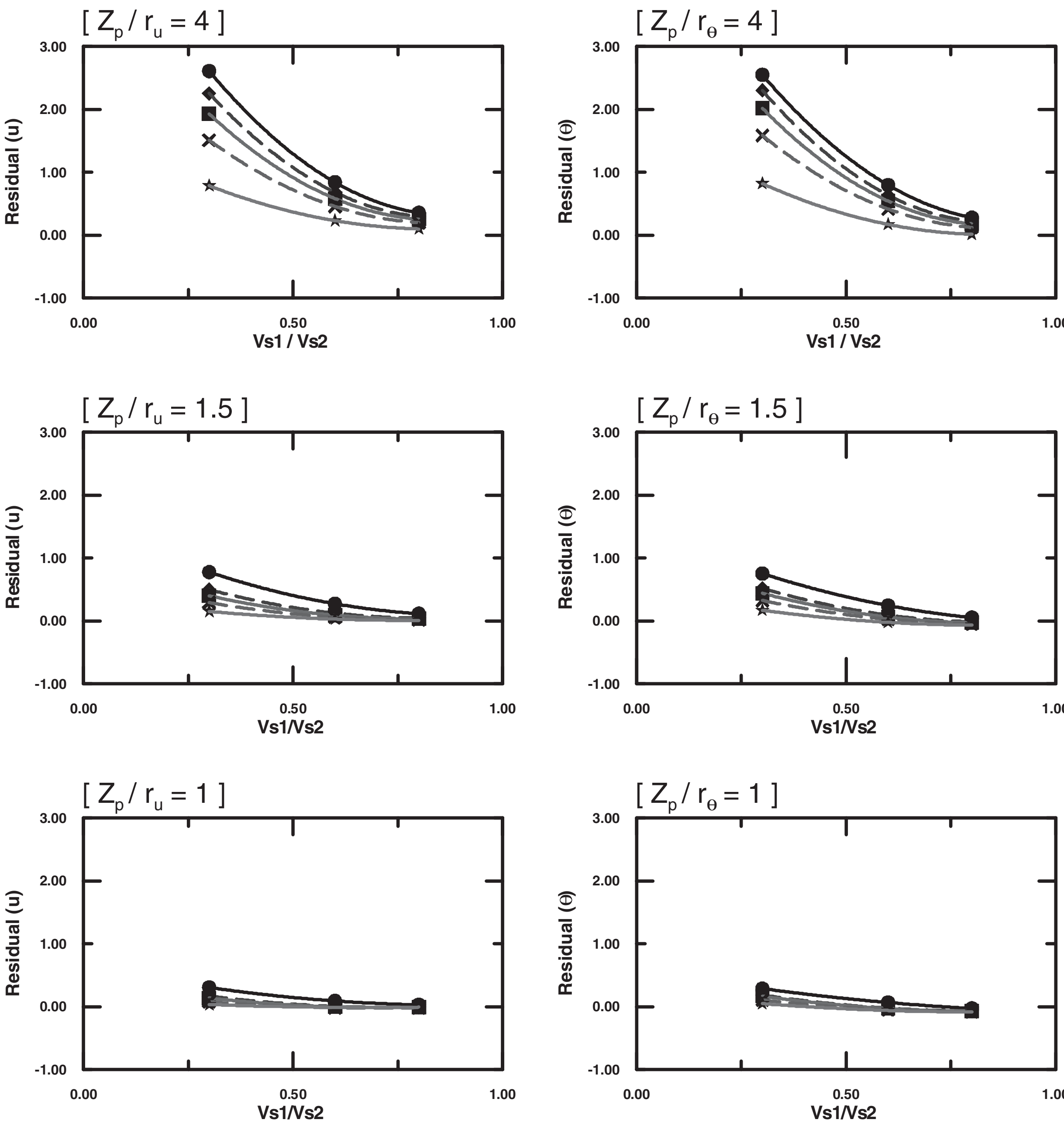

Fig. 2.4 (b) : Static stiffness residuals for nonuniform layer over halfspace
(Normalized Profile Depth, Z_p/r = 4.0, 1.5, 1.0)

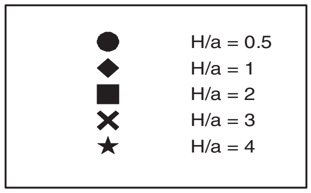

$$\text{Residual}\ \ (u) = \frac{K_{u,\,Half} - K_u}{K_u}$$

$$\text{Residual}\ \ (\theta) = \frac{K_{\theta,\ Half} - K_\theta}{K_\theta}$$

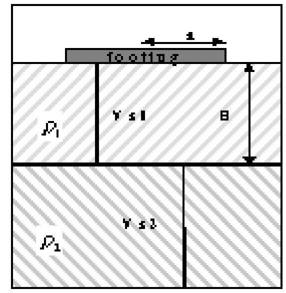

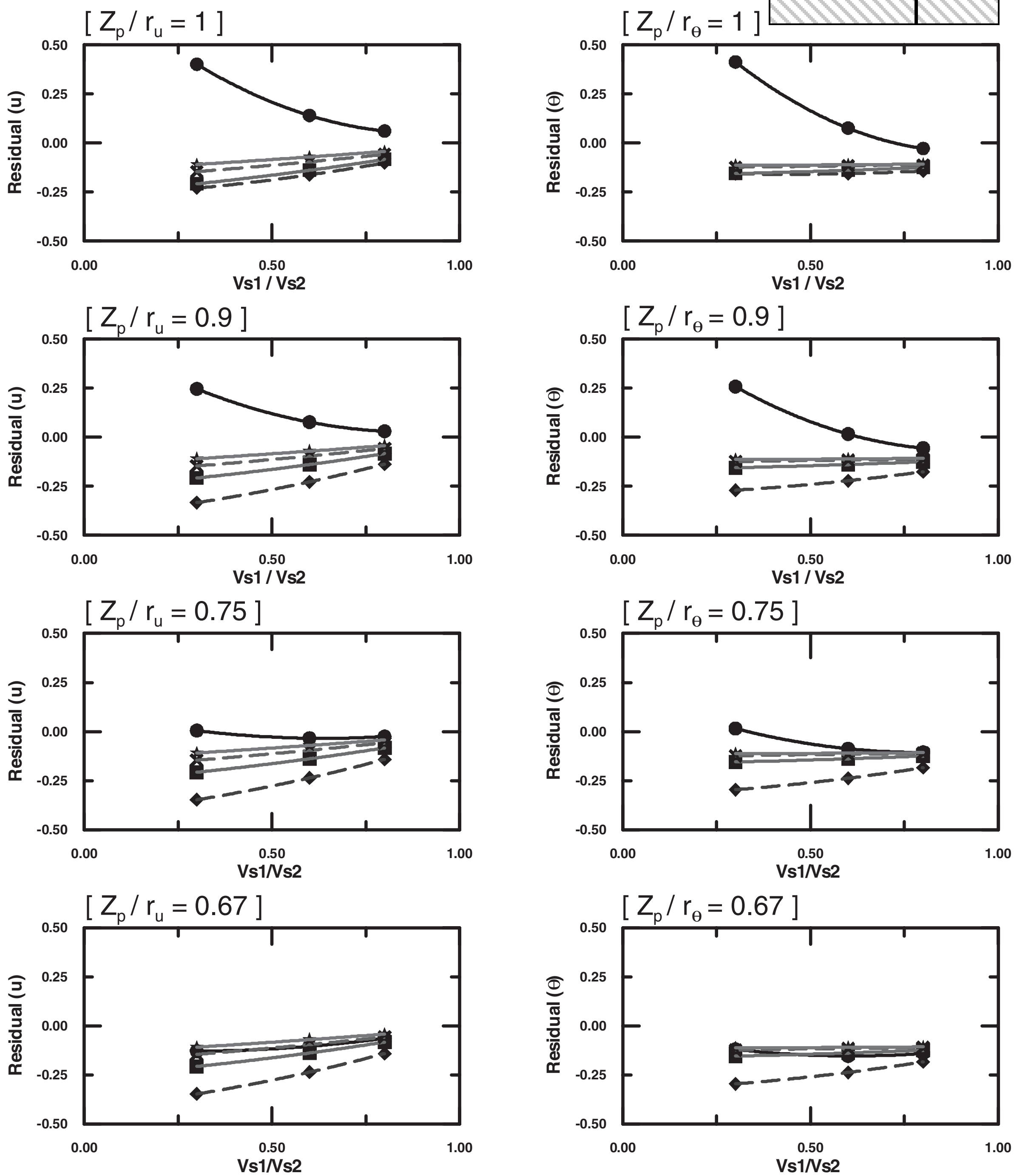

Fig. 2.4 (c) : Static stiffness residuals for finite soil layer over halfspace
(Normalized Profile Depth, Z_p/r = 1.0, 0.9, 0.75, 0.67)

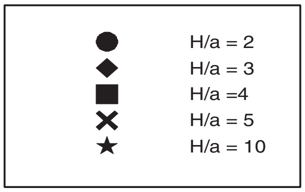

$$\text{Residual}\ (u) = \frac{K_{u,\,Half} - K_u}{K_u}$$

$$\text{Residual}\ (\theta) = \frac{K_{\theta,\,Half} - K_\theta}{K_\theta}$$

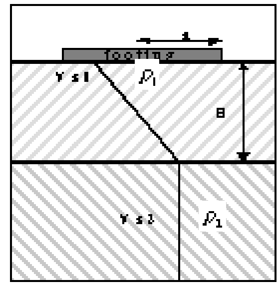

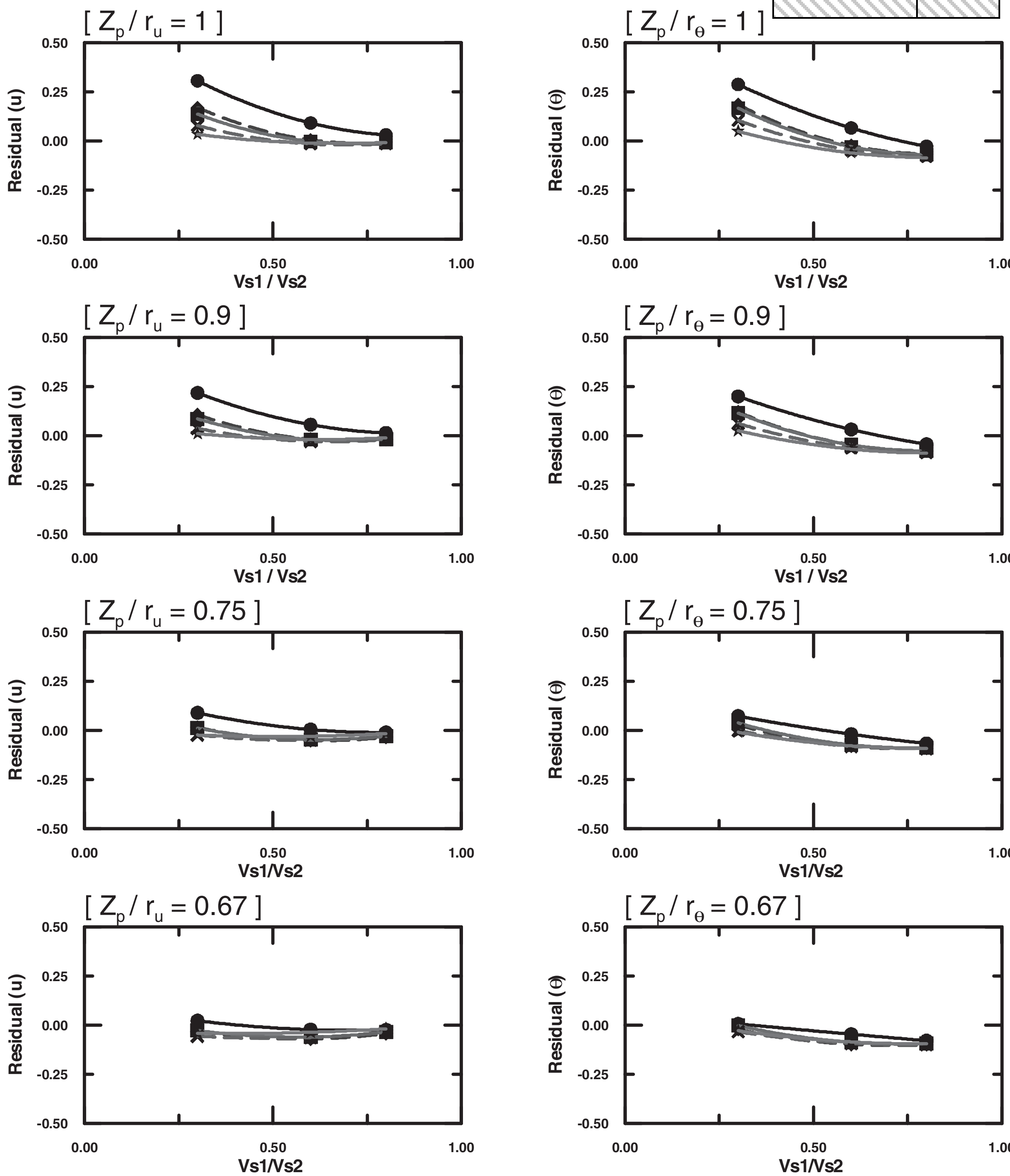

Fig. 2.4 (d) : Static stiffness residuals for nonuniform layer over halfspace
(Normalized Profile Depth, Z_p/r = 1.0, 0.9, 0.75, 0.67)

For profiles with a strong contrast in shear wave velocity, it is of use to investigate the accuracy of the finite soil layer over a rigid base model, as compared to the effective halfspace models invoked above. To directly investigate the errors in the finite soil layer over a rigid base model for different two-layer systems, residuals associated with this model are computed as

$$Residual\ (u) = (K_{U,FL} - K_U)/\ K_U$$

$$\text{Residual}\ (\theta) = (K_{\theta,FL} - K_\theta)/\ K_\theta \tag{2.7}$$

As a first-order approximation, stiffnesses $K_{U,FL}$ and $K_{\theta,FL}$ are evaluated using the square foundation halfspace stiffness values from Eq. 2.5 with the finite soil layer correction indicated in Eq. 2.4(b) for $H/a \geq 2$. Fig. 2.4(e) shows residuals for a range of velocity ratios (V_{S1}/V_{S2}) and profile depths (H/a). The results indicate that for $H/a \geq 2$, the residuals associated with the use of the rigid base model are small ($< \sim 5\%$) for $V_{S1}/V_{S2} < 0.5$. Hence, for simplified analyses, use of the finite soil layer over a rigid base model is recommended for profiles with a uniform velocity layer overlying a material with twice the surface layer's V_S. For other site conditions investigated, the profile is generally best modeled as a halfspace with velocities computed over normalized profile depths of $Z_p/r_u = Z_p/r_\theta = 0.75$.

The second consideration associated with the development of effective profile velocity is the reduction of modulus with cyclic shear strain. The NEHRP recommended provisions correlate modulus reduction with the ground motion parameter S_D as indicated in Table 2.2. As noted in the Appendix, however, the coefficients in Table 2.2 can significantly overestimate the nonlinearity of the soil response. A better estimate of modulus reduction effects is obtained by deconvolving the design-basis free-field motion through the soil column using a 1-D ground response analysis program such as SHAKE91 (Idriss and Sun, 1991). The resulting strain-dependent soil properties across the appropriate profile depth can then be used to evaluate halfspace velocity.

Representation of Noncircular Foundation Shapes

As noted previously, the static stiffnesses of arbitrarily shaped foundations can often be evaluated using the relations in Eq. 2.3 provided foundation radii are computed that match the area (r_u) and moment of inertia (r_θ) of the actual foundation. This formulation can break down, however, as the aspect ratio of the foundation increases. Plotted in Fig. 2.5 are ratios of static impedance for rectangular foundations (computed according

Table 2.2: Code-prescribed values of soil modulus and V_s degradation with effective long period ground acceleration, S_D (BSSC, 1998)

	Ground Acceleration Coefficient, S_D			
	≤ 0.10	≤ 0.15	≤ 0.20	≥ 0.30
G/G_{max}	0.81	0.64	0.49	0.42
$V_s/(V_s)_{max}$	0.90	0.80	0.70	0.65

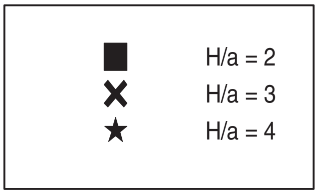

$$\text{Residual }(u) = \frac{K_{u,FI} - K_u}{K_u}$$

$$\text{Residual }(\theta) = \frac{K_{\theta,FI} - K_\theta}{K_\theta}$$

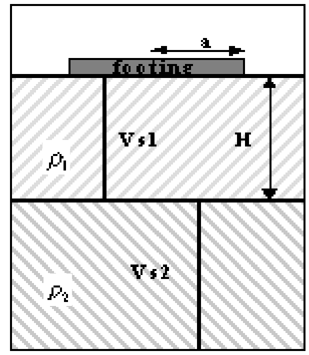

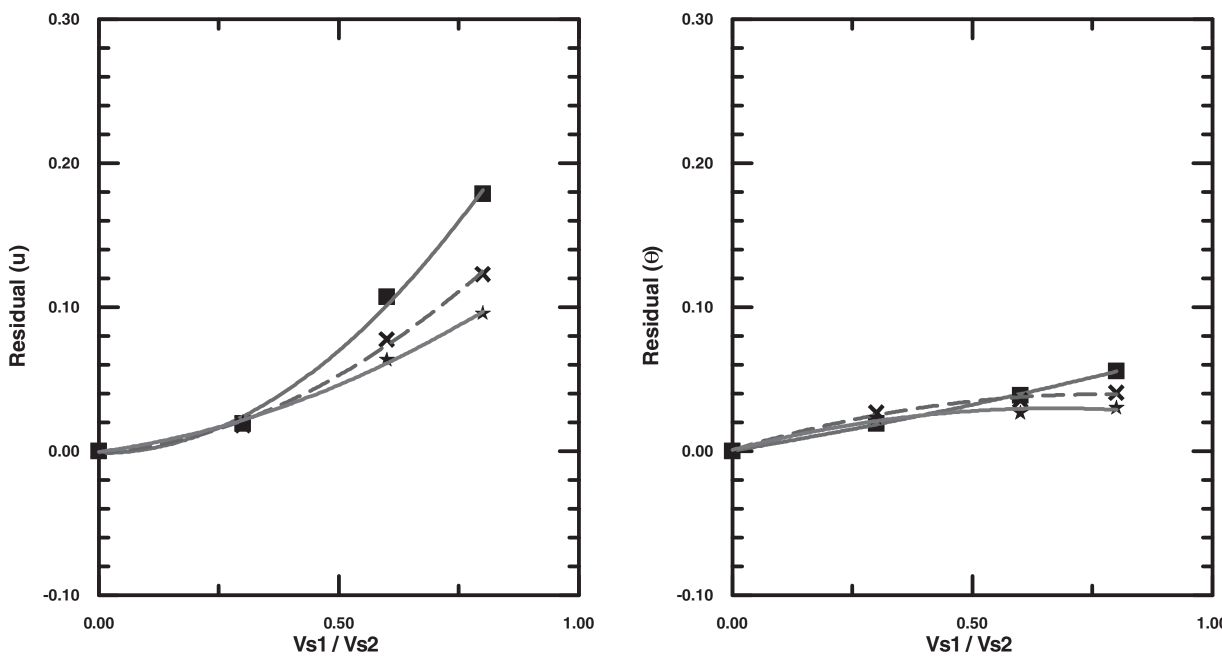

Fig. 2.4 (e) : Static stiffness residuals for finite soil layer over rigid base model

to Gazetas, 1991) to static impedance for the equivalent disk foundation. The disk solution underpredicts the actual static stiffness for aspect ratio, $L/B > 2$, but is less than a 20% effect up to $L/B > 6$. For aspect ratios larger than $L/B>6$ (strip footings) it is recommended that the impedance for circular foundations be increased according to the ordinates in Fig. 2.5.

Modeling of Discontinuous Foundations

The static stiffness equations in Eq. 2.3 assume a continuous foundation system supports the entire building structure (e.g., mats, continuous spread footings underlying walls that are continuous around the building perimeter, spread footings interconnected by grade beams and/or a base slab). Continuous foundations that are nonrigid (i.e. flexible), are discussed in 2.2.3. The discussion here focuses on structures founded on discontinuous foundation elements (e.g. continuous spread footings supporting discontinuous walls, independent spread footings).

Foundation stiffnesses can be derived for independent footings using Eq. 2.3 or 2.4, provided the foundation radii are computed to match the dimensions of the actual foundation elements. As recommended in the NEHRP code, the rocking impedance for structures founded on several independent footings can be approximately computed as

$$K_\theta = \sum k_{zi} \cdot y_i^2 \tag{2.8}$$

where k_{zi} represents the vertical foundation stiffness of an individual footing, and y_i represents the normal distance from the centroid of the i^{th} footing to the rocking axis of the foundation.

Foundation stiffnesses for continuous footings underlying discontinuous walls (e.g. tilt-up structures) should be evaluated separately for each wall. Solutions for long rectangular foundations in Gazetas (1991) can be used, or modifications to the disk foundation stiffness according to Fig. 2.5 can be invoked. These stiffnesses can then be used in a substructure analysis of the wall response. An example of the calculation of wall footing impedance is provided in the Appendix for a tilt-up structure in Hollister, California.

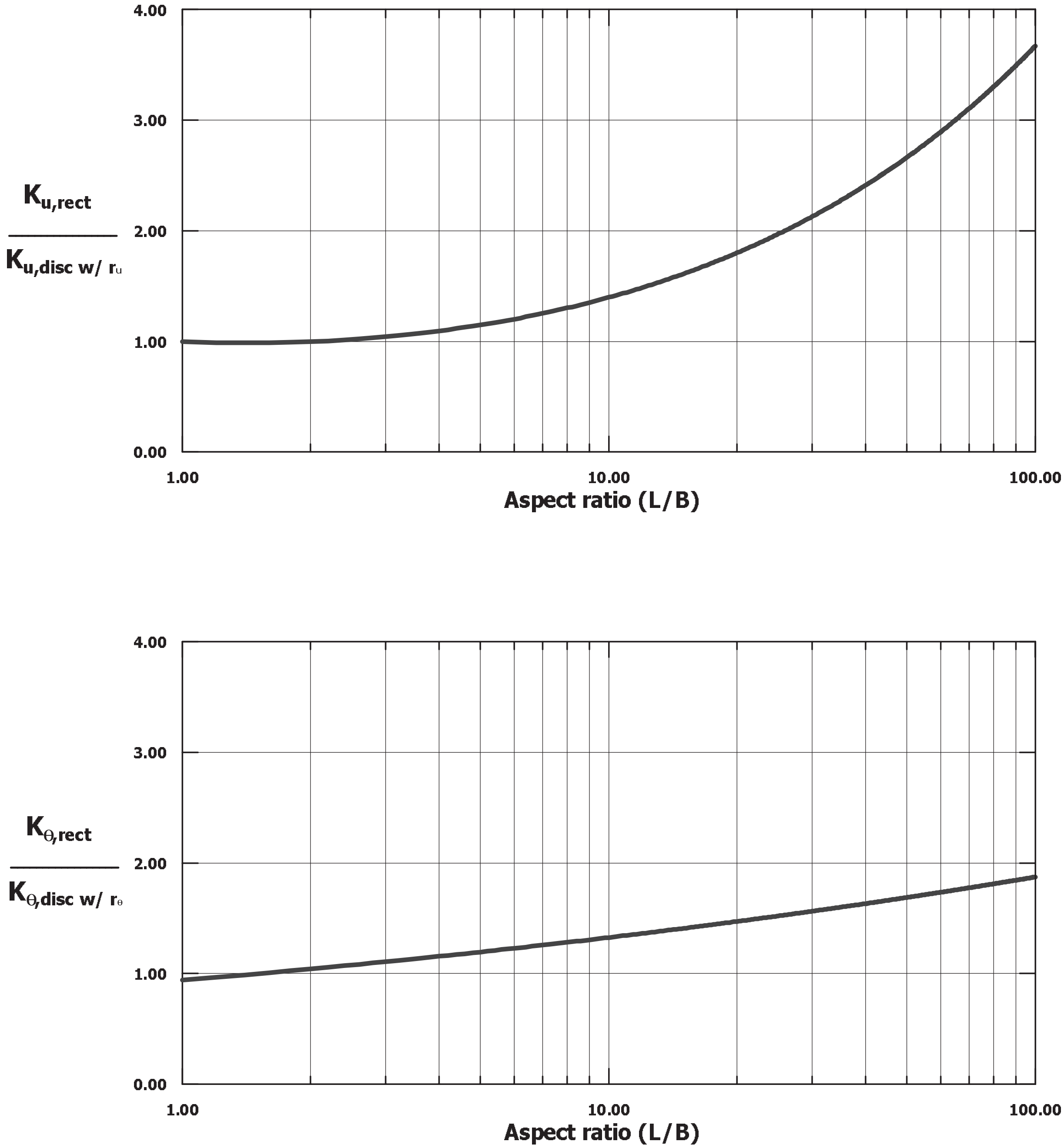

Fig. 2.5 : Ratio of static stiffness of rectangular foundation to equivalent disc foundation

2.2.3 Dynamic Modifiers for Stiffness and Damping

Foundation impedance for both the translation and rocking modes is frequency dependent and complex-valued. As noted in Eq. 2.2, the α factors express the frequency dependence of the real stiffness, while β factors express the frequency dependence of damping.

The α_j and β_j factors for a rigid disk foundation resting on a halfspace are plotted in Fig. 2.6 using the formulation of Veletsos and Verbic (1973). Within the frequency range of common engineering interest, these factors can be applied to nonuniform soils provided a representative halfspace velocity is selected (as discussed in Section 2.2.2). Based on analysis (Dobry and Gazetas, 1986) and case history data (Stewart et al., 1998), the factors in Fig. 2.6 can also be applied to noncircular foundation shapes, provided the foundation aspect ratio is less than four. Note from Eqs. 2.2 that the static foundation stiffnesses (K_U, K_θ) that should be used for the evaluation of dashpot coefficients (c_U, c_θ) are based on an assumed disk foundation shape. Accordingly, a modified static stiffness using the aspect ratio correction in Fig. 2.6 should not be used in the calculation of foundation damping with Eqs. 2.2. In the limiting case of a strip foundation, the α_j factors are nearly one for practical purposes, whereas β_u=0.67 and β_θ=0.38 (independent of frequency).

As can be seen in Fig. 2.6, a key issue associated with the evaluation of damping factors β_j at low frequencies is characterization of the effective soil hysteretic damping ratio β. It is known from laboratory testing of soil that β is a function of soil type and the amplitude of shear strains in the soil. Typical values of β are about 1 to 15% for sand and low-plasticity cohesive soils, and about 2 to 10% for clays with a plasticity index of about 30 to 40 (Vucetic and Dobry, 1991; Stokoe, 1999). The low end of the quoted ranges would apply to low-level shaking ($S_D < 0.1$), the high end to relatively severe shaking ($S_D > 0.4$). More precise guidelines for the selection of β are currently under development.

For embedded foundations, Elsabee and Morray (1977) suggest that a combination of static stiffness values from Eq. 2.4 with the dynamic factors in Fig. 2.6 provides a reasonable representation of dynamic foundation impedance for $e/r < 0.5$. Case history data analyzed by Stewart et al. (1998) suggest this practice is acceptable for building structures. However, for deeper embedment, a more rigorous solution, such as that developed by Apsel and Luco (1987), can significantly improve the results, particularly for high-frequency structures.

For flexible foundations, analyses by Iguchi and Luco (1982) and a case history discussed in Stewart et al. (1998) suggest that the rocking impedance solution for rigid foundations obtained through the use of Eqs. 2.2-2.3 and Fig. 2.6 can be significantly in error for the wall/foundation configuration shown in Fig. 2.7(a) (a stiff core of shear walls resting on a continuous base slab, no perimeter walls). For such cases, it is necessary to account for the reduction in foundation stiffness and damping associated with the flexibility of the base mat. The key parameter governing the influence of foundation flexibility effects on rocking impedance is the ratio of the soil-to-foundation rigidity,

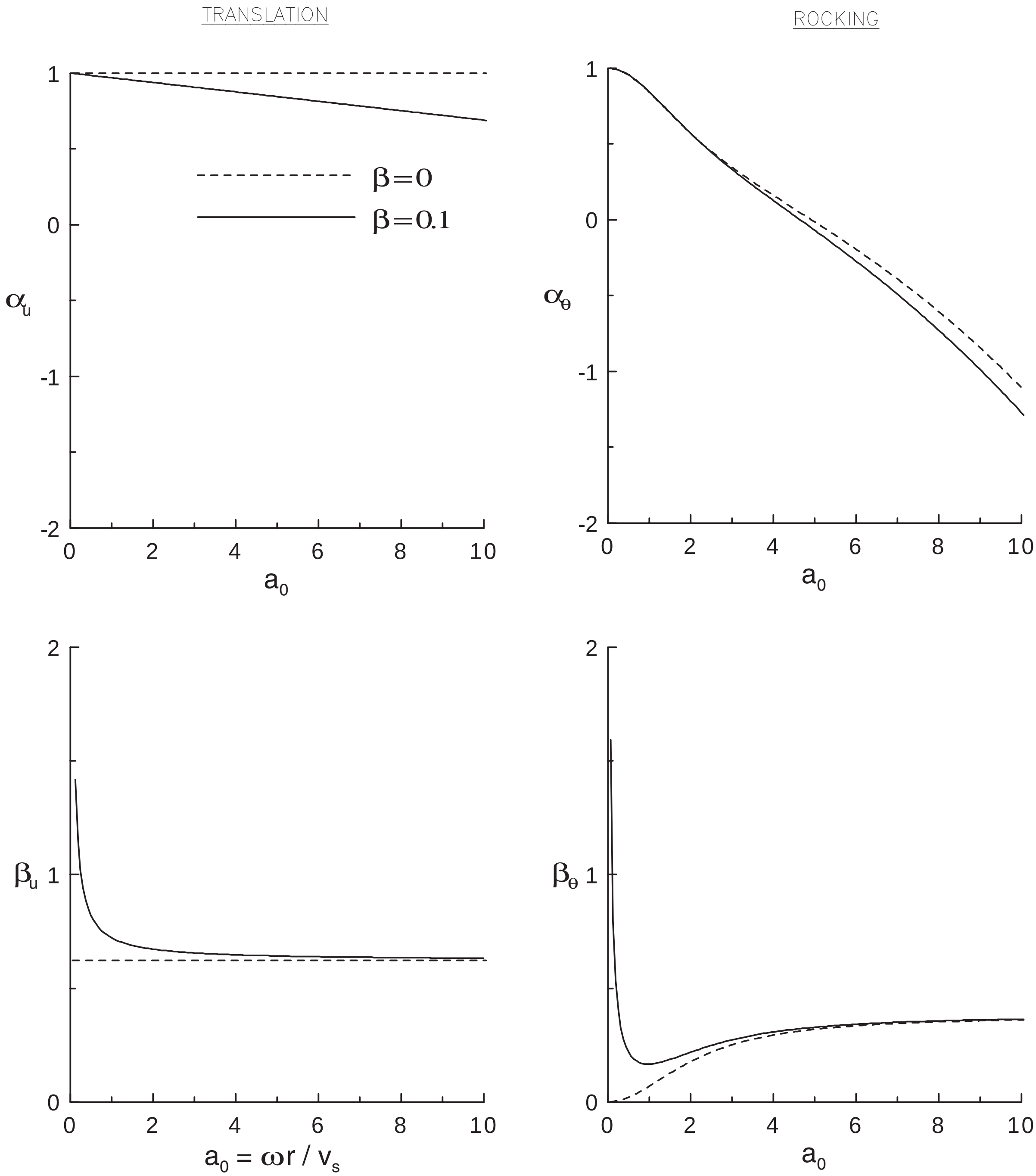

Fig. 2.6: Foundation stiffness and damping factors for elastic and viscoelastic halfspaces, $\upsilon = 0.4$ (after Veletsos and Verbic, 1973)

$$\eta = \frac{Gr^3}{D} \tag{2.9}$$

in which G is the soil dynamic shear modulus and D is the foundation's flexural rigidity,

$$D = \frac{E_f t_f^3}{12\left(1-\upsilon_f^2\right)} \tag{2.10}$$

where E_f, t_f, and ν_f are the Young's modulus, thickness, and Poisson's ratio of the foundation, respectively. Values of α_θ and β_θ for rigid core shear walls of various radii on slab foundations are plotted in Fig. 2.7(b) based on the analysis of Iguchi and Luco (1982). These dynamic modifiers are formulated for use with the standard static stiffnesses calculated using Eqs. 2.2-2.3. The dynamic modifiers in Fig. 2.7(b) should be used in lieu of those in Fig. 2.6 for structures with the configuration indicated in Fig. 2.7(a).

2.3 APPLICATIONS AND CONCLUSIONS

There are two general applications of impedance functions: (1) quantification of foundation spring and dashpot coefficients for use in structural response analyses and (2) analysis of period lengthening ratios and foundation damping factors for response-spectrum-based analysis of seismic structural response. The subject buildings for this study cannot be readily modeled as lumped-mass systems (mass is principally distributed along walls in the concrete building and along the roof diaphragm in the tilt-up building). Hence, period-lengthening ratios and foundation damping factors are not the ideal representation of SFSI effects in these cases. Rather, SFSI effects were evaluated by comparing the response of the building-specific structural models for fixed-base conditions (infinite foundation stiffness, zero damping) and flexible-base conditions (stiffness and damping represented by impedance functions). Results of these comparisons are presented in Chapters 3 and 4. Example calculations of impedance functions are appended to the end of this chapter.

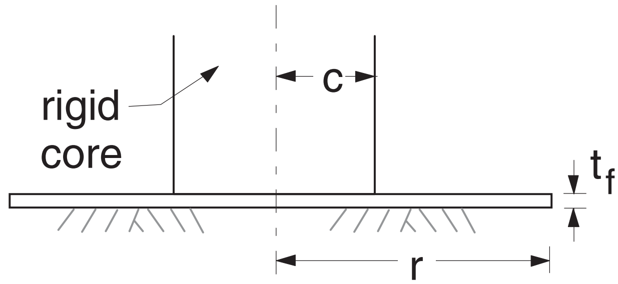

Fig. 2.7(a): Disk foundation with rigid core

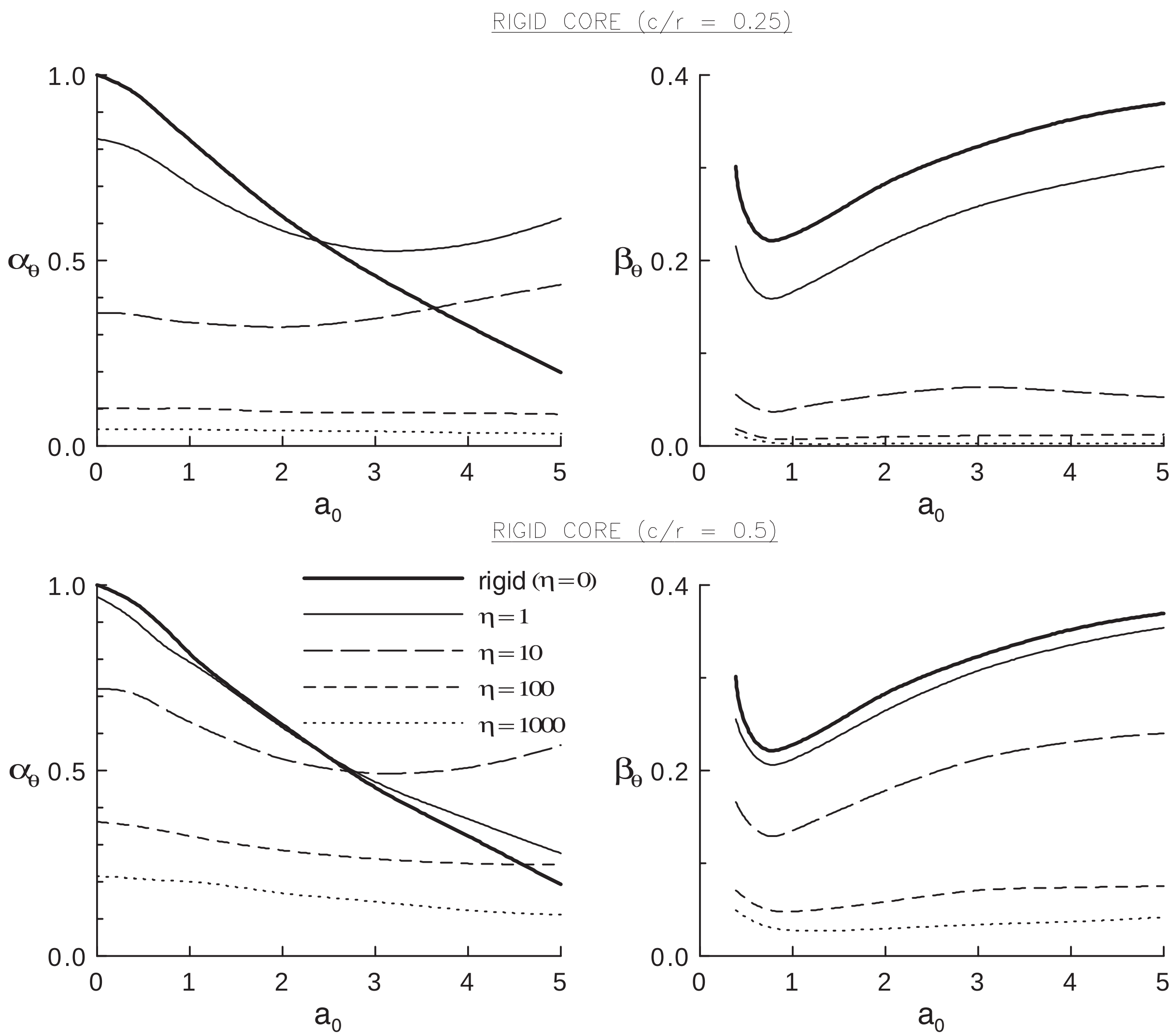

Fig. 2.7(b): Rocking stiffness and damping factors for building with rigid core walls on flexible foundations (Iguchi and Luco, 1982)

APPENDIX 2: A SITE-SPECIFIC ANALYSIS OF IMPEDANCE FUNCTIONS

A2.1: STEEL REINFORCED CONCRETE BUILDING, BERKELEY, CALIFORNIA

The impedance function for this site was evaluated using the simplified procedures in Chapter 2 (based on the impedance of a disk foundation) and the impedance solutions for square foundation shapes by Wong and Luco (1985) as implemented in the computer code DYNA4 (Novak et al., 1993). Both formulations assume a rigid foundation slab, which is justified given the presence of shear walls around the building perimeter (see Section 2.2.3).

Soil Conditions

The soil profile for the site, shown in Fig. A2.1(a), was compiled from borings located along a BART tunnel alignment approximately 100 to 200 ft. from the site. No in-situ measurements of shear wave velocity (V_s) are available, but V_s was estimated based on correlations with void ratio and geologic age by Fumal and Tinsley (1985) and correlations with SPT blow count by Seed et al. (1984). Strain- compatible soil properties were evaluated using the profile in Fig. A2.1(a) in deconvolution analyses with the ground response program SHAKE91 (Idriss and Sun, 1991). The deconvolution analysis was performed using the ground motion recorded at the Gilroy #2 station during the 1989 Loma Prieta earthquake. This representative ground motion was selected based on de-aggregation results from probabilistic seismic hazard analysis for the site, and the PGA was scaled to match the PGA of the 10% in a 50-year constant hazards spectrum. Other time histories were considered, but the computed shear strain profiles, and hence profiles of strain compatible soil properties, were found to be fairly insensitive to the time history.

Simplified Analysis

Actual foundation dimensions are 64 x 90 ft. Equivalent radii of disk foundations can then be calculated as r_u=43 ft., and r_θ=40 and 47 ft. (transverse and longitudinal directions, respectively). Based on the best-estimate small strain V_s profile in Fig. A2.1(a), representative shear wave velocities for the site are calculated over profile depths of 0.75r_u for translation and 0.75r_θ for rocking as 802 ft/s (translation) and 798 ft/s and 808 ft/s (transverse and longitudinal rocking, respectively). Effective strain-dependent shear wave velocities are computed using two techniques: (1) reduction factors in Table 2.2 for $S_D > 0.3$ and (2) the results of the previously described ground response analyses, which yield representative shear wave velocities of 644 ft/s (translation) and 641 ft/s and 649 ft/s (transverse and longitudinal rocking, respectively). The resulting shear moduli are used with a Poisson's ratio of 0.33 (Table 2.1) in Eq. 2.3 to calculate the following static stiffnesses:

Modulus Reduction based on Table 2.2

K_u = 2.07 E08 (lb/ft)

$(K_\theta)_{trans}$ = 2.54 E11 (lb.ft/rad)

$(K_\theta)_{long}$ = 4.22 E11 (lb.ft/rad)

Modulus Reduction based on Ground Response:

K_u = 3.18 E08 (lb/ft)

$(K_\theta)_{trans}$ = 3.90 E11 (lb.ft/rad)

$(K_\theta)_{long}$ = 6.49 E11 (lb.ft/rad)

Comparing these values, it is readily apparent that the modulus reduction factors in the NEHRP Provision significantly overestimate the soil nonlinearity at this site.

To construct full impedance functions, the static stiffness values are multiplied by the frequency-dependent dynamic modifiers α_j and β_j in Fig. 2.6 (for $j = u$ and θ). Using the static soil stiffness values derived from ground response analyses, the estimated impedance functions are as shown in Fig. A2.1b (gray lines).

DYNA4 Analyses

DYNA4 analyses of the impedance of rectangular foundations are based on equivalent dimensions of square foundations ($2a$ x $2a$). These equivalent dimensions are a=38 ft. for translation, and a=35 and 41.5 ft. for rocking (transverse and longitudinal directions, respectively). DYNA has a limited range of soil profile geometries that can be modeled. In particular, the ratio of the thickness of the linearly varying portion of a nonuniform profile (H) to the foundation dimension has a minimum value of H/a=2.0, whereas for the Berkeley site profile this ratio is actually H/a=0.60 to 0.72. In addition, the ratio of the ground surface velocity (V_{s1}) to the velocity at depth (V_{s2}) in DYNA can assume only a discrete number of values, the most appropriate of which is V_{s1}/V_{s2}=0.8 for the subject site. Given the above constraints, the degraded shear wave velocity profile in Fig. A2.1(a) was modified to an "equivalent" profile with H/a=2.0 and V_{s1}/V_{s2}=0.8, and the same average V_s to depth $2a$ as the profile in Fig. A2.1(a). Using these foundation and soil properties, the frequency-dependent foundation impedance functions were evaluated as shown in Fig. A2.1b (black lines).

Comparison

The static stiffness values from different analyses are listed below.

	K_u (lb/ft)	$K_{\theta,trans}$ (lb.ft/rad)	$K_{\theta,long}$ (lb.ft/rad)
Simplified analysis: degraded V_s from Table 2.2	2.07 E08	2.54 E11	4.22 E11
Simplified analysis: degraded V_s from Ground Response	3.18 E08	3.90 E11	6.49 E11
DYNA 4	2.80 E08	3.32 E11	5.53 E11

The simplified and DYNA4 impedance functions based on best-estimate shear wave velocity data are in reasonable agreement. The differences result from the different representations of the same velocity profile necessitated by DYNA4 limitations, as discussed above. As noted previously, the static impedance values calculated from the degraded velocity profile invoking the shear modulus reduction factors from the NEHRP *Provisions* are significantly too low, indicating that these provisions significantly overestimate soil nonlinearity in this case. The variations of stiffness and damping with frequency by the two analysis schemes are nearly identical.

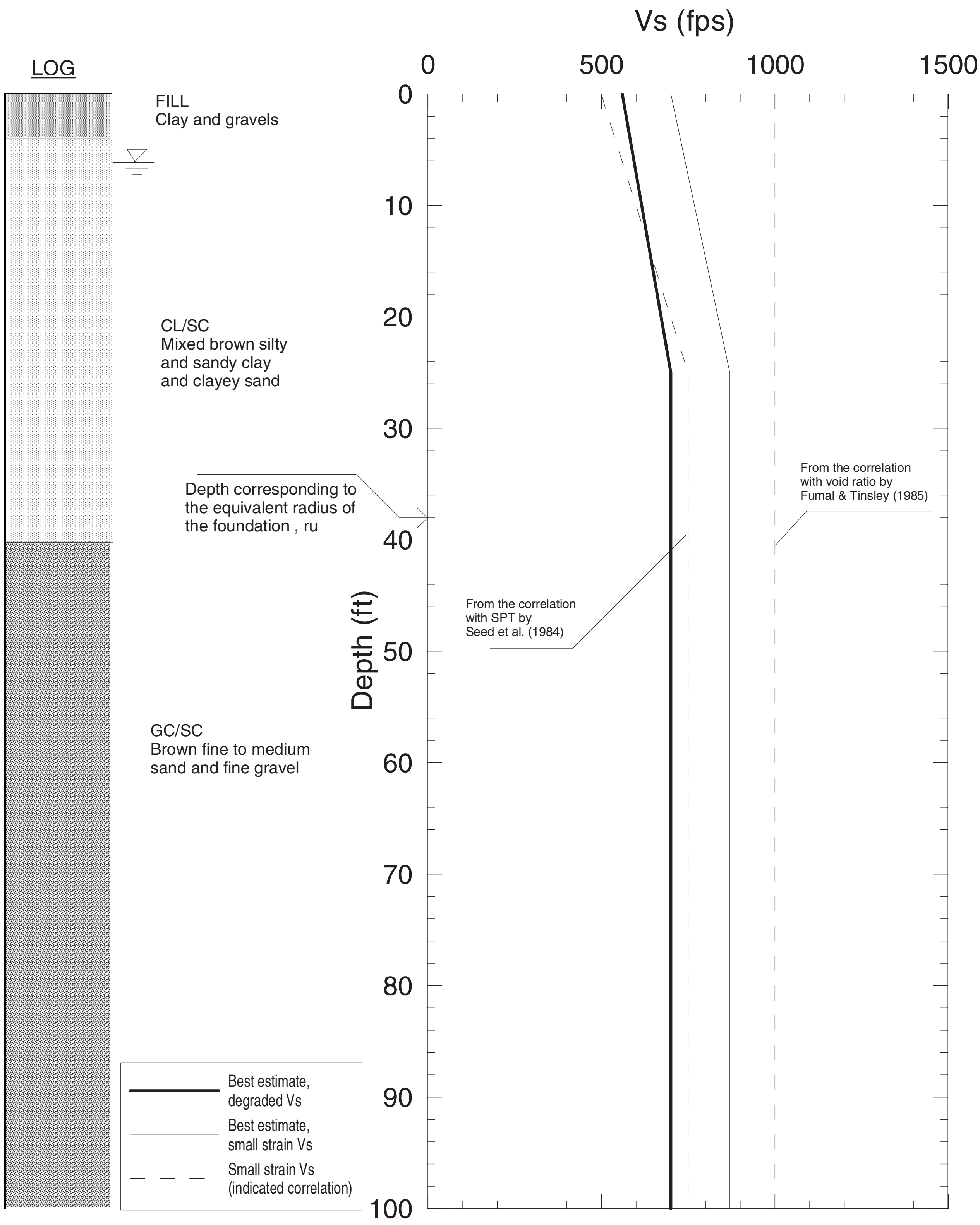

FigA2.1(a) : Generalized soil profile for the Berkeley site.

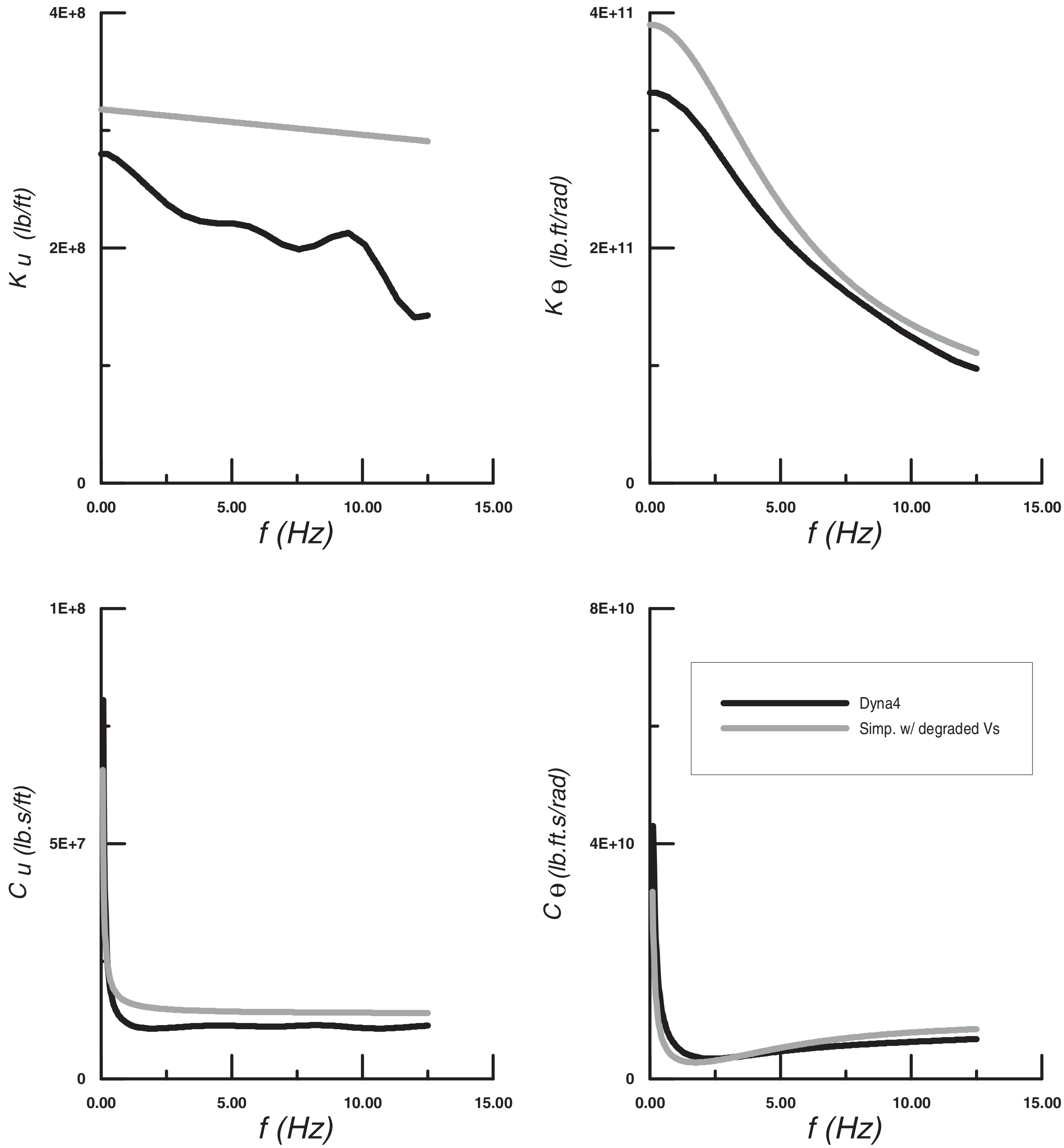

Fig.A2.1(b) : Foundation stiffness and damping constants of E-W for the Berkeley site

A2.2: TILT-UP BUILDING, HOLLISTER, CALIFORNIA

A single impedance function representing the entire foundation system of this tilt-up building was not evaluated. Rather, the foundation impedance for in-plane deformations of end walls was evaluated using the simplified procedures in Chapter 2 (based on the impedance of a disk foundation) and the impedance solutions for arbitrarily shaped foundations by Dobry and Gazetas (1986).

Soil Conditions

The soil profile shown in Fig. A2.2(a) is based on subsurface exploration at Hollister City Hall, located near the site. The V_s profile shown in Fig. A2.2(a) is based on downhole measurements by Shannon & Wilson/Agbabian Associates (1980). Strain-compatible soil properties were evaluated using the profile in Fig. A2.2(a) in deconvolution analyses with the ground response program SHAKE91 (Idriss and Sun, 1991). The deconvolution analysis was performed using the ground motion recorded at the Hollister free-field station near the site during the 1989 Loma Prieta earthquake. The profile of strain-compatible shear wave velocity from these analyses is shown in Fig. A2.2(a).

Simplified Analysis

The end walls for this building are 100 ft. long by 0.5 ft. wide. The foundation width is not known but is assumed to be 3 ft. Equivalent radii of disk foundations can then be calculated as r_u=9.8 ft. (translation) and r_θ=23.8 ft. (in-plane rocking). Based on the best-estimate small strain V_s profile in Fig. A2.2(a), representative shear wave velocities for the site are calculated over profile depths of $0.75r_u$ for translation and $0.75r_\theta$ for rocking as 500 ft/s (translation) and 518 ft/s (rocking). Effective strain-dependent shear wave velocities are computed using both reduction factors in Table 2.2 for S_D >0.3 and ground response analyses. The resulting shear moduli are used with a Poisson's ratio of 0.4 (Table 2.1) in Eq. 2.3 to calculate static stiffnesses for an equivalent disk-shaped foundation. These stiffnesses are then modified according to Fig. 2.5 due to the long aspect ratio of these end wall foundations (L/B = 33) to yield the following static stiffness estimates:

Modulus Reduction Based on Table 2.2
K_u = 4.22 E07 (lb/ft)
K_θ = 4.03 E10 (lb.ft/rad)
Modulus Reduction Based on Ground Response:
K_u = 9.53 E07 (lb/ft)
K_θ = 9.53 E07 (lb.ft/rad)

As with the Berkeley site, the NEHRP modulus reduction provisions are seen to overestimate significantly the soil nonlinearity at this site.

Using the frequency-dependent dynamic modifiers α_j and β_j in Fig. 2.6 (for $j = u$ and θ), the static stiffnesses are modified using Eqs. 2.2 to evaluate the estimated impedance functions shown in Fig. A2.2(b) Results are shown with and without the aspect ratio correction for static stiffness noted above. Note that the aspect ratio correction for static stiffness (solid, gray line) *is* recommended for static stiffness, but *is not* appropriate for evaluation of damping (dashed gray line is preferable).

Dobry and Gazetas (1986) Analysis

Impedance solutions for foundations with arbitrary aspect ratio (*L/B*) by Dobry and Gazetas (1986) were evaluated for the end wall foundations using a value of *L/B*=33. These analyses were performed two ways, once with halfspace velocities computed from effective profile depths recommended in this report (based on dimensions for an equivalent disk foundation) and again with effective profile depths recommended in Gazetas (1991) of 67 ft. (0.67L) for translation and 33 ft. (0.33L) for rocking. The resulting frequency-dependent foundation impedance functions (Gazetas, 1991 depths only) are shown in Fig. A2.2b (black lines).

Comparison

The static stiffness values from different analyses are listed below.

	K_u (lb/ft)	K_θ (lb.ft/rad)
Simplified analysis: Degraded Vs from Table 2.2	4.22 E07	4.03 E10
Simplified analysis: Degraded Vs from Ground Response	9.53 E07	9.07 E10
Dobry and Gazetas: Degraded Vs, profile depth from eq. disk fndn. dimension	9.31 E08	8.95 E10
Dobry and Gazetas: Degraded Vs, profile depth recommended by Gazetas	1.16 E09	9.19 E10

The middle two rows of the above table illustrate that the static stiffness associated with the degraded profiles are very similar for the simplified analysis (which has an aspect ratio correction) and the Dobry and Gazetas (1986) recommendations. Further, as shown in the last two rows, the effect of varying the profile depths is small for this site, due to the relatively uniform soil conditions near the ground surface. The frequency dependence of the stiffness results is negligible in translation, and strongly dependent on foundation aspect ratio (*L/B*) for rocking. The disk approximation significantly overestimates the frequency-dependent reduction in rocking stiffness. It is noteworthy that this reduction is similar for the circular and oblong foundation when expressed with respect to normalized frequency $\alpha_0 = \omega r_\theta / v_s$ for disks and $\alpha_0 = \omega B / v_s$ for rectangular foundations (where ω=circular frequency).

The primary difference between damping estimates in the simplified analysis and Dobry and Gazetas (1986) procedures is at small frequencies, where hysteretic soil damping dominates the damping for disk foundations. Damping values at large frequencies are identical for the two procedures, provided that the damping estimate from the simplified analysis is based on the equivalent disk static stiffness without alteration for aspect ratio effects (as noted above and in Section 2.2.3).

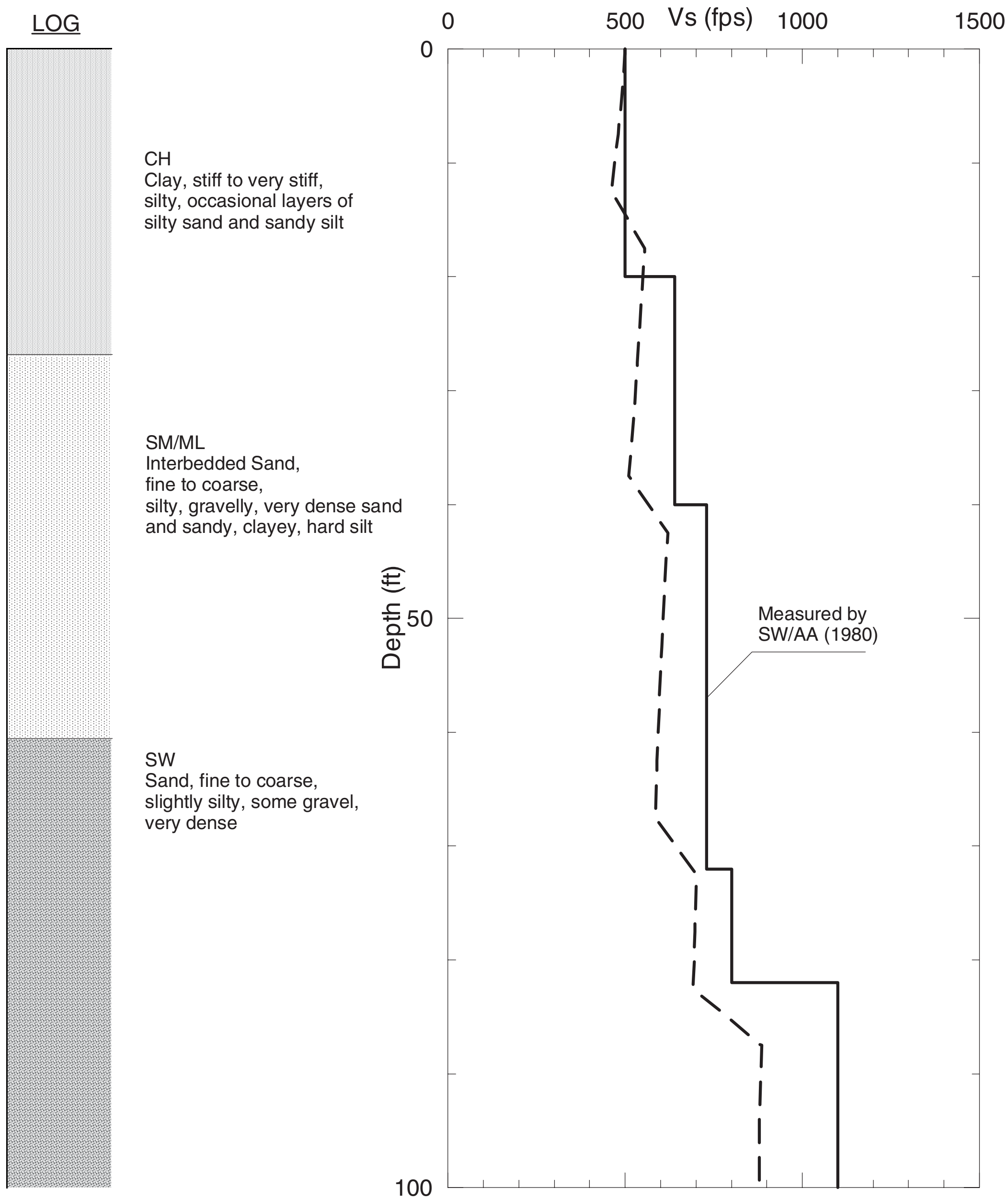

Fig.A2.2(a) : Generalized soil profile for the Hollister site.

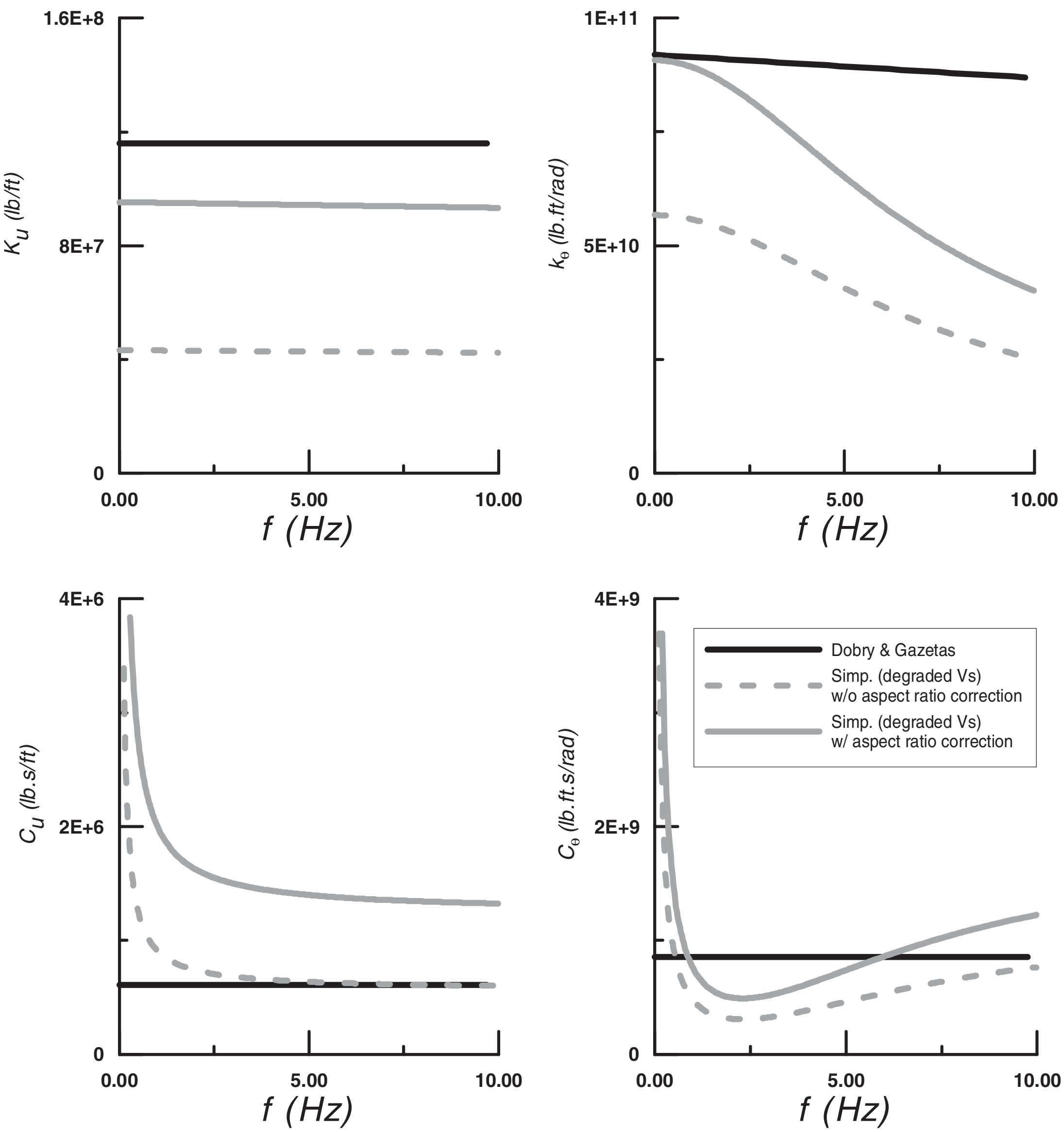

Fig.A2.2(b) : Foundation stiffness and damping constants of E-W for the Hollister site

REFERENCES

Apsel, R.J. and Luco, J.E. (1987). "Impedance functions for foundations embedded in a layered medium: an integral equation approach," *J. Earthquake Engrg. Struct. Dynamics*, 15(2), 213-231.

Building Seismic Safety Council, BSSC (1998). "NEHRP Recommended provisions for seismic regulations for new buildings, Part 1, Provisions and Part 2, Commentary" *Rpt. No. FEMA 302 & 303*, Federal Emergency Management Agency, Washington D.C.

Dobry, R. and Gazetas, G (1986). "Dynamic response of arbitrarily shaped foundations," *J. Geotech. Engrg.*, ASCE, 112(2), 109-135.

Elsabee, F. and Morray, J.P. (1977). "Dynamic behavior of embedded foundations," *Rpt. No. R77-33*, Dept. of Civil Engrg., MIT, Cambridge, Mass.

Fumal, T.E. and Tinsley, J.C. (1985). "Mapping shear-wave velocities of near-surface geologic materials," *Prof. Paper 1360*, U.S. Geological Survey.

Gazetas, G. (1991). "Foundation Vibrations," Chapter 15 of *Foundation Engineering Handbook*, 2nd Edition, H.-Y. Fang (ed.).

Idriss, I.M. and Sun, J.I. (1991). "SHAKE91: A computer program for conducting equivalent linear seismic analyses of horizontally layered soil deposits," Ctr. For Geotech. Modeling, Univ. of California, Davis.

Iguchi, M. and Luco, J.E. (1982). "Vibration of flexible plate on viscoelastic medium," *J. Engrg. Mech.*, ASCE, 108(6), 1103-1120.

Kausel, E. (1974). "Forced vibrations of circular foundations on layered media," *Rpt. No. R74-11*, Dept. of Civil Engrg., MIT, Cambridge, Mass.

Novak, M., Sheta, M., El-Hifnawy, L., El-Marsafawi, H., and Ramadan, O. (1993). "DYNA4: A computer program for calculation of foundation response to dynamic loads," Users Manual, Vol. 1, Geotechnical Research Centre, Univ. Western Ontario, London, Ontario, Canada.

Roesset, J.M. (1980). "A review of soil-structure interaction," in *Soil-structure interaction: The status of current analysis methods and research*, J.J. Johnson, ed., Rpt. No. NUREG/CR-1780 and UCRL-53011, U.S. Nuclear Regulatory Com., Washington DC, and Lawrence Livermore Lab., Livermore, CA.

Seed, H.B., Wong, R.T., Idriss, I.M., and Tokimatsu, K. (1984). "Moduli and damping factors for dynamic analyses of cohesionless soils," *Rpt. No. UCB/EERC-84/14*, Earthquake Engrg. Research Ctr., Univ. of California, Berkeley.

Shannon and Wilson/Agbabian Associates, SW/AA (1980). "Geotechnical and strong motion data from U.S. accelerograph stations," *NUREG/CR-0985*, Vol. 5, Prepared for U.S. Nuclear Regulatory Commission.

Stewart, J.P., Seed, R.B. and Fenves, G.L. (1998). "Empirical Evaluation of Inertial Soil-Structure Interaction Effects," *Rpt. No. PEER-98/07*, Pacific Earthquake Engineering Research Center, University of California, Berkeley, 205 pgs.

Stokoe, K.H., Darendeli, M.B., Andrus, R.D., and Brown, L.T. (1999). "Dynamic soil properties: laboratory, field and correlation studies," *Earthquake Geotech. Engrg*., Vol. 3, 811-845, Balkema Publishers, Brookfield, VT.

Veletsos, A.S. and Meek, J.W. (1974). "Dynamic behavior of building-foundation systems," *J. Earthquake Engrg. Struct. Dynamics*, 3(2), 121-138.

Veletsos, A.S. and Verbic, B. (1973). "Vibration of viscoelastic foundations," *J. Earthquake Engrg. Struct. Dynamics*, 2(1), 87-102.

Vucetic, M. and Dobry, R. (1991). "Effect of soil plasticity on cyclic response," *J. Geotech. Engrg*., 117 (1), 89-107.

Wong, H.L. and Luco, J.E. (1985). "Tables of impedance functions for square foundations on layered media," *Soil Dyn. Earthquake Engrg.*, 4(2), 64-81.

3 Building Vulnerability Studies: Tilt-up Buildings

3.1 INTRODUCTION AND STRUCTURAL SYSTEM

Tilt-up wall structures have been widely used for industrial and commercial buildings throughout the United States. The tilt-up construction method became popular for constructing low-rise structures due to the economy in construction cost and time this method provides. Wall panels in tilt-up buildings are cast horizontally on the floor slab, tilted up by a crane to their final position, and are then connected to the foundation. The primary structural system consists of the concrete wall panels and a wood roof diaphragm connected to the walls through ledger beams attached to the walls.

Past earthquakes have revealed that tilt-up construction is susceptible to structural damage during earthquakes. The most common cause of damage is related to the performance/failure of roof-to-wall connections.

Observed performance of buildings along with data from instrumented buildings and experimental studies have provided valuable information about the seismic performance of tilt-up buildings. However, available modeling techniques still do not provide design professionals with simple yet robust analysis procedures that can reliably evaluate forces in critical components of tilt-up buildings.

The object of this study was to develop a simple analysis methodology that would enable the user to evaluate connection forces and deformations as well as the roof diaphragm demands for a given ground motion. Once the model was developed, correlation studies were undertaken to validate the model. Finally, sensitivity studies were done to assess the influence of variations in modeling parameters and to assess whether characteristics of near-fault ground motion (directivity) has an important effect on the response of tilt-up buildings.

The primary structural system of tilt-up wall structures consists of concrete wall panels and a wood roof diaphragm (Fig. 3.1). Wall panels are cast horizontally on grade and then tilted up by a crane to their final position and connected to the foundation. Individual wall panels are then connected to one another using cast-in-place pilasters, steel plates or chord splicing at the roof level to create a perimeter wall system.

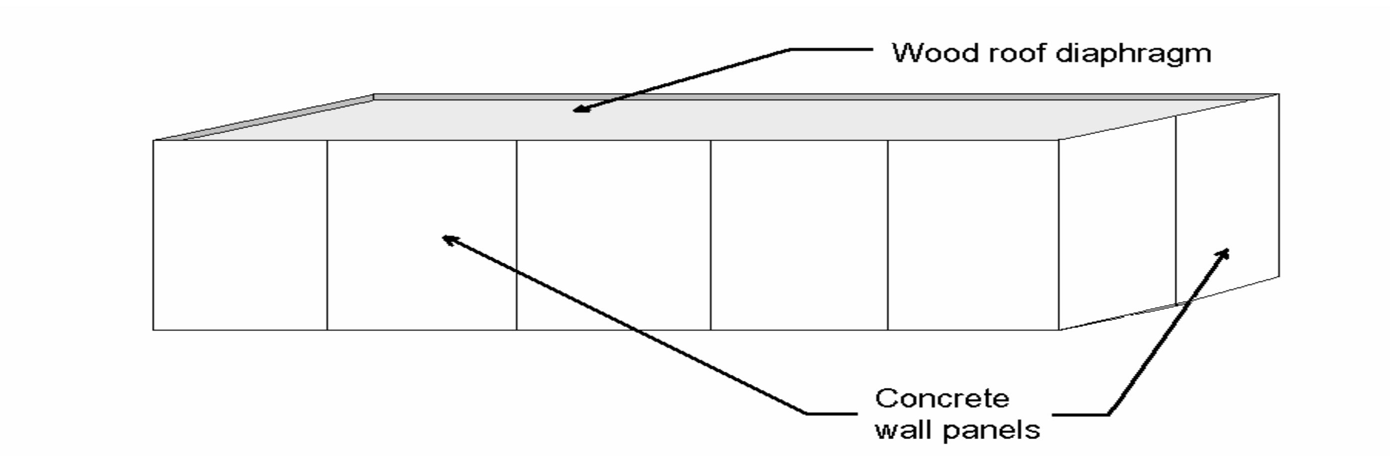

Fig. 3.1 Primary structural system of tilt-up buildings

The primary components of the roof system are typically: glulam beams, purlins, subpurlins, and plywood sheathing. The glulam beams are supported directly on pilasters built into the wall panels (Figs. 3.2, 3.3). Solid-sawn purlins frame to the glulams, while subpurlins frame to the purlins. Plywood sheathing made of 8-foot by 4-foot plywood panels overlay the whole roof system (Fig. 3.3). A ledger beam that is attached to the perimeter wall panels is used to connect the plywood sheathing to the wall panels.

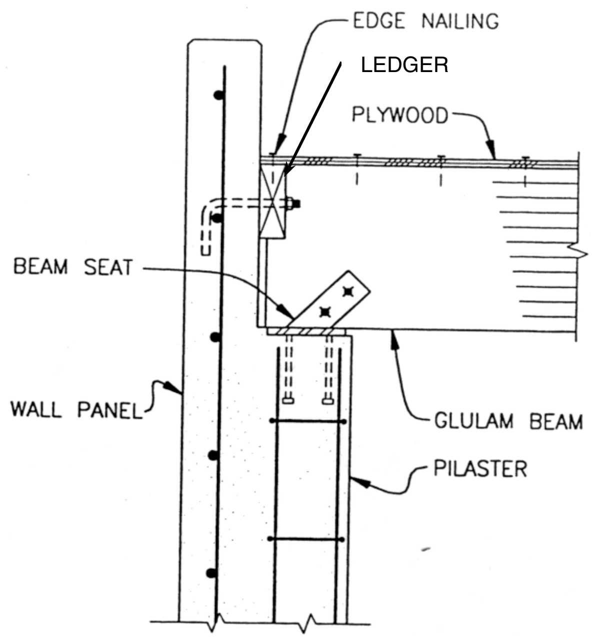

Fig. 3.2 Typical pre-1973 pilaster to glulam beam connection (Hamburger et al., 1996)

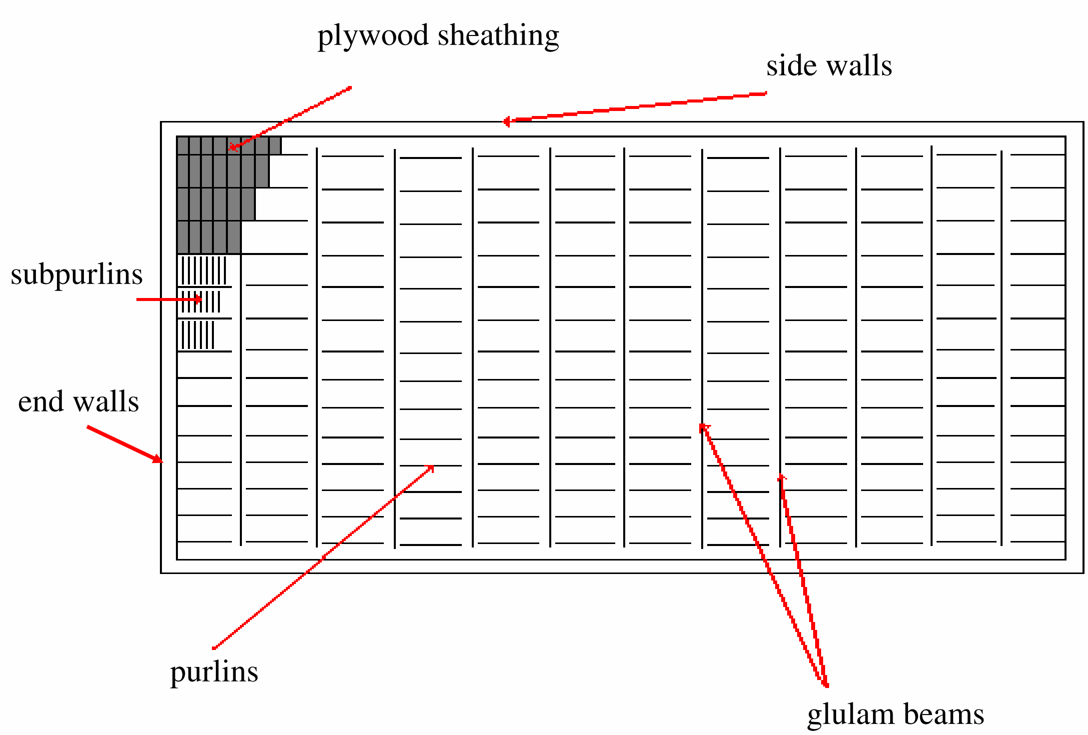

Fig. 3.3 Tilt-up building roof system

3.2 STRUCTURAL RESPONSE

Data obtained in earthquakes from instrumented buildings have helped researchers and design professionals better understand the seismic response of tilt-up wall buildings (Fig. 3.4). The end walls behave essentially rigidly, without significant amplification of the motion from the base to the top of the wall. However, significant amplification is observed in the roof diaphragm, with measured accelerations at the center of the diaphragm that are 2 to 3 times those measured at the end walls (Carter et al., 1993). This is shown in Fig. 3.5 where transmissibility functions (which represent the ratio of an output motion to an input motion in the frequency domain) are plotted for several channels of CSMIP Station # 47391 recorded in the 1989 Loma Prieta Earthquake. The function labeled ‘Ch3/Ch8’ shows that the amplitude of the motions at the base and the top of the end walls are similar, whereas the function labeled ‘Ch4/Ch7’ shows significant amplification of mid-diaphragm motions relative to motion at the base of the side walls.

Experimental studies have also been conducted to study the response of tilt-up buildings. Two small-scale complete tilt-up systems were tested at the University of Illinois (Fonseca, 1997; Fonseca et al., 1996). It was concluded that the behavior of the roof diaphragm was the major factor controlling the response of the building. Force versus displacement data along the length of the diaphragm and comparison of the calculated effective stiffness for each loading stage revealed that the stiffness of the structural system degraded as the amplitude of the imposed displacements and the number of loading cycles were increased.

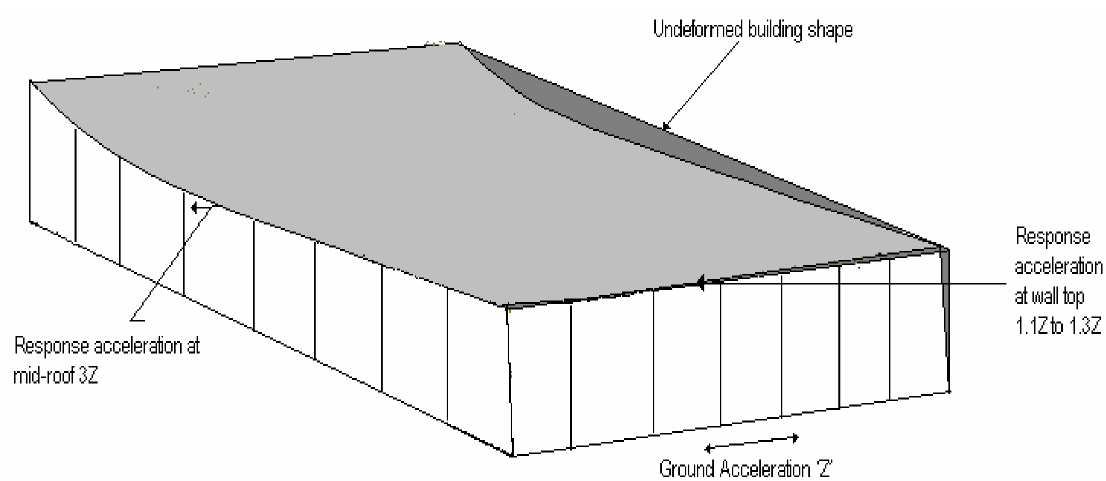

Fig. 3.4 Tilt-up building response under lateral loads

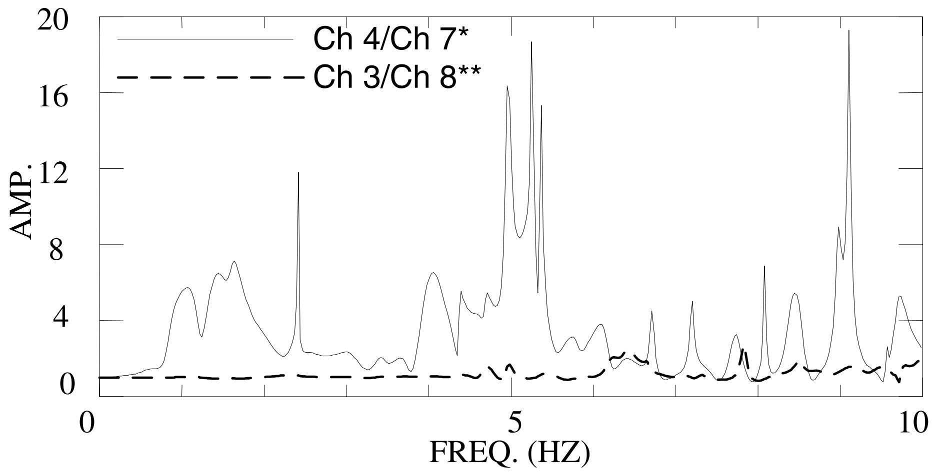

* Mid-diaphragm/base of side walls
** Top of end walls/base of end walls

Fig. 3.5 Transmissibility functions for Hollister building, Loma Prieta earthquake (Stewart and Stewart, 1997)

3.3 OBSERVED PERFORMANCE

The first evidence of the potential seismic vulnerability of tilt-up buildings was observed following the 1964 Alaska earthquake (Carter et al., 1993). Severe structural damage was also noted following the 1971 San Fernando earthquake (Frazier et al., 1971). Most of the observed failures were attributed to inadequate connection details, leading to changes in the Uniform Building Code. New provisions in 1973 and 1976 required positive, direct connection of the concrete walls to the roof diaphragm, continuous ties between chords, the addition of subdiaphragms, and increased design forces. Further changes to the UBC (1991), including an increase in connection design forces of 50% at the mid-span of the diaphragms, were implemented following the 1989 Loma Prieta earthquake. However, even with these code changes and the retrofit of many deficient tilt-up buildings, more than 400 tilt-up wall structures in the Los Angeles area experienced significant structural damage during the 1994 Northridge earthquake (Holmes et al., 1996; Hamburger et al., 1996). General causes of damage were related to the failure of the connections between the wall panels and the roof diaphragm, as well as failures of connections between adjacent wall panels. The majority of the observed failures at the roof-to-wall connections may be classified as follows (Fig. 3.6):

1. Glulam-pilaster connection:
    - Splitting crack in the concrete pilaster under the glulam beam seats due to lack of confinement in the pilaster.

- Bolts pulling through the ends of glulam beams.
- Breaking off or bending of anchor bolts welded to the bottom of the base plate.

2. Purlin-wall connection:
   - Steel strap pullout due to inadequate embedment.
   - Gross section fracture of steel strap at wall face.
   - Failure of strap at first bolt hole (net section fracture).
   - Wood splitting in purlin due to tension at bolt location.
3. Nail pullout from ledger attached to wall panels.
4. Cross-grain bending failure of ledger.

Glulam-pilaster connection failure

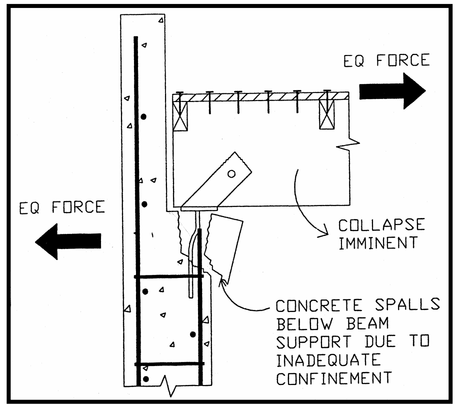

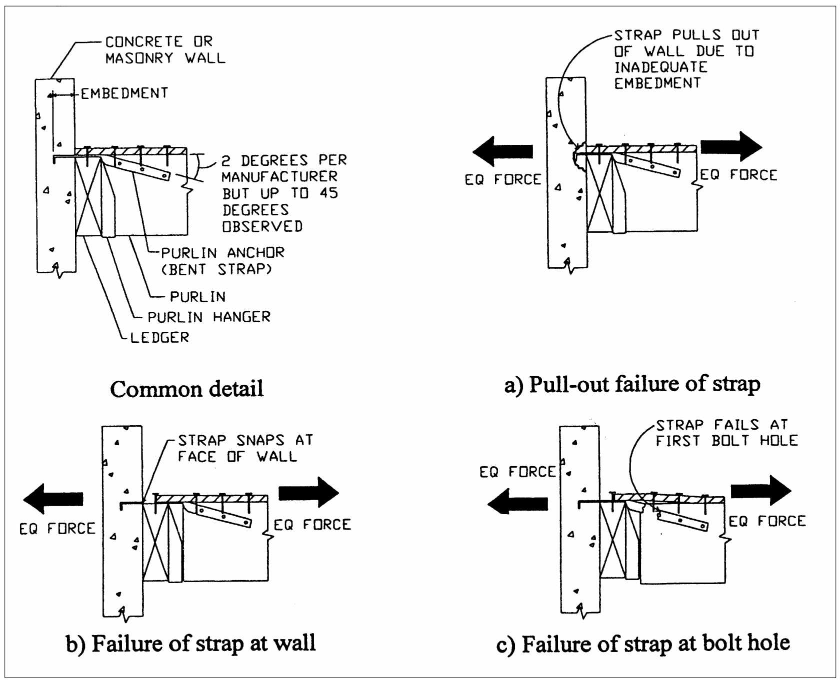

Common detail

a) Pull-out failure of strap

b) Failure of strap at wall

c) Failure of strap at bolt hole

Purlin-wall connection failures

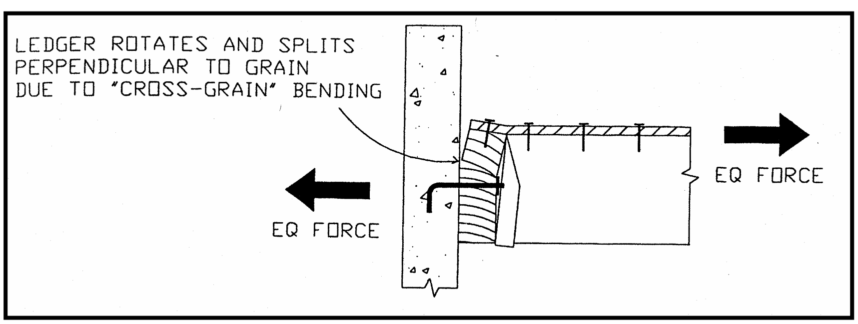

Cross-grain bending failure of ledger

Fig. 3.6 Roof-to-wall connection failures (Holmes et al., 1996)

3.4 EXPERIMENTAL STUDIES

Experimental research was reviewed to obtain relevant information on the behavior of tilt-up wall buildings and their components. The experimental studies were classified into four general areas:

1. Response of individual nailed connections (e.g., Dolan, 1989),
2. Response of tilt-up wall panels (e.g,. Ewing and Adham, 1985),
3. Response of diaphragms (e.g., ABK, 1981; Porter et al., 1990; Pardoen et al., 1999),
4. Response of complete tilt-up systems (e.g., Fonseca et al., 1996; Fonseca, 1997).

A few references for each topic are provided. For a more detailed list of references, see Carter, Hawkins and Wood (1993).

The main focus of this review was diaphragm and connection tests, since studies of system performance indicated that the roof diaphragm was the key feature controlling the response of tilt-up buildings, and that connection damage was the most important cause of structural damage.

Relatively little experimental data exist for wood roof diaphragms subjected to in-plane cyclic loading (See References R.2). A review of the data from plywood diaphragm tests was conducted to identify relevant data (Table 3.1). Typical test variables investigated include nail size and spacing, plywood thickness, influence of blocking and chords, sheathing orientation, and influence of roofing.

No test data on the behavior of diaphragm-wall connections was identified. However, new connection tests are currently being performed at UC Irvine (Del Carlo and Pardoen, 1999), which are part of a coordinated research project that includes this study. A complete interpretation of these test results has not yet been completed.

3.4.1 ABK (1981) Tests

The ABK research program involved dynamic and static loading of 20-ft by 60-ft diaphragms (See Fig. 3.7). Fourteen diaphragm configurations were tested. However, diaphragm N, which was blocked and chorded, with ½ in. plywood and 8d nails spaced at 4 in. on center at edges, and 12 in. on center at intermediate bearings, best represents diaphragms in tilt-up buildings (ABK, 1981). The peak values for force and deformation at each loading level for the quasistatic tests of diaphragm N are plotted in Fig. 3.8. The displacement values are measured at the point of load application. Bilinear force-displacement relations for the diaphragm were estimated from the test data, and are also plotted on Fig. 3.8. Important parameters in the bilinear relation include: initial stiffness, yield force, and post-yield stiffness. A yield force of 12 kips, an initial stiffness of 20 kip/in. and a post-yield stiffness of approximately 35% of the initial value were estimated from the test data.

A majority of diaphragm tests are conducted on bare roofs, i.e., no roofing materials are included. It is possible that roofing materials significantly influence both the stiffness and strength of the diaphragm, but these effects have not been thoroughly investigated.

The only tests that investigated the influence of roofing materials on diaphragm response were conducted by ABK (1981). Diaphragm D (unblocked, chorded) and diaphragm C (unblocked, unchorded) were tested with roofing materials whereas diaphragm B (unblocked, chorded) was tested without roofing materials. A comparison of the initial stiffness of D and B (Fig. 3.9) indicates that roofing materials result in an increase in overall diaphragm stiffness of 33% at a displacement level of 0.3 in. and an even higher contribution is observed at higher displacement levels. However, these tests do not indicate whether the impact of roofing materials would be as significant for blocked diaphragms. Furthermore, insufficient data exist to reliably assess the influence of roofing materials for larger displacement levels where debonding may occur and thus a loss of strength may be possible. Therefore, until additional information is available, a reasonable approach would be to neglect the influence of roofing materials on stiffness and strength of the diaphragm.

Table 3.1 Review of diaphragm tests

Reference	Number of Diaphragms Tested	Diaphragm Material	Diaphragm Size	Type of Loading	Experimental Variables
Countryman and Colbenson (1954)	15	plywood	24′ x 24′	Static one-directional	Blocking Panel arrangement Nail spacing Loading direction
Dolan (1989)	22 20	plywood waferboard	8′ x 8′	Static one-directional Static cyclic Sinusoidal loading Earthquake motion	Sheathing orientation Nail spacing Vertical load
ABK (1981)	5 6 3	plywood 1" x 6" sheathing metal deck	8′ x 8′	Load reversals Forced vibration (earthquake motion)	Plywood thickness Roofing material Blocking and chords
UCI (1999)	7	plywood	16′ x 20′	Racking	Nail spacing Sub-purlin spacing Loading direction

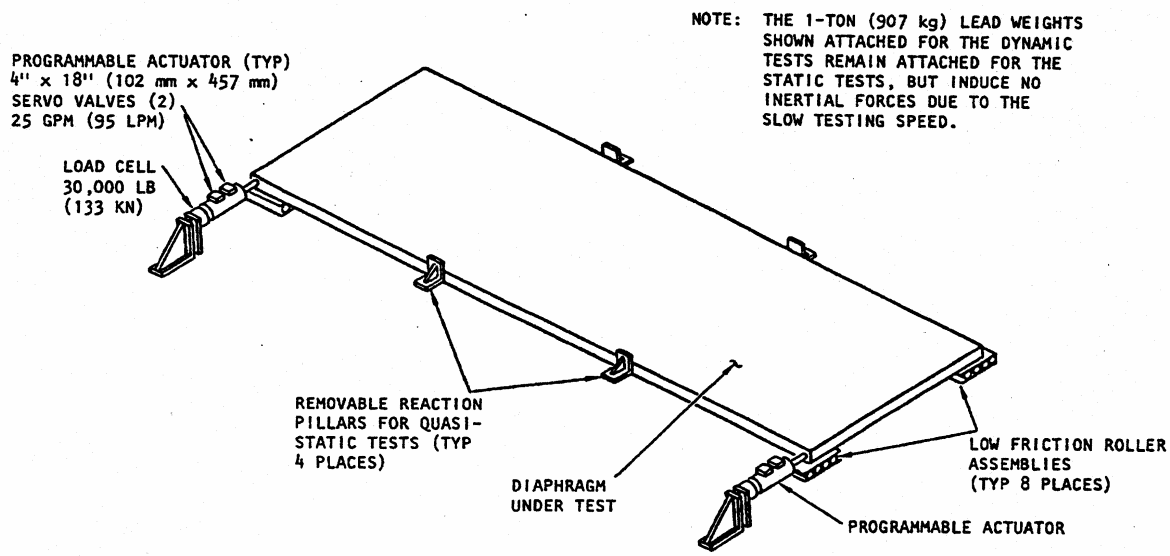

(a) Quasi–static tests.

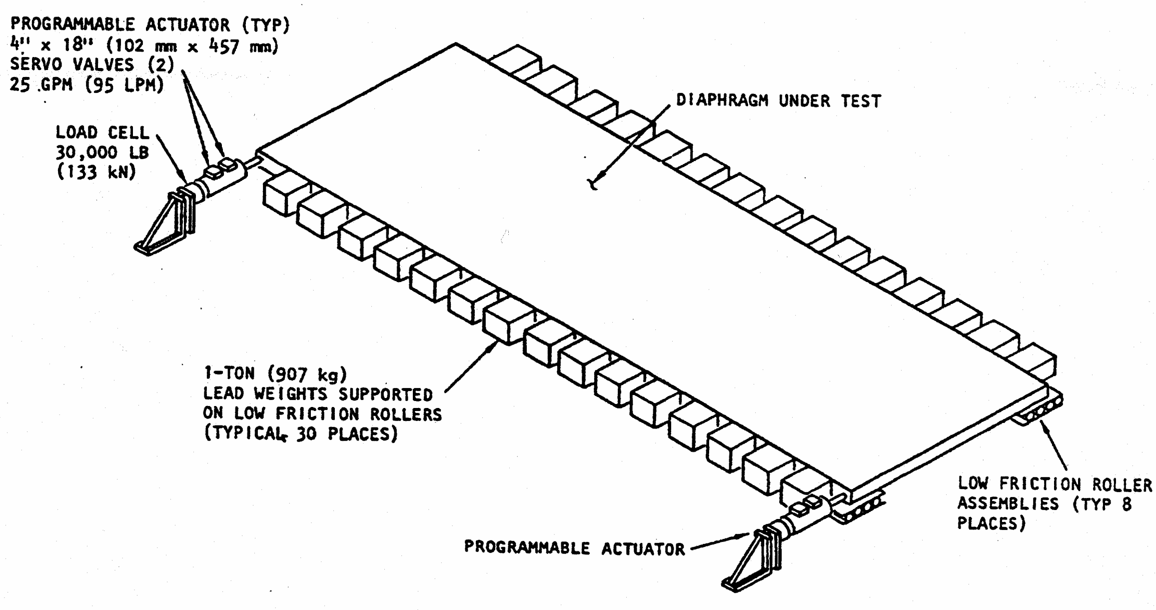

(b) Dynamic tests.

Fig. 3.7 Test configuration for ABK diaphragm tests (ABK, 1981)

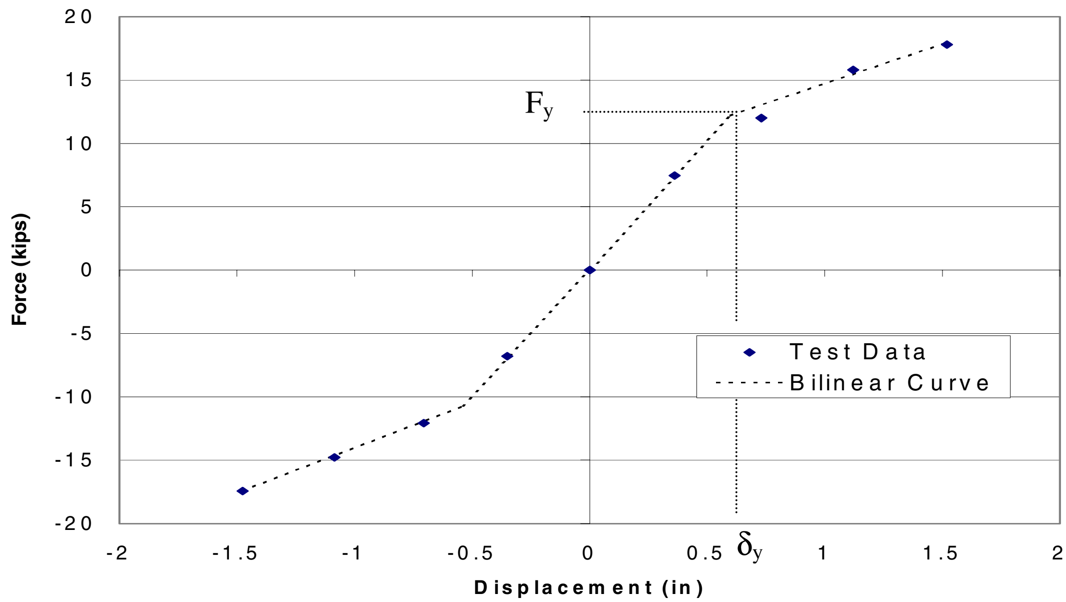

Fig. 3.8 Force vs. displacement for ABK diaphragm N

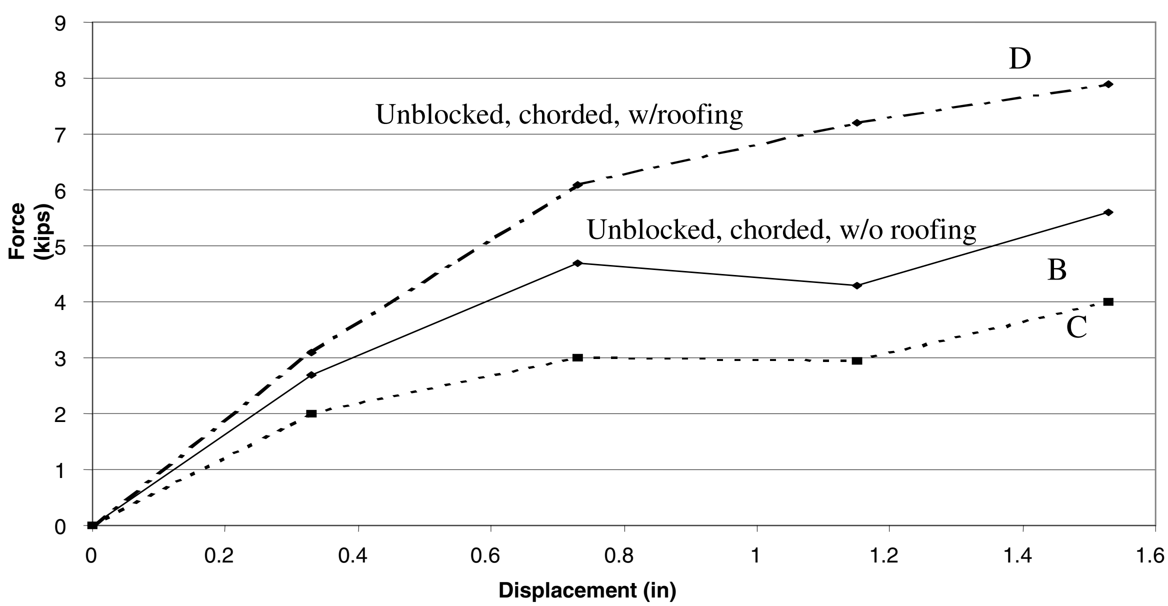

Fig. 3.9 Force vs. displacement for ABK diaphragms B, C, and D.

3.4.2 UC Irvine Tests

The diaphragms tested at UC Irvine are representative of those used in typical California buildings (Pardoen et al., 1999), and add substantially to the database of diaphragm tests. The tests were conducted on single 20-ft. by 16-ft. panels. Six specimens were tested (Table 3.2). The nailing used for the specimens replicates that used in the study building in Fremont, California. Four specimens were tested with nail spacings 6 in. o.c. for ledger and continuous edges, and 6 in. o.c. for other edges, whereas two specimens were constructed with a denser nailing pattern (2 in. o.c. for ledger and continuous edges, and 3 in. o.c. for other edges). For both specimens, the nail spacing on intermediate bearings was 12 in. o.c. Specimen 1 is referred to as the control specimen with changes in load-displacement relations for other specimens noted relative to the load-displacement relation for the control specimen. Load-displacement relations are plotted in Fig. 3.10, with a maximum displacement of approximately 5 in. Based on the test results for specimen 1, an initial stiffness of 12.5 k/in., a yield force of 10 kips, and a post-yield stiffness of 15% were selected for the control specimen to be representative over the range of displacements expected. For the dense nailing pattern, representative values are 16 k/in., 20 kips, and 35%, respectively. Parameters influencing the diaphragm stiffness and strength will be discussed in Section 3.5.

Table 3.2 UCI diaphragm test matrix (Pardoen et al., 1999)

TEST #	NAME	NAILING			TEST PROTOCOL	SUB-DIAPHRAGMS**
		Edge	Cont. Edge	Field		
1	Control	6	6	12	ATC* 24	2 X 4 @ 16 in. o.c.
2	Alternate Geometry	6	6	12	ATC 24	2 X 4 @ 16 in. o.c
3	Dense Nailing	3	2	12	ATC 24	2 X 4 @ 16 in. o.c.
4	Fling	6	6	12	Fling	2 X 4 @ 16 in. o.c.
5	Control	6	6	12	ATC 24	2 X 4 @ 24 in. o.c.
6	Dense Nailing	3	2	12	ATC 24	2 X 4 @ 24 in. o.c.

* Applied Technology Council, 1992

** Spacing of 2 X 4s varied

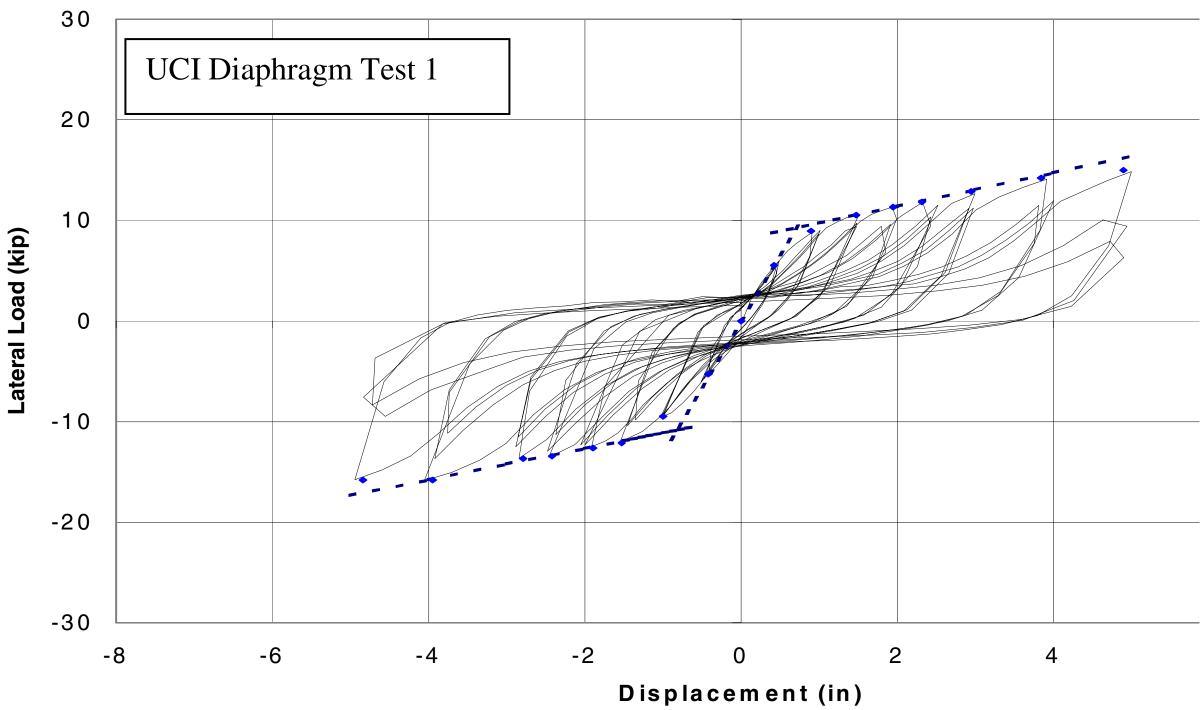

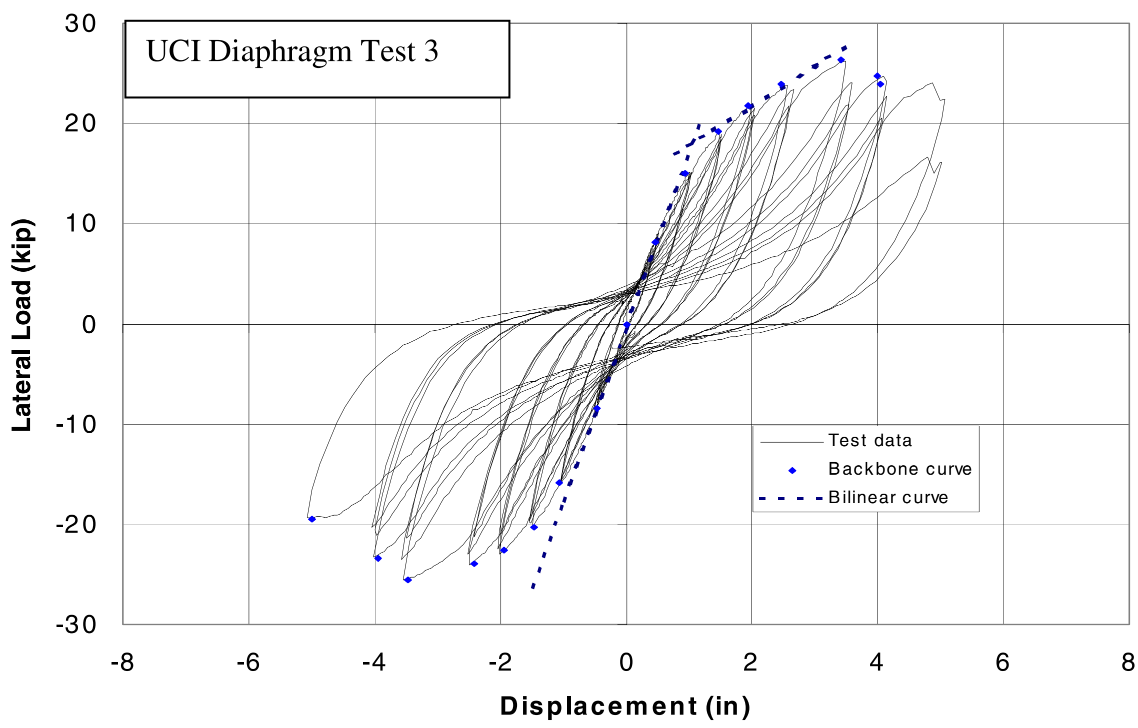

Fig. 3.10 Force vs. displacement for UCI diaphragm tests 1 and 3

3.5 GENERALIZED DIAPHRAGM STIFFNESS AND STRENGTH VALUES

In general, estimates of diaphragm strength and stiffness are necessary for a range of diaphragm characteristics, since test data may not be available for all diaphragm conditions. To accomplish this, the test results are extrapolated to account for variations in diaphragm geometry, nail spacing, and plywood thickness, as well as the effect of roofing materials using Equation 3.1 (modified from Hamburger et al., 1996). Data from the UCI control specimen are used to normalize the stiffness value in Eq. 3.1, that is; extrapolations are made from UCI's "control" specimen. (Sect. 3.4.2, Fig. 3.10) To account for variable nail spacing, a weighted average of the nail spacing was calculated for each specimen. For the control specimen, the nail spacing is 6 in. (Table 3.2). The stiffness and strength properties are determined as:

$$K_d = 12.5k/in \times \left(\frac{D/16'}{L/20'}\right) \times \left(\frac{F_{plywood}}{0.5''}\right) \times F_{nailsize} \times \left(\frac{6"}{s}\right) \times F_{roofing} \tag{3.1}$$

$$F_y = 10^k \times \left(\frac{D}{16'}\right) \times \left(\frac{F_{plywood}}{0.5''}\right) \times F_{nailsize} \times \left(\frac{6"}{s}\right) \times F_{roofing}$$

where, K_d is the stiffness of the diaphragm section, D is the depth, and L is the width of the diaphragm section in feet, $F_{plywood}$ is the plywood thickness in inches, $F_{nailsize}$, is 1.0 for 10d nails, s is the weighted average of the nail spacing for the diaphragm section and $F_{roofing}$ is 1.0.

Equation 3.1 was modified from that presented by (Hamburger et al., 1996) to account for new data from the UCI tests (Pardoen et al., 1999), as well as to re-evaluate the previous data (Countryman and Colbenson, 1954; ABK, 1981). Table 3.3 lists yield strength, stiffness values, and key parameters in Eq. 3.1 for various tests. Note that in Table 3.3 specimens within a test group were compared with each other; i.e., the first specimen in a test group was assumed to be the control specimen and extrapolations made from this specimen were compared with the actual stiffness and yield strength values of the next specimen. For example, for the first test group, extrapolations were made from the stiffness value (R1, C1). The computed stiffness (R2, C3) was then compared with the actual stiffness, (R2, C1). (R2, C4) gives the ratio of the computed stiffness to the actual stiffness, and (R2, C5) gives the error in predicting the actual stiffness.

All nails used in the ABK tests were 8d nails, whereas only 10d nails were used in the UCI tests. Although 8d and 10d nails were used in the tests by Countryman et al., (1954), plywood thickness, blocking, and joist spacing were also varied within these tests. Therefore, no direct comparison can be made using these data to evaluate the effects of nail size on initial stiffness and yield force.

Results in Table 3.3 reveal that the values produced with Eq. 3.1 do not always agree with test data (variations of 3% to 74% are indicated). Limited data and the lack of a systematic evaluation of parameters in the existing test programs inhibit the ability to conduct a comprehensive study to develop a more reliable equation. Therefore, given these limitations, diaphragm properties should be selected based on available test data that best represent the diaphragm being evaluated, and sensitivity studies should be conducted to assess potential response variation. This is taken up in Section 3.8.

Table 3.3 Comparison of actual and calculated (Eq. 3.1) stiffness and yield strength values for various diaphragm tests

		C1		C2						C3		C4	C5		
		Stiffness (kip/in)		Strength	D	L	s	t	nail	Keqn	Fy	Keqn/K	Error %	Fy_eqn/Fy	Error %
		Initial	Post-yield	(kips)	(ft)	(ft)	(in)	(in)	10d	Eqn.3.1	Eqn.3.1				
	1954 Diaphragm Tests														
		Comparison between diaph. D and F													
R1	Diap. D	25.0	-	14.4	24	24	6	3/8	8d	25.0	14.4	1.00	0	1.00	0
R2	Diap. F	37.1	-	19.7	24	24	3	3/8	8d	50.0	28.8	1.35	35	1.46	46
		Comparison between diaph. A and O													
	Diap. A	48.0	-	16.8	24	24	5.79	3/8	8d	48.0	16.8	1.00	0	1.00	0
	Diap. O	62.3	-	23.0	24	24	5.79	1/2	8d	64.0	22.4	1.03	3	0.97	3
	UCI Diaphragm Tests														
	Test 2	12.5	15%	9.3	16	20	6	1/2	10d	12.5	9.3	1.00	0	1.00	0
	Test 5	16.0	35%	20.0	16	20	2.69	1/2	10d	27.9	20.8	1.74	74	1.04	4
	ABK Diaphragm Tests														
	Diap. N	20.0	35%	12.0	20	20	4	1/2	8d	20.0	12.0	1.00	0	1.00	0
	Diap. P**	36.0	50%	21.5	20	20	4	3/4	8d	30.0	18.0	0.83	17	0.84	16
	Diap. P**	36.0	50%	21.5	20	20	4	8/9	8d	36.0	21.6	1.00	0	1.00	0
	Diap. P**	36.0	50%	21.5	20	20	4	1	8d	40.0	24.0	1.11	11	1.12	12

** For Diaphragm P, one layer of ¾" plywood panels was overlaid by rows of ¾" thick plywood panels at right angles to the first layer with 2' gaps between rows. Therefore, the plywood thickness is less than 1 ½", but greater than ¾", and several values in this range are included to allow comparison.

3.6 ANALYTICAL MODELING

Analytical models for tilt-up wall buildings have been developed in prior research programs (Carter et al., 1993). Models range from simple elastic models that exclude end walls and connections (Mehrain and Silver, 1988; Mehrain and Graf, 1990), to detailed inelastic models that include the effect of soil under the end walls (Adham et al., 1989). Simple elastic models may not be easily used to account for inelastic response of the diaphragm and the connections, and may tend to overestimate forces. Finite element models allow detailed modeling of the system (Hawkins et al., 1994), but such models take considerable time and effort to construct, analyze and assess, particularly if nonlinear response is considered. The most widely used approach is to model the diaphragm by inelastic spring or truss elements (Hamburger et al., 1996; Mehrain and Silver, 1988; Mehrain and Graf, 1990). Although various models have been proposed, a methodology to determine connection forces through these models is not yet well developed.

Simple nonlinear models appear to offer the greatest potential for design office applications. However, a review of models employed in previous studies identified that one or more of the following items were often omitted: end walls, side walls, soil-foundation-structure interaction (SFSI), connections and glulam beams.

A systematic study was undertaken as part of this project to assess the level of model detail required to obtain reliable results and to study the influence of inelastic response on connection demands.

3.6.1 Simple Nonlinear Modeling of Tilt-up Buildings

Computer programs for 3D nonlinear analysis are not well developed or widely used by the design professional community; therefore, a series of 2D models were developed to represent the 3D response of a tilt-up building. The building evaluation was carried out by combining three separate models representing portions of the building using the DRAIN-2DX program (Prakash et al., 1993). The three models consist of:

1. The diaphragm: to model the in-plane stiffness and strength of the roof.
2. The internal frame: to model the side walls (Fig. 3.11), the out-of-plane bending stiffness of the roof, connections between the roof and the side walls, the internal steel columns supporting the roof, and wall-to-foundation connections.
3. The end walls: to model the stiffness of the end walls (Fig. 3.11), the foundation, and the soil.

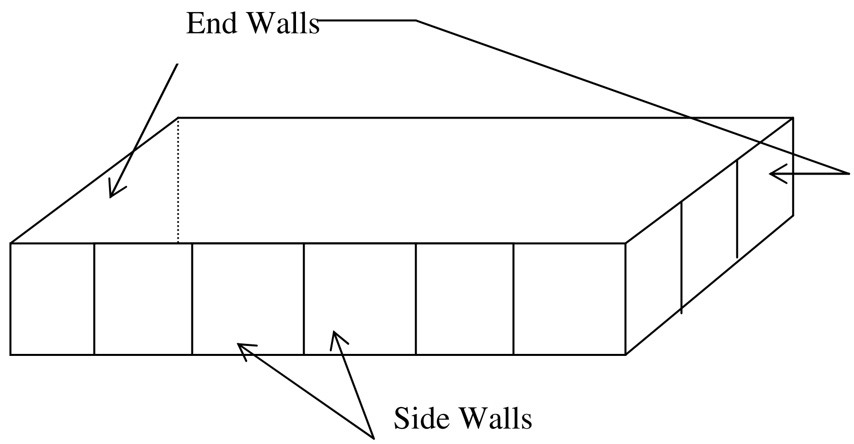

Fig. 3.11 Tilt-up building walls

Each of these models is discussed in detail in the following sections:

1. Diaphragm model

Nonlinear beam elements were used to model the in-plane behavior of the diaphragm. element modeling options were limited to those available in Drain-2DX (Powell, 1993). The diaphragm was modeled using Drain-2DX element type02, which only allows bilinear flexural response (no cyclic stiffness degradation). Rotations at the ends of the elements (Fig. 3.12) were fixed; therefore, only lateral translation is allowed (i.e., a “shear beam” model).

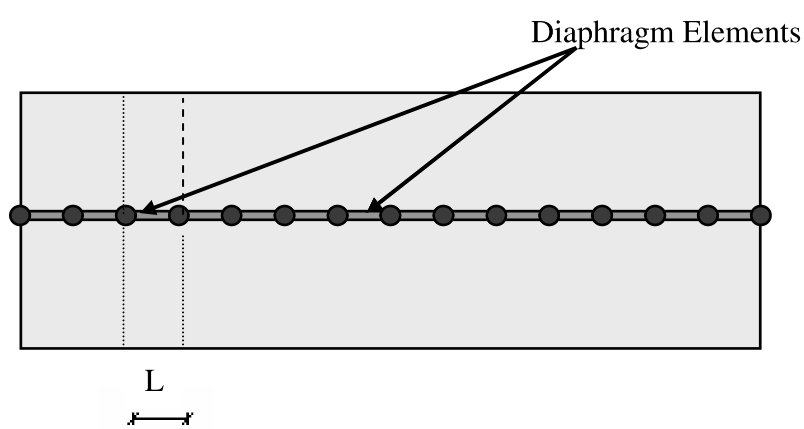

Fig. 3.12 Diaphragm elements

The yield strength and stiffness of each beam element is selected to represent the behavior of the diaphragm. The bending stiffness for each element is calculated as $K_d = 12E_d I_d / L^3$, where E_d is Young's modulus, I_d is moment of inertia, and L is length of the diaphragm element (Fig. 3.12). The stiffness value, K, is calculated using Eq. 3.1 based on the properties of the diaphragm; the length is selected to be a convenient value for modeling purposes (Sect. 3.5). The bending stiffness, EI, of the beam element is then computed. In Drain-2DX, an arbitrary value of Young's Modulus, E_d, was used and the inertia, I_d, was computed to give the E_dI_d value calculated from $K_d = 12E_d I_d / L^3$. The yield moment for the diaphragm elements were calculated as $M_y=V_y \times L/2$ (Fig. 3.13), where $V_y = F_y$ was determined using Eq. 3.1 (Sect. 3.5).

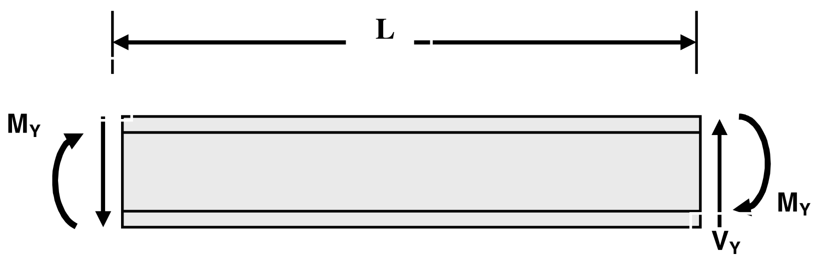

$$M_Y = \frac{V_Y \times L}{2}$$

Fig. 3.13 Yield moment calculation for diaphragm elements

2. The internal frame model

The out-of-plane bending stiffness of the side walls, bending stiffness of the diaphragm and the glulam beams, and the stiffness of the connections between the roof diaphragm and the side walls were included in the internal frame model (Fig. 3.14). Equivalent columns were used to represent pilasters and the walls on both sides of the pilasters. The tributary wall length was calculated based on ACI318-95 Section 8.10 requirements for T-beams.

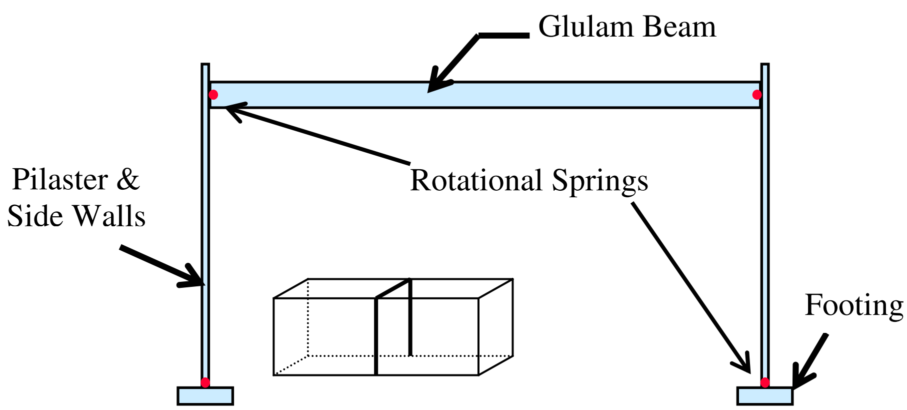

Fig. 3.14 Components of the internal frame model

The nonlinear load-deformation behavior of the pilaster-to-footing and roof-to-side wall connections were represented by rotational springs. Simple models of each connection type were developed to determine force deformation relations, as discussed in the following sections:

(a) Pilaster-footing connection

The location of slabs at the base of the side walls determine how the rotational stiffness is calculated for each connection. For example, if slabs are shown on both sides of the wall in the drawings, the connection may be assumed to be rigid, however if a gap exists on one side, the point of fixity may be lower for loading in one direction (Fig. 3.15).

Moment-rotation (M-θ) curves were computed considering the extension and slip of the reinforcement at the point of fixity. Slip of reinforcement was calculated using the methodology described by Alsiwat and Saatcioglu (1992) for hooked bars. For the rotation levels of interest, the contribution of slip was found to be negligible for a typical condition (Fig. 3.16; see Section 3.7 for additional information on the building). Therefore, only extension of the tension reinforcement was considered in computing the M-θ relations.

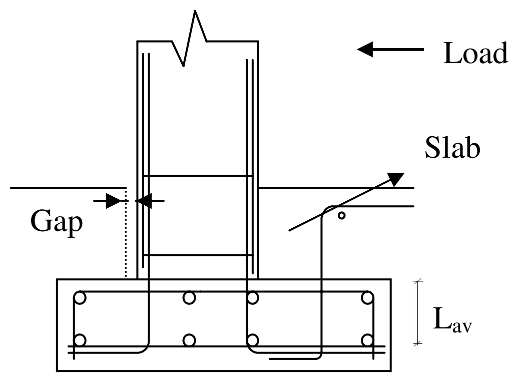

Fig. 3.15 Pilaster-footing connection with gap on one side

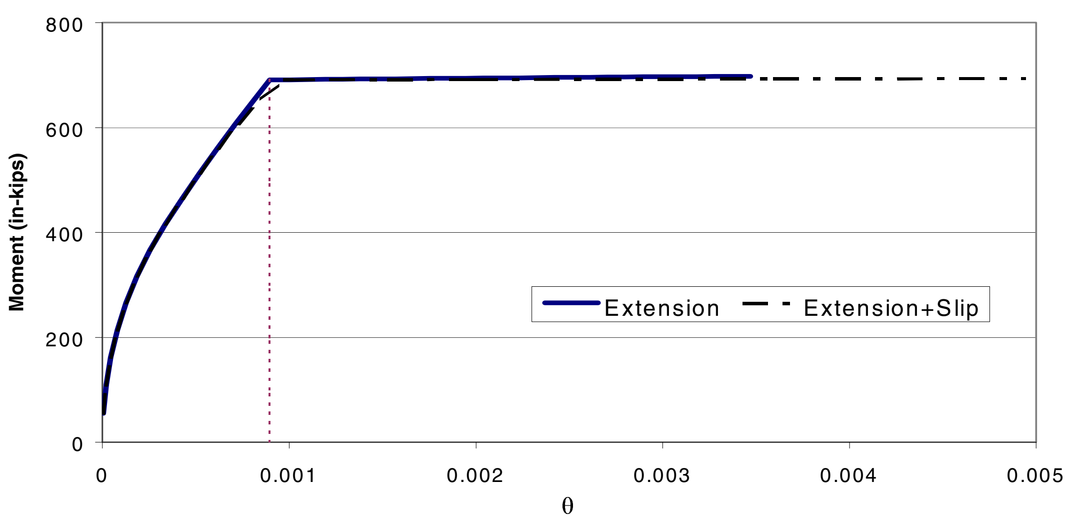

Fig. 3.16 Moment vs. rotation for pilaster-footing connection — Hollister building

A step-by-step procedure was used to determine the moment-rotation curve. Strain in the tensile reinforcement was incrementally increased, and moment capacity as well as the extension in the tensile reinforcement were calculated for each strain level. The model for calculating extension is shown in Fig. 3.17 and the equations are developed in following pages.

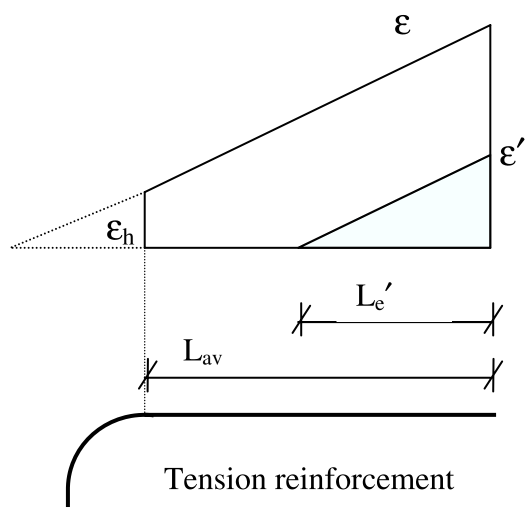

Fig. 3.17 Extension calculation model for pilaster-footing connection

The required length (L_e) for development of each strain level is calculated as (Alsiwat et al., 1992):

$$L_e = f_s \times \left(\frac{d}{4 \times u_e} \right) \tag{3.2}$$

where, L_e is the required length, f_s is the reinforcement stress, d is the diameter of reinforcement, and u_e is the elastic bond stress.

and,

$$u_e = \frac{f_y \times d}{4 \times L_d}, \tag{3.3}$$

$$L_d = \frac{440 \times A_b \times f_y}{K \times \sqrt{f_c'} \times 400} > 300 \text{ mm (SI units)} \tag{3.4}$$

where, A_b is the area of reinforcement, f_y is reinforcement yield strength, f_c' is concrete compression strength, and K is assumed to be equal to 3 x d.

Once L_e is obtained, the extension for that strain level is calculated as,

$$\delta = \frac{\varepsilon \times L_e}{2} \qquad L_e < L_{av} \tag{3.5}$$

$$\delta = \frac{(\varepsilon - \varepsilon_h) \times L_{av}}{2} + \varepsilon_h \times L_{av} \qquad L_e > L_{av} \tag{3.6}$$

where, L_e is the required length, L_{av} is the available length, ε is the strain in the reinforcement, ε_h is the strain in the reinforcement at hook, and δ is the extension.

Then the rotation for each strain level is calculated as the extension of reinforcement over distance of tensile reinforcement to the neutral axis. Moment vs. rotation is plotted (Fig. 3.16) and the rotational stiffness for this connection is obtained as the slope of the curve.

(b) Pilaster-glulam connection

For the roof-to-pilaster/wall connection, it was assumed that the glulam beam seat connection was relatively rigid and that connection strength was limited by yielding of the tension connection in the plane of the roof diaphragm (Fig. 3.18). Rotation was assumed to be mainly due to extension of the straps and/or holddowns, rotating about the bottom of the beam seat as indicated in Fig. 3.18. Elastic and post-yield stiffness values are determined directly from the stress-strain relation for the tension connection.

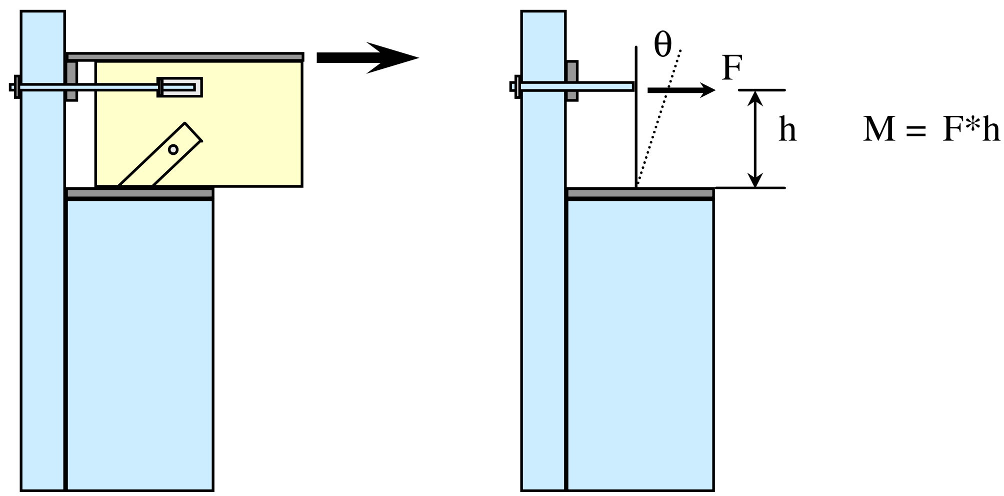

Fig. 3.18 Pilaster-glulam connection modeling

It should be noted that this approach assumes that other failure modes (Sec. 3.3), such as cross-grain bending of the ledger and splitting at the pilaster tip, are prevented. At the completion of the analysis, the beam seat connection should be checked to make sure that it can resist the forces developed in the connections.

If no straps or holddowns are present, the rotational spring model becomes invalid. In that case, it might be more appropriate to model the beam seat connection by an axial spring. Further refinement of the approach may be possible following the completion of the UCI connection tests and a thorough evaluation of the test data.

(c) Side wall-purlin/subpurlin connection:

Equivalent yield moment and rotational stiffness values are computed for subpurlins within the tributary wall length for each connection modeled. Rotation was assumed to be mainly due to extension of the straps and was computed directly from the stress-strain relation of the straps. Connection strength was limited by yielding of the tension connections in the plane of the roof diaphragm (Fig. 3.19). The connection was assumed to be rigid when subjected to compression. Although depending on the quality of the construction or the nailing the connection might rotate about point A (Fig. 3.19), this rotation is not very likely to occur since it would require bending of the diaphragm and kinking in the strap.

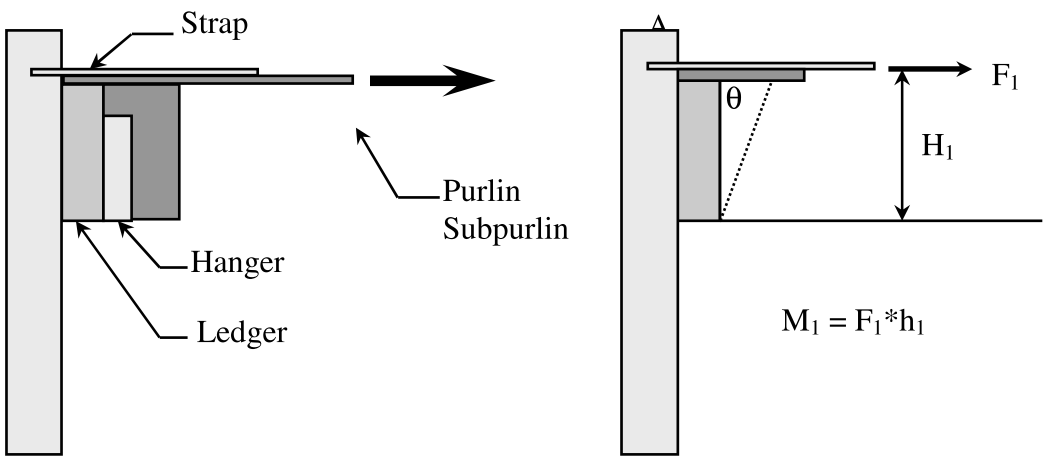

$$M = M_1 + M_2 + M_3 + \ldots + M_n$$

n: number of purlin/subpurlin connections in tributary wall length

Fig. 3.19 Purlin/subpurlin connection modeling

Once M-θ relations were developed, the internal frame was analyzed using Drain-2DX, to determine a "pushover" curve. An equivalent bilinear force-displacement relation was used to represent the pushover curve as indicated on Fig. 3.20 for an example building (See Section 3.7 for additional information on the building). A bilinear spring was used in Drain-2DX (type01) to incorporate the influence of the internal frames on the diaphragm response (Fig. 3.21). A spring was located at each glulam location in the model (Fig. 3.21).

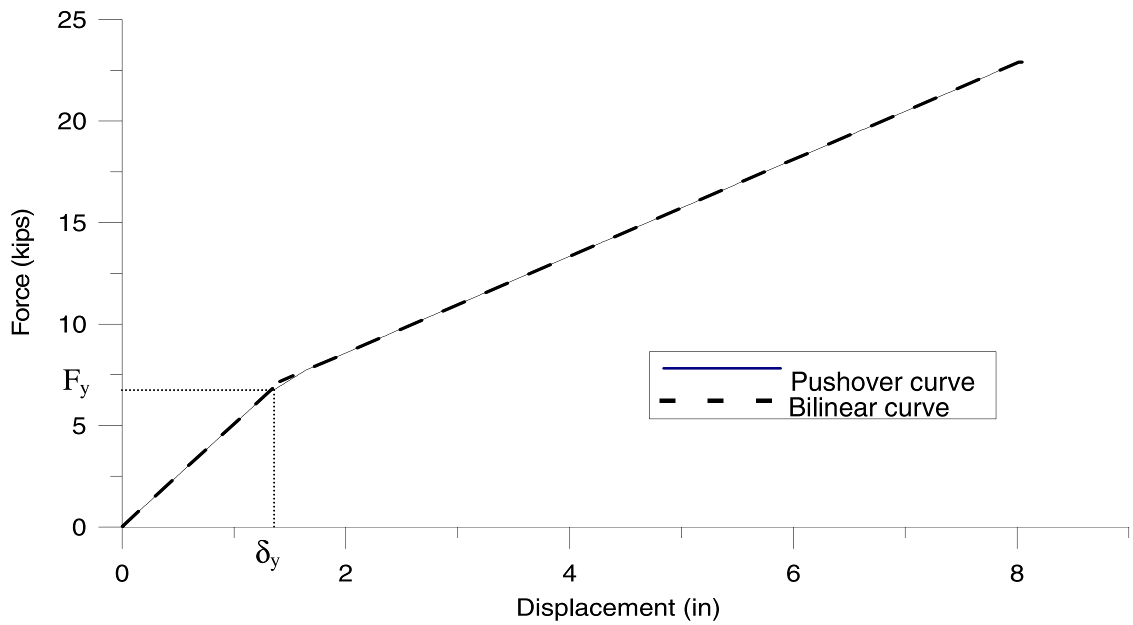

Fig. 3.20 Force vs. displacement curve for internal frame — Hollister building

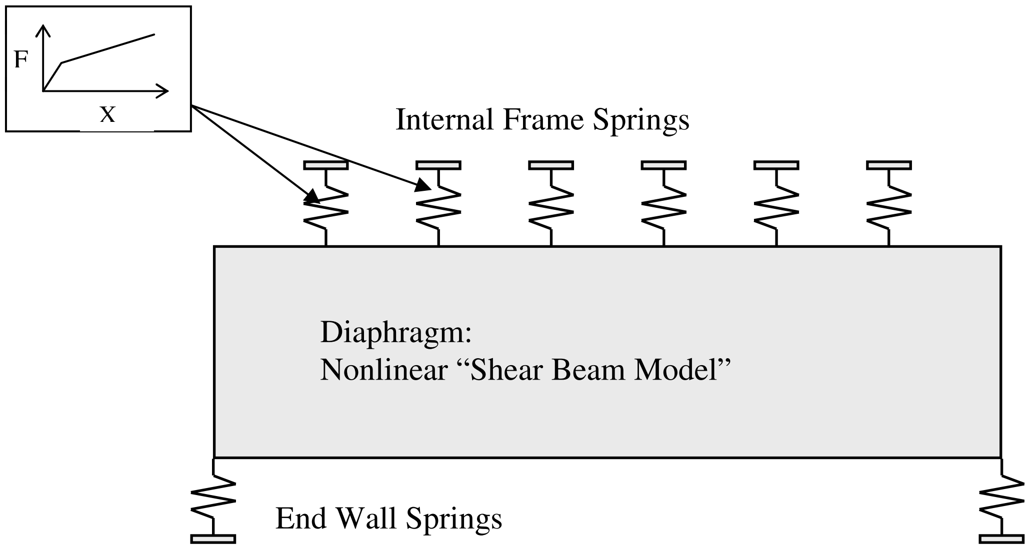

Fig. 3.21 Bilinear springs representing the internal frames

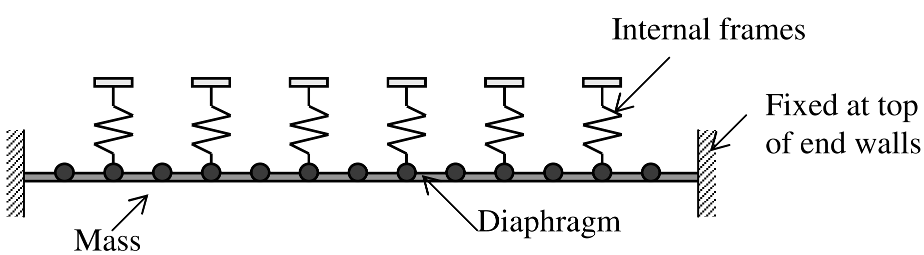

(a) No end walls

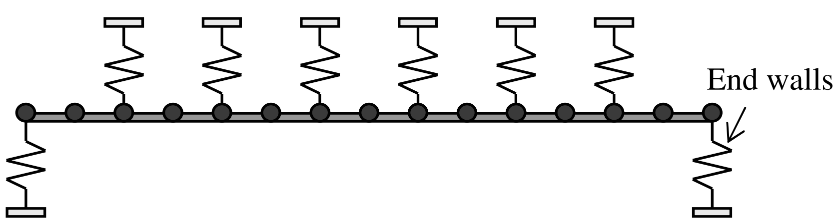

(b) End walls included: walls on fixed or flexible base

Fig. 3.22 Structural system model

3. End walls

The influence of the end walls on building response was investigated using three models: In the first model, the diaphragm was fixed at the top of the end walls (Fig. 3.22a), and the flexibility of the end walls was neglected. This model was used because evaluation of responses from buildings with strong-motion instruments (as well as previous analytical studies) indicate that the large in-plane stiffness of the end walls results in negligible deformations relative to those in the diaphragm.

In the second analysis, the elastic bending and shear stiffness of the end walls with a fixed base were incorporated (Fig. 3.22b). The flexible wall with a fixed base was analyzed assuming the wall to be a cantilever. The lateral stiffness of the wall was calculated by including both flexural and shear deformations as follows:

$$\delta_w = \frac{F{L_w}^3}{3E_c I_w} + \frac{6FL_w}{5A_w G_c} \qquad K_{ew} = F/\delta_w \qquad \text{(Eq. 3.7)}$$

where, F is unit force, L_w is height of the wall, E_c is Young's modulus for concrete, I_w is moment of inertia of the wall about the strong axis, A_w is the area of the wall, G_c is shear modulus for concrete, δ_w is top displacement of the wall, and K_{ew} is the lateral stiffness of the wall.

An alternative approach would be to model the bending stiffness of the end wall as the sum of the bending stiffnesses of the individual wall panels. This would provide a lower-bound estimate of the bending stiffness of the end wall.

The flexibility of the foundation/soil was added to the final analysis model. The procedure to determine the dynamic stiffness and damping coefficients for the wall with a flexible base is presented in Appendix 3-A.

Linear elastic springs (type01) were used to represent the end walls with a fixed and flexible base. The axial stiffness of the spring representing the end wall is calculated as $K_{ew} = E_{es}A_{es}/L_{es}$, where, E_{es} is the Young's modulus of the end wall spring, A_{es} is the cross-sectional area of the end wall spring (truss element), and L_{es} is the length of the spring element.

3.6.2 Damping

In addition to hysteretic damping associated with nonlinear behavior, Rayleigh damping was incorporated for all elements in the model (2%). Rayleigh damping coefficients α and β were calculated for the whole system and applied to each element group with the exception of the end walls on flexible base. Sensitivity studies indicated that the response was insensitive to the selection of the higher mode frequency (3rd, 5th, 7th modes), so 1st and 7th mode frequencies were used to determine the damping coefficients.

In the case of end walls on a flexible base, damping was obtained from soil-foundation-structure interaction studies. A separate stiffness proportional Rayleigh damping coefficient, β, was calculated for this element group as,

$$\beta = \frac{\tilde{C}}{\tilde{K}} \qquad \text{(Eq. 3.8)}$$

where, $\tilde{C}$ is the damping for an end wall on flexible base, and $\tilde{K}$ is the stiffness for an end wall on flexible base.

3.6.3 Masses

Masses were placed along the diaphragm length to account for the mass of the diaphragm and tributary mass from the side walls. Therefore, the mass at each node of the beam elements representing the diaphragm was calculated as, $M = M_{diaph} + \alpha M_{wall}$. The mass contribution of the side walls α was determined by evaluating the dynamic characteristics of the internal frame model. In order to calculate α, two models were prepared for the internal glulam frame. In the first model, the mass of the wall was distributed over the height of the wall. In the second model, the mass was placed at the top of the wall and an equivalent mass was obtained to reproduce the fundamental period of the frame. Periods were compared for this purpose. Masses of the end walls were also included in the fixed- and flexible-base models. For the end walls, it was assumed that either shear deformations dominated and/or there was rotation at the base of the wall. Either case results in a triangular displaced shape over the height of the wall. Therefore, 2/3 of the end wall mass was lumped at the top of the wall.

Since the 3D response of the building was modeled using a series of 2D models, the diaphragm and wall masses were not included separately, but had to be lumped together along the diaphragm length (Fig. 3.23a). Therefore, the model did not include the possibility of the two masses on either side of the connection acting out of phase during an earthquake (Fig. 3.23b).

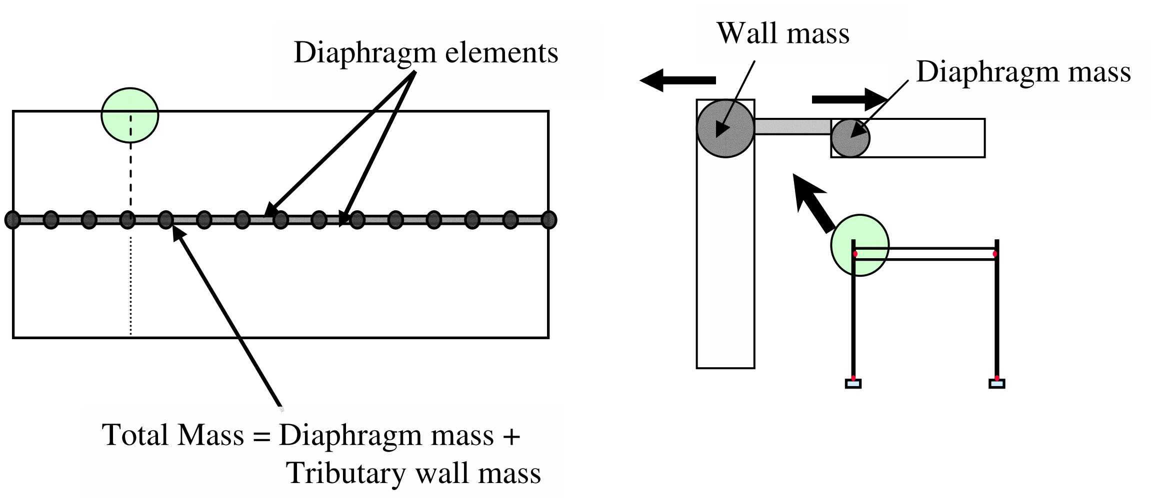

(a) Mass in the model (b) Mass at the connection

Fig. 3.23 Modeling of the building mass

3.6.4 Summary

A general methodology for nonlinear modeling of tilt-up buildings was presented. An overview of the methodology is included in Appendix 3-B. In Sections 3.7 and 3.8, analytical studies are done to validate the modeling approach presented, as well as to assess the sensitivity of the response to changes in important system parameters.

3.7 MODEL VALIDATION—HOLLISTER BUILDING: CSMIP STATION 47391

The proposed modeling methodology was validated using measured responses for the Hollister warehouse building, CSMIP Station 47391 (Huang et al., 1985). The building contains 13 strong-motion instruments as shown in Fig. 3.24. Recorded responses are available for the 1984 Morgan Hill, 1986 Hollister, and 1989 Loma Prieta earthquakes. Responses from the Loma Prieta earthquake were used since the level of shaking in the other earthquakes was relatively small.

Previous studies of the building (Stewart and Stewart, 1997) indicate a fundamental period between 0.6 and 0.7 second during the Loma Prieta earthquake. Period lengthening is observed between approximately 6 and 14 seconds, for mid-roof transverse displacement response (Fig. 3.25), indicating potential damage. The measured responses provide valuable data to validate the modeling methodology.

Available building drawings were collected to assist in creating the structural model. Limited connection information was available; therefore, “best guess” values were used to model key connection parameters. Sensitivity studies were conducted to assess response variations due to changes in element and connection properties.

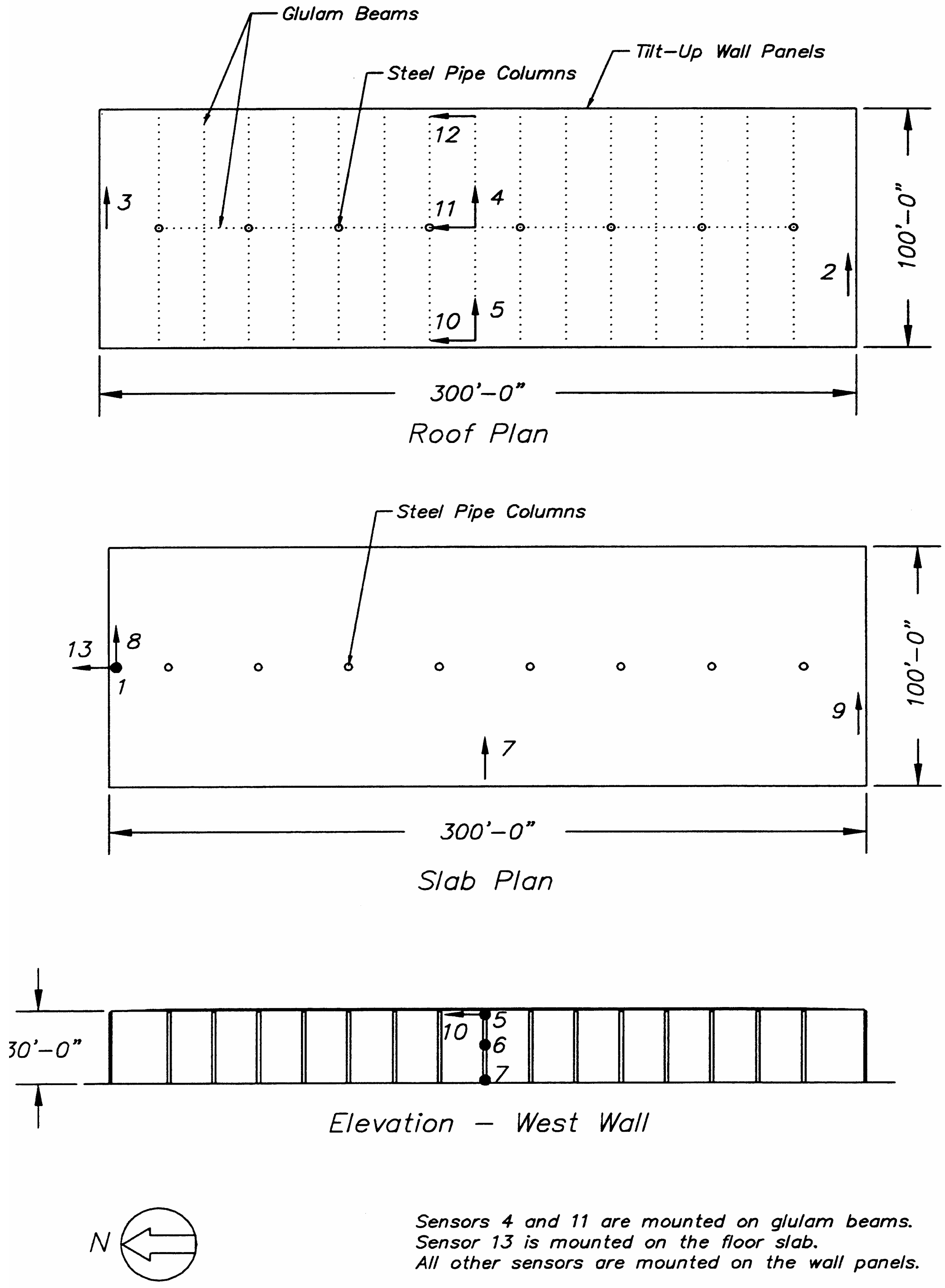

Fig. 3.24 Hollister warehouse — strong motion instrument locations

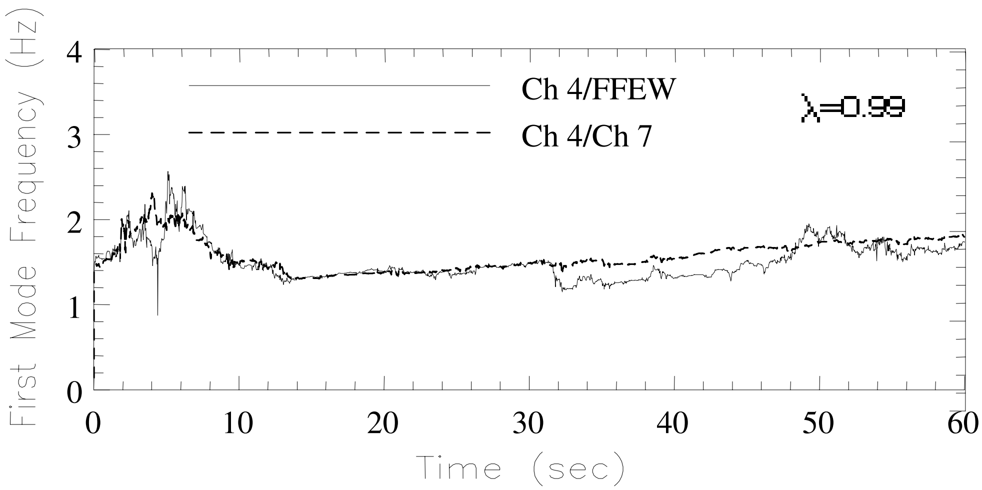

Fig. 3.25 Time variation of first mode parameters — Hollister building, Loma Prieta earthquake (Stewart and Stewart, 1997)

3.7.1 The Building Model

1. The diaphragm

The general layout of the Hollister building is presented in Fig. 3.26. The building was modeled for responses in the east-west direction only. To account for the variation in nail spacing and plywood thickness along the length of the roof diaphragm, the diaphragm was divided into 4 zones (Fig. 3.27). Diaphragm details ($F_{plywood}$, $F_{nailsize}$, s, $F_{roofing}$) were evaluated for each zone using information on the structural drawings. For nail spacing, weighted averages were used to account for variations within each zone. Stiffness and yield force values for each diaphragm element were calculated using the generalized stiffness equations (Sect. 3.5). Resulting values are given in Table 3.4. It should be noted that the 1.33 factor for the presence of roofing was used here for correlation purposes only because debonding of roofing materials was not expected. Including the factor is not recommended for design purposes. A post-yield stiffness equal to 15% of the initial stiffness was used for all element groups based on data from the UCI control specimen.

Table 3.4 Diaphragm stiffness and yield force values for Hollister building

Element Group	D (ft)	L (ft)	$F_{plywood}$	$F_{nailsize}$	s (in)	$F_{roofing}$	K (kips/in)	F_y (V_y) (kips)
1	98.5	23.25	1.5	1.0	2.7	1.33	295	255
2	98.5	9.0	1.5	1.0	3.5	1.33	585	195
3	98.5	9.0	1.0	1.0	3.6	1.33	375	125
4	98.5	9.0	1.0	1.0	5.6	1.33	245	80

Element properties for input into the DRAIN-2DX program were calculated as follows:

$$K_d = 12E_d I_d / L^3 \quad and \quad M_y = V_y L/2$$

where, E_d is Young's modulus (arbitrarily set at 10,000 ksi), I_d is moment of inertia, L is length of the diaphragm element, M_y is yield moment, V_y is yield force (F_y), and K_d is the elastic stiffness. Calculated moment of inertia and yield moment values are presented in Table 3.5.

Table 3.5 Diaphragm moment of inertia and yield moment values for Hollister building

Element Group	L (ft)	I (in^4)	M_y (in-kips)
1	23.25	53,510	35,750
2	9.0	6,140	10,600
3	9.0	3,950	6,810
4	9.0	2,560	4,425

2. The internal frame:

(a) The frame: The internal frame consisted of a 5-1/8 in. x 25 ½ in. glulam beam, an 8-in. diameter steel pipe at the middle of the glulam span, 14 in. x 14 in. pilasters, and 5 ½ in. thick by 30 ft. high wall panels. An equivalent column was used to model the pilasters and an effective flange width of 24.5 in. on both sides of the pilaster, based on ACI 318-95 requirements for T-beams (Section 8.10). The equivalent column was assumed to be fully cracked, and an effective moment of inertia of $0.5I_g$ was used.

(b) Connections:

- Pilaster/footing connections: Footing details were not available for the Hollister building. Drawings provided by PG&E for a tilt-up building in Fremont, California, were used and assumed to be representative of those existing in the Hollister building.

  The moment-rotation relations were obtained using the procedure described in Section 3.6.1a. It was assumed that there were no gaps on either side of the wall panels and pilasters at the slab level, and thus, the connections were assumed to be rigid. The yield moments were determined using a cross-section analysis for the given concrete and reinforcement properties.

- Roof-wall connections: The only information available for the roof-to-wall connections consisted of details of the beam seat connection, where a single bolt was used to connect the glulam beam to the pilaster. Straps were assumed to be present at the subpurlins. The rotational stiffness of the connection in tension was calculated as described in Sections 3.6.1a and 3.6.1c. The connection was assumed to be rigid when subjected to compression.

(c) Masses: Masses were lumped at the nodes of beam elements modeling the diaphragm. The masses were calculated as $M = M_{diaph} + \alpha M_{wall}$. A value of α of 0.4 was calculated using the procedure described in Sect. 3.6.3.

3. *End walls*

Stiffness values for the end walls of the Hollister building were obtained using the procedure outlined in Sect. 3.6.1. Only in-plane loads were modeled and the walls were assumed to remain elastic. The influence of the soil on structural response was estimated by modeling the foundation for the end wall to be a strip footing on the surface of a homogenous halfspace (Appendix 3-A). Based on the procedure outlined in Appendix 3-A, the following values were computed for the building:

	For [E-W] direction	For [N-S] direction
Fixed Base	K = 2.62e+08 (lb/ft)	K = 8.88e+08 (lb/ft)
Flexible Base	$\tilde{K}$ = 2.15e+07 (lb/ft)	$\tilde{K}$ = 1.60e+08 (lb/ft)
	$\tilde{C}$ = 4.41e+04 (lb.sec/ft)	$\tilde{C}$ = 3.73e+05 (lb.sec/ft)

The Rayleigh damping coefficient for the end walls on a flexible base was calculated as $\beta = \tilde{C}/\tilde{K}$ = 0.00205 for the analysis in the east-west direction ($\tilde{\xi}$ = 6%).

The length (L_{es}), and the cross-sectional area (A_{es}) of the spring used to model the stiffness and damping of the end walls were arbitrarily selected to be 10.0 and 1.0, respectively, to allow the calculation of the appropriate stiffness ($K_{ew} = E_{es} A_{es} / L_{es}$; where, K_{ew} is either K or $\tilde{K}$).

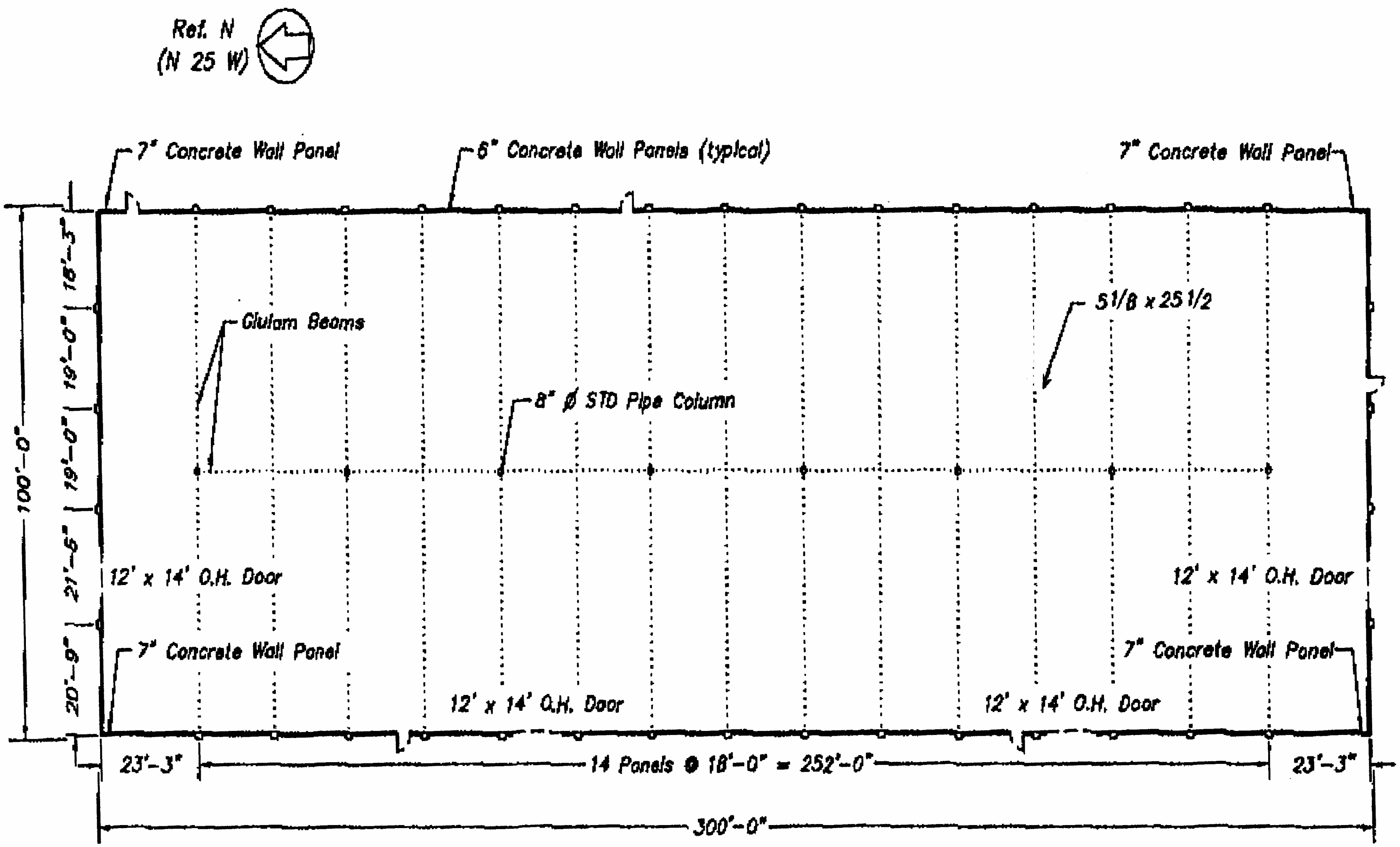

Fig. 3.26 Hollister building layout

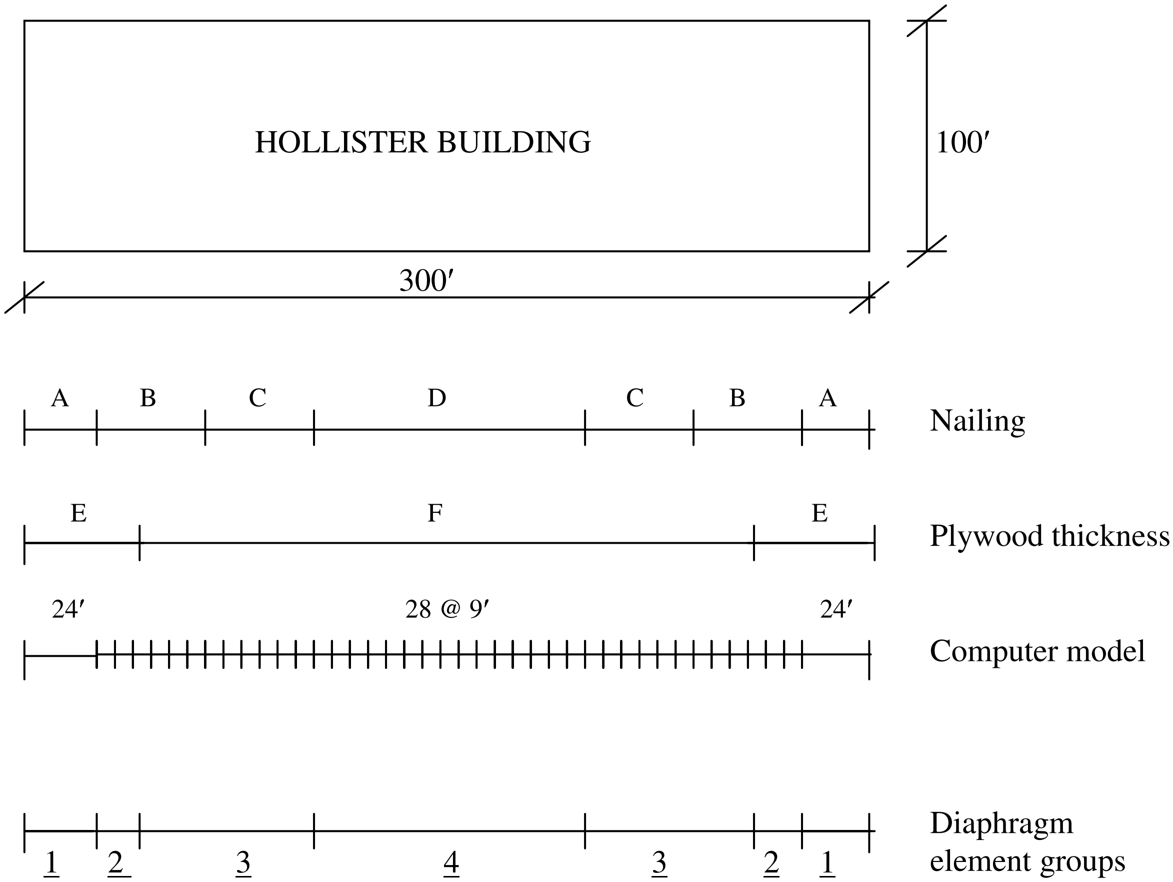

NAILING (o.c.)	A	B	C	D
Boundaries and continuous edges	1 ¾"	2"	2 ½"	4"
Edges	3"	4"	4"	6"
Field	12"	12"	12"	12"

PLYWOOD THICKNESS	
E	F
¾"	½"

Fig. 3.27 Hollister warehouse — diaphragm element groups

3.7.2 Correlation Studies

(a) Internal frame assessment: The first step in the correlation study was to conduct a pushover analysis on the internal frame model. A bilinear force-deformation relation was determined to represent the pushover curve (Fig. 3.20). Effective stiffness and yield force values were determined from Figure 3.20 as 5.13 k/in. and 7.4 kips, respectively. These values were used as the properties for the internal frame springs in the diaphragm model.

(b) Periods and damping: From the initial analysis, the fundamental period with no end walls was determined to be T= 0.66 sec. Using the computed 1st and 7th mode frequencies, Rayleigh damping coefficients for 2% damping were calculated and included in the model.

(c) Structural response: The mid-diaphragm displacement history was computed using the model and compared with the response history calculated using measured acceleration history data from the Loma Prieta earthquake (Fig. 3.28). The diaphragm-model analysis was repeated including the end walls on fixed and flexible base. Resulting mid-diaphragm displacement responses are compared in Fig. 3.29. The “no walls”, “walls on fixed base”, and “walls on flexible base” cases resulted in essentially the same response. Further studies to verify this finding for other soil conditions are described in Section 3.8. A direct comparison of the computed fixed- and flexible-base responses is shown in Fig. 3.30. All three cases had a fundamental period of 0.66 second. New damping coefficients were calculated and included in the model for each case; however, since the fundamental periods were almost identical, the coefficients for each case were essentially the same.

The internal frame spring force history at mid-diaphragm is plotted in Fig. 3.31. The greatest displacement and thus the maximum internal frame force was experienced at this point. Using the force-displacement relation for the internal frames, the maximum force experienced was located on the graph for the given roof displacement (Fig. 3.32). The connection moment and rotations at this force level were then evaluated based on the assumed connection model. At the maximum force level, the total rotation for the roof-to-wall connection was determined from the analysis as θ=0.00141 radian. The deformation was calculated using the connection model described in Sections 3.6.1a and 3.6.1c. The strain in the strap was then calculated as ε =0.00543 ($\varepsilon / \varepsilon_y$ = 0.00543/0.00114 = 4.75) for a strap length of 7 in. A strain level of 0.5% does not appear to be excessive; however, insufficient test and damage data exist to assess what constitutes an excessive strain level. Experimental studies of various connection systems are needed to address this issue.

The shear force histories for critical diaphragm elements were also examined. Shear force response for the diaphragm elements right next to the end walls is plotted in Fig. 3.33. No yielding occurs in diaphragm elements in this specific case. The calculated moments and the yield moments along the diaphragm length are plotted in Fig. 3.34. The figure reveals that for the Hollister building the critical diaphragm elements in case of a more severe earthquake are not the elements right next to the end walls but the ones at the ends of the two weakest diaphragm element groups (element groups 3 and 4 in Fig. 3.27).

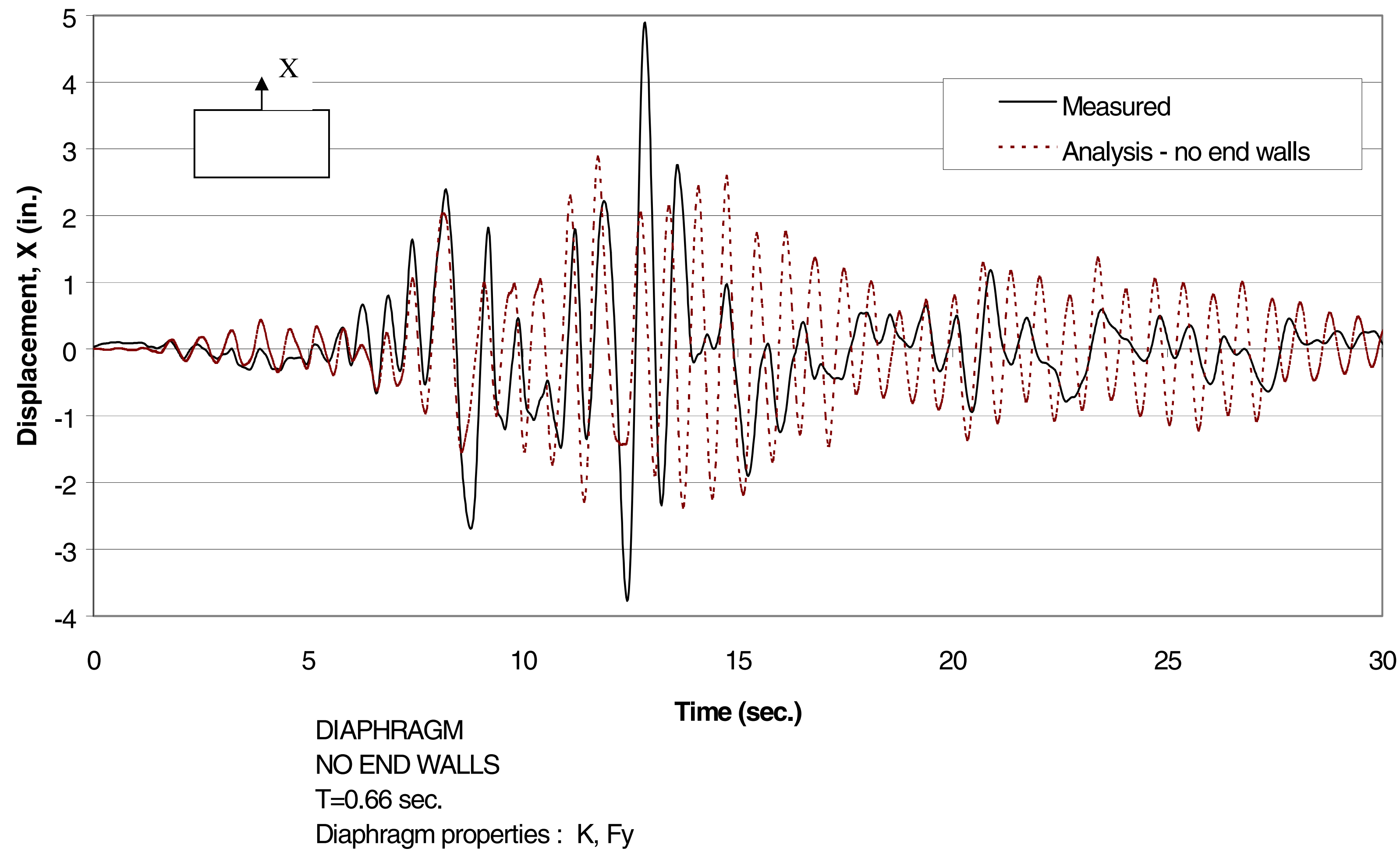

Fig. 3.28 Hollister building—Loma Prieta earthquake: Mid-diaphragm displacement response — No end walls

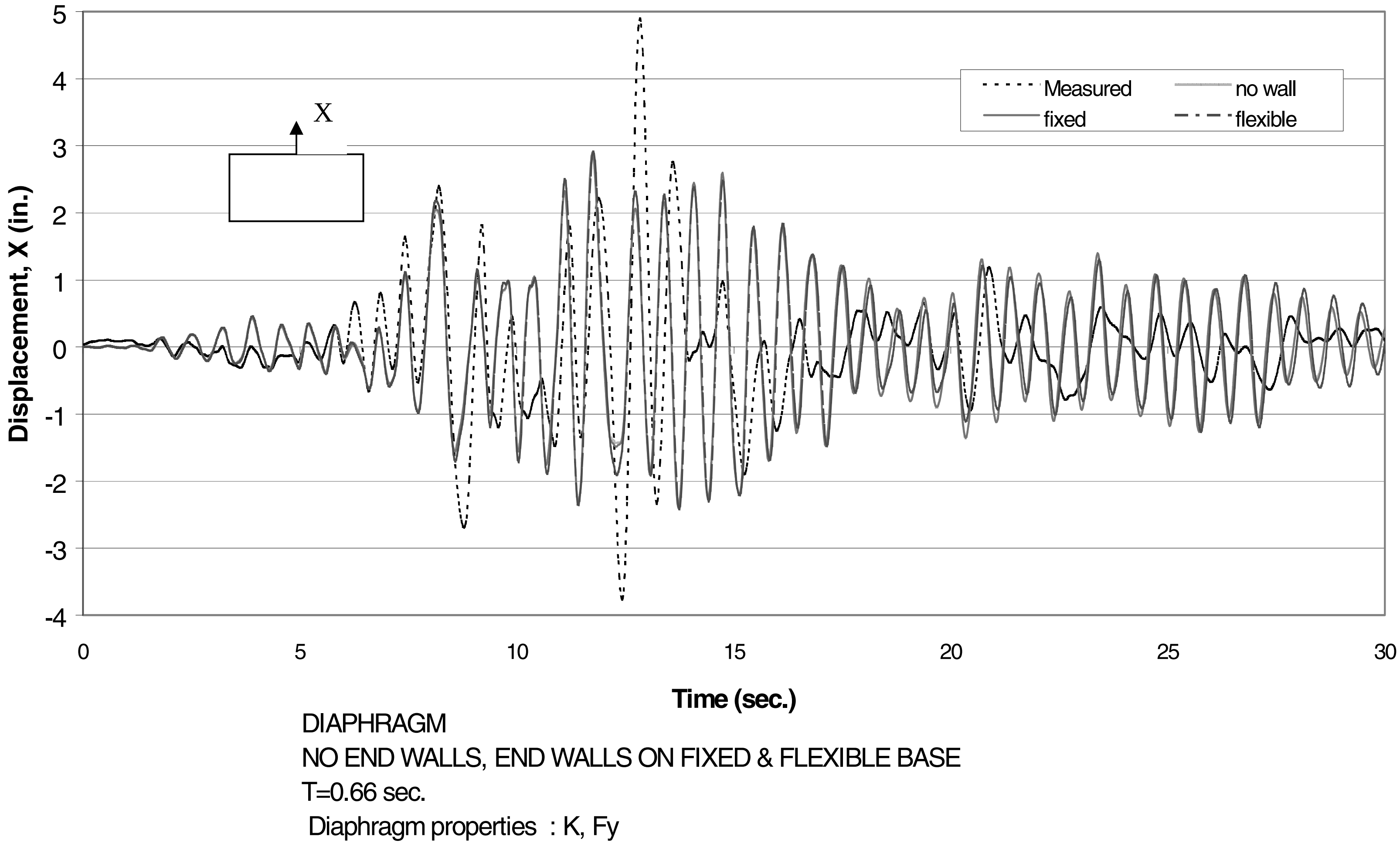

Fig. 3.29 Hollister building—Loma Prieta earthquake: Mid-diaphragm displacement response correlation—No end walls, end walls on fixed and flexible base

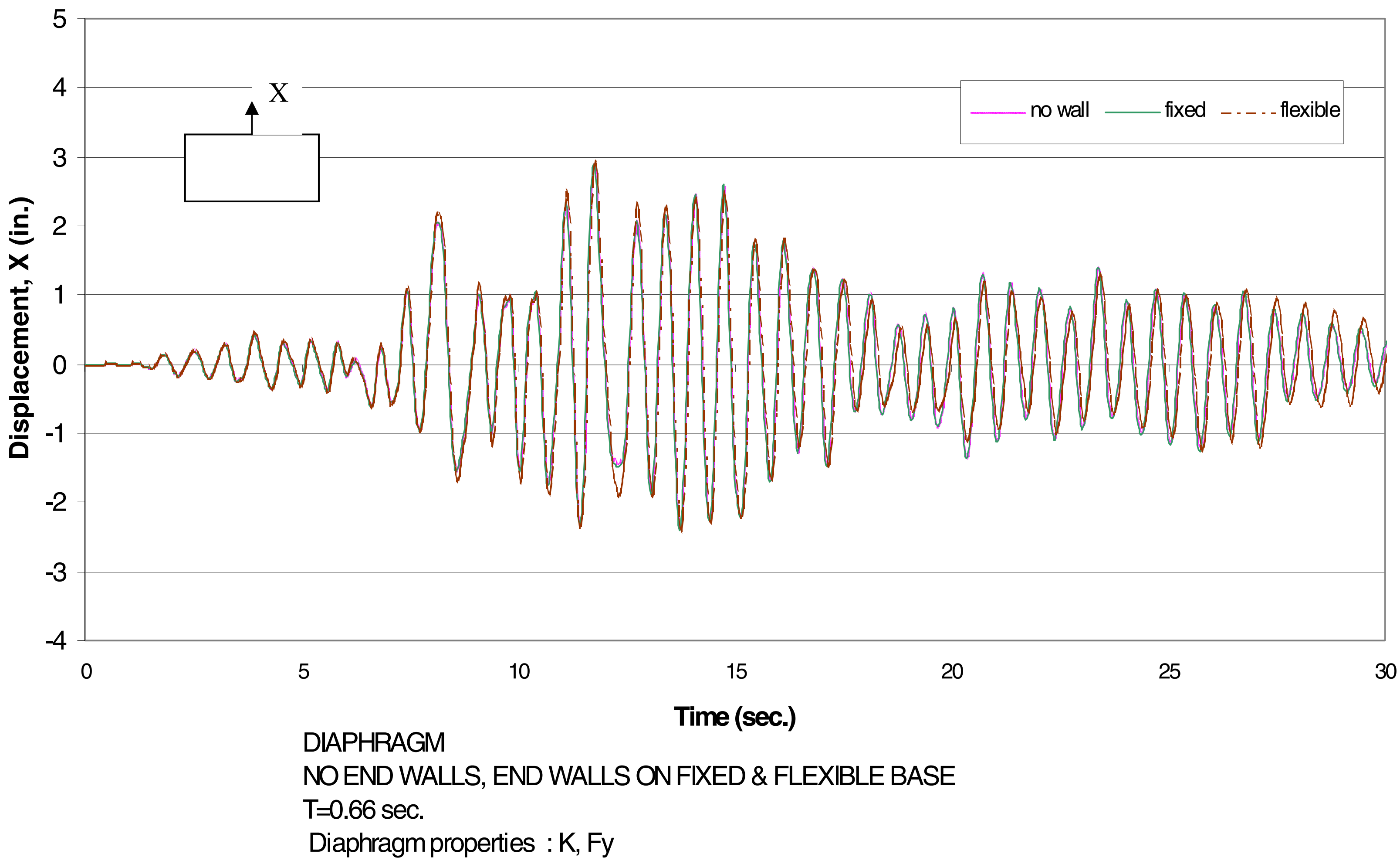

Fig. 3.30 Hollister building—Loma Prieta earthquake: Mid-diaphragm displacement response: — No end walls, end walls on fixed and flexible base

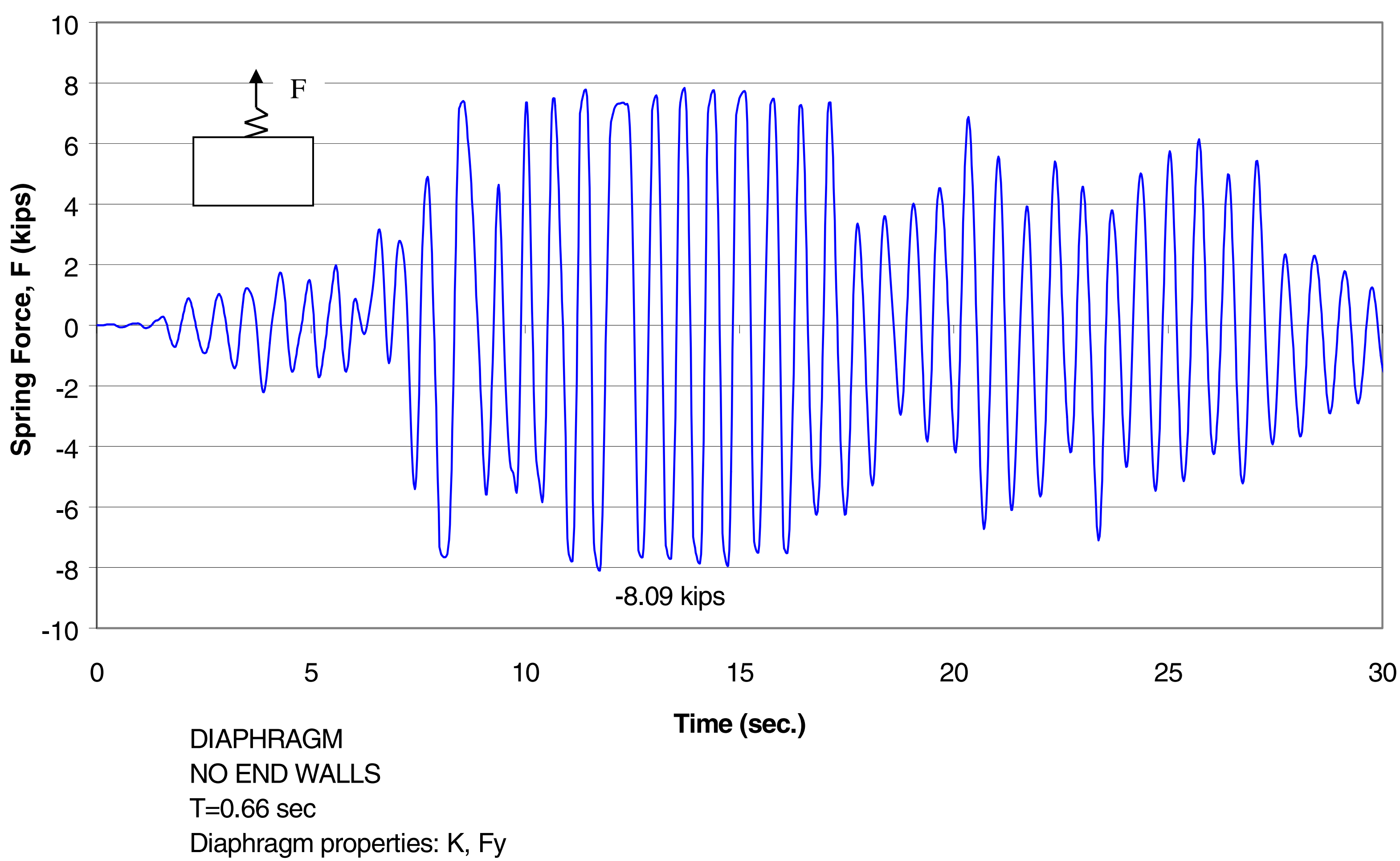

Fig. 3.31 Hollister building—Loma Prieta earthquake: Mid-diaphragm internal frame force—No end walls

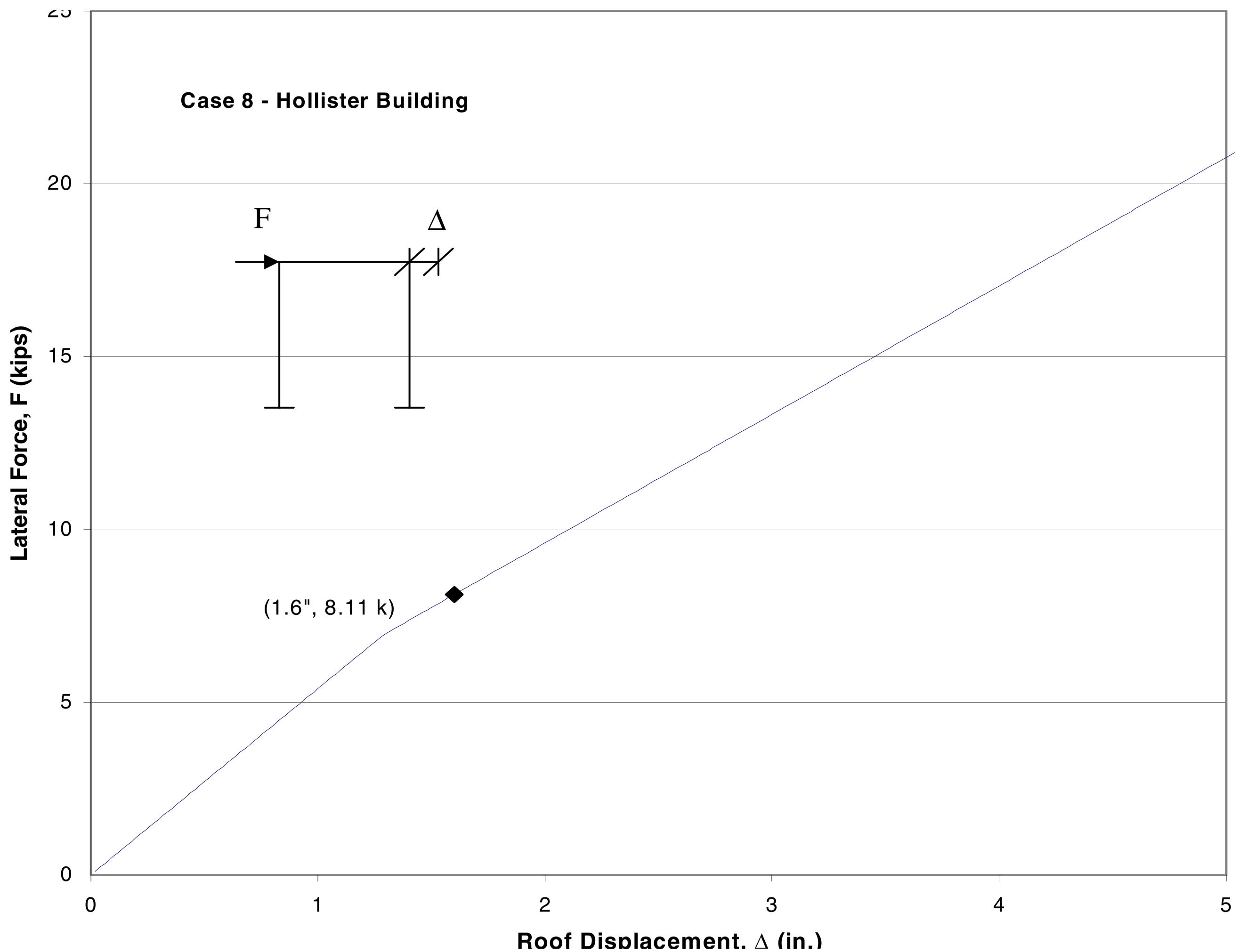

Fig. 3.32 Force vs. displacement curve for a typical internal frame—Hollister building

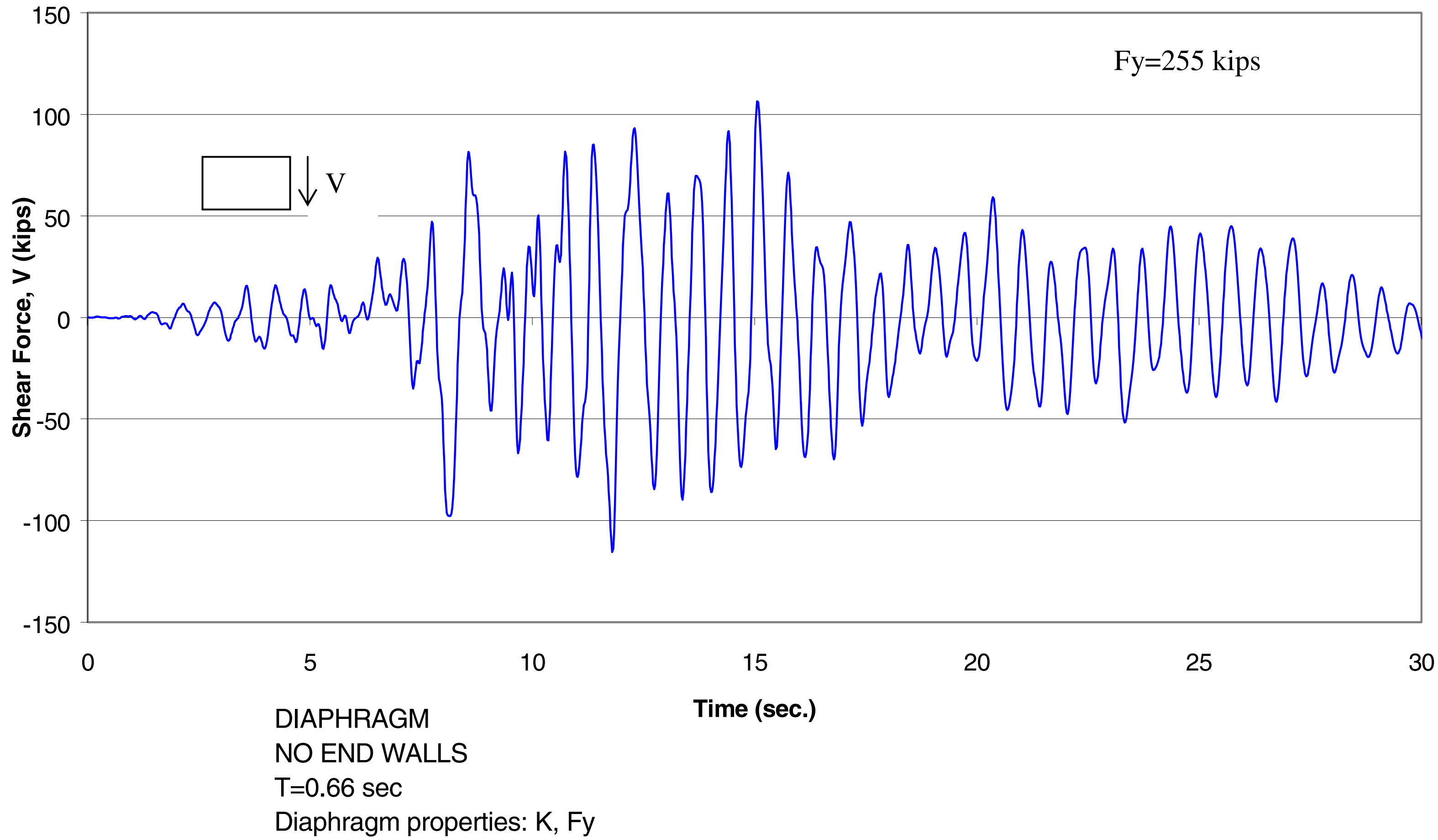

Fig. 3.33 Hollister building—Loma Prieta earthquake: Diaphragm shear force history, diaphragm edge—No end walls

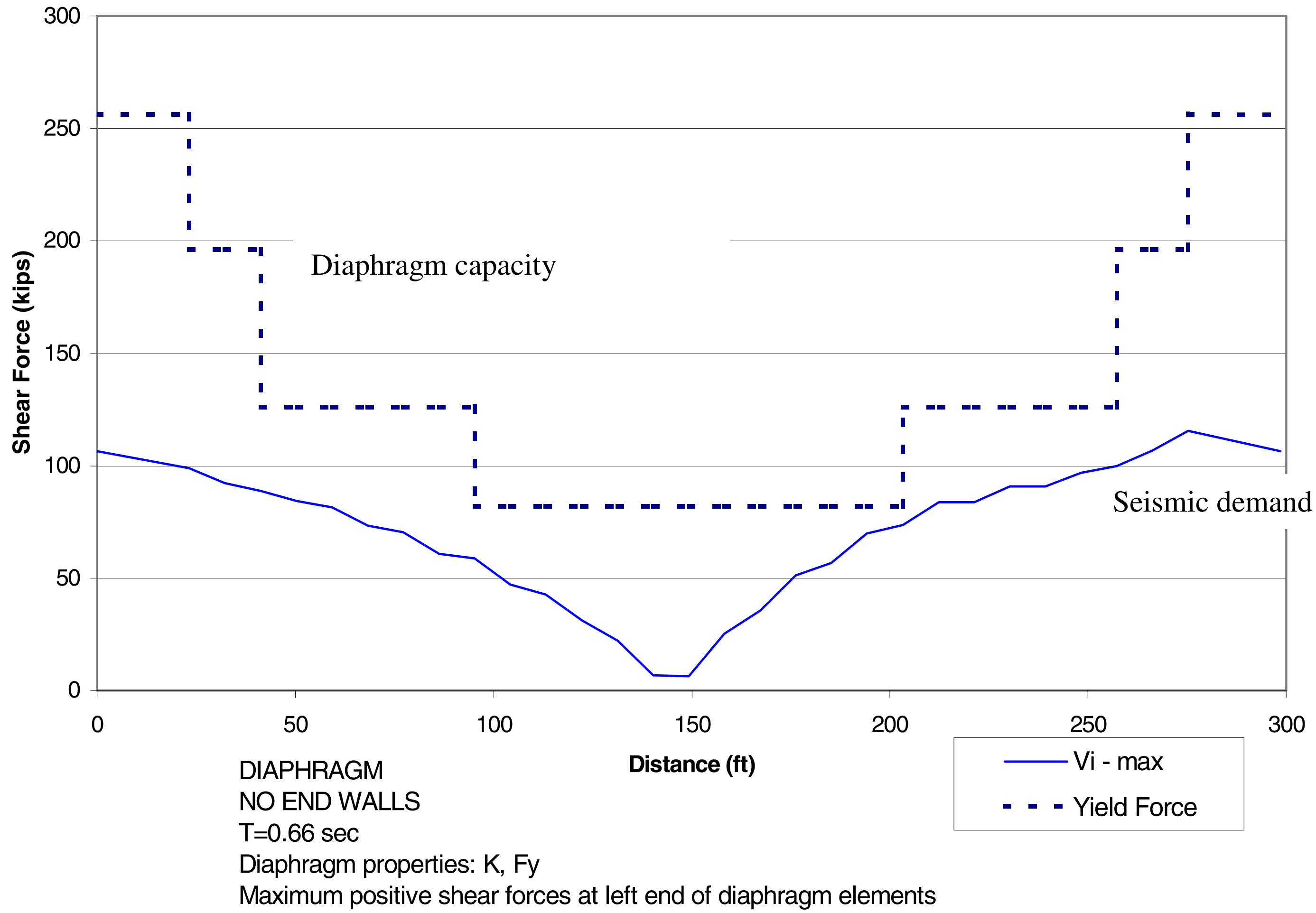

Fig. 3.34 Hollister building—Loma Prieta earthquake: Maximum shear force along diaphragm length—No end walls

3.7.3 Summary

The Hollister building was used for correlation purposes because of the availability of measured response. The building was a typical older tilt-up building that was selected to be representative of California buildings.

The model was developed based on the analysis approach described in Section 3.6, on drawings provided as well as best guess-values.

Correlation studies reveal:

- Displacement correlation for the peak cycles is reasonably good. However, the model is slightly stiffer than the actual building.
- Displacement correlation beyond 15 seconds is poor. This is likely to be due to the low level of response as well as the procedures that are used/available to model damping.
- Yielding is not observed in the diaphragm.
- Mid-diaphragm displacement response is not significantly influenced for models that include the end walls.
- Mid-diaphragm displacement response is not influenced by SFSI due to the geometry of the foundation of Hollister building and the favorable soil conditions.

Analysis results for Hollister building were computed based on given data and best estimates. To assess potential variation in response due to the modeling assumptions, sensitivity studies are conducted in Section 3.8

3.8 SENSITIVITY STUDIES

Hollister building was used for correlation purposes because of the availability of measured response. However, limited information was available on the building and best guess values were used in the analysis. Moreover, limited experimental studies lead to assumptions in the model. Sensitivity studies were performed to investigate the impacts of variations in the following factors on building response:

1. Diaphragm stiffness
2. Connection stiffness/strength
3. Wall tributary length
4. Glulam beam stiffness
5. Damping
6. Soil flexibility

In addition to these items, the influence of ground motion directivity on structural response was studied. The sections that follow describe the effect of each factor.

1. Diaphragm stiffness: The diaphragm stiffness values used in the correlation study were determined using UCI test results and the formulation presented in Eq. 3.1. Limitations in the testing program and assumptions made in the model development lead to uncertainties in the application of this model to field conditions. Therefore, it is important to assess the sensitivity of the structural response to the key modeling parameters. Modeling reliability can be improved as new test data are produced.

   The elastic stiffness of the diaphragm was varied by +/- 15% to assess sensitivity of the response correlation due to relatively minor changes in diaphragm stiffness (e.g., a 15% change in diaphragm stiffness may result if the nail spacing is changed by 1 in. to 5 in. or 7 in., versus the 6 in. spacing used for the original analysis). The “walls on fixed base” model was selected for the analyses because the end walls and the SFSI do not influence results significantly (See Appendix 3-D for an example input file). The fundamental period increased to T=0.70 sec. with the 15% diaphragm stiffness decrease, and decreased to T=0.63 sec. with the increase in diaphragm stiffness. The maximum displacement increased by almost 50% with a 15% decrease in diaphragm stiffness, resulting in a much better mid-diaphragm displacement response correlation (Fig. 3.35). A 15% increase in diaphragm stiffness resulted in only a 12% decrease in the maximum displacement (Fig. 3.36).

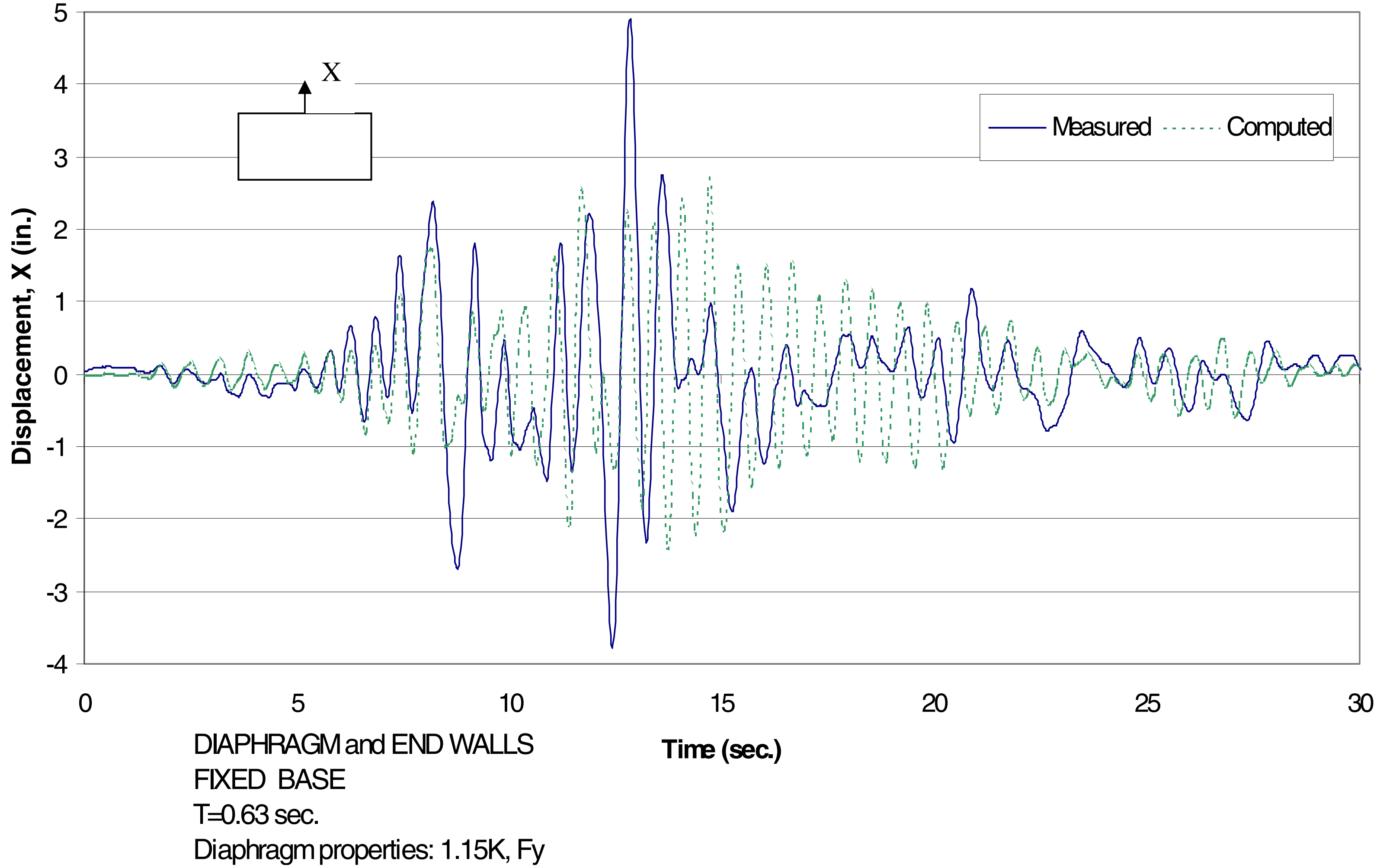

Fig. 3.35 Hollister building—Loma Prieta earthquake: Mid-diaphragm displacement response correlation: 15% increase in diaphragm stiffness

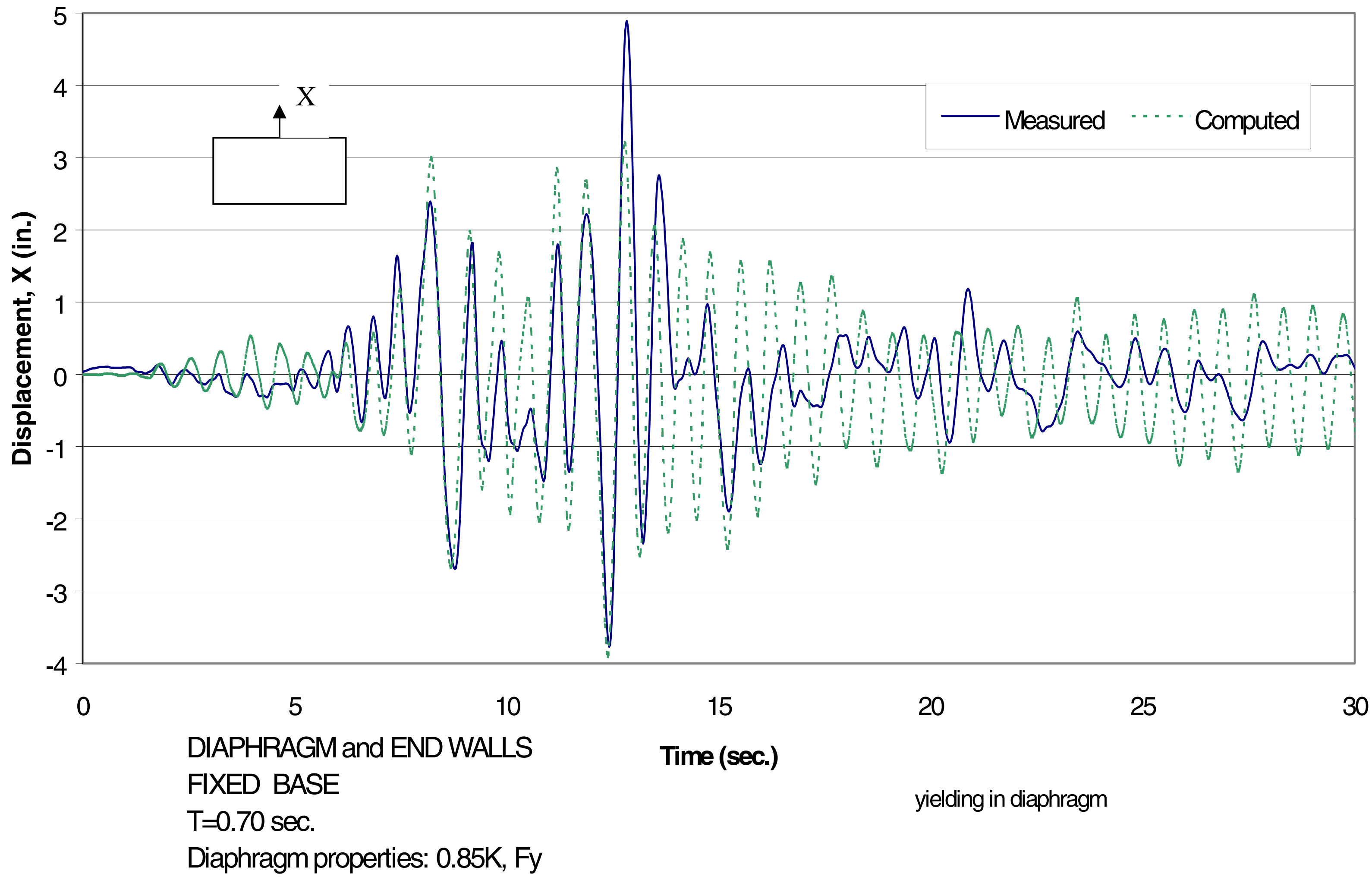

Fig. 3.36 Hollister building—Loma Prieta earthquake: Mid-diaphragm displacement response correlation: 15% decrease in diaphragm stiffness

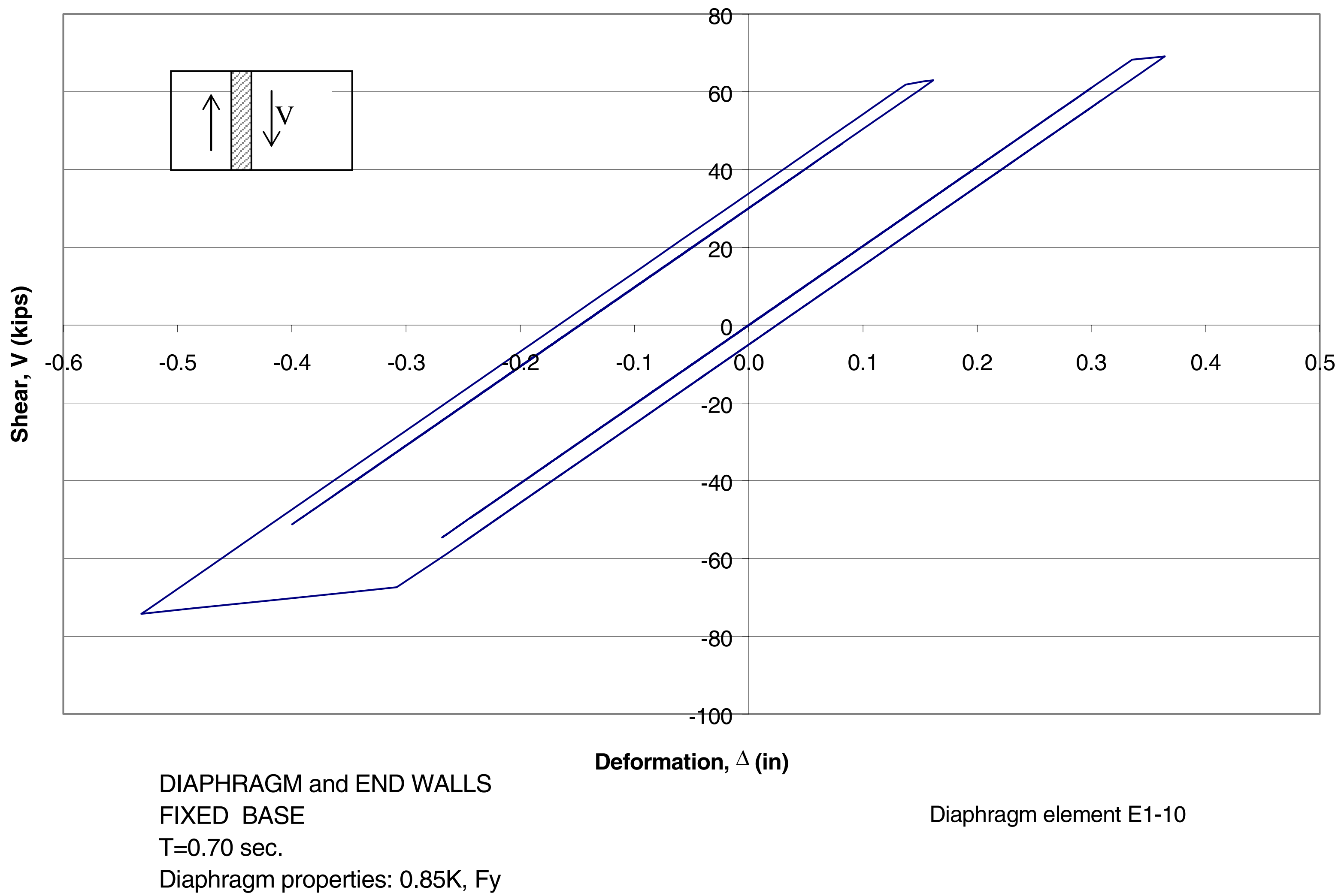

Fig. 3.37 Hollister building—Loma Prieta earthquake: Shear vs. deformation for roof diaphragm element 1-10: 15% decrease in diaphragm stiffness

Yielding of the diaphragm was noted only for the case where the elastic stiffness of the diaphragm was decreased by 15%. Yielding was only observed in the diaphragm elements (Fig. 3.37) at both ends of the weakest diaphragm element group (element group 4 in Fig. 3.27).

The sensitivity of the displacement response is a result of the shape of the displacement curve (see Fig. 3.38). The analyses indicate that significantly improved displacement response correlation can be achieved with only minor changes in diaphragm stiffness. For a smooth displacement spectrum, that would likely be linear in the period range of interest, peak displacement response would not be very sensitive to changes in diaphragm stiffness of +/- 15%. Based on the limited data available, the correlation studies suggest that the modeling approach reasonably represent behavior of the diaphragm, which is a significant aspect of modeling tilt-up systems. Additional studies should be done for other instrumented tilt-up buildings (e.g. Redlands; CSMIP, 1992) and any relevant data should be incorporated as it becomes available. Systematic experimental studies of diaphragm behavior are also needed to improve modeling.

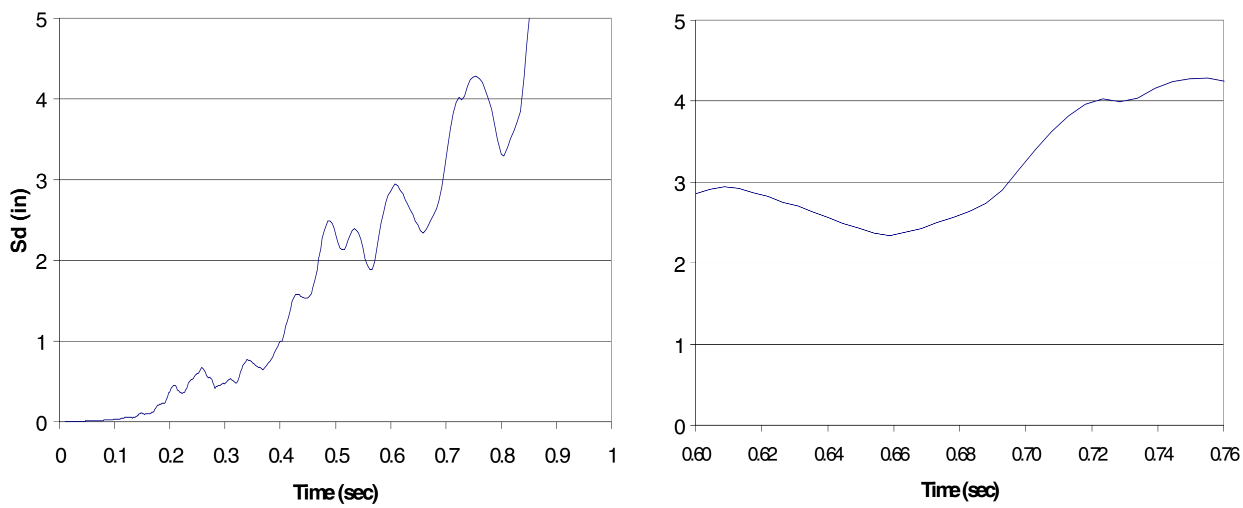

Fig. 3.38 Displacement curve for Hollister building, Loma Prieta earthquake

2. Connection stiffness/strength: Connection stiffness and strength values were varied to assess their influence on the effective stiffness (e.g. see Fig. 3.20) of the internal frame and the system response. Table 3.6 lists various rotational stiffness values and the resulting effective stiffness and strength values:

Table 3.6 Variations in connection stiffness and strength values

		K, stiffness (x 10^6 k/in)							
Connection No. (Fig. 3.38)	M_Y	Case 1	Case 2	Case 3	Case 4	Case 5	Case 6	Case 7	Case 8
1	890	∞	2	∞	∞	∞	∞	∞	∞
2	675	2	2	0.7	0.7	0.7	0.7	0.7	∞ M_Y=890k
3	600	2	2	2	1	2	0.6	2 M_Y=900k	2
4	100000	∞	∞	∞	∞	2	∞	∞	∞
K_{eff} k/in		5.1	5.1	5.1	5.1	5.1	5.1	5.1	5.4
F_{yeff} kips		7.1	7.6	6.5	6.7	6.4	6.4	8.3	7.0

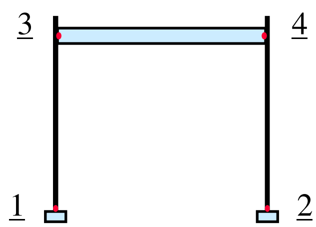

Fig. 3.39 Internal frame connections

The rotational stiffness values given in Table 3.6 represent a range of conditions. For example, for connection 2 (Fig. 3.39), two stiffness values (0.7 x 10^6 and 2.0 x 10^6) represent the condition with a gap on one side of the footing (see Fig. 3.15), and the third value (∞) represents a fixed base. A value of 2.0 x 10^6 is representative of the initial stiffness, whereas 0.7 x 10^6 represents a secant stiffness to the yield level (Fig. 3.16). A rigid-plastic connection was used for the fixed-base condition.

Table 3.6 reveals that the effective stiffness and yield strength of the springs representing the internal frame are relatively insensitive to changes in connection stiffness, Changes in K_{eff} are generally less than 5%, whereas F_{yeff} varies by as much as 30%. This result implies that the stiffness of the internal frames depends primarily on the wall panels and glulam, and the strength depends primarily on the connection strength. Figures 3.40 and 3.41 plot mid-diaphragm displacement response and shear forces along the diaphragm for the reference analysis as well as analyses in which the yield strength of the springs representing the internal frames are varied by +/- 15%. Shear force responses are not significantly different. In this case, the peak displacement is also not significantly different; however, displacement peaks for other cycles show more variation. Therefore, the potential variation of the yield strength of the internal frames should be considered in assessing connection performance.

3. Wall tributary length: The tributary length of the wall was calculated using ACI 318 requirements for T-beams (Section 8.10), resulting in an effective overhanging flange of 24.5 inches on both sides of the pilaster. To assess the influence of this assumption on overall response, a model with an effective overhanging flange width equal to the distance from the face of the pilaster to the wall mid-point (maximum possible) was evaluated. The fundamental period of the model decreased by 11%, from 0.70 to 0.62 second. The resulting responses are presented in Fig. 3.42. For the ground motions measured in the Loma Prieta earthquake, the correlation between measured and model mid-diaphragm responses is worse. However, as noted earlier, for a smooth spectrum, displacement response would be relatively insensitive to this change. The ACI value is used for the correlation studies.

4. Glulam stiffness: In the initial internal frame analysis (Sect. 3.8.2), the glulam beam was the only source of bending stiffness. Based on calculations, the stiffness of the glulam beam was increased by 100% to account for the contribution of the out-of-plane bending of the roof diaphragm to the lateral stiffness of the internal frame. The resulting effective stiffness and yield strength values, 5.4 k/in. and 7.5 kips respectively, were close to the values reported in Table 3.6 for various connection cases, and thus, would not result in a significant difference in the system response. Therefore, no plots are included, and when modeling the internal frame, it is recommended to consider the glulam stiffness only, neglecting the contribution of the diaphragm.

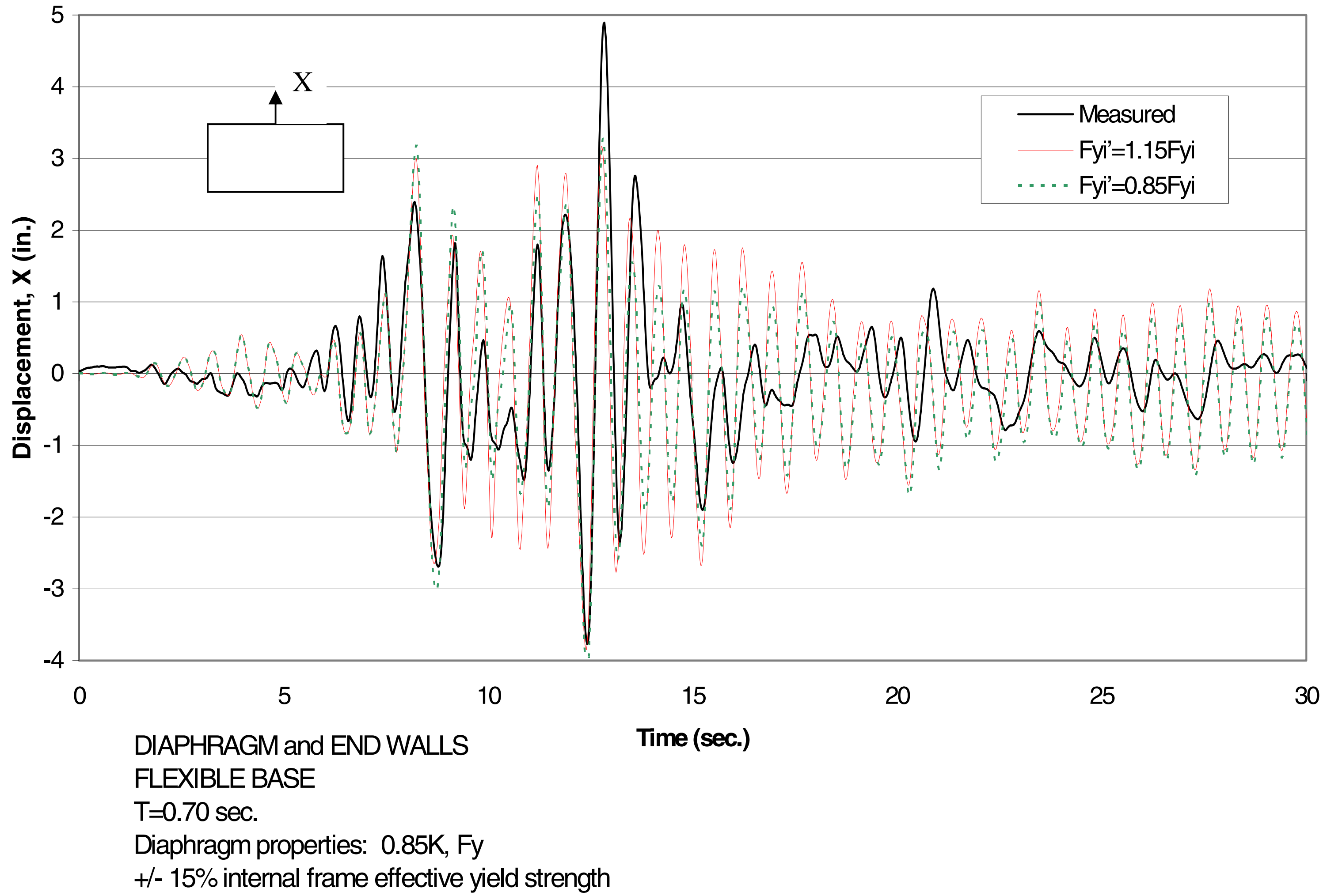

Fig. 3.40 Hollister building—Loma Prieta earthquake: Mid-diaphragm displacement response correlation +/-15% internal frame effective yield strength

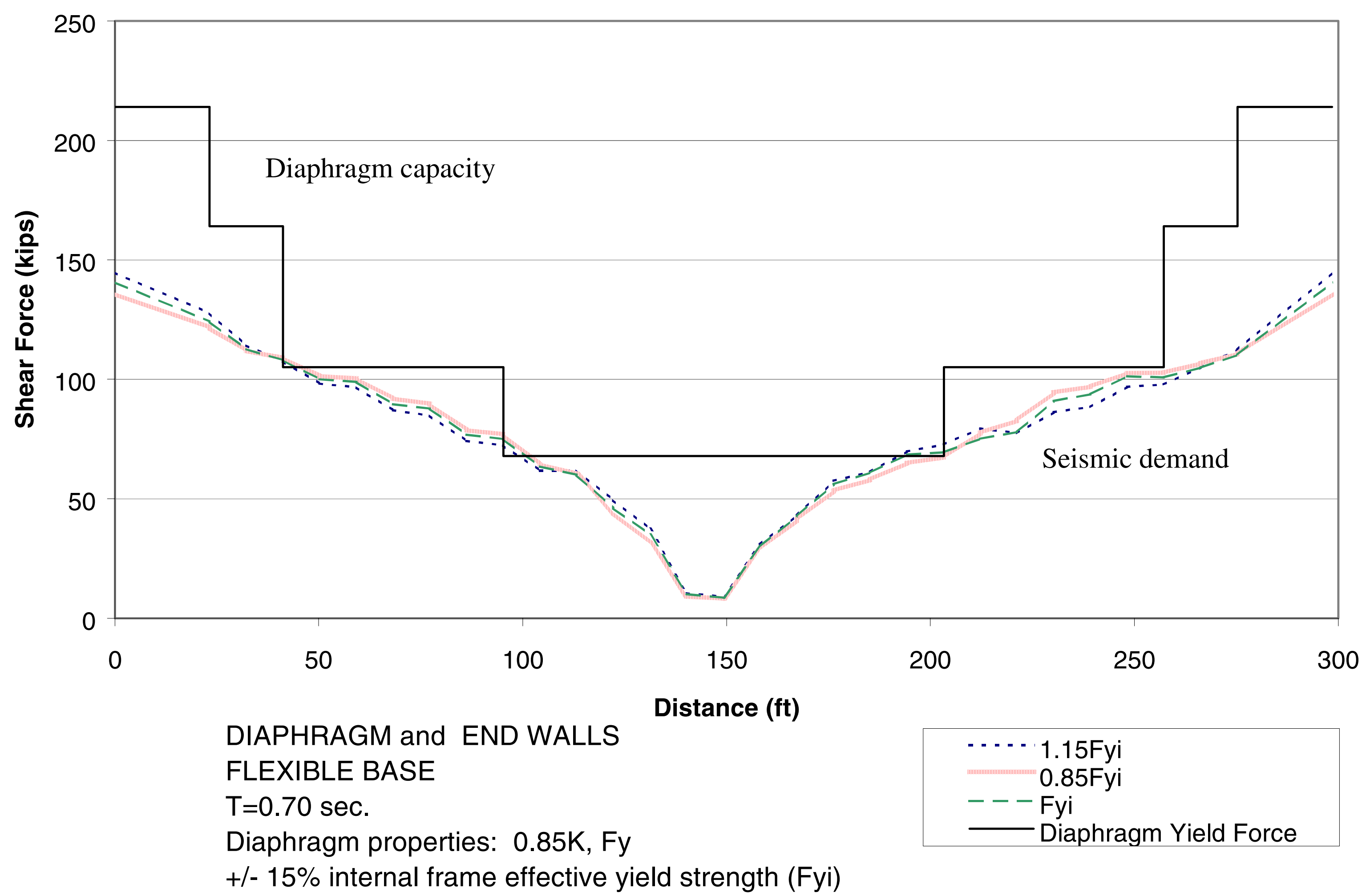

Fig. 3.41 Hollister building—Loma Prieta earthquake: Maximum shear force along diaphragm length +/-15% variation in internal frame effective yield strength

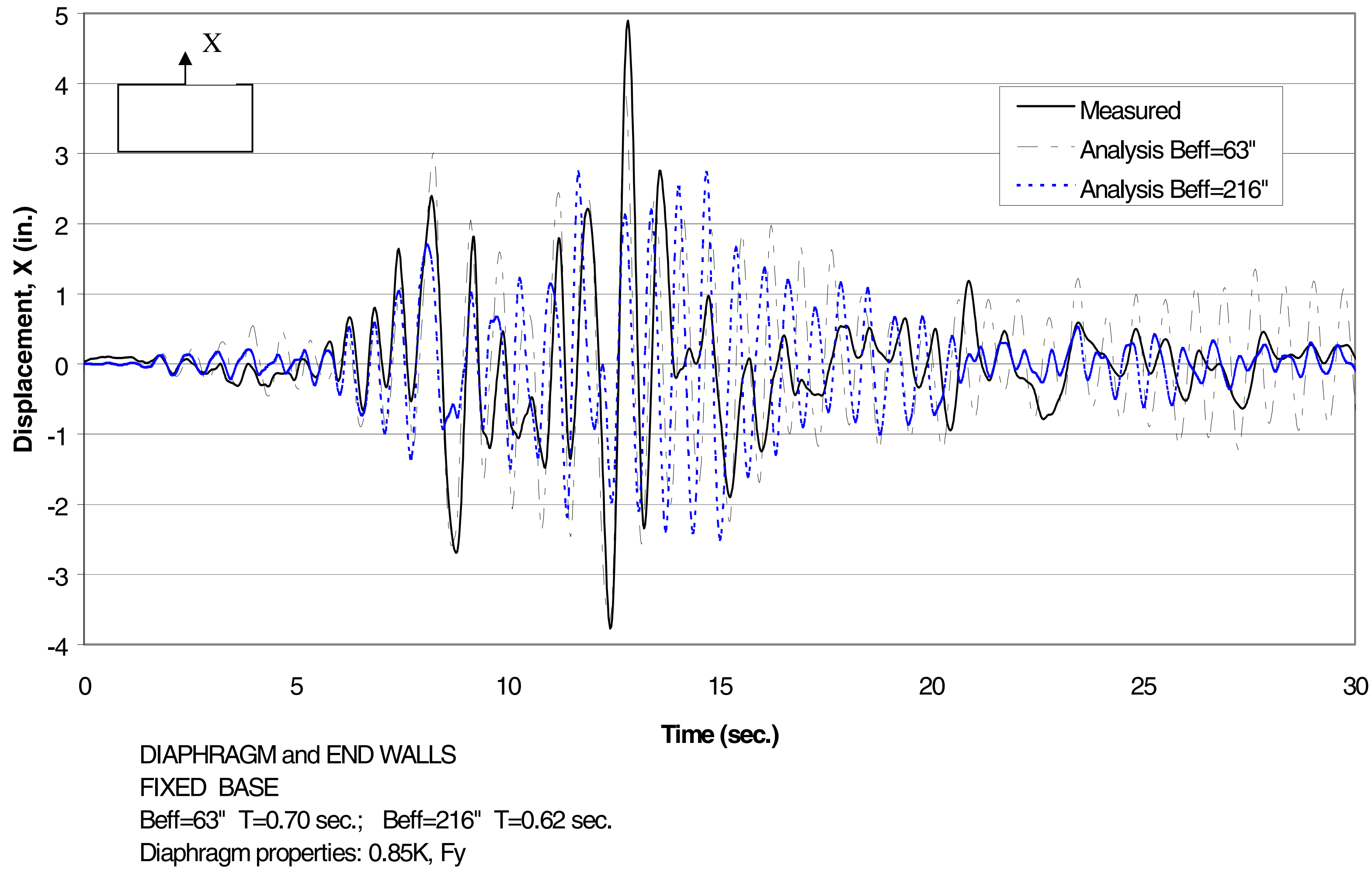

Fig. 3.42 Hollister building—Loma Prieta earthquake: Mid-diaphragm displacement response correlation
Variation in wall effective width

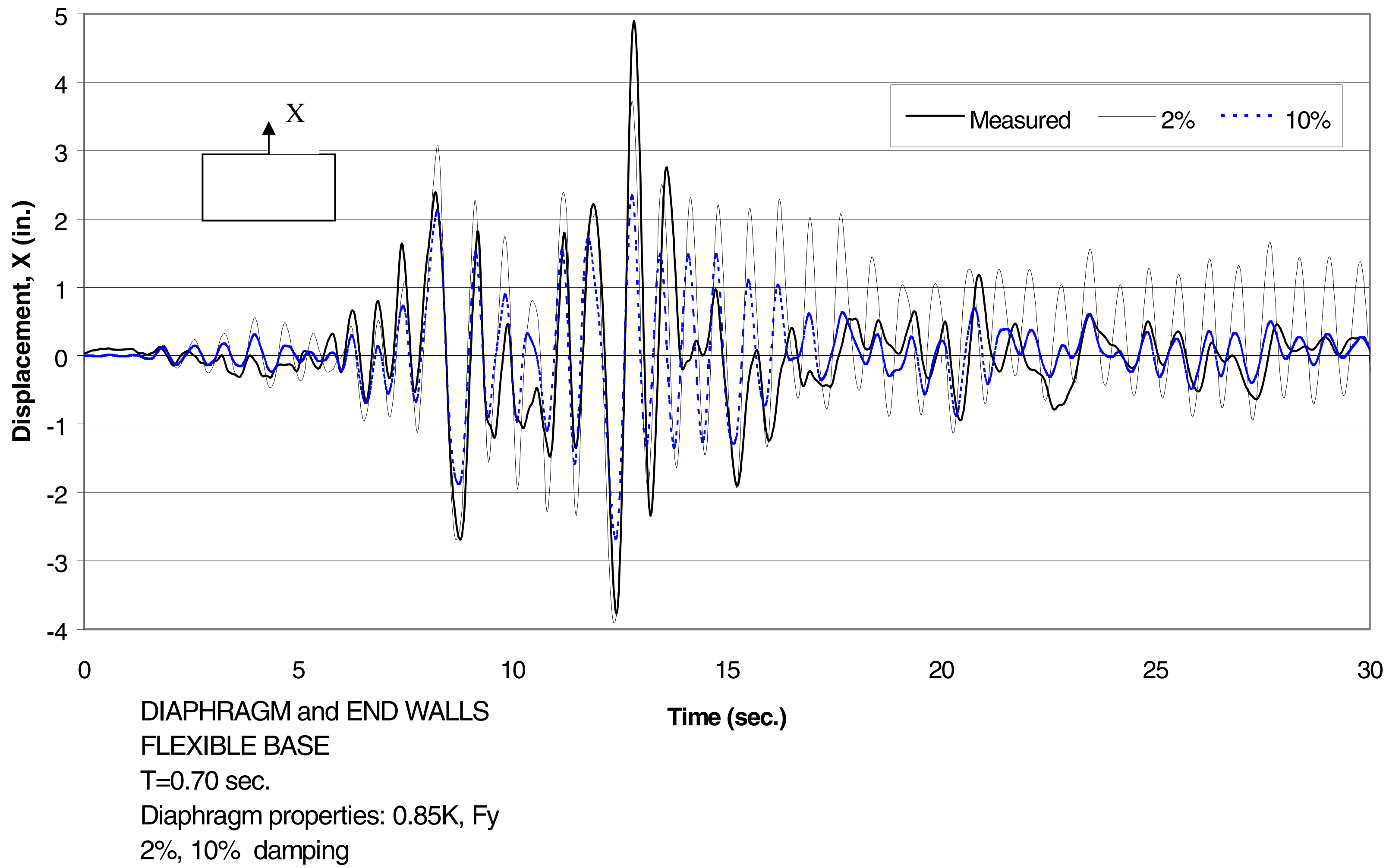

Fig. 3.43 Hollister building—Loma Prieta earthquake: Mid-diaphragm displacement response correlation for 2% and 10% damping

5. Damping: Mid-diaphragm displacement response correlation was poor beyond the peak displacement cycles for all cases where 2% Rayleigh damping was used (See Fig. 3.28-3.41). The response beyond the peak displacement cycles is generally elastic; therefore, no hysteretic damping occurs (e.g., see Fig. 3.37). Apparently, due to diaphragm damage, effective viscous damping increases after the peak displacement cycles. To assess the impact of damping, the system was evaluated for viscous damping ratios of 5% and 10%. Results are presented in Fig. 3.43 for diaphragm response correlation of 2% and 10% damping. With 2% damping, the correlation is good until the peak displacements are reached, but poor afterwards. For 10% damping, peak displacement responses are not as well captured. However, a considerably better correlation is noted for displacements beyond 15 seconds (Fig. 3.43). The poor correlation after the peak values for 2% damping can be attributed to lack of hysteretic damping for post-yield elastic cycles (Fig. 3.44a). For this ground motion, after the peak displacements are reached, elements remain elastic, eliminating the hysteretic damping (Fig. 3.37).

   Typically, computer programs do not allow the viscous damping ratio to vary with time. An element that allows hysteretic damping in the elastic range after inelastic diaphragm response occurs could be implemented in DRAIN-2DX for tilt-up systems (Fig. 3.44b). In general, use of 2% viscous damping is recommended, since peak displacement responses are of most interest.

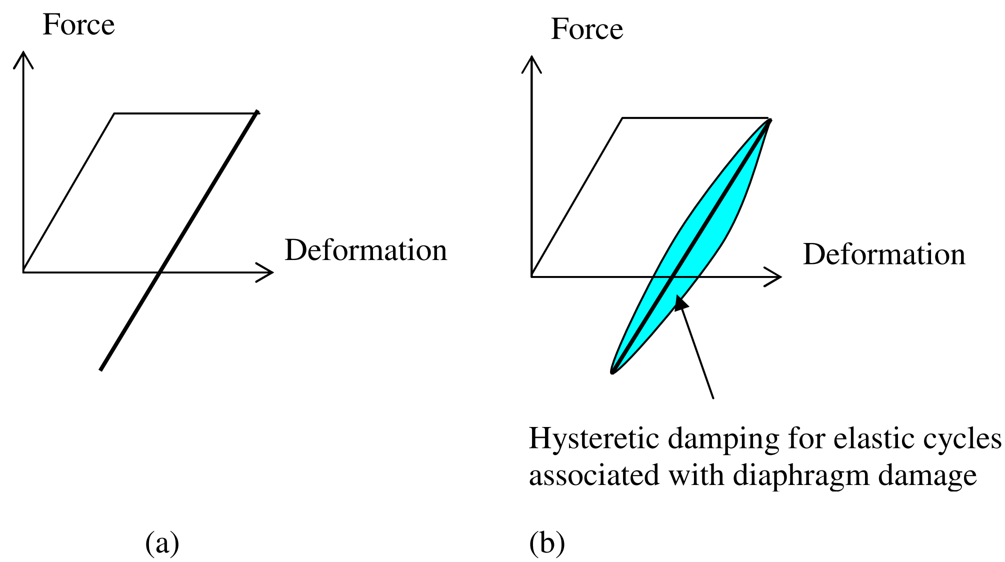

Fig. 3.44 Damping model for tilt-up buildings

6. Soil flexibility: Due to the soil and foundation properties of the Hollister building, response for “walls on flexible base” is almost identical to response for “walls on fixed base”. To assess the influence of more flexible soil and foundation conditions, the shear wave velocities were decreased by 50% (a very flexible-base condition for the Hollister building) to produce new estimates of $\tilde{K}$ and $\tilde{C}$, which are denoted $\tilde{K}'$ and $\tilde{C}'$ respectively. The resulting wall stiffness, $\tilde{K}'$, is 6.0 x 10^6 lb./ft. (28% $\tilde{K}$), and the damping, $\tilde{C}'$, is 2.5 x 10^4 lb.sec./ft. (58% $\tilde{C}$). A 50% reduction in soil stiffness resulted in a period increase from T=0.70 sec. to T=0.72 sec., and an 18% increase in peak displacements at mid-diaphragm (Fig. 3.45). Although the increase in peak displacements at the top of an end wall (Fig. 3.46) was as much as 2.8 times that of the less flexible case ($\tilde{K}$, $\tilde{C}$), the end wall peak displacement (0.3 in.) was still small compared with the mid-diaphragm peak displacement of 3.9 in. These results suggest it is unlikely that soil-foundation-structure interaction will be significant for tilt-up buildings. A parametric study could be undertaken to confirm this conclusion.

7. Near field ground motions-directivity: The purpose of this part of the study was to assess whether characteristics of near-field ground motion (directivity) have any important effect on the response of tilt-up buildings. A database of ground motion records was collected and records were categorized according to magnitude, soil condition, and parameters describing rupture directivity effects. Selected ground motions from the database were then used to assess the importance of near-fault ground motions on the response of the Hollister building. Each record was scaled to a common peak ground acceleration, which was selected to be the average peak ground acceleration for the selected records. Details of the procedure and results of the analyses are presented in Appendix 3-C. Conclusions are discussed in the following paragraph.

   To assess the impact of directivity, forces in the internal frames, and diaphragm shears and displacements are compared. The results indicate that forward directivity has a significant influence on the response of the Hollister building. Shears and displacements in the diaphragm elements increased on average by approximately 30% to 60% in critical locations as defined in Appendix 3-C for records with forward directivity compared with records in the category backward/neutral. Maximum internal spring forces increased, on average, by 9% to 16% in response to ground motions containing forward directivity, as compared to backward/neutral. However, more comprehensive studies are needed to develop specific recommendations to account for the influence of forward directivity on building response.

   These analyses were undertaken to assess the importance of near-field ground motions on the behavior of tilt-ups using inelastic nonlinear models and actual ground motions. The results indicate that near-field ground motions have the greatest impact on the diaphragm response. Future studies should focus on identifying specific features of the near-field ground motions and the diaphragm that experiences the greatest impact.

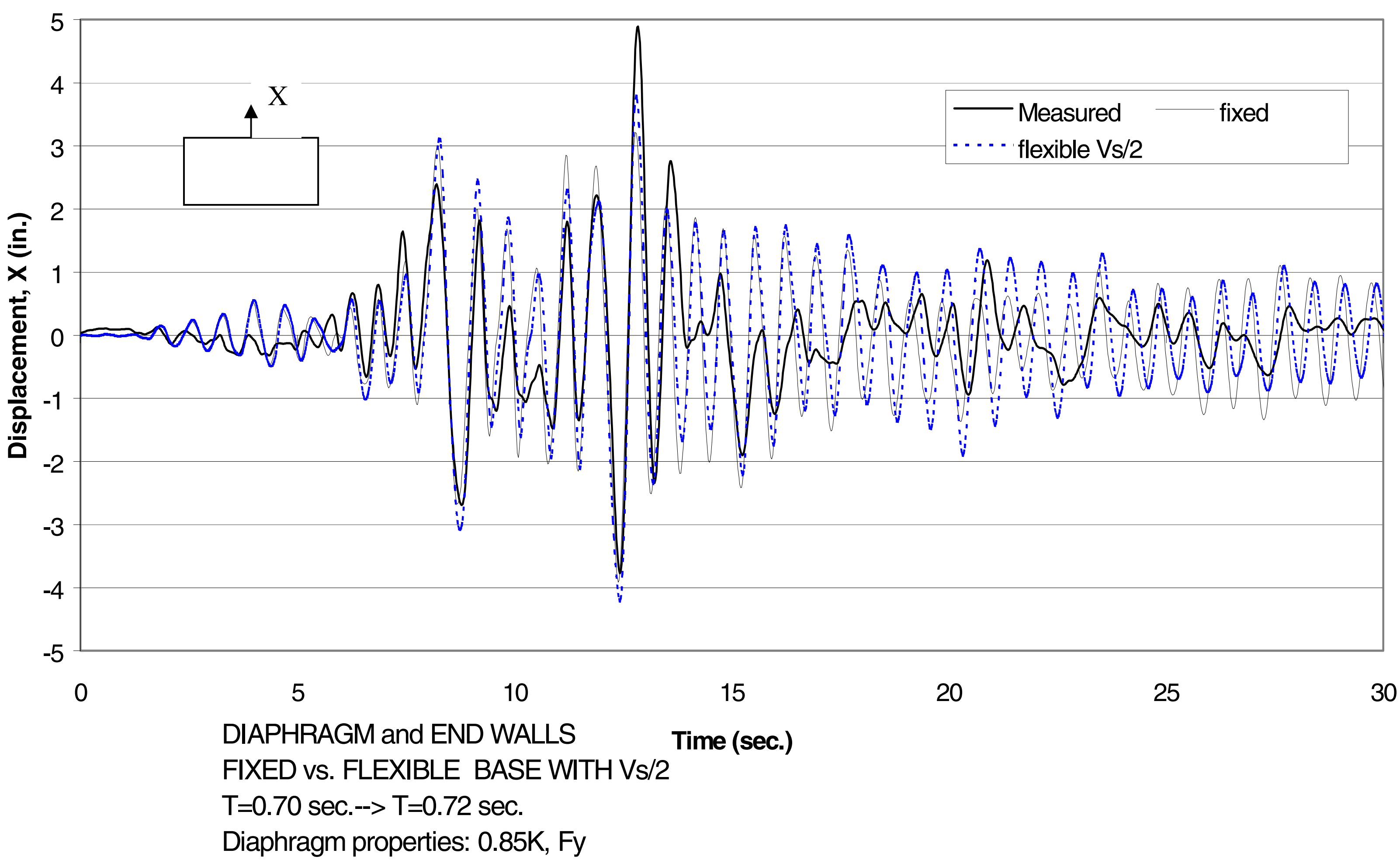

Fig. 3.45 Hollister building—Loma Prieta earthquake: Mid-diaphragm displacement response correlation—Increase in soil flexibility (Shear wave velocity $V_s/2$)

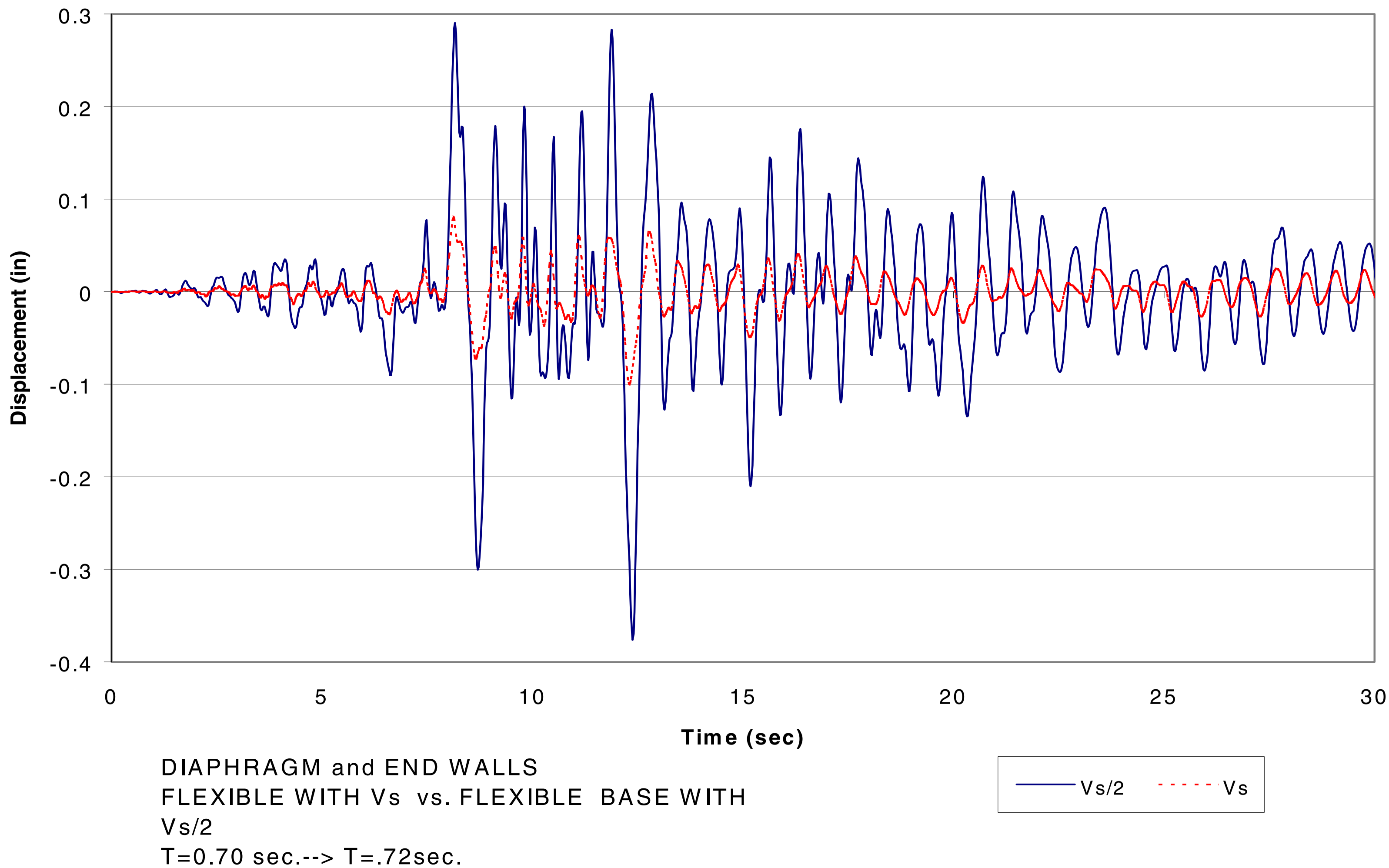

Fig. 3.46 Hollister building—Loma Prieta earthquake: Displacement response comparison at top of end wall: Shear wave velocities V_s vs. $V_s/2$

3.9 CONCLUSIONS

A simple nonlinear model was developed for the analysis of tilt-up buildings. The model enables the user to evaluate connection forces and deformations as well as the demand in the roof diaphragm for a given ground motion. An instrumented building (CSMIP Station 47391) was used to validate the modeling methodology. Although limited information was available for the building, the correlation studies showed that the simple model was capable of representing the measured mid-diaphragm displacement response reasonably well.

Sensitivity studies were done to assess potential response variations. Parameters considered included: diaphragm stiffness, connection stiffness/ strength, wall tributary length, glulam beam stiffness, system damping, and soil-foundation-structure interaction. The influence of forward/backward directivity of near-field ground motions was also studied.

The sensitivity studies, as well as previous studies, indicate that diaphragm stiffness has a considerable impact on the response of tilt-up buildings. An equation presented by Hamburger et al. (1996) to estimate diaphragm stiffness and strength values for a range of diaphragm characteristics (e.g., diaphragm geometry, nail spacing, plywood thickness, and presence of roofing materials) was reviewed. The expression was modified based on the review of existing and new test data. The results indicate that further studies are needed to better understand diaphragm response. However, with current information, the equation provides a reasonable approach to determining the stiffness and strength for a broad range of diaphragm conditions. Sensitivity studies are recommended for design and evaluation to account for uncertainties in modeling the diaphragm.

Simple models were developed to represent the diaphragm-to-wall connections. It is shown that +/- 15% variations to the connection stiffness/strength do not result in significant changes in the diaphragm response. For the tilt-up wall panels, ACI318 values for effective slab widths provide a reasonable approach to estimate the tributary wall length on either side of the pilasters. Variations in glulam stiffness have little impact on the response of internal frames; therefore, it is appropriate to neglect the contribution of the diaphragm and use the glulam beam stiffness only.

Sensitivity studies showed that a 2% damping ratio resulted in good response correlation until the peak displacements were reached, but higher damping ratios (e.g. 10%) were needed to improve correlation in the post-peak displacement range. However, with current modeling options, a 2% damping ratio is recommended to predict peak displacement responses, which are of most interest. Since most computer programs do not allow the viscous damping ratio to vary with time, an element that allows hysteretic damping in the elastic range after inelastic diaphragm response occurs could be implemented to improve the modeling options.

Due to the soil and foundation properties of Hollister building, soil-foundation-structure interaction is not significant. Increasing soil flexibility results in larger peak displacements; however, the impact becomes significant only with large increases in soil flexibility (50%). Even with very flexible soil conditions, the displacements at the top of the end wall remain small relative to those in the diaphragm. Unless very flexible soil conditions exist, it is unlikely that SFSI will be significant for tilt-up buildings.

Sensitivity studies indicate that near-field ground motion (directivity) has a significant influence on the response of tilt-up buildings. Maximum internal frame forces, and shears and displacements in the diaphragm elements increase by 9 to 16%, and 30 to 60%, respectively, for ground motions containing forward directivity relative to ground motions with the same peak ground acceleration but with neutral or backward directivity. The results indicate that near-field ground motions have the greatest impact on the diaphragm and that the influence is significant. Although the results presented can be used to estimate the impact of near-field ground motions on given tilt-up buildings, more comprehensive studies are needed to identify specific features of the near-field ground motions and to develop specific recommendations.

APPENDIX 3-A SOIL-FOUNDATION-STRUCTURE INTERACTION

The dynamic stiffness and damping of the end walls on soil (the so-called flexible-base condition) were calculated to evaluate the effects of soil-structure interaction on building response. This appendix describes the analysis procedure for the soil-foundation impedance function, and how the impedance was merged with “fixed-base” wall stiffness to evaluate an effective “flexible-base” stiffness and damping for the end walls.

A critical parameter controlling foundation impedance functions is the profile of soil shear stiffness (G) with depth. Small strain shear modulus, G is typically evaluated from measurements of shear wave velocity (V_s) as $G = V_S{}^2 \times \rho$, where ρ is mass density for soil ($\text{lb.sec}^2/\text{ft}^4$).

The shear wave velocity profile was estimated for the Hollister Warehouse site using in-situ measurements from nearby downtown Hollister (Stewart and Stewart, 1997). Using the analysis program SHAKE (Schnabel et al, 1972; revised 1991), the strain-dependent shear wave velocity profile was estimated. These analyses were performed using the free-field time history for the Hollister site. Shear wave velocities within the soil region beneath the foundation that most influences lateral and rocking behavior (depths of 1.33L for lateral, 0.67L for rocking, where 2L is the foundation length) were then evaluated.

The foundation for the end wall was assumed to be a strip footing of length 2L on the surface of a homogenous halfspace. The static stiffness values were calculated as (Gazetas, 1991):

$$K_X = \frac{2GL}{2-\nu}\left(2+2.50X^{0.85}\right) - \frac{0.2}{0.75-\nu}GL\left(1-\frac{B}{L}\right)$$

$$K_{ry} = \frac{G}{1-\nu} I_{by}{}^{0.75}\left[3\left(\frac{L}{B}\right)^{0.15}\right]$$

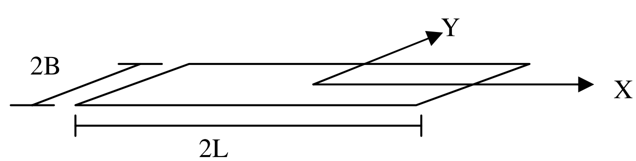

where, K_x: Horizontal (static) stiffness in lateral direction, K_{ry}: Rocking (static) stiffness around lateral axis, ν: Poisson’s ratio for soil, I_{by}: Moment of inertia of the section about y axis, L, B: are as defined in the above figure, and $X = \frac{A}{4L^2} = \frac{B}{L}$, A: Area of the section.

The static stiffness values are modified to account for dynamic effects by multiplying by the following coefficients:

Translation: $k_x \cong 1$

Rocking: $k_{ry} \cong 1 - 0.30 a_o \qquad \nu < 0.45$

$$k_{ry} \cong 1 - 0.25 a_o \left(\frac{\mathrm{L}}{\mathrm{B}}\right)^{0.30} \qquad \nu \approx 0.50$$

$$where,\ a_o = \omega B / \ V_S$$

The damping coefficients for lateral and rocking response are calculated as:

Translation: $C_x \cong \rho V_S A$

Rocking: $C_{ry} \cong \left(\rho V_{La} / b_y\right) \tilde{c}_{ry}$

$\tilde{c}_{ry} = f\ (L/\mathrm{B}, \mathrm{a_o}) \qquad$ as determined from Fig. A - 1 below

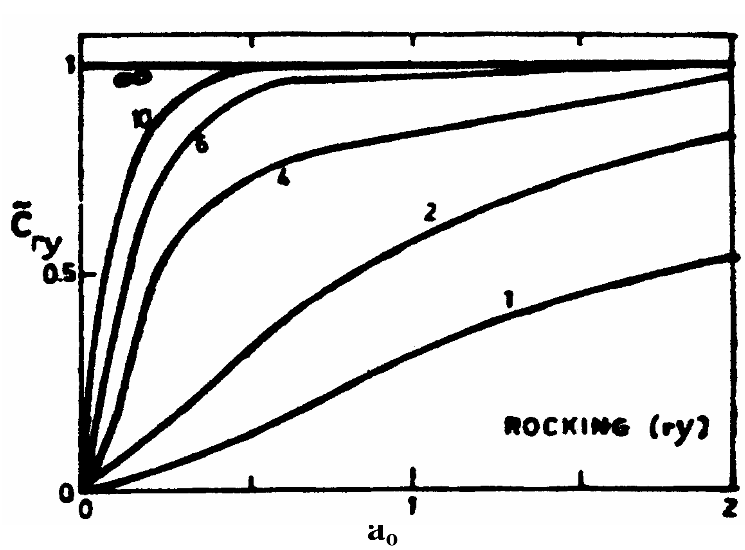

Fig. 3-A-1 $\tilde{c}_{ry}$ for various L/B ratios (Gazetas, 1991)

The composite stiffness and damping of the wall soil system is evaluated using expressions derived by Stewart and Fenves (1998). The effective fundamental mode frequency and damping ratio are calculated as:

$$\tilde{\omega} = \sqrt{\frac{1}{1/\ \omega^2 + 1/\ \omega_u{}^2 + 1/\ \omega_r{}^2}}$$

$$where \qquad \omega_u = \sqrt{\frac{\mathrm{K}_x k_x}{\mathrm{m}}} \quad \omega_r = \sqrt{\frac{\mathrm{K}_r k_r}{\mathrm{m}}} \quad \omega = \sqrt{\frac{K}{\mathrm{m}}} \qquad and \quad K\text{: wall stiffness}$$

$$\tilde{\xi} = \left(\frac{\tilde{\omega}}{\omega_x}\right)^3 \xi_x + \left(\frac{\tilde{\omega}}{\omega_r}\right)^3 \xi_r + \left(\frac{\tilde{\omega}}{\omega}\right)^3 \xi$$

$$where \qquad \xi_x = \frac{C_x}{2m\omega_x} \qquad \xi_r = \frac{C_r}{2m\omega_r} \qquad \xi = \frac{C}{2m\omega}$$

The effective spring stiffness and dashpot coefficient for the wall/soil system are then calculated as $\tilde{K} = m\tilde{\omega}^2$ and $\tilde{C} = 2m\tilde{\omega}\xi$.

APPENDIX 3-B MODELING PROCESS — STEPS

General Methodology:

1. Internal Frame Model
   (a) Connection models
   - Foundation
   - Roof diaphragm/wall connections

   (b) Pushover analysis
   (c) Bi-linear force deformation curve → Effective stiffness and yield force values
   (d) Tributary mass calculation for sidewalls at roof level (α)
2. Diaphragm model
   (a) Internal frame springs: K and F_y from bi-linear curve
   (b) Diaphragm elements: K and F_y extrapolated using Eq. 3.1 and appropriate test results
   (c) End walls: 3 analyses
   - No end walls
   - Walls on fixed base: K for end springs
   - Walls on flexible base: $\tilde{K}$, $\tilde{C}$ and β calculated

   (d) Total mass calculation: $M = M_{diaph} + \alpha\, M_{wall}$
   (e) Eigenvalue Analysis → T, ω → Rayleigh damping coefficients
   (f) Structural analysis
   - Internal Frame Force vs. Time → Max internal frame force (mid-diaphragm)
3. Internal Frame Model
   - For max spring force: Connection moment and rotation
   - Connection model: Connection force and deformation; ductility
4. Evaluation

APPENDIX 3-C SIGNIFICANCE OF FORWARD DIRECTIVITY EFFECTS ON TILT-UP BUILDINGS

1. Classifying Ground Motions by Rupture Directivity

The initial phase of this part of the study was to develop a list of near-fault strong ground motion recordings, categorized into sets of records with and without significant rupture directivity effects. The records were classified into three categories: forward, backward, and neutral, based on the direction of rupture along the fault and the alignment of slip direction with source-site azimuth. Either forward or backward directivity is possible when the direction of slip on the fault is aligned with the site. Forward directivity results when the rupture propagates toward the site, whereas backward directivity occurs when the fault ruptures away from the site. Neutral directivity happens when the site is not aligned with the slip direction, so the rupture path passes by the site and creates no significant directivity effect (neither forward nor backward).

Forward directivity is commonly characterized by a single large-velocity pulse of short duration. This pulse contains most of the seismic energy radiating in the direction of rupture. Backward directivity produces motions of long duration and small amplitudes. (Somerville, et al. 1997) Consider two records from the 1992 Landers earthquake (Fig. 3-C1). The Lucerne record displays forward directivity effects, whereas the Joshua Tree exemplifies backward directivity effects.

Somerville et al. (1997) presents a procedure that allows ground motions to be classified as forward, backward, or neutral by using a “rupture directivity parameter.” The parameter is based on the angle at which the site is located from the hypocenter (dip-slip faults) or epicenter (strike-slip faults) relative to the direction of rupture propagation, as well as a measurement of how much of the fault ruptures toward the site. The records with a large value of the rupture directivity parameter exhibit forward directivity while those with zero or negative values are characteristic of backward or neutral directivity. Earthquake ground motions in the Pacific Engineering and Analysis Strong Motion Catalog (02/17/98) were considered. Only ground motion records with rupture distances of about ten kilometers or less were selected given the study on near-field effects. Additional records were added from other near-field lists (Table 8 of Somerville et al., 1997). To simplify future analysis runs, data was grouped into magnitude bins of 5.5 to 6.5, 6.5 to 7.0, and 7.0 to 7.5. Within each magnitude bin, each record was labeled and grouped as strike-slip or dip-slip. Dip-slip included normal and reverse (thrust) slip mechanisms. Oblique slip mechanisms were characterized as either strike or dip slip, depending on which mechanism was most pronounced.

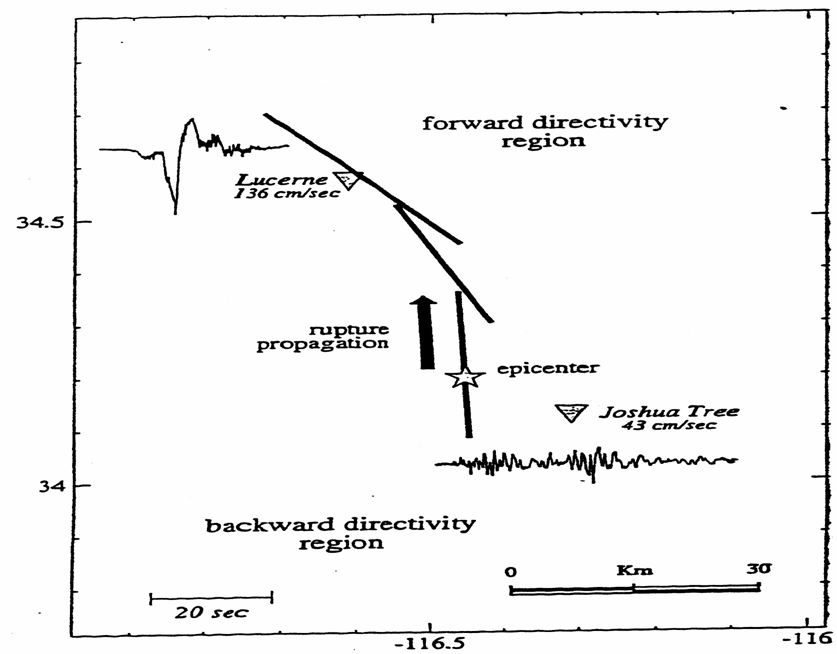

Fig. 3-C1 Map of the Landers region showing the location of the rupture of the 1992 Landers earthquake, the epicenter, and the recording stations at Lucerne and Joshua Tree (Somerville et al., 1997)

The slip mechanism classification determined the parameters and the procedure for calculating the rupture directivity parameter. The rupture directivity parameter for strike-slip cases required a length ratio, X, and an angle, θ, where X is the fraction of fault along the strike that ruptures toward the site, and θ is the angle between the fault plane and ray path from the epicenter to the site. For dip-slip cases, a width ratio, Y, and angle ϕ were used, where Y is the fraction of fault up-dip that ruptures toward the site, and ϕ is the angle between the fault plane and ray path from the hypocenter to the site.

For cases where the required parameters, X and θ or Y and ϕ, were not available (e.g., Table 8 of Somerville et al.), they were evaluated based on site location and published fault rupture models listed in Table 3-C1. The map of each fault area provided either epicenter or focus locations from which the direction of rupture propagation would be inferred, along with other necessary fault rupture information depending on the slip mechanism (Fig. 3-C2).

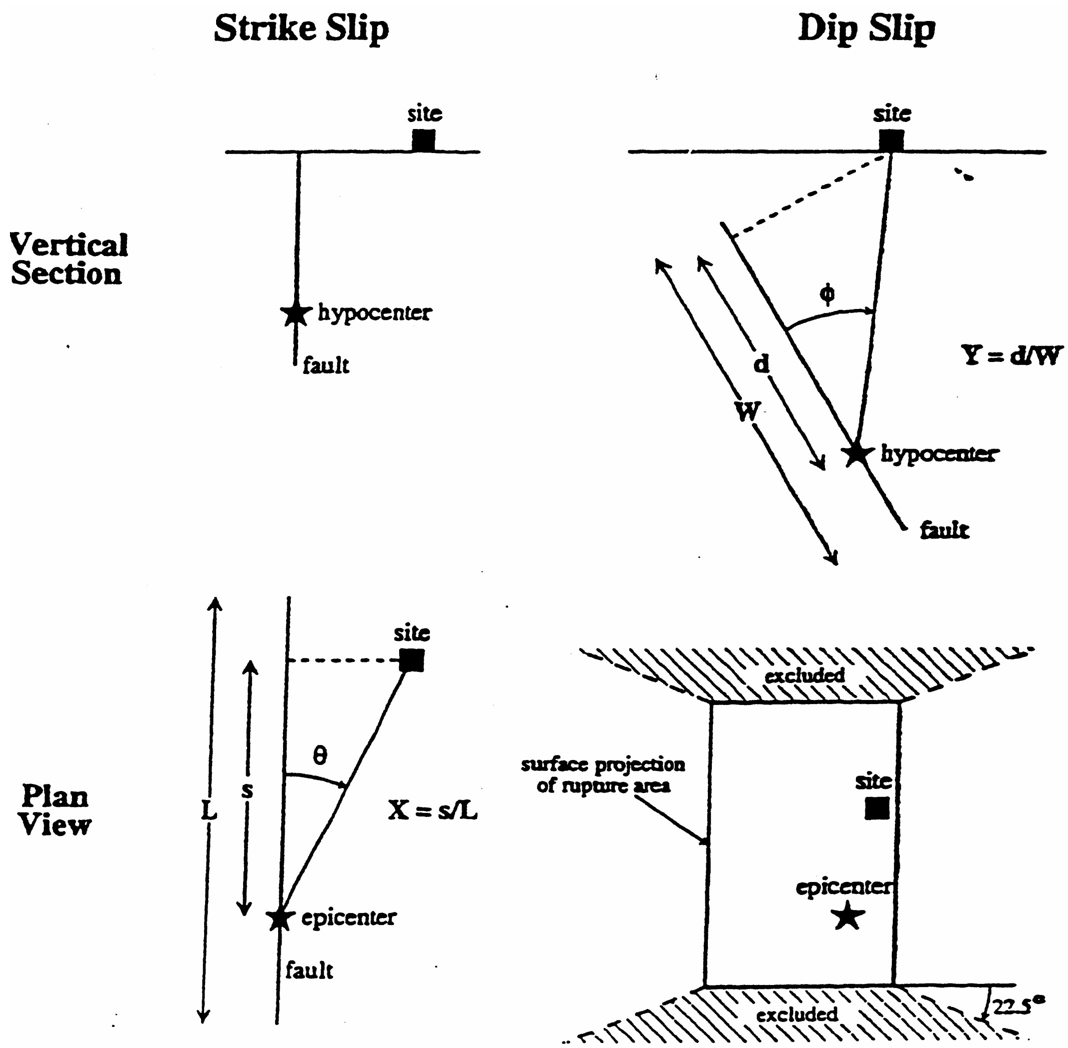

Fig. 3-C2 Definition of rupture directivity parameters X and θ for strike-slip faults and Y and ϕ for dip-slip faults, and region off the end of the dip-slip faults excluded from the model (Somerville et al., 1997)

Once all necessary geometric parameters were obtained, the rupture directivity parameters (RDP) were calculated as $X\cos\theta$ and $Y\cos\phi$ for strike-slip and dip-slip cases, respectively. The degree to which various values of those parameters can be considered representative of forward, backward or neutral rupture directivity was assessed based on empirical relations by Somerville et al. (1997). As shown in Fig. 3-C3, these relations correlate the rupture directivity parameter to period-dependant amplification or de-amplification of spectral accelerations relative to predictions from attenuation relations (e.g., Abrahamson and Silva, 1997). Based on spectral acceleration factors at T=2 seconds, spectral acceleration ratios<0.9 and >1.1 at T=2 seconds were considered representative of backward and forward directivity, respectively, with intermediate values considered to be neutral. The resulting classifications of specific ground motions as backward, forward or neutral were checked against a list compiled by Naeim and Somerville (1998).

Based on these criteria and Somerville's empirical results of Fig. 3-C3, the following values of RDP were selected for this study:

	Backward	Neutral	Forward
Strike-slip	< 0.2	0.2-0.55	> 0.55
Dip-slip	< 0.25	0.25-0.65	> 0.65

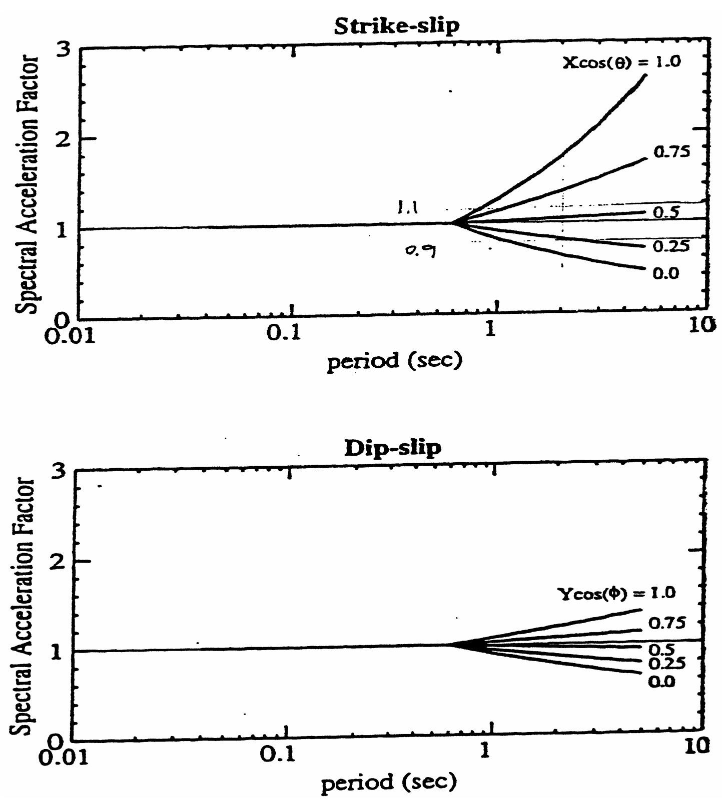

Fig. 3-C3 Empirical model of the response spectral amplitude ratio, showing its dependence on period and on the directivity functions—Xcosθ for strike-slip and Ycosϕ for dip-slip (Somerville et al., 1997)

Response histories were sorted, within each magnitude bin, by their directivity descriptor: forward (f), backward (b), and neutral (n). For cases where a discrepancy existed between the forward, backward, and neutral descriptor using the values given above and those given by Naeim and Somerville, our classification was used if the difference was due to the result of slip mechanism, and theirs was used if the cause was not apparent.

The final list of ground motions, displayed as Table 3-C1, consists of over 100 records, many of which were newly classified for this study. The additional records include measurements obtained in the following earthquakes: Parkfield 1966, Coyote Lake 1979, Coalinga 1983, Chalfant Valley 1986, Superstition Hills 1987, Whittier Narrows 1987, and Cape Mendocino 1992. Soil conditions for each site using the Geomatrix Classification System (key found at bottom of Table 3-C1) are also listed in Table 3-C1.

Records were selected from Table 3-C1 for the analysis of tilt-up buildings. From the magnitude bin 6.5 to 7.0, fifteen records with forward, five with backward, and nine with neutral directivity effects were selected. Five records with magnitudes above 7.0 were also selected. The selected ground motion records are given in Table 3-C2.

2. Influence of Directivity on Response of Tilt-up Buildings

Since the DRAIN-2DX computer program was used for the analysis, only a single horizontal component was used to assess the influence of directivity on building response. Records in Table 3-C1 were rotated, as required, to obtain fault-normal and fault-parallel components using strike angles listed in Table 3 of Somerville et al. 1997 (Appendix 3-C2), or the strike angles mentioned in CDMG or USGS strong-motion data reports. Sources of the strike angles are noted in Appendix 3-C1, which corresponds to the earthquakes in Table 3-C1.

Nineteen records were selected to assess directivity effects, ten with forward directivity and nine with backward or neutral directivity. Records were selected for magnitudes between 6.5 to 7, for short rupture distances, and for a variety of soil conditions (Table 3-C3). Only fault-normal components were used in the forward directivity group since, according to the Somerville report, the fault-normal records contributed most to directivity effects.

For response history analysis, each record was scaled to a common peak ground acceleration as indicated in column 4 (“PGA”) of Table 3-C3.

Of particular interest in this study is how directivity would influence demands on the Hollister Building diaphragm and connections between the diaphragm and tilt-up wall panels. Three beam elements for the DRAIN-2DX model (1, 4, 10, Fig. 3-C4) were selected to monitor diaphragm response. These elements were selected because an abrupt change in stiffness and strength occurred at each location due to a difference in nail spacing. The corresponding yield moments of the sections are shown in Fig. 3-C4. At the selected diaphragm locations, yield and maximum displacement, and maximum shear were obtained for each record. Connection forces and deformations were evaluated by monitoring the "internal frame springs" at the quarter- and midpoints of the diaphragm (Points A and B, respectively, Fig. 3-C4). Peak and yield forces were compared to assess the demands on the connections. Given the connection model, the ratio of maximum spring force to yield force is also equal to the ratio of maximum displacement to yield displacement.

Displacement and acceleration response relations for the internal frame springs, and shear vs. displacement hysteresis relations for the diaphragm elements were plotted for each record. From the plots, diaphragm end elements (E1-1) remained elastic for all the records, while middle- and quarter-length element joints often yielded many times. A typical relation is plotted in Fig. 3-C5. Maximum (average) element joint displacements ranged from 0.5 to 2 in. and maximum shear ranged from 80 to 180 kips. The greatest shear occurred at the diaphragm ends and greater displacement always occurred toward the middle. Capacity at yield for each of these elements, as calculated from element properties, are listed below:

Diaphragm Element	E1-1	E1-4	E1-10
Yield Force (kips)	214	105	68
Yield Displacement (in)	0.867	0.3355	0.3355

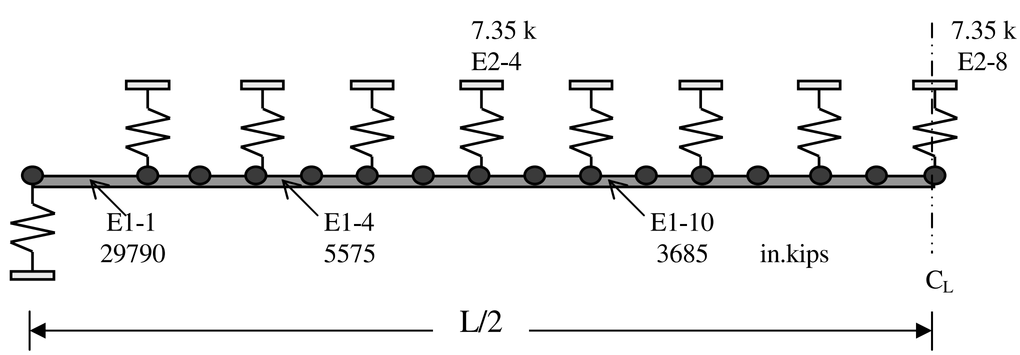

Fig. 3-C4 Tilt-up building model— elements and yield forces

In the internal frame springs, peak forces were 8 to 11 kips, with greater force in the middle spring. The yield force for all of the springs is 7.35 kips. Therefore, inelastic connection behavior is expected. Table 3-C4 presents average forces and displacements for the forward and backward/neutral directivity records, along with the standard deviation and the ratio of maximum force and displacement to the yield value.

In comparing forward and backward/neutral directivity, it was observed that earthquake records with forward directivity caused higher maximum forces and displacements for all elements than did the earthquake records with backward/neutral directivity. On average, forward directivity led to maximum spring forces 9% and 16% greater than backward/neutral directivity for the element at quarter-length (E2-4) and at mid-length (E2-8), respectively. For the diaphragm, a greater discrepancy was observed: 29% higher at the end (E1-1), 60% higher at the change in nailing (E1-4), and 40% higher at the midpoint (E1-10). A more detailed quantitative comparison is shown in Table 3-C5.

TABLE 3-C1: GROUND MOTION CHARACTERISTICS AND RUPTURE DIRECTIVITY PARAMETERS

Location	Year	Date	Time	Mag	Mech.	Record	Station	R. Dist	Soil	X	θ	Y	φ	Source	ss / ds	RDP	direct.	Somer.
Imperial Valley	1940	519	437	7		0USGS	117 El Centro Array #9	8.3	D	0.15	19.17	0.53	19.24		ss	0.14	b	*
Parkfield	1966	628	426	6.1		0CDMG	1015 Cholame #8	9.2	B	0.68	16.48	0.77	38.85		ss	0.65	f	*
Parkfield	1966	628	426	6.1		0CDMG	1014 Cholame #5	5.3	C	0.67	7.93	0.77	20.49		ss	0.66	f	*
Parkfield	1966	628	426	6.1		0CDMG	1013 Cholame #2	0.1	D	0.66	0.003			1	ss	0.66	f	
Parkfield	1966	628	426	6.1		0CDMG	1438 Temblor pre-1969	9.9	A	0.83	11			1	ss	0.81	f	
Parkfield	1966	628	426	6.1			097 Temblor, CA, Station 2	4.4	HR	0.66	9.47	0.77	23.89		ss	0.65	f	*
San Fernando	1971	209	1400	6.6		2CDMG	279 Pacoima Dam	2.8	B	0.17	69.62	0.67	10.71		ds	0.66	f	*
Gazli, USSR	1976	517		6.8		2	9201 Karakyr	3	A	0.16	5.08	0.66	48.86		ds	0.43	n	*
Tabas, Iran	1978	916		7.4		2	9101 Tabas	3	B	0.59	11.46	0.26	3.01		ds	0.26	n	*
Coyote Lake	1979	806	1705	5.7		0CDMG	57382 Gilroy Array #4	4.5	D	0.53	20			2	ss	0.50	n	
Coyote Lake	1979	806	1705	5.7		0CDMG	57217 Coyote Lake Dam (SW Abut)	3.2	A	0.08	40			2	ss	0.06	b	
Coyote Lake	1979	806	1705	5.7		0CDMG	47379 Gilroy Array #1	9.3	A	0.5	40			2	ss	0.38	n	
Coyote Lake	1979	806	1705	5.7		0CDMG	47381 Gilroy Array #3	6	D	0.5	28			2	ss	0.44	n	
Coyote Lake	1979	806	1705	6.5		0CDMG	47380 Gilroy Array #2	7.5	D	0.5	35			2	ss	0.41	n	
Imperial Valley	1979	1015	2316	6.5		0CDMG	5155 EC Meloland Overpass FF	0.5	D	0.55	1			2	ss	0.55	f	*
Imperial Valley	1979	1015	2316	6.5		0USGS	5028 El Centro Array #7	0.6	D	0.66	0.37	0.88	0.94		ss	0.66	f	*
Imperial Valley	1979	1015	2316	6.5		0USGS	5054 Bonds Corner	2.5	D	0.13	25.53	0.88	13.08		ss	0.12	b	*
Imperial Valley	1979	1015	2316	6.5		0USGS	5055 Holtville Post Office	7.5	D	0.45	22.52	0.88	35.38		ss	0.42	n	*
Imperial Valley	1979	1015	2316	6.5		0USGS	412 El Centro Array #10	8.6	D	0.64	17.42	0.88	37.3		ss	0.61	f	*
Imperial Valley	1979	1015	2316	6.5		0USGS	5053 Calexico Fire Station	10.6	D	0.3	40.61	0.88	43.97		ss	0.23	n	*
Imperial Valley	1979	1015	2316	6.5		0UNAM/UCSD	6616 Aeropuerto Mexicali	8.5	D	0.03	19.89	0.88	2.38		ss	0.03	b	*
Imperial Valley	1979	1015	2316	6.5		0UNAM/UCSD	6619 SAHOP Casa Flores	11.1	C	0.11	66.27	0.88	42.77		ss	0.04	b	*
Imperial Valley	1979	1015	2316	6.5		0USGS	952 El Centro Array #5	1	D	0.69	8.43	0.88	21.21		ss	0.68	f	*
Imperial Valley	1979	1015	2316	6.5		0USGS	955 El Centro Array #4	4.2	D	0.63	15.63	0.88	33.91		ss	0.61	f	*
Imperial Valley	1979	1015	2316	6.5		0USGS	5165 El Centro Differential Array	5.3	D	0.65	11.18	0.88	26.19		ss	0.64	f	*
Imperial Valley	1979	1015	2316	6.5		0	6618 Agrarias	0.8	SL	0.08	13.26	0.88	4.12		ss	0.08	b	*
Imperial Valley	1979	1015	2316	6.5		0	942 El Centro Array #6, Huston Rd.	1.2	D	0.67	2.65	0.88	6.75		ss	0.67	f	*
Imperial Valley	1979	1015	2316	6.5		0	958 El Centro Array #8, Cruickshank Rd.	3.8	SL	0.66	8.07	0.88	19.66		ss	0.65	f	*
Imperial Valley	1979	1015	2316	6.5		0	6622 Compuertas	4.5	SL	0.15	37	0.88	23.07		ss	0.12	b	*
Imperial Valley	1979	1015	2316	6.5		0	9301 El Centro Differential Array 1	5.5	SL	0.65	11.18	0.88	26.19		ss	0.64	f	*
Imperial Valley	1979	1015	2316	6.5		0	9302 El Centro Differential Array 2	5.5	SL	0.65	11.18	0.88	26.19		ss	0.64	f	*
Imperial Valley	1979	1015	2316	6.5		0	9304 El Centro Differential Array 3	5.4	SL	0.65	11.18	0.88	26.19		ss	0.64	f	*
Imperial Valley	1979	1015	2316	6.5		0	9305 El Centro Differential Array 4	5.2	SL	0.65	11.18	0.88	26.19		ss	0.64	f	*
Imperial Valley	1979	1015	2316	6.5		0	9306 El Centro Differential Array 5	5.1	SL	0.65	11.18	0.88	26.19		ss	0.64	f	*

Imperial Valley	1979	1015	2316	6.5	0	335 Imperial County FF	7.4	SL	0.67	15.45	0.88	35.27		ss	0.65	f	*
Mammoth Lakes	1980	525	1634	6.3	3CDMG	54099 Convict Creek	9	D	mult. fault planes, ss and ds, no clear expression of directivity, source:3								
Coalinga	1983	502	2342	6.4	3USGS	1162 Pleasant Valley P.P. - yard	8.5	D			0.54	13	4	ds	0.53	n	
Morgan Hill	1984	424	2115	6.2	0USGS	1652 Anderson Dam (Downstream)	2.6	D	0.57	7	0.7	14.69		ss	0.57	f	*
Morgan Hill	1984	424	2115	6.2	0CDMG	57217 Coyote Lake Dam (SW Abut)	0.1	A	0.82	6.33	0.7	18.8		ss	0.82	f	*
Morgan Hill	1984	424	2115	6.2	0CDMG	57191 Halls Valley	3.4	C	0.06	9.35	0.7	2.68		ss	0.06	b	*
Nahanni, Canada	1985	1223		6.8	3	6097 Site 1	6	A	0.04	75.59	0.45	25.29		ds	0.41	n	*
Nahanni, Canada	1985	1223		6.8	3	6098 Site 2	8	A	0.09	44.22	0.33	38.24		ds	0.26	n	*
N. Palm Springs	1986	708	920	6	3USGS	5072 Whitewater Trout Farm	7.3	C	0.18	30.76	0.63	31.78		ss	0.15	b	f
N. Palm Springs	1986	708	920	6	3USGS	5071 Morongo Valley	10.1	C					5	ss	--	n	
N. Palm Springs	1986	708	920	6	3USGS	5070 North Palm Springs	8.2	D	0.36	37.99	0.64	14.41		ss	0.28	n	f
N. Palm Springs	1986	708	920	6	3USGS	5073 Cabazon	16.3	D	0.57	45.86	0.64	6.48		ss	0.40	n	f
N. Palm Springs	1986	708	920	6	3CDMG	12149 Desert Hot Springs	8	D	0.43	7.57	0.58	37.27		ss	0.43	n	*
N. Palm Springs	1986	708	920	6	3	5997 Devers Hill Substation	4.1	SL	0.21	52.6	0.64	14.95		ss	0.13	b	f
N. Palm Springs	1986	708	920	6	3	12025 Palm Springs Airport	9.6	SL	0.43	45.72	0.64	10.08		ss	0.30	n	f
Chalfant Valley	1986	721	1442	6.2	0CDMG	54171 Bishop - LADWP South St	9.2	D	0.45	10			6	ss	0.44	n	
Superstition Hills	1987	1124	1316	6.7	0USGS	286 Superstition Mtn.	4.3	A					7	ss	--	n	
Superstition Hills	1987	1124	1316	6.7	0USGS	5051 Parachute Test site	0.7	D					7	ss	--	f	
Whittier Narrows	1987	1001	1442	6	2USC	90019 San Gabriel - E Grand Av #	9	A			0.34	78	8	ds	0.07	b	
Whittier Narrows	1987	1001	1442	6	2USC	90094 Bell Gardens - Jaboneria #	9.8	D			0.5	29	8	ds	0.44	n	
Whittier Narrows	1987	1001	1442	6	2USC	90066 El Monte - Fairview Av #	9.8	D			0.2	83	8	ds	0.02	b	
Loma Prieta	1989	1018	5	6.9	3CDMG	47006 Gilroy - Gavilan Coll.	11.6	B	0.5	23.21	0.83	10.79		ss	0.46	n	*
Loma Prieta	1989	1018	5	6.9	3CDMG	57007 Corralitos	5.1	B	0.12	44.03	0.83	5.85		ss	0.09	b	*
Loma Prieta	1989	1018	5	6.9	3CDMG	58065 Saratoga - Aloha Ave	13	D	0.5	22.76	0.83	9.18		ss	0.46	n	f*
Loma Prieta	1989	1018	5	6.9	3CDMG	47379 Gilroy Array #1	11.2	A	0.5	23.02	0.83	10.3		ss	0.46	n	*
Loma Prieta	1989	1018	5	6.9	3	57180 Lexington Dam (left abutmnt)	6.3	B	0.4	33.24	0.83	8.79		ss	0.33	n	f*
Loma Prieta	1989	1018	5	6.9	3	Los Gatos Presentation Center	3.5	A	0.45	13.88	0.83	6.72		ss	0.44	n	f*
Erzican, Turkey	1992	313		6.8		95 Erzican	0	D (?)	0.33	9.65	0.84	3		ss	0.33	n	f*
Landers	1992	628	1158	7.3	0CDMG	22170 Joshua Tree #	11.6	C	0.1	45	0.47	37.09		ss	0.07	b	*
Landers	1992	628	1158	7.3		Lucerne Valley	1.1	A	0.6	5	0.47	0.63		ss	0.60	f	*
Cape Mendocino	1992	425	1806	7.1	2CDMG	89005 Cape Mendocino #	8.5	A					9	ds	--	n	
Cape Mendocino	1992	425	1806	7.1	2CDMG	89156 Petrolia #	9.5	D					9	ds	--	b	
Northridge	1994	117	1231	6.7	2CDMG	24207 Pacoima Dam (upper left) #	8	A	0.19	77.27	0.85	3.03	10	ds	0.85	f	
Northridge	1994	117	1231	6.7	2USGS	00000 LA Dam	2.6	B	0.1	80	0.85	15.1	10	ds	0.82	f	
Northridge	1994	117	1231	6.7		5968 Rinaldi Receiving Station FF	7.1	C	0.06	83.54	0.85	20.61		ds	0.80	f	*
Northridge	1994	117	1231	6.7		6273 Sylmar Converter Sta E FF	6.1	SL	0.08	83.09	0.85	14.94		ds	0.82	f	*

Northridge	1994	117	1231	6.7		306 Sylmar Converter Station FF	6.2	SL	0.12	79.31	0.85	16.23		ds	0.82	f	*
Northridge	1994	117	1231	6.7	2USGS	0655 Jensen Filter Plant #	6.2	D	0.13	79.11	0.85	16.02		ds	0.82	f	*
Northridge	1994	117	1231	6.7	2USGS	0637 Sepulveda VA #	8.9	D	0.17	66.34	0.79	28.62		ds	0.69	f	*
Northridge	1994	117	1231	6.7	2CDMG	24207 Pacoima Dam (downstr) #	8	B	0.19	77.27	0.85	3.03		ds	0.85	f	*
Northridge	1994	117	1231	6.7	2CDMG	24088 Pacoima Kagel Canyon #	8.2	B	0.19	61.09	0.85	8.64		ds	0.84	f	n*
Northridge	1994	117	1231	6.7	2CDMG	24514 Sylmar - Olive View Med FF #	6.4	D	0.05	87.02	0.85	8.38		ds	0.84	f	*
Northridge	1994	117	1231	6.7	2CDMG	24279 Newhall - Fire Sta #	7.1	D	0.54	59.89	0.85	6.01		ds	0.85	f	*
Northridge	1994	117	1231	6.7	2CDMG	24087 Arleta - Nordhoff Fire Sta #	9.2	D	0.19	47.74	0.81	26.58		ds	0.72	f	n*
Northridge	1994	117	1231	6.7	2	5356 Newhall, 26835 Pico Cyn. Bl.	7.2	SL	0.81	37.08	0.85	13.62	10	ds	0.83	f	
Kobe	1995	116	2046	6.9	0CEOR	0 Kobe University	0.2	A	0.41	9.74	0.79	19		ss	0.40	n	f*
Kobe	1995	116	2046	6.9	0	0 KJMA (Kobe)	0.6	B	0.3	11.28	0.79	16.84		ss	0.29	n	f*
Kobe	1995	116	2046	6.9	0CUE	0 Takatori	0.3	E	0.2	19.14	0.79	18.95		ss	0.19	b	f*
Kobe	1995	116	2046	6.9	0CEOR	0 Port Island (0 m)	2.5	E	0.31	20.18	0.79	26.71		ss	0.29	n	f*
Kobe	1995	116	2046	6.9	0	0 OSAJ	8.5	E	0.67	32.3	0.7	61.3		ss	0.57	f	f*

GEOMATRIX CLASSIFICATION SYSTEM OF SUBSURFACE CHARACTERISTICS
A = Rock. Instrument on rock (Vs > 600 mps) or <5m of soil over rock.
B = Shallow (stiff) soil. Instrument on/in soil profile up to 20 m thick overlying rock.
C = Deep narrow soil. Instrument on/in soil profile at least 20m thick overlying rock, in a narrow canyon or valley no more than several km wide.
D = Deep broad soil. Instrument on/in soil profile at least 20m thick overlying rock, in a broad valley.
E = Soft deep soil. Instrument on/in deep soil profile with average Vs < 150 mps.

* = same as on Somerville list,
used Somerville's when preceeded by letter

TABLE 3-C2: LIST OF GROUND MOTION RECORDS FOR FUTURE STUDIES

CATEGORIZED BY MAGNITUDE AND DIRECTIVITY

Year	Earthquake	Source	Station No.	Station Name	Mag.	Fault Mech.	Rup. Dist. (km)	Soil Type
M = ~6.5 - ~7.0								
Forward Directivity								
1971	San Fernando	CDMG	279	Pacoima Dam	6.6	th	2.8	B
1979	Imperial Valley	USGS	952	El Centro Array #5	6.5	ss	1	D
1979	Imperial Valley	USGS	5158	El Centro Array #6	6.5	ss	1	D
1979	Imperial Valley			El Centro: Meloland Overpass	6.5	ss	0.5	D
1987	Superstition Hills	USGS	5051	Parachute Test Site	6.7	ss	0.7	D
1989	Loma Prieta	CDMG	58065	Saratoga: Aloha Ave.	6.9	ob	13	D
1989	Loma Prieta		57180	Lexington Dam	6.9	ob	6.3	B
1989	Loma Prieta			Los Gatos Presentation Center	6.9	ob	3.5	A
1992	Erzican, Turkey		9401	Erzican, Turkey	6.7	ss	2	D(?)
1994	Northridge	CDMG	24514	Sylmar: Olive View Medical Center	6.7	th	6.4	D
1994	Northridge	CDMG	24279	Newhall Fire Station	6.7	th	7.1	D
1994	Northridge		5968	Rinaldi	6.7	th	7.1	C
1995	Kobe		0	JMA	6.9	ss	0.6	B
1995	Kobe	CEOR	0	Kobe University	6.9	ss	0.2	A
1995	Kobe	CUE	0	Takatori	6.9	ss	0.3	E
Backward Directivity								
1940	Imperial Valley	USGS	117	El Centro Array #9	7	ss	8.3	D
1979	Imperial Valley	USGS	5054	Bonds	6.5	ss	2.5	D
1979	Imperial Valley	UNAM	6616	Aeropuerto	6.5	ss	8.5	C
1979	Imperial Valley		6618	Agrarias	6.5	ss	0.8	D
1989	Loma Prieta	CDMG	57007	Corralitos	6.9	ob	5.1	B
Neutral								
1976	Gazli, USSR		9201	Karakyr	6.8	th	3*	A
1979	Imperial Valley	USGS	5055	Holtville Post Office	6.5	ss	7.5	D
1985	Nahanni, Canada		6097	Site 1	6.8	ds	6	A
1985	Nahanni, Canada		6098	Site 2	6.8	ds	8	A

1987	Superstition Hills	USGS	286	Superstition Mountain	6.7	ss	4.3	A
1989	Loma Prieta	CDMG	47006	Gilroy: Gavilan College	6.9	ob	6.1	A
1989	Loma Prieta	CDMG	47379	Gilroy #1	6.9	ob	11.2	A
1994	Northridge	CDMG	24088	Pacoima: Kagel Canyon	6.7	th	8.2	B
1994	Northridge	CDMG	24087	Arleta	6.7	th	9.2	D
M > 7.0								
Foward Directivity								
1992	Landers			Lucerne Valley	7.3	ss	1.1	A
Backward Directivity								
1992	Cape Mendocino	CDMG	89156	Petrolia	7.1	th	9.5	D
1992	Landers	CDMG	22170	Joshua Tree	7.3	ss	11.6	C
Neutral								
1992	Cape Mendocino	CDMG	89005	Cape Mendocino	7.1	th	8.5	A
1978	Tabas, Iran		9101	Tabas	7.4	th	3*	B

TABLE 3-C3: GM RECORDS USED IN REPORT
WITH SCALING FACTORS AND UNIT CONVERSIONS

FILENAME	Points	EQ file	PGA (g)	Factor	Units	Unit Conv	Accn Ftr	Duration (s)	M	RD	Soil[4]
forward											
ERZI	**1038**	**ER92erzd**	0.421	1.276	cm/s^2	0.394	**0.50291**	**20.76**	6.7	2	D(?)
IVA5	**1968**	**IV79ar5d**	0.367	1.464	cm/s^2	0.394	**0.5769**	**39.36**	6.5	1	D
IVA6	**1950**	**IV79ar6d**	0.421	1.276	cm/s^2	0.394	**0.50291**	**39**	6.5	1	D
IVEM	**1995**	**IV79emod**	0.587	0.915	g	386.4	**353.729**	**39.9**	6.5	0.5	D
KOBE	**3000**	**KB95kobj**	1.09	0.493	cm/s^2	0.394	**0.19424**	**60**	6.9	0.6	B
LGPC	**1248**	**LP89lgpc**	0.626	0.858	cm/s^2	0.394	**0.33822**	**24.96**	6.9	3.5	A
NEWH	**3000**	**NR94newh**	0.723	0.743	cm/s^2	0.394	**0.29284**	**60**	6.7	7.1	D
SHPT	**1115**	**SH87ptsd**	0.35	1.535	g	386.4	**593.255**	**22.3**	6.7	0.7	D
LSTG	**1995**	**LP89stgd**	0.454	1.184	g	386.4	**457.355**	**39.9**	6.9	13	D
NSYM	**3000**	**NR94sylm**	0.732	0.734	cm/s^2	0.394	**0.28924**	**60**	6.7	6.4	D
backward/neutral											
IVBD	**1880**	**IV79bond**	0.781	0.688	cm/s^2	0.394	**0.27109**	**37.6**	6.5	2.5	D
CNS1	**1026**	**CN85st1d**	0.841	0.639	g	386.4	**246.896**	**20.52**	6.8	6	A
IVAG	**1415**	**IV79agra**	0.174	3.088	g	386.4	**1193.33**	**28.3**	6.5	0.8	D
IVHP	**1885**	**IV79hvpd**	0.242	2.221	g	386.4	**858.013**	**37.7**	6.5	7.5	D
LCLS	**1995**	**LP89clsd**	0.587	0.915	g	386.4	**353.729**	**39.9**	6.9	5.1	B
LGIL	**1998**	**LP89gild**	0.438	1.227	g	386.4	**474.062**	**39.96**	6.9	6.1	A
NRAL	**3000**	**NR94nord**	0.237	2.267	cm/s^2	0.394	**0.89335**	**60**	6.7	9.2	D
NPKC	**2000**	**NR94pkcd**	0.509	1.056	g	386.4	**407.935**	**40**	6.7	8.2	B
SHSM	**1110**	**SH87supd**	0.63	0.853	g	386.4	**329.586**	**22.2**	6.7	4.3	A
			avg=0.53737								

TABLE 3-C4: COMPARISON OF FORWARD AND BACKWARD EFFECTS IN EACH SELECTED ELEMENT WITH AVERAGES AND STANDARD OF DEVIATION

FORWARD DIRECTIVITY

EQ	**Glulam Springs**		**Diaphragm**					
element	E 2-4	E 2-8	E 1-1		E 1-4		E 1-10	
	max force (k)	max force (k)	max shear (k)	max disp (in)	max shear (k)	max disp (in)	max shear (k)	max disp (in)
ERZI	10.115	13.631	-203.43	-0.7762	-168.47	-1.5555	-105.36	-2.422
IVA5	-8.131	-9.836	161.96	0.6132	134.51	0.8586	79.195	1.3486
IVA6	-7.924	-10.088	160.013	0.6058	118.35	0.527	94.26	1.967
IVEM	-7.915	-9.391	140.67	0.5326	117.5	0.5097	87.67	1.6962
KOBE	9.61	13.035	-192.78	-0.7299	-160.7	-1.396	-102.25	-2.2947
LGPC	-9.243	12.488	-220.56	-0.8351	-156.79	-1.316	-103.47	-2.3448
NEWH	8.532	-11.747	-188.12	-0.7122	-149.15	-1.159	111.19	2.6618
SHPT	-8.521	-10.9	189.94	0.7191	142.85	1.0297	99.64	2.1876
LSTG	-7.94	-9.435	168.92	0.6395	116.89	0.4971	70.72	1.0009
NSYM	-7.746	-9.148	154.84	0.5862	113.19	0.4212	95.707	1.4272
avg =	***8.57***	***10.97***	***178.123***	***0.675***	***137.84***	***0.927***	***94.946***	***1.9351***
stdev =	**0.81923**	**1.64962**	**24.7532**	**0.09443**	**20.6131**	**0.42297**	**12.514**	**0.54353**
yield force =	7.35	7.35	228.93	0.86676	109.015	0.33552	54.507	0.33552
Fmax/Fy =	1.16567	1.4925	0.77807	0.77874	1.26441	2.76282	1.7419	5.76741

BACKWARD/NEUTRAL DIRECTIVITY

	max force (k)	max force (k)	max shear (k)	max disp (in)	max shear (k)	max disp (in)	max shear (k)	max disp (in)
IVBD	-7.779	8.795	-145.79	-0.552	114.26	0.4431	-72.38	-1.0689
CNS1	-7.4833	8.175	-106.61	-0.4036	93.37	0.2874	60.54	0.583
IVAG	8.88	10.79	-203.48	-0.7704	-159.64	-1.3743	94.71	1.9855
IVHP	7.72	10.002	-145.63	-0.5514	-109.97	-0.355	-88.05	-1.7121
LCLS	-8.213	-9.935	176.32	0.6676	137.96	0.9294	91.7	1.8616
LGIL	7.37	7.875	-78.85	-0.2985	-80.84	-0.2488	-54.43	-0.3351
NRAL	-8.13	-10.382	142.43	0.5393	128.61	0.7377	95.71	2.0262
NPKC	8.418	10.761	-181.27	-0.6862	-138.38	-0.938	-102.22	-2.2936
SHSM	-7.146	8.288	102.72	0.3889	-76.47	-0.3407	-64.47	-0.7444
avg =	***7.90437***	***9.4448***	***138.348***	***0.5238***	***112.693***	***0.6283***	***80.468***	***1.4012***
stdev =	**0.55334**	**1.16233**	**41.4491**	**0.15693**	**28.8522**	**0.38843**	**17.637**	**0.72326**
yield f (disp) =	7.35	7.35	228.93	0.86676	109.015	0.33552	54.507	0.33552
Fmax/Fy =	1.07542	1.285	0.60432	0.60431	1.03373	1.87252	1.4763	4.17607

TABLE 3-C5: COMPARISON OF FORWARD AND BACKWARD EFFECTS BY PERCENTAGE

Glulam Spring

	Max Spring Force (k)	Fmax/Fyield	Max Displacement (in)	FD % > B/ND
element 2-4				
forward directivity	8.568	1.1657	1.6717	9.26%
backward/neutral	7.866	1.0702	1.53	
element 2-8				
forward directivity	10.970	1.4925	2.1404	16.14%
backward/neutral	9.445	1.285	1.8429	

Diaphragm

	Max Shear Force (k)	Vmax/Vy	Max Displacement (in)	dmax/dy	
element 1-1					
forward	178.123	0.77807	0.67498	0.77874	28.62%
backward/neutral	138.606	0.60545	0.52477	0.60544	
element 1-4					
forward	137.840	1.26441	0.92698	2.76282	59.38%
backward/neutral	113.227	1.03863	0.58163	1.73353	
element 1-10					
forward	94.946	1.74191	1.93508	5.76741	39.94%
backward/neutral	80.020	1.46807	1.382778	4.1213	

LOMA PRIETA - LOS GATOS PRES. CTR.

Roof Diaphragm Element 1-1

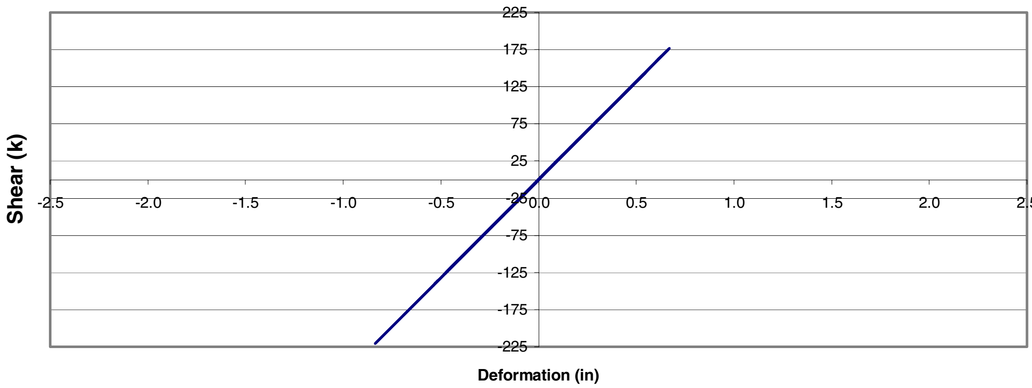

Roof Diaphragm Element 1-4 (27)

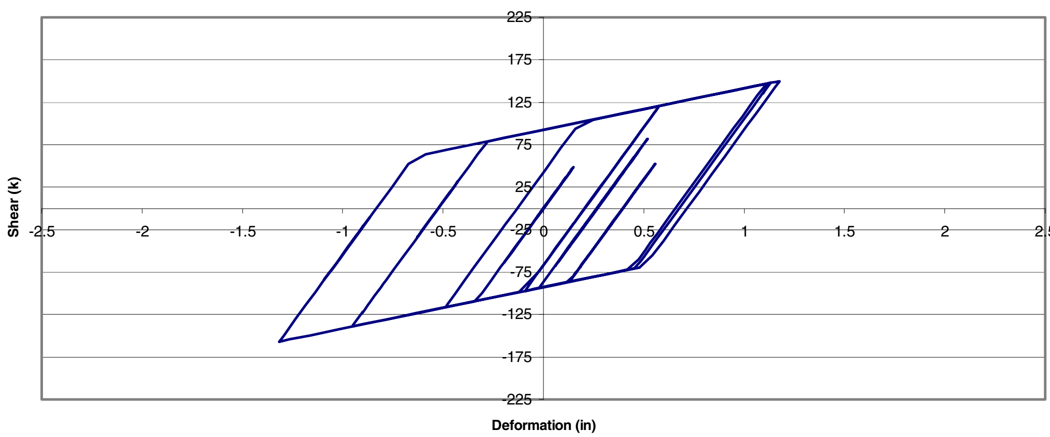

Roof Diaphragm Element 1-10 (21)

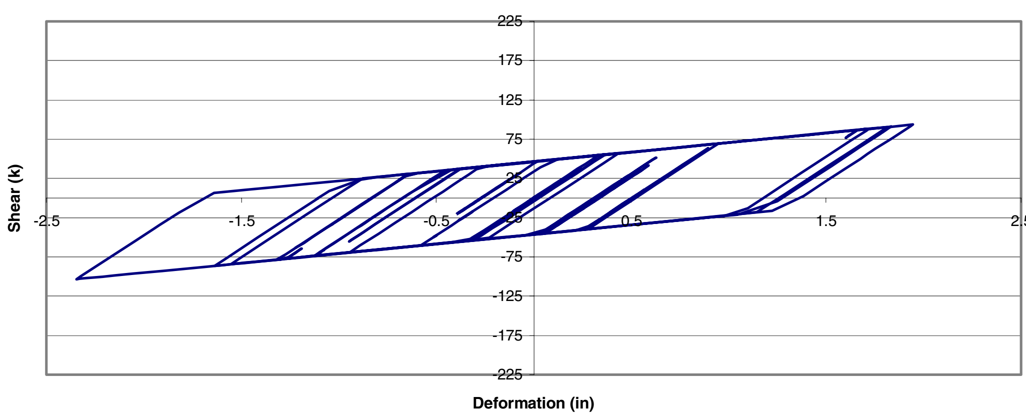

Fig. 3-C5: Shear vs. Deformation

Appendix 3-C1

Sources for Rupture Directivity Parameters and Strike and Dip Angles
in Table A which were not on the Somerville, et al. list.

1. Parkfield 1966

Archuleta, R. J.; Day, S. M. "Dynamic rupture in a layered medium: the 1966 Parkfield earthquake," *Bulletin of the Seismological Society of America*, 70, 3, June 1980, pages 671-689.

Shoja-Taheri, J. "Parkfield, California, earthquake of June 1966: interpretation of the strong motion records," *Earthquake Engineering & Structural Dynamics*, 8, 6, Nov.-Dec. 1980, pages 527-544.

2. Coyote Lake, 1979

Brady, A. G.; et al., Processed Data From the Gilroy Array and Coyote Creek Records, Coyote Lake, California Earthquake of 6 August 1979. Open File Report 81-42. U. S. Geological Survey, [Menlo Park, CA] page 2.

3. Mammoth Lakes 1980

Archuleta, R. J.; et al. "Source parameters of the 1980 Mammoth Lakes, California, Earthquake Sequence," *Journal of Geophysical Research*, 87, B6, June 10, 1982, pages 4595-4607, Paper No. 2B0360.

McJunkin, R. D.; Kaliakin, N. A., "Strong-motion records recovered from the Mammoth Lakes, California, Earthquake of 30 September 1981," California Division of Mines and Geology, Office of Strong Motion Studies, Sacramento, 1981, 22 leaves.

McJunkin, R. D.; et al. "Strong-motion records recovered from the Mammoth Lakes, California, earthquakes of 6 January 1983," OSMS Report 83-1.1 (rev.1), Office of Strong Motion Studies, California Div. of Mines and Geology, Sacramento, 1983, 31 pages.

McJunkin, R. D.; Bedrossian, T. L. "Mammoth Lakes earthquakes, May 25-27, 1980, Mono County, California," *California Geology*, 33, 9, Sept. 1980, pages 194-201

4. Coalinga, 1983

Scholl, R. E.; Stratta, J. L. "Coalinga, California Earthquake of May 2, 1983," EERI Reconnaissance Report No. 84-03, Jan 1984.

5. North Palm Springs, 1986

Huang, M. J.; et al. "Processed strong motion data from the Palm Springs earthquake of 8 July 1986: part I, ground-response records," OSMS 87-01, California Office of Strong Motion Studies, Sacramento, June 1987, 256 pages.

Hartzell, S.; Langer, C.; Mendoza, C. "Rupture histories of eastern North American earthquakes," *Bulletin of the Seismological Society of America*, 84, 6, Dec. 1994, pages 1703-1724.

6. Chalfant Valley, 1986

Bryant, W. A.; et al. "Report on the Chalfant Valley, California earthquake -- July 12, [sic] 1986," EERI Special Earthquake Report, Nov. 1986, 8 pages

Kahle, J. E.; Bryant, W. A.; Hart, E. W. "Fault rupture associated with the July 21, 1986, Chalfant Valley earthquake, Mono and Inyo counties, California," *California Geology*, 39, 11, Nov. 1986, pages 243-245

Maley, R.P.; Etheredge, E.C.; Acosta, A., U.S. Geological Survey strong-motion records from the Chalfant Valley, Open-file report (Geological Survey (U.S.)) 86-0568; Strong-motion network data report 11, U.S. Geological Survey, [Menlo Park, Calif.], 1986, 19 leaves.

7. Superstition Hills, 1987

Huang, M. J., et al., CSMIP Strong-Motion Records From the Superstition Hills, Imperial County, California Earthquakes of 23 and 24 November 1987. CSMIP Report No. OSMS 87-06. CDMG [Sacramento, Calif.], 24 December 1987.

8. Whittier Narrows, 1987

Hartzell, S.; Iida, M. "Source complexity of the 1987 Whittier Narrows, California, earthquake from the inversion of strong motion records," *Journal of Geophysical Research*, 95, B8, Aug. 10, 1990, pages 12475-12485.

Lin, J.; Stein, R. S. "Coseismic folding, earthquake recurrence, and the 1987 source mechanism at Whittier Narrows, Los Angeles Basin, California," *Journal of Geophysical Research*, 94, B7, July 10, 1989, pages 9614-9632.

Linde, A. T.; Johnston, M. J. S. "Source parameters of the October 1, 1987 Whittier Narrows earthquake from crustal deformation data," *Journal of Geophysical Research*, 94, B7, July 10, 1989, pages 9633-9643.

9. Cape Mendocino, 1992

Shakal, A., CSMIP strong-motion records from the Petrolia, California earthquakes of April 25-26, 1992, Report (California. Office of Strong Motion Records) no. OSMS 92-05, California Division of Mines and Geology, Office of Strong Motion Studies, Sacramento, Calif., 1992, 74 pages.

10. Northridge, 1994

Web site: "http://www-rcf.usc.edu/~mtodorov/USC_NOR.GIF'

APPENDIX 3-D EXAMPLE DRAIN-2DX INPUT FILE

Example input file:

```
!UNITS L in F k   [Inserted by NONLIN-Pro]
*STARTXX
    HOlfix    0    0 1 0 0           ONE STORY DIAPHRAGM AND GLULAM FRAME MODEL
!  Analysis of 1 story RC tilt-up building using Nonlinear Dynamic Procedure
!  Case Study, Inelastic diaphragm and glulam frame model
!  Hollister Building, Loma Prieta Earthquake
!  FEBRUARY  1999
!  Ayse O. Kulahci, RA, UCLA
!  John W. Wallace, Ph.D., P.E., UCLA
!  Using DRAIN version 1.10
!  Diaphragm stiffness values for s=5"
!  Fixed base
*NODECOORDS
!234567890123456789012345678901234567890123456789012345678901234567890
C    01010     -1791         0
C    01310      1791         0
C    02010     -1791       1.0
C    02310      1791       1.0
C    01020     -1512         0
C    01300      1512         0
C    02020     -1512       1.0
C    02300      1512       1.0
C    03010     -1791     -10.0
C    03310      1791     -10.0
!  Generation of remaining nodes
!2345678901234567890123456789012345678901234567890123456789001234567890
L    01020     01300     00010            0.0
L    02020     02300     00010            0.0
*RESTRAINTS
!234567890123456789012345678901234567890123456789012345678901234567890
S 101     01010     01310       300
S 101     01020     01300       010
! fix nodes for glulam springs
S 111     02010     02310       010
S 111     03010     03310       300
*MASSES
! Diaphragm mass (12 psf)*98.5ft*9ft/386.4/1000 = 0.0275
! Diaphragm mass (12 psf)*98.5ft*16.125ft/386.4/1000 = 0.0493
! Side walls (participating mass) 40%=0.0462 (Sec. 3.3)
! Side walls (participating mass) 40%=0.0766
!2345678901234567890123456789012345678901234567890123456789012345678901234567890123456789
S 010    0.3861     01010     01310      0300
.295577           :2% Rayleigh damping-1st&7th modes (Sec. 3.2)
S 010    0.1259     01020     01300      0280
.295577           :2% Rayleigh damping -1st&7th modes
S 010   0.07369     01030     01290      0010
.295577           :2% Rayleigh damping -1st&7th modes
```

```
*ELEMENTGROUP
    2    1    0      0.0007940                   BEAMS- DIAPHRAGM
!   stiffness types, ecc. types, yield surface types
    4    1    4
!   Beam section: Diaphragm properties based on UCI(1998)
!234567890123456789012345678901234567890123456789012345678901234567890123456789
0
!   #    Modulus     Harden   Area    Inertia  Kii  Kjj  Kij    Ashear Poisson
    1   10000.0      0.15   10000.0   44590.5  4.0  4.0  2.0
    2   10000.0      0.15   10000.0   5116.21  4.0  4.0  2.0
    3   10000.0      0.15   10000.0   3288.66  4.0  4.0  2.0
    4   10000.0      0.15   10000.0   2135.57  4.0  4.0  2.0
!   Eccentricity Types
!   Not used at this time
!234567890123456789012345678901234567890123456789012345678901234567890
    1       0.0       0.0       0.0       0.0
!   yield strengths
!234567890123456789012345678901234567890123456789012345678901234567890
    1    1   29791.0   29791.0
    2    1    8830.2    8830.2
    3    1    5676.0    5676.0
    4    1    3685.8    3685.8
!   element nodal assignments
!   beams
!23456789012345678901234567890123456789012345678901234567890123456789
    1     01010     01020      0010    1    0    1    1
    2     01020     01030      0010    2    0    2    2
    3     01030     01040      0010    2    0    2    2
    4     01040     01050      0010    3    0    3    3
    9     01090     01100      0010    3    0    3    3
   10     01100     01110      0010    4    0    4    4
   21     01210     01220      0010    4    0    4    4
   22     01220     01230      0010    3    0    3    3
   27     01270     01280      0010    3    0    3    3
   28     01280     01290      0010    2    0    2    2
   29     01290     01300      0010    2    0    2    2
   30     01300     01310      0010    1    0    1    1
*ELEMENTGROUP
    1    1    0      0.0007940                    INTERNAL FRAME SPRINGS
!   property types
    1
!        modulus     st-har     Area     Fyt       Fyc     Fbuck   tol
!234567890123456789012345678901234567890123456789012345678901234567890
    1     5.125      0.10       1.0      7.35      7.35    0     0.01 !
! elements
!234567890123456789012345678901234567890123456789012345678901234567890
    1     01020     02020      0020    1
   15     01300     02300              1
*ELEMENTGROUP
    1    1    0      0.0007940                      END WALL SPRINGS
!   property types
    1
!   end walls on fixed base
!        modulus     st-har     Area     Fyt       Fyc     Fbuck   tol
!234567890123456789012345678901234567890123456789012345678901234567890
    1    218167      0.10       1.0 999999999 999999999    0     0.01 !
! elements
!234567890123456789012345678901234567890123456789012345678901234567890
    1     01010     03010      0300    1
    2     01310     03310              1
```

```
*SECTION
! Section to get total force in internal frame springs
        0.                                SECTION
!
    2    1    -1512.    0
        0.         0.        0.
        0.         1.        0.
        0.         0.        0.
        0.         0.        0.
    2    2    -1296.    1
    2    3    -1080.    1
    2    4     -864.    1
    2    5     -648.    1
    2    6     -432.    1
    2    7     -216.    1
    2    8        0.    1
    2    9      216.    1
    2   10      432.    1
    2   11      648.    1
    2   12      864.    1
    2   13     1080.    1
    2   14     1296.    1
    2   15     1512.    1
*RESULTS
!  nodes (Every node - displacements and accelerations)
!234567890123456789012345678901234567890123456789012345678901234567890123456789
NSD    111     01010     01310        10
NSD    111     02010     02310        10
NSD    111     03010     03310       300
NSA    111     01010     01310        10
! all elements
E      111
! all sections
S      111
*ACCNREC
!234567890123456789012345678901234567890123456789012345678901234567890123456789
! Loma Prieta Earthquake (Acc. Ch.8, Hollister Building)
 HOLL       GRNDACE8             (8F8.3)             LOMA PRIETA EQ
 1504    8    0    1       1.0     0.394      0.02       0.0
*PARAMETERS
OS       1    1    1    1    0
OD       1         1              0      0.02    0              0
DC  1    0    0    0
*MODE
    7              0    0    0
*ACCN                                                LOMA PRIETA EQ
     30.08 1504    1      0.02
2     HOLL       1.0       1.0
*STOP
```

REFERENCES

ABK, A Joint Venture (1981). "Methodology for Mitigation of Seismic Hazards in Existing Unreinforced Masonry Buildings: Diaphragm Testing." ABK-TR-03, Agbabian Associates, El Segundo, CA.

Abrahamson N. A.; and Silva, W. J. (1997). "Equations for Estimating Horizontal Response Spectra and Peak Acceleration from Western North American Earthquakes: A Summary of Recent Work." *Seismological Research Letters*, Vol. 68,No. 1, Jan.-Feb. 1997.

Adham, S. A.; Anderson, R. W.; Kariotis, J. C.; and Al Mostafa, A. (1989). "Evaluation of Tilt-up-wall Structural Systems Affected by the Whittier Narrows Earthquake." Agbabian Associates, *Report No. R-8828-6283*. El Segundo, CA.

Alsiwat, J. M.; and Saatcioglu, M. (1992). "Reinforcement Anchorage Slip under Monotonic Loading." *Journal of Structural Engineering*, Vol. 118, No. 9, 1992, pp. 2421-2438.

Carter, J. W., III; Hawkins, N. M.; and Wood, S. L. (1993). " Seismic Response of Tilt-up Construction." Civil Engineering Studies, Structural Research Series No. 581, Dept. of Civil Engineering, University of Illinois at Urbana-Champaign, Urbana, IL.

Countryman, D.; and Colbenson, P. (1954) "Summary of 1954 Horizontal Plywood Diaphragm Tests." Douglas Fir Plywood Association. *Laboratory Report No.63*.Tacoma, WA.

Del Carlo, D.; and Pardoen, G. C. (1999). "Strength and Stiffness of Timber Connections and Diaphragms." Civil and Environmental Engineering Department, University of California, Irvine, CA.

Dolan, J. D. (1989). "The Dynamic Response of Timber Shear Walls." *Ph. D. Dissertation* submitted to the Faculty of Graduate Studies, University of British Columbia, Canada.

Ewing, R. D.; and Adham, S. A. (1985) "Guidelines for Mitigation of Seismic Hazards in Tilt-up-wall Structures- Phase 2." Agbabian Associates. *Report No. R-8216-5771*. El Segundo, CA.

Fonseca, F. S.; Wood, S. L.; and Hawkins, N. M. (1996). "Measured Response of Roof Diaphragms and Wall Panels in Tilt-up Systems Subjected to Cyclic Loading." *Earthquake Spectra,* Earthquake Engineering Research Institute, Vol.12, No.4, pp.783-802.

Fonseca, F. S. (1997). “Cyclic Loading Response of Reinforced Concrete Tilt-up Structures with Plywood Diaphragms.” *Ph. D. Dissertation* submitted to the Graduate College, University of Illinois, Urbana, IL.

Frazier, G. A.; Wood, J. H.; and Housner, G. W. (1971). “Earthquake Damage to Buildings.” *Engineering Features of the San Fernando Earthquake February 9, 1971, EERL 71-02*; P.C. Jennings, editor; Earthquake Engineering Research Laboratory, California Institute of Technology, Pasadena, CA.

Gazetas, G. (1991). “Foundation Vibrations.” *Foundation Engineering Handbook*, 2nd Edition; H. Y. Fang, editor; Van Nostrand Reinhold, New York, NY.

Hamburger, R. O.; Harris, S. K.; Martin, S. C.; McCormick, D. L.; and Somerville, P. G. (1996). “Response of Tilt-up Buildings to Seismic Demands: Observations and Case Studies From the 1994 Northridge Earthquake.” *EQE International*, Inc., San Francisco, CA.

Hawkins, N. M.; Wood, S. L.; and Black, E. (1996). “Evaluation of Repair and Rehabilitation Strategies for Tilt-up Construction.” Unpublished Report for NSF. (NSF CMS 94-146354)

Hawkins, N. M.; Wood, S. L.; and Fonseca, F. S. (1994). “Evaluation of Tilt-up Systems.” *Proceedings.* Fifth U.S. National Conference on Earthquake Engineering, Earthquake Engineering Research Institute, Vol. III, 1994, pp. 687-696.

Holmes, W. T.; and Somers, P.; technical editors (1996). “Tilt-up-wall Buildings.” *Earthquake Spectra,* Earthquake Engineering Research Institute, Supplement C to Volume 11, pp.99-123.

Huang, M. J.; Shakal, A. F.; Parke, D. L.; Sherburne, R. W.; and Nutt, R. V. (1985). “Processed Data from the Strong-Motion Records of the Morgan Hill Earthquake of 24 April 1984-Structural Response Records.” *Report No. OSMS 85-05.* California Strong Motion Instrumentation Program, California Department of Conservation, Division of Mines and Geology, Office of Strong Motion Studies, Sacramento, CA.

Mehrain, M.; and Graf, W. P. (1990). “Dynamic Analysis of Tilt-up Buildings.” *Proceedings.* Forth U.S. National Conference on Earthquake Engineering, Earthquake Engineering Research Institute, Vol. II, pp. 299-307.

Mehrain, M.; and Silver, D. (1988). “Concrete Wall Anchorage Forces in Industrial Buildings with Flexible Roof Diaphragms.” *Proceedings.* Ninth World Conference on Earthquake Engineering, Vol. V, Tokyo- Kyoto, Japan.

Naeim, F.; and Somerville, P. G. (1998). “Earthquake Records and Design.” *95% Draft EERI Monograph*, Earthquake Engineering Research Inst., Oakland, CA.

Pardoen, G. C.; Hamilton, C. H.; Del Carlo, D.; and Kazanjy, R. P. (1999). “Stiffness Properties of Large Timber Panels for Seismic Retrofit of Buildings.” Civil and Environmental Engineering Department, University of California, Irvine, CA.

Porter, M. L.; Yeomans, F. S.; and Johnson, A. W. (1990). “Assembly of Existing Diaphragm Data.” U.S-Japan Coordinated Program for Masonry Building Research Report 5.2-1, College of Engineering, Iowa State University, Ames.

Powell, G. H. (1993). “DRAIN-2DX Element Description and User Guide for Element Type01, Type02, Type04, Type06, Type09, and Type15.” *Report No.UCB/SEMM-93/18*. Department of Civil Engineering, University of California, Berkeley, CA.

Prakash, V.; Powell, G. H.; and Campbell, S. (1993). “DRAIN-2DX Base Program Descriptions and User Guide.” *Report No. UCB/SEMM-93/17*. Department of Civil Engineering, University of California, Berkeley, CA.

“Research Report 138.” (1980) American Plywood Association, Tacoma, WA.

Schnabel, P. B.; Lysmer, J.; and Seed, H. B. (1972). “SHAKE: A Computer Program for Earthquake Response Analysis of Horizontally Layered Soil Deposits.” *Report No. UCB/EERC-72/12*, Earthquake Engineering Research Center, University of California, Berkeley, CA. (1991 modifications by Idriss, I.M. and Sun, J.I.)

Somerville, P. G.; Smith; Graves, R. W.; and Abrahamson, N. A. (1997). “Modification of Empirical Strong Ground Motion Attenuation Relations to Include the Amplitude and Duration Effects of Rupture Directivity.” *Seismological Research Letters*, Vol. 68, No. 1, pages 199-222.

Stewart, J. P.; and Fenves, G. L. (1998). "System Identification for Evaluating Soil-Structure Interaction Effects in Buildings from Strong Motion Recordings." *Earthquake Engineering and Structural Dynamics*, Vol. 27, 869-885.

Stewart, J. P.; and Stewart, A. F. (1997). "Analysis of Soil-Structure Interaction Effects on Building Response from Earthquake Strong Motion Recordings, from 58 Sites." *Report No. UCB/EERC-97/01*, Earthquake Engineering Research Center, University of California, Berkeley, CA.

Uniform Building Code. (1973). International Conference of Building Officials, Whittier, CA.

Uniform Building Code. (1976). International Conference of Building Officials, Whittier, CA.

Uniform Building Code. (1991). International Conference of Building Officials, Whittier, CA.

R2. Additional References

Bouwkamp, J. G.; Hamburger, R. O.; and Gillengerten, J. D. (1994). "Degradation of Plywood Roof Diaphragms under Multiple Earthquake Loading." *Data Utilization Report CSMIP/94-02*. California Strong Motion Instrumentation Program, Sacramento, CA.

Easley, J. T.; Foomani, M.; and Dodds, R. H. (1982). "Formulas for Wood Shear Walls." *Journal of the Structural Division*, *ASCE*, 108, ST11, Nov. 1982, pages 2460-2478, Proc. Paper 17460.

Ficcadenti, S.; Steiner, M.; Pardoen, G.; and Kazanjy, R. (1998). "Cyclic Load Testing of Wood-Framed, Plywood Sheathed Shear Walls Using ASTM E564 and Three Loading Sequences." *Proceedings*, Sixth U.S. National Conference on Earthquake Engineering, Earthquake Engineering Research Inst., Oakland, CA.

Haroun, M. A.; Salama, A. E.; and Hilmy, S. I. (1994). "Retrofit of Wall-Foundation Connections of Precast R/C Tilt-Up Walls." *Proceedings*, Fifth U.S. National Conference on Earthquake Engineering, Earthquake Engineering Research Inst., Oakland, CA, Vol. III, 1994, pages 737-746.

Itani, R. Y.; and Cheung, C. K. (1984). "Nonlinear Analysis of Sheathed Wood Diaphragms." *Journal of Structural Engineering,* 110, 9, Sept. 1984, pages 2137-2147.

Johnson, M. A.; and Fonseca, F. S. (1998). "Seismic Response of Reinforced Concrete Tilt-Up Wall Panels." *Proceedings*, Sixth U.S. National Conference on Earthquake Engineering, Earthquake Engineering Research Inst., Oakland, CA.

Karacabeyli, E.; and Ceccotti, A. (1998). "Nailed Wood-Frame Shear Walls for Seismic Loads: Test Results and Design Considerations." *Structural Engineering World Wide 1998*, Paper T207-6, Elsevier Science Ltd., Oxford, England.

Mehrain, M.; and Jacobson, L. (1998). "Case Study of Diaphragm Considerations in Performance Based Design." Structural Engineering World Wide 1998 [computer file], Paper T187-5, Elsevier Science Ltd., Oxford, England.

4 Steel Reinforced Concrete Building

4.1 INTRODUCTION

The Pacific Gas and Electric Company substation, located at the corner of Hearst Avenue and McGee Street in Berkeley, California, was built in 1909. Originally, the plane dimension of this 31-ft. high, single-story, concrete and steel structure was approximately 44 ft. in the east-west direction, and 56 ft. in the north-south direction. In 1923, the building was expanded to the present configuration of 63 ft. in the east-west direction and 90 ft. in the north-south direction. Figure 4.1 presents the footprint of the original and expanded building.

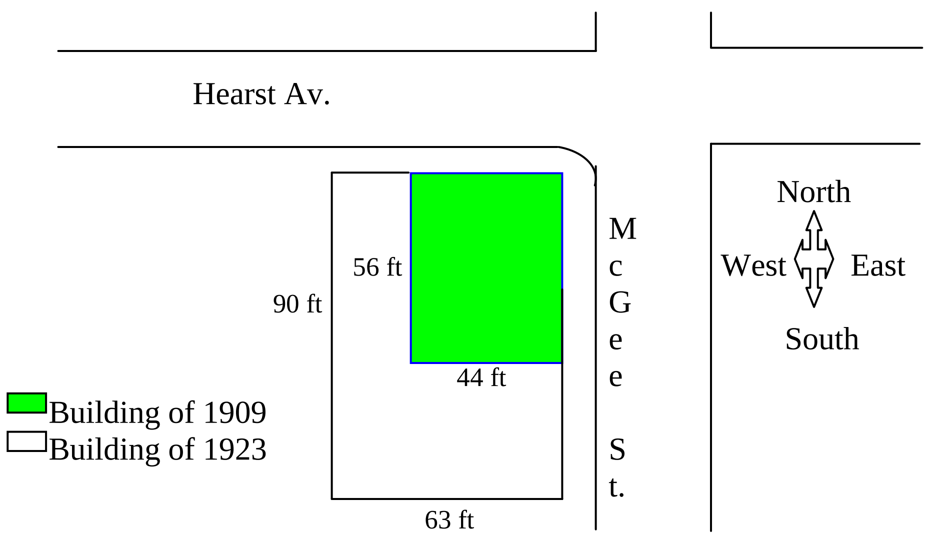

Fig. 4.1 Pacific Gas and Electric Co. building

The 1923 expansion of the building consisted of the following: (1) demolition of the original south exterior wall, (2) extension of the original north and east exterior walls, which were tied to the new south and west walls, (3) extension of the original west wall by 16 ft. in the south direction [The original west exterior wall, which remained after the expansion, will be referred to as the interior wall in this report], (4) addition of an interior wall tied to the new west wall and the southern end of the original west wall, and (5) addition of a 12.5-ft. high gallery, approximately 90 ft. (north-south) by 14 ft. (east-west), at the east side of the building. Architectural and Structural views of the building are presented in Figs. 4.2, 4.3 and 4.4. The openings of the north and east wall have all been filled in with nonstructural materials. The apparent openings in the west wall, except the one at the southern end, are actually solid reinforced concrete cast integrally with the rest of the wall.

The lateral force-resisting system of the building consists of steel moment frame and reinforced concrete shear walls (Fig. 4.3 a, b, and c), which are tied together by a reinforced concrete roof. The roof is also supported by steel trusses and built-up steel columns, which form the primary vertical load-resisting system (Fig. 4.3. b and c). Many of the steel columns are partially embedded in the reinforced concrete walls (Fig. 4.3.a).

The objective of this study is to develop a strategy for evaluating the dynamic response of the building, as well as to assess the applicability of the FEMA 273 guidelines for evaluating this type of structure. One of the major focuses is the influence of the numerous openings in the roof (Fig. 4.4) and the exterior walls (Fig. 4.2), which affect the strength and the stiffness of the structural system.

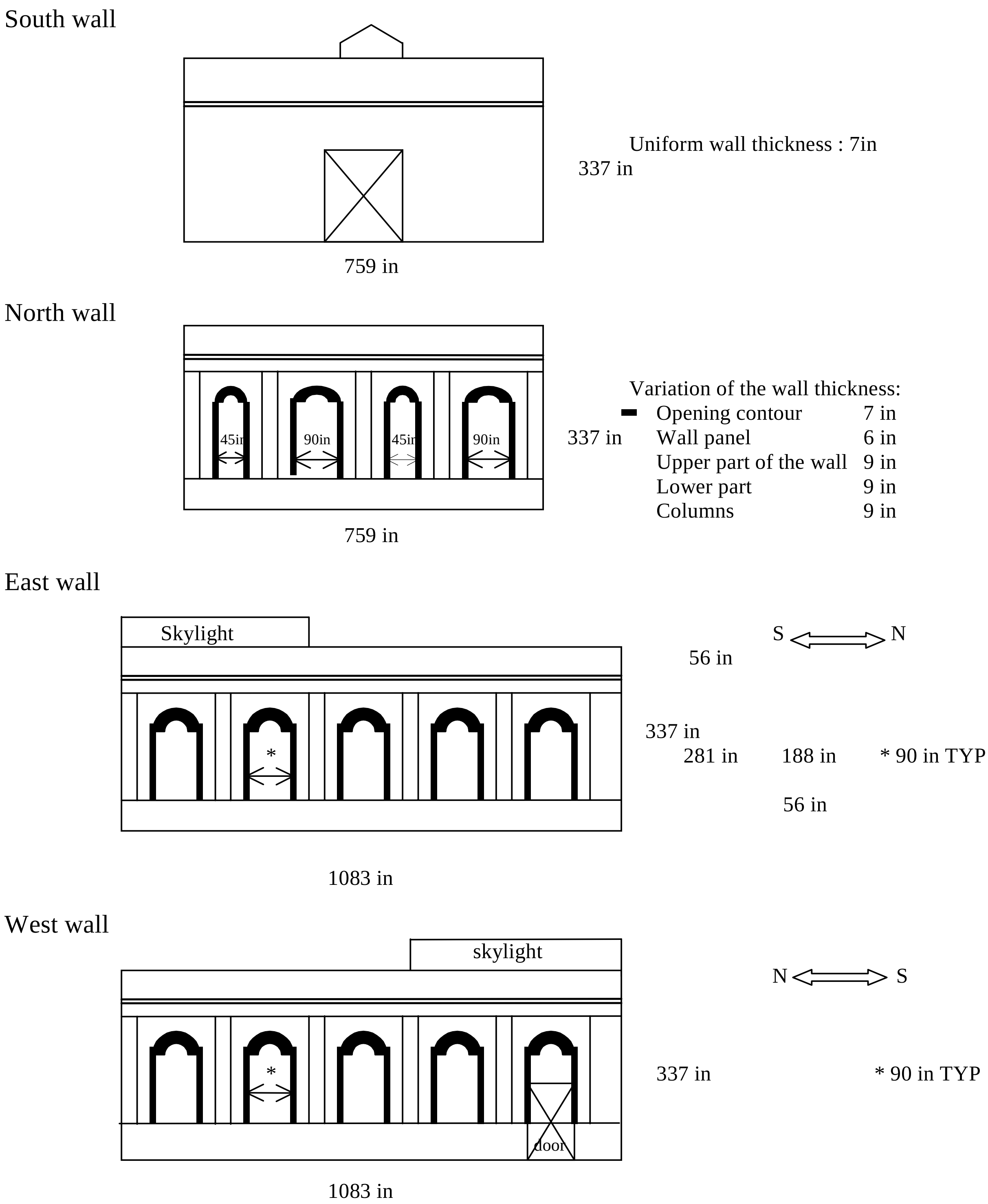

Figure 4.2 Architectural views

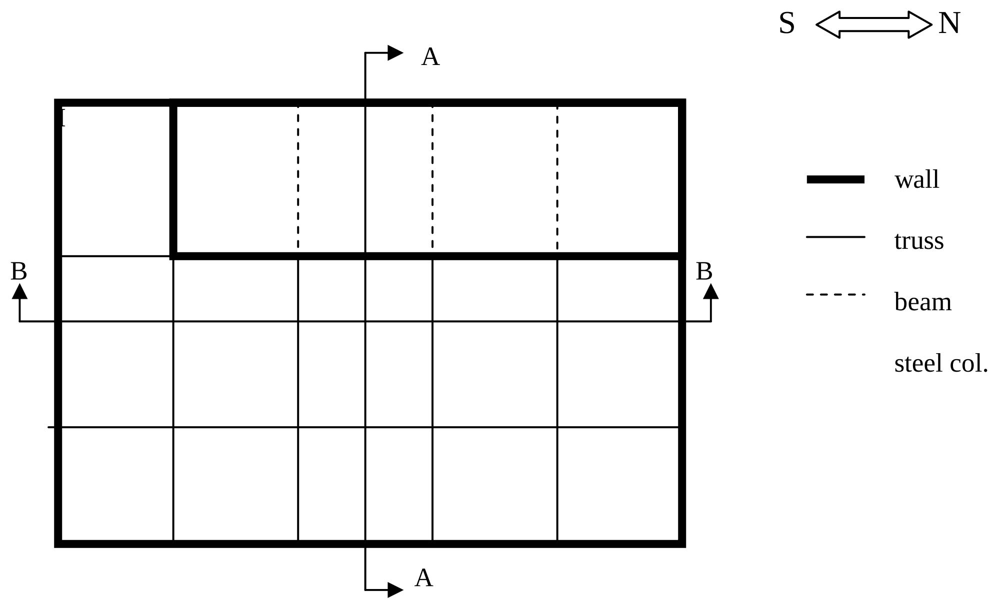

Fig. 4.3(a) Top view (cut below the roof)

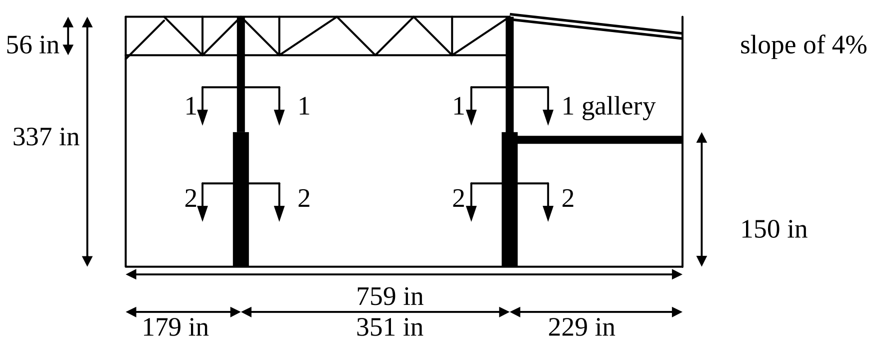

Section 1-1

Section 2-2

View of a steel column: 4 angles 4x3x5/16, web thickness : ¼ ″

Fig. 4.3(b) East-west elevation A-A

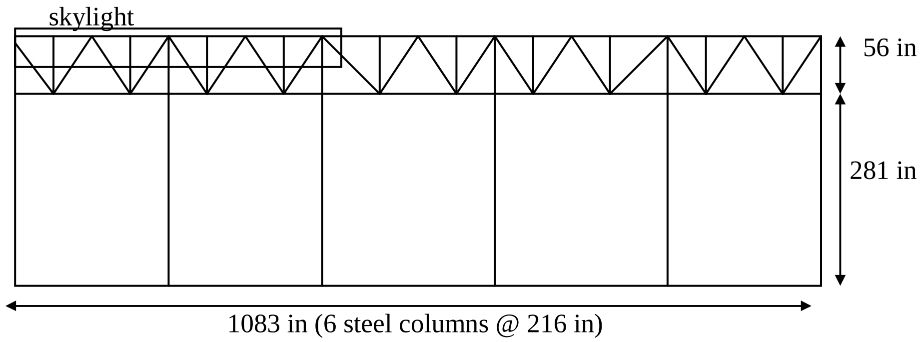

Fig. 4.3(c) North-south elevation B-B

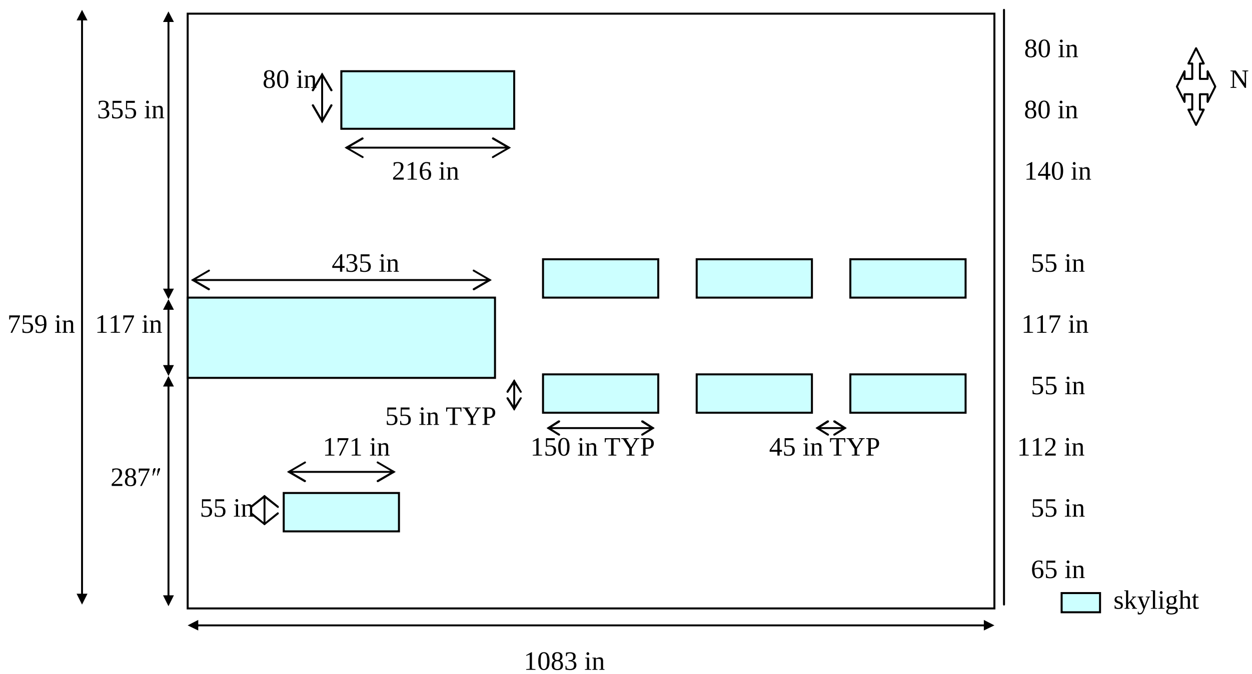

Fig. 4.4 Plan view of the roof

4.2 MODELING

A variety of structural modeling options are considered for this building, from complex linear finite element models to sophisticated frame element models. In the following sections, descriptions of the models are presented and assumptions made in their application are discussed.

4.2.1 General Assumptions

Due to the complex geometry of the building, several assumptions are made to simplify the modeling. These simplifications include:

- The relatively minor architectural features of the walls are neglected. The exterior wall thickness is varied over the wall height as noted in Fig. 4.2 for the detailed finite element model. For “simpler” models, considering a beam analogy, a uniform wall thickness of 7 in. is used for each element.
- The window openings in the walls are approximated as rectangular.
- The steel columns embedded in the wall are considered as part of the wall (Fig. 4.3a).
- The strength and stiffness of the skylight (over the opening at the south end of the roof) are neglected.
- Steel beams embedded in the roof slab are neglected (mass and stiffness).
- The trusses are considered massless.
- The roof is considered to be flat.

4.2.2 Material Properties

Both structural steel and reinforced concrete were used as construction materials. Due to a lack of material-specific data for this building, material properties representative of those commonly used at the time of the construction are assumed (Table 4.1). Sensitivity studies could be used to assess the impact of these assumptions; however, the primary focus of the project is to investigate modeling and evaluation approaches for the building. Given this focus, use of typical material properties is appropriate.

Table 4.1 Material properties

	Material Weight lb/ft3	Poisson's ratio ν	Modulus of elasticity ksi	Yield Stress ksi
Concrete	150	0.2	3600	——
Reinforcing Steel	490	0.3	29000	45
Structural Steel	490	0.3	29000	36

4.2.3 Building Lateral Strength Evaluation

The lateral strength of the building at the roof level, at the bottom of the openings (56 in. from the base of the walls), and at the base of the building for both X and Y direction (Fig. 4.5) is estimated using the wall nominal shear strength, $V_n = (2\sqrt{f_c^{'}} + \rho f_y)A_{cv}$. Calculations indicated that shear strength, versus flexural strength, is the controlling failure state for the walls. This value is compared to the weight of the structure supported. The results are presented in Table 4.2.

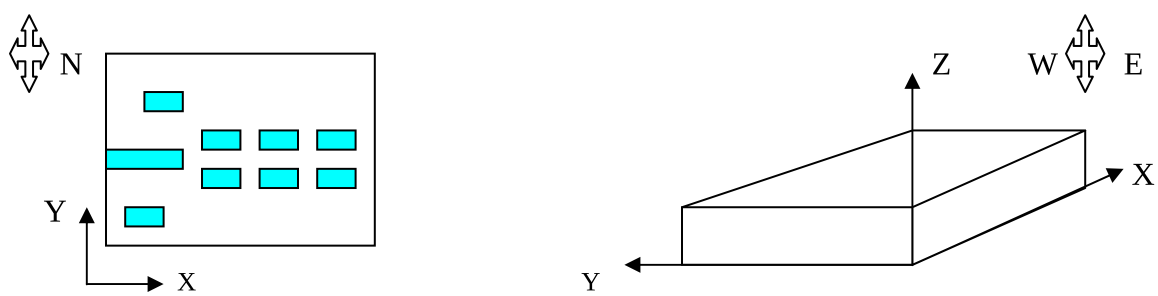

Fig. 4.5 Roof elevation and 3-D view of the building

Table 4.2: Lateral strength resistance of the structure

	Lateral strength (kips)		Weight above the	Ratio lateral strength / weight	
	X direction	Y direction	Intersection plane (kips)	X direction	Y direction
at roof level (@ 337 in)	4510	2600	214	21.1	12.2
at the bottom of openings (@56 in)	3705	1990	843	4.4	2.4
at the base (@ 0 in)	4510	2600	1255	3.64	2.1

The lateral strength capacity is at least twice the weight of the structure supported, and significantly greater than required by code (UBC 97). The flexural strength between the wall openings is estimated to be slightly higher than the shear capacity.

4.2.4 Finite Element Model

(a) Model description

Due to the relatively complex building geometry and structural system, initial modeling efforts focused on developing a fairly detailed finite element model of the building. In this model, referred to as the FE Model in this report, beams, columns and trusses are represented by frame elements, whereas walls and slabs (roof and floor) are modeled by shell elements. These shell elements include membrane and bending effects, in order to represent in-plane and out-of-plane deformations.

Three different categories of frame elements are used: a built-up I-shaped section to represent the columns (Fig. 4.3a), and single-angle and double-angle shapes to represent the truss members.

Five different shell element thicknesses are needed to describe the walls and slabs (3, 5.75, 6.5, 7.25, and 8.75 in.). The finite element mesh for the walls and slabs is defined based on the following criteria: locations of openings, connection of concrete and structural steel sections, connection between wall and slab panels, and changes in element thicknesses. The mesh used for the building is depicted in Appendix 4-A1.

(b) Analysis of the FE model

The model is analyzed for a variety of conditions to study building response characteristics. The first analysis consists of subjecting the model to gravity loads and static lateral loads at the roof level, in order to study the roof behavior. The applied lateral loads are equal to the roof masses multiplied by 1g. This is roughly consistent with using an unreduced UBC-94 spectrum for short-period buildings. The lateral acceleration is applied in the north-south direction (X global reference axis of the model) for the first analysis, and in the east-west direction (Y reference axis) for the second analysis (Fig. 4.5). The self-weight multiplier is used in SAP 2000 to generate the desired vertical and lateral loads for this condition, and a uniform load of 20 psf is assigned to the central part of the gallery slab (on an area of 20 square feet) to represent the weight of the anchored mechanical equipment. The main results obtained by analyzing this model follow:

- The fundamental period is 0.13 sec. and the associated mode shape involves out-of-plane (breathing) movement of the interior wall and roof. A summary of the 5 first modes are provided in Table 4.3. Because the periods and mode shapes involve localized breathing of wall and roof segments, the building responds quite differently than typical buildings. Three hundred modes have to be considered to obtain approximatively 90% mass participation (Appendix 4-F), although Ritz vectors could be used to reduce the number of modes required.

Table 4.3 Five first modes of the FE model

Mode number	Period (sec)	Cumulative Mass participation	
		X	Y
1	0.133	0.004	12.91
2	0.116	0.009	13.17
3	0.114	0.010	27.07
4	0.099	0.012	28.27
5	0.098	7.281	28.29

- The maximum displacements at the roof level for a 1g static load applied in each direction (Fig. 4.5) are presented in Table 4.4. The displacement values at the roof level are very small, indicating that the building is really stiff. However, due to the wall and roof "breathing", larger wall displacements will occur between the base and the top (roof level).

Table 4.4 Maximum displacements at the roof level
due to a static 1g force applied at the roof level in one direction

Load case	Displacements (in)	
	X direction	Y direction
1 g in the N-S direction	0.040	0.003
1 g in the E-W direction	0.006	0.130

- The sum of the lateral forces resisted in each wall is displayed in Table 4.5 for both loading directions with the nomenclature of Fig. 4.6. The stress is evaluated at the standard two-by-two Gauss integration points of each shell element and then extrapolated to the nodal points; therefore, a small difference exists (less than 2 %) in the total force distribution between each loading case.

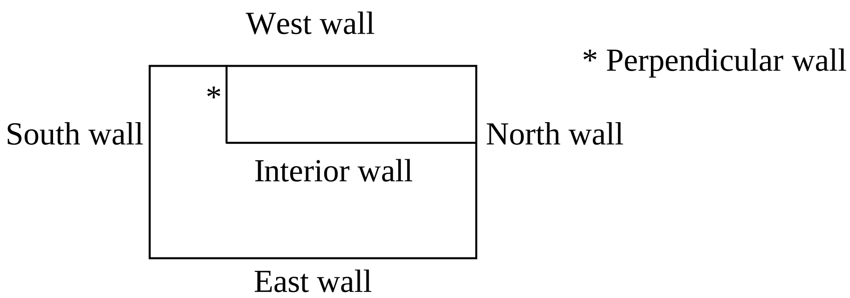

Fig. 4.6 Wall nomenclature

Table 4.5 Force distribution in each wall at the roof level for the FE model

	Force Distribution (kips)	
Walls	1 g in the N-S direction	1 g in the E-W direction
East	48	1
West	53	2
Interior	73	3
South	1	74
North	1	70
Perpendicular	1	30
Sum	177	180

- The maximum principal compressive stress at the roof level for both loading cases considered is less than 1 ksi (Appendix 4-A2), which is less than the concrete compressive strength of 4 ksi. The maximum principal tensile stress at the roof level is less than 10% of the concrete compressive strength. Given the distributed reinforcement and the embedded steel sections within the roof, adequate reinforcement exists to resist these stresses.

The static analysis was used to investigate load paths and force/stress demands within the roof (for a static lateral force equal to 1g). However, some difficulties were encountered using the FE model, such as:

- When using shell elements, the results are mesh dependent. Therefore, several meshes may be required to ensure that reasonable results are obtained (i.e., convergence is achieved).

- Due to the numerous openings, and thus the presence of stress concentration, a fine mesh is needed (in particular around the openings) to counterbalance the infinite stress developed by the program.
- The model is computationally intensive because of the use of this fine mesh; to run a response spectrum analysis can take up to eleven hours on a 300Mhz PC: therefore, it is difficult to make changes to the model and reanalyze it in a reasonable time.
- The results are somewhat difficult to review given that the principal and shear stresses must be re-evaluated each time.

Because of these limitations, a simpler model, which uses frame elements in place of shell elements to model the walls and the gallery level slab, was created.

4.2.5 Frame Element Model

(a) Model description

In the second model developed for the building (Appendix 4-B1), the walls, the gallery slab, the steel columns and trusses are modeled using frame elements. However, the roof is still modeled by shell elements to maintain continuity with the walls. As well, a simple model would be difficult to develop considering the numerous random openings. This model will be referred to as the frame element model (FR) in this report.

The finite element mesh for the roof is defined based on the location of the roof openings as well as the location of the frame elements used to model the wall panels, the steel columns and the truss elements.

The use of simple analogous frames for shear wall analysis (Stafford & Girgis, 1984) was considered. In this approach, a wall panel is modeled using frame elements as shown in Figs. 4.7(a) and (b). The geometry of the element is selected to accurately model the bending, shear and axial stiffness of the wall. Hinges are used between the elements so that flexural stiffness is not overestimated.

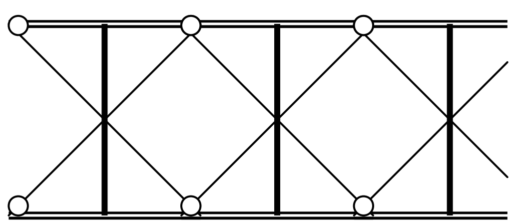

Fig. 4.7(a) Braced wide column module

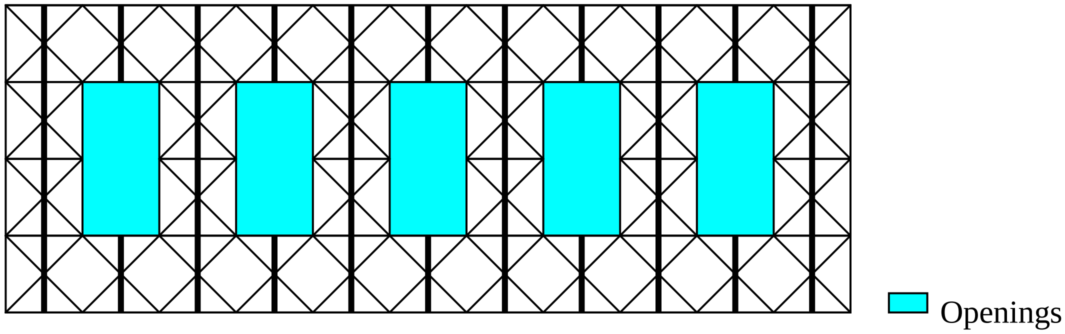

Fig. 4.7(b) Model of a wall with braced wide column module

This method was unrealistic for the building due to the large number of openings and the geometry of the building. Too many elements were required to model a wall, with more than 80 elements needed for the east wall alone. To simplify the modeling, a column analogy is used that excludes the diagonal braces (Figs. 4.7(c) and 4.11). This model is justified based on the aspect ratio of the structural wall elements between the openings, which typically have aspect ratios (height/width) greater than 1.5. For this range of aspect ratio, flexural deformations are more important than shear.

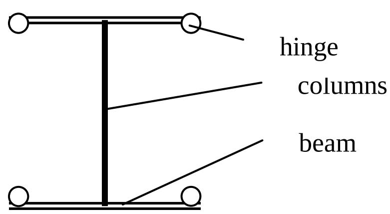

Fig. 4.7(c) Module developed for the FR model

The modeling procedure for a typical wall (west wall, Fig. 4.8) is described in greater detail as follows:

- The columns are defined by the width, thickness, and height of the wall segment considered (Fig. 4.9). Locations for frame elements modeling the side walls are selected to provide continuity for the steel columns supporting the roof trusses and the roof.
- The beams are defined using the same general approach that was used for the columns (Figs. 4.10-4.11). Three kinds of beams are defined for the north, east and west walls: the upper and lower part of the wall, where there are no openings, and the middle of the wall where openings exist.

- The moment of inertia, shear area, and axial area for the beams and columns are defined based on the cross section. This approach is similar to the strip method for slabs (Hillerborg 1956), which allows the designer, when no external load is required to be carried by torsion, to consider the slab as a composition of orthogonal strips. This approach has been verified in this report for a wall similar to the west wall (Appendix 4-C).
- The beams are generally considered massless in order not to double the mass of the wall. This assumption is part of the model evaluation process presented in Appendix 4-C. The mass of the beam is included only where the beam is located above or below an opening.
- Massless short frame elements (Fig. 4.11) are also used to connect the shell elements modeling the roof with the horizontal beam near the top of the wall. Without this element, the wall and roof could separate between the vertical columns.

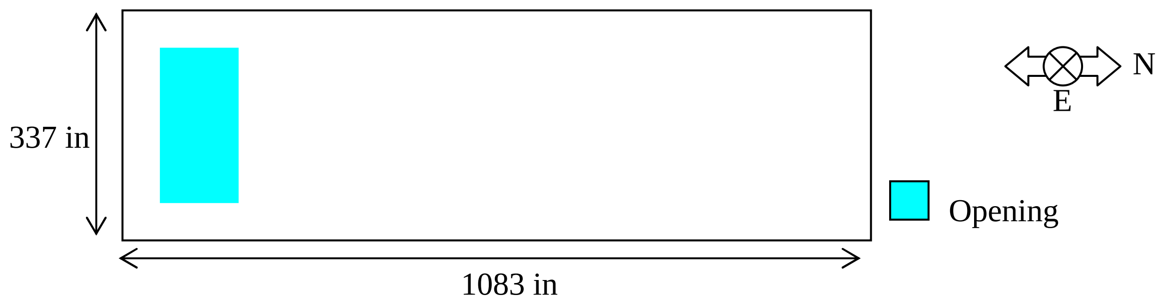

Fig. 4.8 West wall elevation

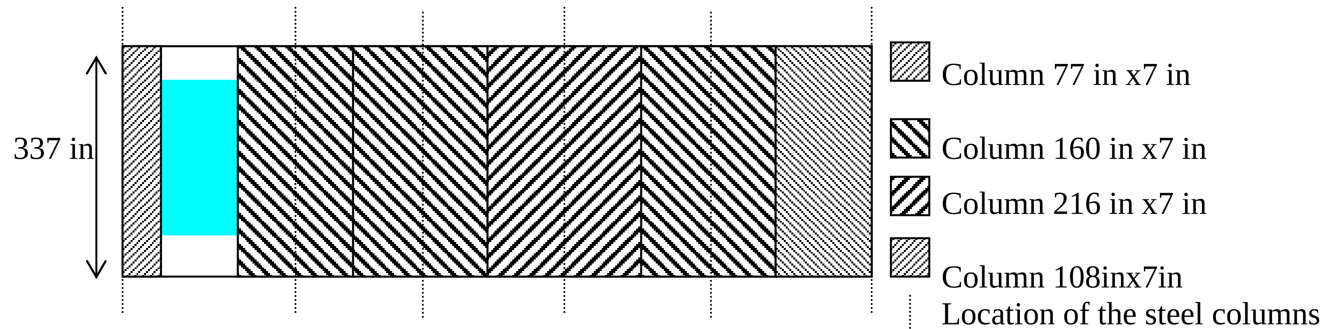

Fig. 4.9 Model of the columns

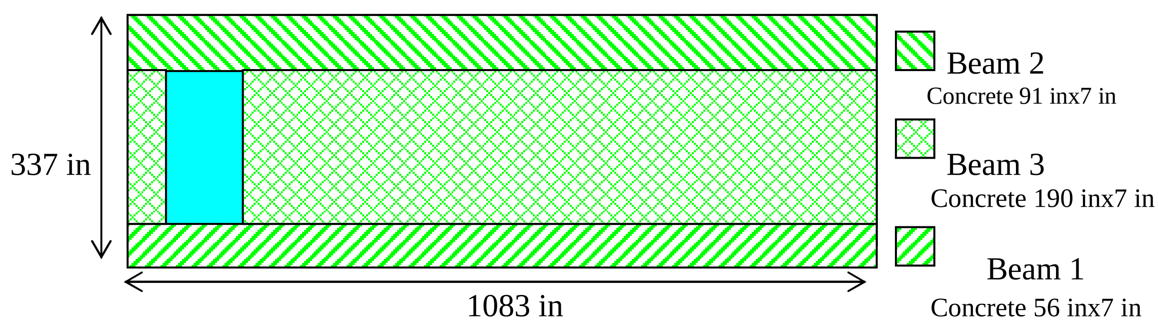

Fig. 4.10 Model of the beams

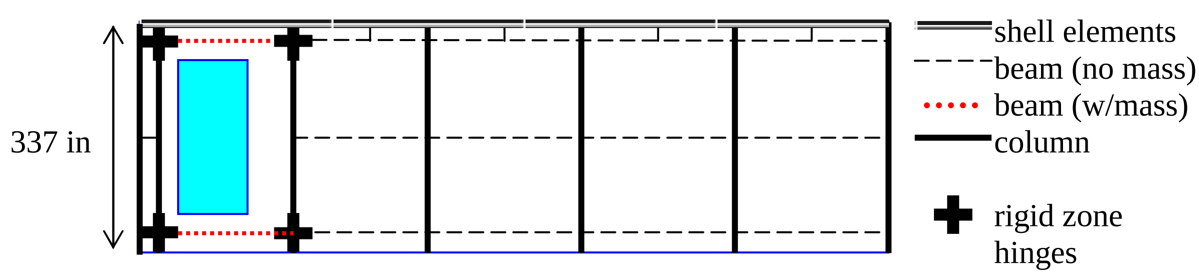

Fig. 4.11 Model of the west wall

(b) Analysis of the FR model

A static analysis equivalent to a 1g lateral acceleration at the roof level is conducted to compare the lateral forces resisted by the columns representing the wall panels with the results obtained with the FE model. The FE model is used as a reference, considering that it represents the best available model for a building of this type. As well, several meshes were considered for the FE model to check convergence of the results. The main results obtained by analyzing this new model follow:

- The fundamental period is 0.12 sec, which is consistent with the fundamental period of the FE model.
- The first five modes are described in the Table 4.6, and are in reasonable agreement with the modes of the FE model (Table 4.3). In general, the mode shapes correspond to localized breathing of wall segments and roof.

Table 4.6 Five first mode shapes of the frame element model

Mode number	Period (sec)	Cumulative Mass participation	
		X	Y
1	0.124	0.025	8.86
2	0.109	0.053	22.12
3	0.097	0.066	22.12
4	0.093	0.066	22.14
5	0.091	0.367	35.11

- The maximum displacements at the roof level for a 1g static load applied in one direction (Fig. 4.5) are presented in Table 4.7; although some variations are noted between the FE (Table 4.4) and FR models, the displacements for the FR model are reasonable, especially given the very low magnitudes.

Table 4.7 Maximum displacements at the roof level
due to a static 1g force at the roof level in one direction

Displacements	X direction (in)		Y direction (in)	
	FR	FE	FR	FE
1g in the N-S direction	0.04	0.01	0.006	0.003
1g in the E-W direction	0.006	0.006	0.08	0.13

- The sum of the lateral forces resisted in each wall is displayed in Table 4.8 for both loading directions with the nomenclature of Fig. 4.6. The results of the analyses of the FR and FE models suggest that the FR model gives very reasonable results. Forces estimated by the FR model are within 20% of the forces estimated by the FE model for the walls resisting significant forces.

Table 4.8 Force distribution in each wall at the roof level for the FE model

FORCE (kips)	1g in the N-S direction			1g in the E-W direction		
Model	FR	FE	FR /FE	FR	FE	FR/FE
East	56	48	1.17	1	1	----
West	53	53	1.00	4	2	----
Interior	60	73	0.82	5	3	----
South	3	1	----	65	74	0.88
North	7	1	----	70	70	1.00
Perpendicular	0	1	----	35	30	1.17
Sum	179	177		180	179	

- The maximum principal tensile and compressive stress at the roof level for both loading cases considered (Appendix 4-B2), are in the same range than for the FE model. By using the FR model, only slight differences are noted at the roof level.

The analysis results for the frame and the finite element models are similar. Both models capture periods, mode shapes, displacements and force distribution for the building. However, the FR model requires less effort to construct and is computationally less intensive. For these reasons, the frame model is used in the following sections to evaluate the building.

4.3 BUILDING EVALUATION

The FR model developed in section 4.2 was chosen to evaluate the expected performance of the building according to FEMA 273 guidelines. The earthquake hazard for the site is described by the spectrum provided by PG&E (Appendix 4-D: 10% in 50 years).

The first step is to define if a static analysis will represent accurately the building behavior, or if a dynamic analysis is necessary. Comparing the static and dynamic response of a simple wall (Appendix 4-E) indicates that dynamic actions produce out-of-plane moments as much as 10 times greater than those obtained by a static analysis. The breathing of the wall and roof also imposes deformations on the roof trusses and interior columns that cannot be accounted for in a static analysis. Given these issues, the linear or nonlinear static procedures presented in FEMA 273 are not consistent with the mode shapes of the building. Moreover, the use of the nonlinear dynamic procedure was not considered a realistic option (either for this project, or for a consulting office evaluating a building of this type) when working on such a complex building. The Linear Dynamic Procedure (LDP) of FEMA 273 is then the most appropriate method available; therefore it is applied. The use of the LDP is reassessed based on analysis results.

The procedure described in Section 3.2.7. of FEMA 273 was used to establish spectral demands. The 10-percent-in-50-years PG&E spectrum (Appendix 4-D) was imposed along one axis of the building, and 30% of this spectrum was applied along the orthogonal axis. Two analyses were conducted: 100% in the X-direction (north-south) and 30% in the Y-direction (east-west) [SPEC 1], and 30% in the X-direction and 100% in the Y-direction [SPEC 2]. Thirty modes (Appendix 4-F) were considered to achieve approximately 90% mass participation.

Demand values for moment, shear, axial load, and deformation were taken from the LDP analysis results and scaled by three different factors, C1, C2 and C3, (for force controlled actions, the demand will be divided by the same factor later in the procedure). The various factors take into account, respectively, the relation between the maximum inelastic displacements and the displacements calculated for linear elastic response, the effect of hysteresis shape on the maximum displacement response, and the increase in displacements due to second-order effects. These factors are defined according to Section 3.3.2.3(A) of FEMA 273. A value of C1= 1.375 was computed by linear interpolation given a characteristic ground motion period T_0 of 0.3 sec defined from the PG&E response spectrum. C2 was taken as 1, based on a collapse prevention limit state for framing type 2 (Table 3-1 FEMA 273) and C3=1 was assumed based also on an estimate of T_0 = 0.3 sec. The simple approach, applying linear interpolation, was used to determine C1 because the building response does not fit the model used for equation 3-13 of FEMA 273. However, the value used for C1 does not influence the results for force-controlled actions, which constitute a significant portion of the elements for the building (as discussed in the following pages).

Capacities are evaluated using standard approaches. For reinforced concrete panels, the moment capacity is evaluated for an extreme fiber concrete strain of 0.003. The BIAX program (Wallace, 1996) is used to determine the moment-axial load interaction diagram for each section. Concrete is modeled as unconfined using the relation by Hognestad (1951), for a peak stress of 4,000 psi at a strain of 0.002. An elastic, perfectly-plastic, stress-strain relation with a yield stress of 40 ksi is used for the reinforcing bars. The shear strength of reinforced concrete elements is calculated using Eq.11-3 of ACI 318-95 (which is consistent with FEMA 273). Given the low level of axial stress due to gravity load and overturning moments obtained from the SAP 2000 analyses for the walls, the influence of axial load on shear strength is neglected. Sample calculations are given in Appendix 4-G.

Capacities for steel elements are determined using AISC LRFD (1995) procedures. A yield stress of 45 ksi is assumed based on the information provided in the structural drawings. For the roof-truss elements, failure modes for gross-section-yielding (GSY), net section fracture (NSF) and block shear (BS) are checked for 5/8" diameter rivets according to the drawings. Sample calculations are provided in Appendix 4-H.

Acceptance criteria for each element is checked using the FEMA 273 recommendations (Section 3.4.1 and 3.4.2.) as outlined below:

- Deformation-controlled actions are used for flexure in the interior steel columns and out-of-plane bending for the walls.

$$m\kappa Q_{CE} > Q_{UD} \qquad (4-1)$$

- Force-controlled actions are used for the other elements of the building.

$$\kappa Q_{CL} > \frac{Q_{UF}}{C_1 * C_2 * C_3} \qquad (4-2)$$

where *m* is the element demand modifier to account for the expected ductility of the deformation associated with the action for the given performance level, and κ is a knowledge factor. According to Section 2.7.2 (FEMA 273), κ of 0.75 should be used for this case to compensate the minimum level of knowledge concerning the structure.

Given the large number of elements that made up the structural system, it was not realistic within this project to evaluate each of them. Therefore, for each type of element, several elements are selected in critical regions (defined from the SAP 2000 analysis results) to assess expected building performance, as well as to present the overall approach.

Results of the LDP are presented in four sections:

(a) Roof: displacement and general behavior,

(b) Walls: moment and shear capacity (the east and west walls were considered to be the most critical elements, considering the numerous openings),

(c) Built-up steel columns supporting the roof: moment and shear capacity, buckling, resistance in compression,

(d) Roof truss members: moment and shear capacity, resistance in compression and tension.

4.3.1 Fixed-Base Model

Because construction details for the wall to foundation connections are not available, two analyses are conducted, one for a fixed-base condition and the other for a pinned-base condition. Specific results for the fixed-base model are presented and discussed in the following paragraphs. Results for the pinned-base model will be presented later.

The fundamental period of the fixed base model is 0.12 sec., which is consistent with the fundamental period of the FE model (also fixed base).

(a) Roof

The displacement at the roof level have been defined from the SAP 2000 model and are presented in Table 4.9.

Table 4.9: Displacement results at the roof level (*C1*C2*C3)

	Spec 100% X - 30% Y	Spec 30% X - 100% Y
Max Displacement in X dir. (in)	0.03	0.01
Max Displacement in Y dir. (in)	0.02	0.05
Max Drift in X dir. (%)	0.007	0.003
Max Drift in Y dir. (%)	0.005	0.015

Note: FEMA 273 provisions are likely poor for periods of less than 0.3 sec because the values of C1 are too small to correctly estimate the inelastic displacements. However, the building is very stiff; the building is behaving in the elastic range, and so the value used for C1 has negligible impact on the evaluation.

(b) Walls

Because of the numerous openings in the north and east walls, the strength is reduced relative to other locations and thus the demand/capacity ratio of these elements is higher. Results are presented for the east and north walls, which are likely to have the highest demand/capacity ratios compared to the other walls. The demand applied to each element is based on the results of the SAP 2000 analysis.

It is important to notice that:

- The demand values displayed in the following tables are multiplied by the factor C1*C2*C3 (Section 3.3.2.3.A FEMA 273), and so are fictitious. They are designed to represent displacements and not forces. These values are appropriate for deformation-controlled elements but they will be divided by the factor C1*C2*C3 for force controlled elements.
- For the out-of-plane moment, assumed to be deformation-controlled, the element demand modifier, m, has been defined equal to 4 (Table 6-11 of FEMA 273). The in-plane-moment and the shear are considered force-controlled actions.

East Wall: Wall sections between the large openings are evaluated using standard procedures. Cross section and material information to define the moment capacity of these panels are presented in Appendix 4-G.

(i) Demand obtained from analysis

Table 4.10(a) Maximum demand on the east wall panels

Load case	P (k)	Vx (k)	Vy (k)	Mx (kip-in)	My (kip-in)
100% X, 30% Y	29	69	4	261	5 743
30% X, 100% Y	36	68	11	778	4 034

(ii) Capacity

The moment capacities are obtained with BIAX Program (Wallace, 1996) from P-M interaction diagrams. Assumptions and input files are displayed in Appendix 4-G. Shear capacity is determined using ACI 318 95 & LRFD 95.

Moment capacity $M_{nx} = 1\ 200$ kip-in

$M_{ny} = 21\ 700$ kip-in

Shear capacity $V_n = 2A_{cv}\sqrt{f_c^{'}} + 0.6 f_y d t_w = 162$ kips

(iii) Evaluation

Table 4.10(b) Acceptance criteria

Load case	Vu/ΦVn in-plane	Mx/ΦMnx in-plane	My/ΦMny out-of-plane
100% X, 30% Y	0.42	0.21	0.09
30% X, 100% Y	0.41	0.63	0.06

(iv) Discussion

Ratios displayed in Table 4.10(b) indicate that demands on the element are significantly less than capacity; therefore, acceptable performance is expected. The factor used for C1 (1.375) is not a critical parameter for evaluation of this element, considering the low ratio for the out-of-plane moment.

North Wall: The north wall was extended in 1923. The most recent part of the wall has a lower reinforcement ratio than the original wall; therefore, wall sections from each portion of the wall are considered. Three columns elements representing portions of the wall are evaluated (Fig. 4.12). The first column considered is between the old and the new building.

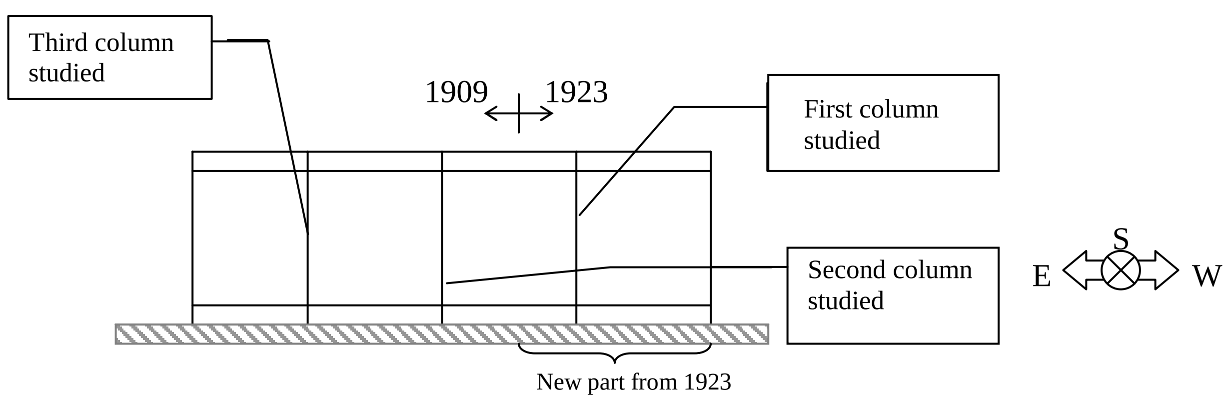

Fig. 4.12 North elevation

1st column (north wall)

(i) Demand obtained from analyses

Table 4.11(a) Maximum demand on the first column of the north wall

Load case	P (k)	Vx (k)	Vy (k)	Mx (kip-in)	My (kip-in)
100% X, 30% Y	24	0.4	44	5 248	26
30% X, 100% Y	10	0.1	117	13 802	10

(ii) Capacity

The same procedure described for the east wall is followed for the evaluation of each portion of the north wall considered. For the first column, the following values are obtained:

Moment capacity $M_{nx} = 32\ 800$ kip-in

$M_{ny} = 1\ 160$ kip-in

Shear capacity $V_n = 190$ kips

(iii) Evaluation

Table 4.11(b) Acceptance criteria

Load case	Vu/ΦVn in-plane	Mx/ΦMnx in-plane	My/ΦMny out-of-plane
100% X, 30% Y	0.23	0.05	0.02
30% X, 100% Y	0.62	0.14	0.01

2nd column (north wall)

(i) Demand obtained from analyses

Table 4.12(a) Maximum demand on the second column of the north wall

Load case	P (k)	Vx (k)	Vy (k)	Mx (kip-in)	My (kip-in)
100% X, 30% Y	6	0.5	20	2 281	67
30% X, 100% Y	14	0.2	52	6 035	26

(ii) Capacity

The same procedure described for the east wall is followed. The following values are obtained:

Moment capacity $M_{nx} = 15\ 900$ kip-in

$M_{ny} = 2\ 080$ kip-in

Shear capacity $V_n = 86$ kips

(iii) Evaluation

Table 4.12(b) Acceptance criteria

Load case	Vu/ΦVn in-plane	Mx/ΦMnx in-plane	My/ΦMny out-of-plane
100% X, 30% Y	0.23	0.05	0.03
30% X, 100% Y	0.61	0.13	0.01

3rd column (north wall)

(i) Demand obtained from analysis

Table 4.13(a) Maximum demand on the third column of the north wall

Load case	P (k)	Vx (k)	Vy (k)	Mx (kip-in)	My (kip-in)
100% X, 30% Y	5	1.0	27	2 303	83
30% X, 100% Y	13	2.1	74	6 205	138

(ii) Capacity

The same procedure described for the east wall is followed. The following values are obtained:

Moment capacity $M_{nx} = 15\ 900\ \text{kip-in}$

$M_{nx} = 2\ 080\ \text{kip-in}$

Shear capacity $V_n = 86\ \text{kips}$

(iii) Evaluation

Table 4.13(b) Acceptance criteria

Load case	Vu/ΦVn in-plane	Mx/ΦMnx in-plane	My/ΦMny out-of-plane
100% X, 30% Y	0.31	0.05	0.04
30% X, 100% Y	0.86	0.13	0.07

The ratios display in Table 4.11(b), 4.12(b), 4.13(b) indicate that the demands on the elements are less than the capacity; therefore, acceptable performance is expected. Note that a factor κ of 0.75 and design material properties, which would lower the demand/ capacity ratios for in-plane actions considerably (concrete strength is likely much higher), are used. Considering the lack of information, this makes the calculation relatively conservative.

(c) Built-up steel columns

The steel columns at the perimeter of the building and along the interior wall are partially embedded in the reinforced concrete wall panels. Given the small displacement response of the building and the low demand, these columns are not considered critical. Demand-to-capacity ratios are calculated for the interior columns supporting the roof and gallery slab. Since steel beams frame into the interior columns at the gallery level on three sides, the columns are evaluated as two components; one from the roof truss to the gallery level and one from the gallery level to the floor. The properties of the columns are displayed in Appendix 4-I. The columns are evaluated for combined axial load and biaxial bending using FEMA 273 recommendations for deformation-controlled, and then all demands have been multiplied by a factor of C1*C2*C3.

The LRFD and FEMA 273 Criteria for biaxial bending and axial load is:

$$\frac{Pu}{\phi_c P_n} \leq 0.2 \qquad \frac{P_u}{2\phi_c P_n} + \left[\frac{M_{ux}}{\phi_b M_{nx}} + \frac{M_{uy}}{\phi_b M_{ny}}\right] < 1 \tag{4-3}$$

and an acceptance criteria for FEMA 273 is:

$$\frac{Pu}{\phi_c P_n} \leq 0.2 \qquad \frac{P}{2P_n} + \left[\frac{M_{ux}}{m_X M_{nx}} + \frac{M_{uy}}{m_Y M_{ny}}\right] < 1 \tag{4-4}$$

Values of m_x = 2 and m_y = 8 are obtained from Table 5-8 (FEMA 273/274), for the collapse prevention limit state. The following results are derived from Eq. 4-4:

Column between roof and gallery slab:

$$\frac{P_u}{2P_n} + \left[\frac{M_{ux}}{2M_{nx}} + \frac{M_{uy}}{8M_{ny}}\right] = 0.02 + 0.007 + 0.22 = 0.25 < 1 \tag{4-5}$$

Column between gallery slab and base:

$$\frac{P_u}{2P_n} + \left[\frac{M_{ux}}{2M_{nx}} + \frac{M_{uy}}{8M_{ny}}\right] = 0.04 + 0.01 + 0.22 = 0.27 < 1 \tag{4-6}$$

These ratios are considerably less than 1; therefore, acceptable behavior is expected. However, it can be argued that the built-up trusses are force-controlled and not deformation-controlled. In this case, the ratios are higher (up to twice higher), but are still less than 0.55. The results are still acceptable.

(d) Trusses

The roof trusses are composed of either single or double angles. Critical elements, defined (from the SAP 2000 model) as the elements with higher demands, are checked for both tension and compression. The properties of the trusses and the calculations for tension are presented in Appendix 4-H. For compression, biaxial bending of the truss elements is considered. Calculations for several critical elements are presented in Table 4.14.

Table 4.14 Properties of the different elements

Section Angle	A (in^2)	I_{XX} (in^4)	I_{YY} (in^4)	S (in^3)	$M_R(kip\text{–}in)$	k
2L 3.5, 2.5, 1/4	2.88	3.60	2.64	1.12	29.12	1
2L 2 , 2 , 1/4	1.88	0.70	1.36	0.50	12.85	1
L 2.5, 2 , 1/4	1.06	0.65	0.37	0.20	6.61	1

For worst case sections, local buckling is not a problem as noted in the following calculations.

unstiffened element: b/t = 2.5/(1/4) = 10 < 76/√fy =12.67 for single angle

b/t = 3.5/(1/4) = 14 < 95/√fy = 15.83 for double angles

stiffened element: hc/ tw = (17.5-7)/(1/4) = 42 < 253 /√fy =42.17

Truss elements evaluated are identified on Figs. 4.13 to 4.15.

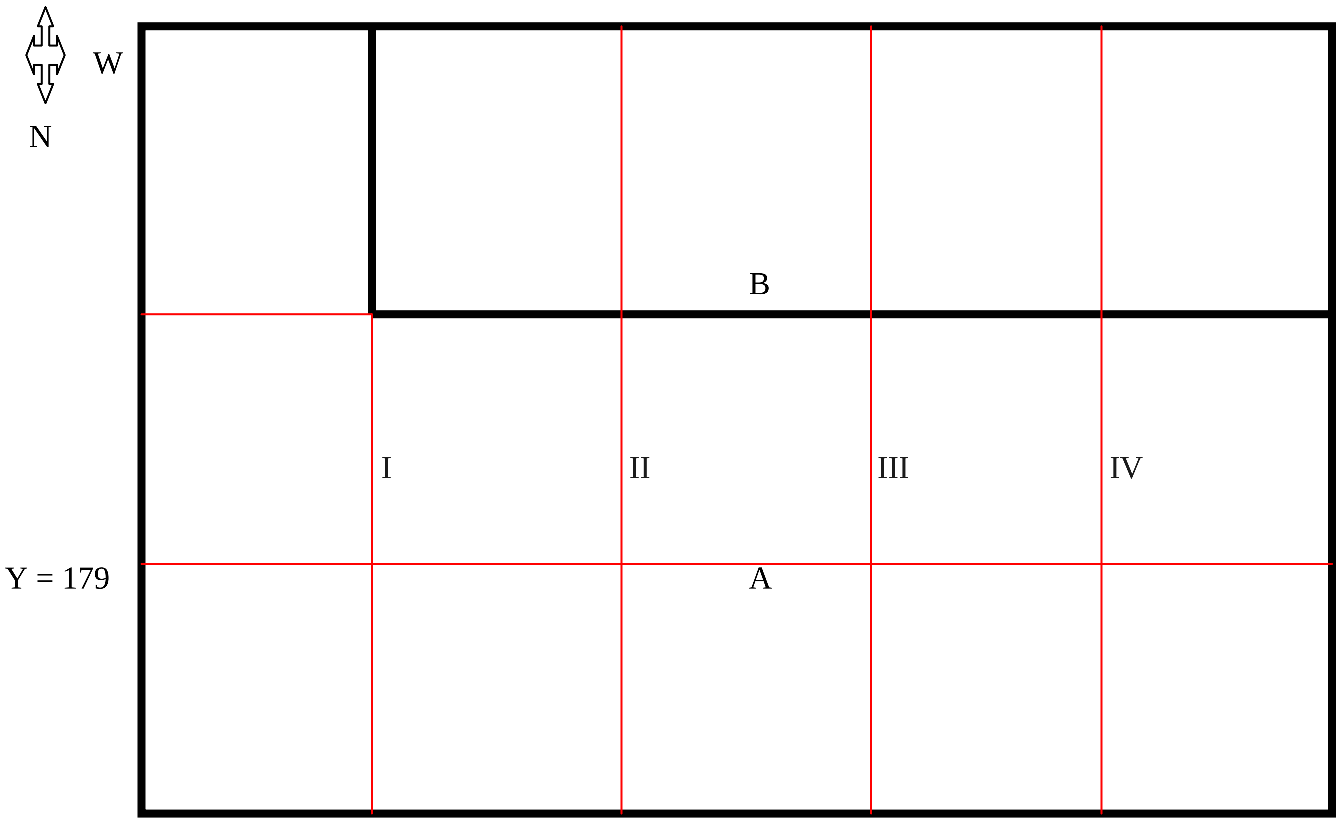

Fig. 4.13 Top views of the trusses

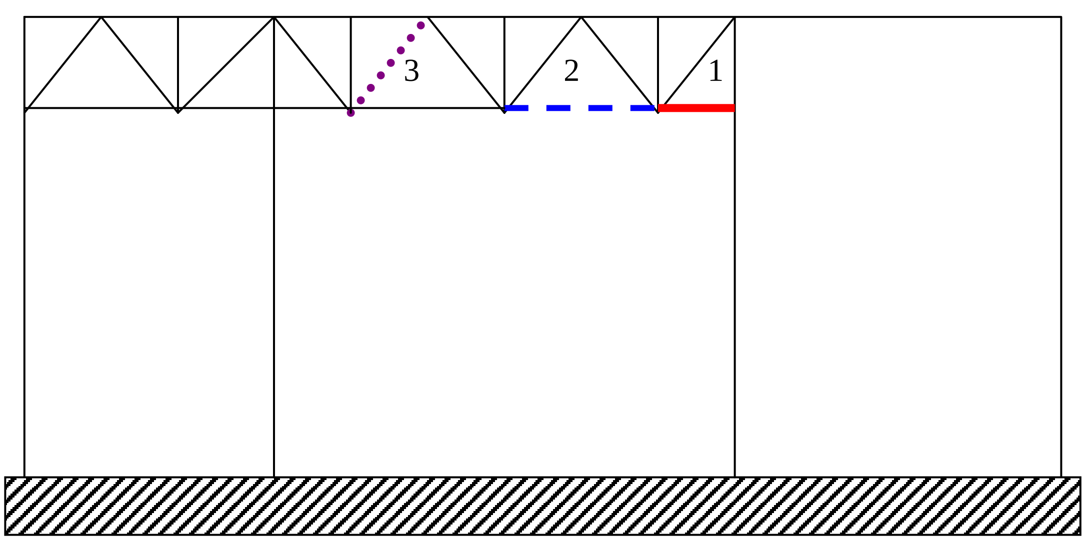

Fig. 4.14 East-west elevation (trusses I, II, III, IV from Fig. 4.13)

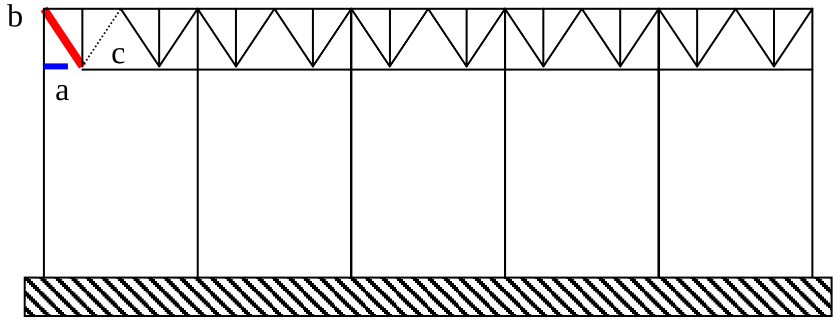

Fig. 4.15 South-north elevation (trusses A, B from Fig. 4.13)

Biaxial Bending equations for FEMA 273 for force-controlled are presented below:

$$\left.\begin{aligned}
&(1)\frac{P_u}{\phi_b P_n} < 0.2 \\
&\qquad \frac{P_u}{2\phi_c P_n} + \left[\frac{M_{ux}}{\phi_b M_{nx}} + \frac{M_{uy}}{\phi_B M_{ny}}\right] < 1 \\
&(2)\frac{P_u}{\phi_b P_n} > 0.2 \\
&\qquad \frac{P_u}{\phi_c P_n} + \frac{8}{9}\left[\frac{M_{ux}}{\phi_b M_{nx}} + \frac{M_{uy}}{\phi_B M_{ny}}\right] < 1
\end{aligned}\right\} \qquad (4-7)$$

$$\frac{P_u}{P_n} + \frac{8}{9}\left[\frac{M_{ux}}{M_{nx}} + \frac{M_{uy}}{M_{ny}}\right] < 1 \qquad (4-8)$$

Applying the acceptance criteria described in FEMA 273 Section 5.4.2.3.A:

The demand, capacity and the evaluation of each element considered are summarized in Tables 4.15 and 4.16.

Table 4.15 South–north trusses

Section Angle	Location *	l	λ	ϕPn (kips)	Pu (kips)	Mux (kip-in)	Muy (kip-in)	Pu/ϕPn	(4-8)
2L 3.5, 2 , 1/4	A a	54	0.64	74.2	39.2	0.92	3.53	0.52	0.57
L 2.5, 2 , 1/4	A b	68	1.80	8.8	7.5	0	0	0.85	0.85

* Refer to Fig. 4.13 and 4.15

Table 4.16 East-west trusses

Section Angle	Location *	l	λ	ϕPn (kips)	Pu (kips)	Mux (kip-in)	Muy (kip-in)	Pu/ϕPn	(4-8)
2L 3.5, 2 , 1/4	III 1	71	0.84	67.1	35.5	7.9	0.11	0.53	0.59
2L 3.5, 2 , 1/4	IV 1	71	0.84	67.1	32.9	6.1	0.34	0.49	0.54
2L 3.5, 2 , 1/4	I 2	122	1.45	36.7	9.2	1.6	0.39	0.25	0.27
2L 3.5, 2 , 1/4	IV2	122	1.45	36.7	24.8	0.9	0.23	0.68	0.69
2L 2.5, 2 , 1/4	III 3	82	1.51	39.8	16.3	0	0	0.41	0.41
2L 2.5, 2 , 1/4	IV 3	82	1.51	39.8	11.0	0	0	0.28	0.28

* Refer to Fig. 4.14 and 4.15
λ is the limiting width-thickness ratios defined by LRFD

All the demands have been multiplied by C1*C2*C3. However, the building is behaving in the elastic range, and the factor C1*C2*C3 is then equal to 1. By using a higher factor, the calculations are more conservative.

The ratios given in Tables 4.15 and 4.16 are all less than one; therefore, the acceptance criteria are satisfied. Results for the fixed base FR model indicate acceptable performance. However, the ratios are higher for the north-south truss elements than for the east-west truss elements, because the deformations are larger in this direction, especially at the south end. This is likely due to the large openings located in the south wall (door) and the skylights in the roof.

4.3.2 Pinned Base Model

Due to the uncertainty associated with the base connection of the walls to the footing, a second analysis is performed assuming that the walls are free to rotate about their weak axis at the base. According to the drawings, the steel columns are considered to be fixed at their base. The results of this analysis are presented in Appendix 4-J. The building is slightly more flexible than the fixed-base model, as expected, and the fundamental period is approximately 25% higher. However, the first mode corresponds to local wall and roof deformations, which are significantly impacted by the support conditions at some locations. Change in the wall fixity at the base does not significantly influence overall building response.

By allowing the walls to rotate about their weak axis, the moments developed in the walls, columns and trusses are slightly larger than those developed for the fixed-base model. Indeed, the period is slightly higher and the acceleration associated with the period is also higher (Appendix 4-D), causing an increase in demand. The ratios obtained are then slightly higher than the one from the fixed base, but are still within acceptable range.

4.4 SOIL-FOUNDATION-STRUCTURE INTERACTION (SFSI)

Soil–foundation-structure interaction (SFSI) is often an important source of flexibility and damping for stiff buildings. Therefore, a simplified analysis is performed to assess the role of SFSI for the building.

To model the building response with SFSI, the FR model is used, and a rigid slab is added at the base. The rigid base assumption simplifies the analysis, and has been found by Lion & Huang (1994) to provide an adequate representation of foundation impedance for flexible slabs supporting thin perimeter walls. The foundation slab is composed of shell elements whose nodes are constrained (body constraint in SAP 2000) so that each node is forced to move rigidly for all displacements. A set of springs and dampers are placed at the center of the slab to model the foundation impedance (Appendix 4-K). The values for the springs and dampers were obtained from a geotechnical study described in Appendix 2-A. Impedance and damping values for a fundamental period of 0.15 sec. are presented in Tables 4.17 and 4.18.

Table 4.17 Damping and stiffness values used to model the SFSI

Translation	Stiffness (kip/in)	Damping (kip/in/s)
X axis *	1.5 E4	8.8 E2
Y axis *	1.5 E4	8.8 E2
Z axis *	1.1 E4	1.7 E3

* Refer to Fig. 4.5.

Table 4.18 Damping and stiffness values used to model the SFSI

Rocking	Stiffness (kip.in/rad)	Damping (kip.in/rad/s)
X axis *	1.5 E4	8.8 E2
Y axis *	1.5 E4	8.8 E2
Z axis*	1.1 E4	1.7 E3

* Refer to Fig. 4.5.

The principal results are presented below:

- The fundamental period is 0.16 sec, which is 26% higher than the fundamental period of the FR model for fixed-base condition.
- The first five mode shapes and their mass participation are presented in Table 4.19.

Table 4.19 Five first mode shapes of the FR with SSI model

		Mass Participation	
Mode shape	Period (sec)	X direction	Y direction
1	0.16	0.1	70.2
2	0.14	61.9	70.3
3	0.12	62.1	72.4
4	0.10	62.3	72.4
5	0.10	62.3	72.4

The two first modes are primarily composed of rocking and translational motions.

- The maximum displacement at the roof level are presented in Table 4.20.

Table 4.20 Maximum displacements at the roof level

Displacements	X direction (in)			Y direction (in)		
	SSI		FR	SSI		FR
	max	relative		max	relative	
100% in X, 30 % in Y	0.24	0.13	0.03	0.10	0.06	0.06
30% in X, 100% in Y	0.07	0.04	0.01	0.32	0.20	0.05

The relative lateral displacements obtained by including the effect of SFSI can be four times higher than fixed-base displacements. However, the displacement increase is due to rigid body translation and rotation of the base, and does not represent a significant seismic demand for the structural elements.

To assess the impact of SFSI on element demands, the FEMA 273 recommendations are used to evaluate the same elements considered in the fixed-base and pinned-base models.

(a) Walls

Assumptions for the wall evaluation are presented in section 4.3.1 (b)

East Wall: Cross section and material information to define the moment capacity of these panels are presented in Appendix 4-G.

(i) Demand obtained from analysis

Table 4.21(a) Maximum demand on the east wall panels

Load case	P (k)	Vx (k)	Vy (k)	Mx (kip-in)	My (kip-in)
100% X, 30% Y	37	58	2	159	5 020
30% X, 100% Y	52	46	7	500	2 096

(ii) Capacity

The moment capacities are obtained with BIAX Program (Wallace, 1996). The shear capacity is determined using ACI 318 95 & LRFD 95.

Moment capacity $M_{nx} = 1\ 200$ kip-in

$M_{ny} = 21\ 700$ kip-in

Shear capacity $V_n = 2A_{cv}\sqrt{f_c^{'}} + 0.6 f_y dt_w = 162$ kips

(iii) Evaluation

Table 4.21(b) Acceptance criteria

	Vu/ϕVn in-plane		Mx/ϕMnx in-plane		My/ϕMny out-of-plane	
Load case	SFSI	FR*	SFSI	FR*	SFSI	FR*
100% X, 30% Y	0.35	0.42	0.13	0.21	0.08	0.09
30% X, 100% Y	0.28	0.41	0.40	0.63	0.03	0.06

* FR refers to the FR fixed-base model

(iv) Discussion

Ratios displayed in Table 4.21(b) indicate that demands on the element are significantly less than capacity; therefore, acceptable performance is expected. Some of these ratios are slightly lower than the values obtained for the fixed-base FR model (Table 4.10(b)). These results are obtained despite the fact that increasing periods lead to higher force demands given the period range for this building. The results may be due to the increase in damping, as well as the impact of SFSI on the mode shapes.

North Wall: Three columns of the wall are evaluated (Fig. 4.12). The first column considered is between the old (1909) and the new (1923) building.

1st column (north wall)

(i) Demand obtained from analyses

Table 4.22(a) Maximum demand on the first column of the north wall

Load case	P (k)	Vx (k)	Vy (k)	Mx (kip-in)	My (kip-in)
100% X, 30% Y	46	0.5	44	5 229	27
30% X, 100% Y	16	0.1	139	16 436	9

(ii) Capacity

The same procedure described for the east wall has been followed.

Moment capacity $M_{nx} = 32\ 800\,\text{kip-in}$

$M_{ny} = 1\ 160\,\text{kip-in}$

Shear capacity $V_n = 190\ \text{kips}$

(iii) Evaluation

Table 4.22(b) Acceptance criteria

	Vu/ϕVn in-plane		Mx/ϕMnx out-of-plane		My/ϕMny out-of-plane	
Loading	SSI	FR	SSI	FR	SSI	FR
100% X, 30% Y	0.22	0.23	0.05	0.05	0.02	0.02
30% X, 100% Y	0.71	0.62	0.17	0.14	0.01	0.01

2nd column (north wall)

(i) Demand obtained from analyses

Table 4.23(a) Maximum demand on the second column of the north wall

Load case	P (k)	Vx (k)	Vy (k)	Mx (kip-in)	My (kip-in)
100% X, 30% Y	18	0.4	20	2 251	56
30% X, 100% Y	17	0.1	62	7 111	18

(ii) Capacity

The same procedure described for the east wall has been followed.

Moment capacity $M_{nx} = 15\ 900\ \text{kip-in}$

$M_{ny} = 2\ 080\ \text{kip-in}$

Shear capacity $V_n = 86\ \text{kips}$

(iii) Evaluation

Table 4.23(b) Acceptance criteria

	Vu/ϕVn in-plane		Mx/ϕMnx out-of-plane		My/ϕMny out-of-plane	
Loading	SSI	FR	SSI	FR	SSI	FR
100% X, 30% Y	0.22	0.23	0.05	0.05	0.03	0.03
30% X, 100% Y	0.70	0.61	0.15	0.13	0.01	0.01

3rd column (north wall)

(i) Demand obtained from analysis

Table 4.24(a) Maximum demand on the third column of the north wall

Load case	P (k)	Vx (k)	Vy (k)	Mx (kip-in)	My (kip-in)
100% X, 30% Y	24	1.0	26	2 284	70
30% X, 100% Y	20	1.0	82	7 250	72

(ii) Capacity

The same procedure described for the east wall is followed.

Moment capacity $M_{nx} = 15\ 900$ kip-in

$M_{ny} = 2\ 080$ kip-in

Shear capacity $V_n = 86$ kips

(iii) Evaluation

Table 4.24(b) Acceptance criteria

	Vu/ϕVn in-plane		Mx/ϕMnx out-of-plane		My/ϕMny out-of-plane	
Loading	SSI	FR	SSI	FR	SSI	FR
100% X, 30% Y	0.29	0.31	0.05	0.05	0.03	0.04
30% X, 100% Y	0.92	0.86	0.15	0.13	0.01	0.07

(iv) Discussion

The ratios obtained from Table 4.22b, 4.23b, 4.24b indicate that the acceptance criteria defined by FEMA 273 are satisfied. These ratios are in most cases slightly higher (up to 15%) than the values found for the fixed-base FR model (Table 4.11b, 4.12b, 4.13b). This can be explained by a different mass participation. In the first ten modes, more than 60% of the mass participation is captured for the SFSI in both directions, whereas only 9% is captured for the FR model.

Moreover, the first mode is higher when considering SFSI, which leads to a higher spectral acceleration.

(b) Built-up steel columns

Demand-to-capacity ratios are calculated for the interior columns supporting the roof and gallery slab, as it has been performed for the fixed-base FR model. The properties of the columns are displayed in Appendix 4-I.

The LRFD and FEMA 273 Criteria, applied for biaxial bending and axial load is:

$$\frac{Pu}{\phi_c P_n} \leq 0.2 \qquad \frac{P_u}{2\phi_c P_n} + \left[\frac{M_{ux}}{\phi_b M_{nx}} + \frac{M_{uy}}{\phi_b M_{ny}}\right] < 1 \tag{4-3}$$

and an acceptance criteria for FEMA 273 is:

$$\frac{Pu}{\phi_c P_n} \leq 0.2 \qquad \frac{P}{2P_n} + \left[\frac{M_{ux}}{m_X M_{nx}} + \frac{M_{uy}}{m_Y M_{ny}}\right] < 1 \tag{4-4}$$

Values of $m_x = 2$ and $m_y = 8$ are obtained from Table 5-8 (FEMA 273/274), for the collapse prevention limit state. The following results are derived from (4-4):

Column between roof and gallery slab:

$$\frac{P_u}{2P_n} + \left[\frac{M_{ux}}{2M_{nx}} + \frac{M_{uy}}{8M_{ny}}\right] = 0.02 + 0.02 + 0.01 = 0.08 < 1 \tag{4-9}$$

Column between gallery slab and base:

$$\frac{P_u}{2P_n} + \left[\frac{M_{ux}}{2M_{nx}} + \frac{M_{uy}}{8M_{ny}}\right] = 0.06 + 0.03 + 0.01 = 0.1 < 1 \tag{4-10}$$

These ratios are slightly lower than the ones obtained for the fixed model. Acceptable performances are expected. By considering the element as force-controlled, these ratios are slightly higher but still acceptable.

(c) Trusses

The same process described in chapter 4.3.1 (d) is applied here, using equations (4-5) and (4-6). The results are summarized in Table 4.25 and 4.26.

Table 4.25 South–north trusses

Section Angle	Location *	l	λ	ϕPn (kips)	Pu (kips)	Mux (kip-in)	Muy (kip-in)	Pu/ϕPn	(4-8)
2L 3.5, 2 , 1/4	A a	54	0.64	74.2	4.7	0	0	0.06	0.03
L 2.5, 2 , 1/4	A c	68	1.80	8.8	7.5	0	0	0.85	0.85

* Refer to Fig. 4.13 and 4.15

Table 4.26 East-west trusses

Section Angle	Location *	l	λ	ϕPn (kips)	Pu (kips)	Mux (kip-in)	Muy (kip-in)	Pu/ϕPn	(4-8)
2L 3.5, 2 , 1/4	III 1	71	0.84	67.1	27	4.8	0.1	0.40	0.43
2L 3.5, 2 , 1/4	IV 1	71	0.84	67.1	20	3.6	0.2	0.30	0.32
2L 3.5, 2 , 1/4	I 2	122	1.45	36.7	8	0.3	1.5	0.22	0.24
2L 3.5, 2 , 1/4	IV2	122	1.45	36.7	13	0.7	0.2	0.35	0.35
2L 2.5, 2 , 1/4	III 3	82	1.51	39.8	8	0	0	0.20	0.20
2L 2.5, 2 , 1/4	IV 3	82	1.51	39.8	6	0	0	0.15	0.15

* Refer to Fig. 4.14 and 4.15
λ is the limiting width-thickness ratios defined by LRFD

All the demands have been multiplied by C1*C2*C3. However, the building is behaving in the elastic range, and the factor C1*C2*C3 is then equal to 1. By using a higher factor, the calculations are more conservative.

The truss members evaluated in the east-west direction have relatively low demand/capacity ratios. Maximum ratio for the north-south direction is considerably higher, indicating potential local failure for much stronger earthquakes, for a single angle truss. However, comparing the ratios obtained from the fixed base FR model, no trend is apparent.

4.5 CONCLUSIONS

A linear dynamic analysis was performed on different models for the PG&E spectrum with a 10% probability of exceedance in 50 years. The linear dynamic procedure (LDP) analysis was chosen in order to model the out-of-plane wall and roof response that could not be captured using a static analysis.

The first model considered was a finite element (FE) model; however, this type of model is cumbersome due to stress concentrations, many hours of computation, and the use of a very fine mesh. A simpler model was then developed using equivalent frame elements instead of shell elements to model the walls and the gallery slab. The analysis results for this model (FR) were in good agreement with the ones obtained with the FE model. Thus, the FR model was used for the dynamic analyses.

Demand-to-capacity ratios were computed using the Linear Dynamic Procedure described in FEMA 273. Acceptance criteria were checked and acceptable results were obtained for both fixed-base and pinned-base FR models. Demand-to-capacity ratios of up to 0.86 for shear, 0.63 for in-plane moment and 0.10 for out-of-plane moment in the walls were obtained. The built-up steel columns had demand-to-capacity ratios between 0.14 and 0.44, and truss member ratios varied between 0.27 and 0.85.

Analyses were also conducted to assess the influence of soil-foundation-structure interaction. By creating a new model, where the SFSI was modeled by a set of springs and dampers, new values of global structural displacements and demand-to-capacity ratios were obtained. Roof displacements increased by up to a factor of four due to the added flexibility of rigid body rocking and translating of the base slab. In contrast, demand-to-capacity ratios tended to increase only slightly due to the higher spectral acceleration associated with the first modes being counteracted by the added damping associated with the foundation-soil-interaction. For more conventional buildings with more significant story and roof mass, these SFSI effects are generally more pronounced. For this building, trends were difficult to assess and overall results were not impacted significantly. Consideration of SFSI is not recommended for this type of structural system.

The building is really stiff and strong. Even though designed as a steel frame, the reinforced concrete can carry most of the loads applied to the structure. A static analysis was judged unrealistic for such a structure and a linear dynamic analysis was conducted. Acceptable performance was estimated for a 10%-probability-of-exceedance-in-5-years spectrum. For a larger demand (2%-probability-of-exceedance-in-50-years spectrum), very localized inelastic response would be expected in the truss elements. However, it is important to notice that out-of-plane wall response could be more significant for buildings without interior walls or gallery slabs.

APPENDIX 4-A1 3-D VIEW OF THE FE MODEL

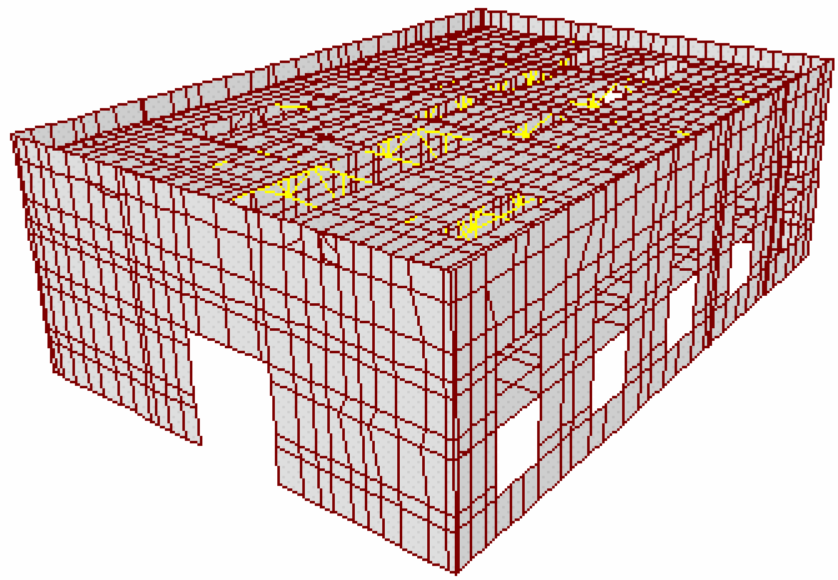

Fig. 4-A1 (a) 3-D view of the FE model

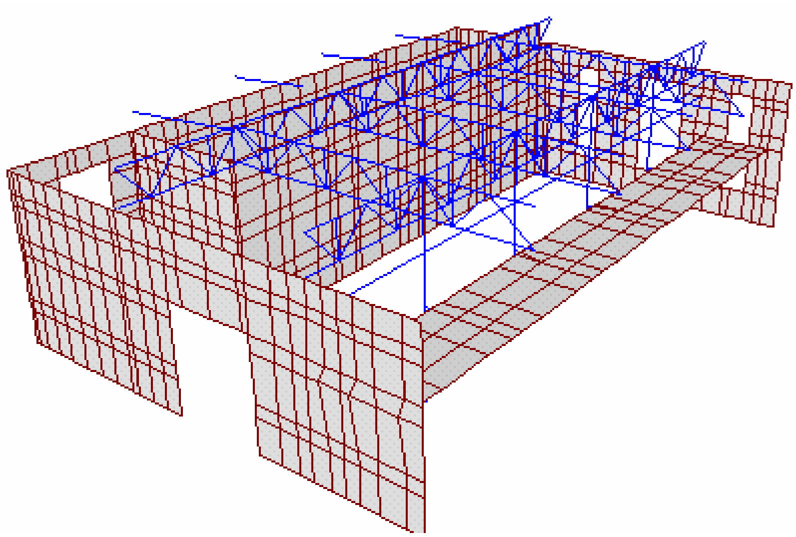

Fig. 4-A1 (b) 3-D view of the FE model without the south wall and the roof

APPENDIX 4-A2 MAXIMUM STRESS AT THE ROOF LEVEL FOR THE FE MODEL

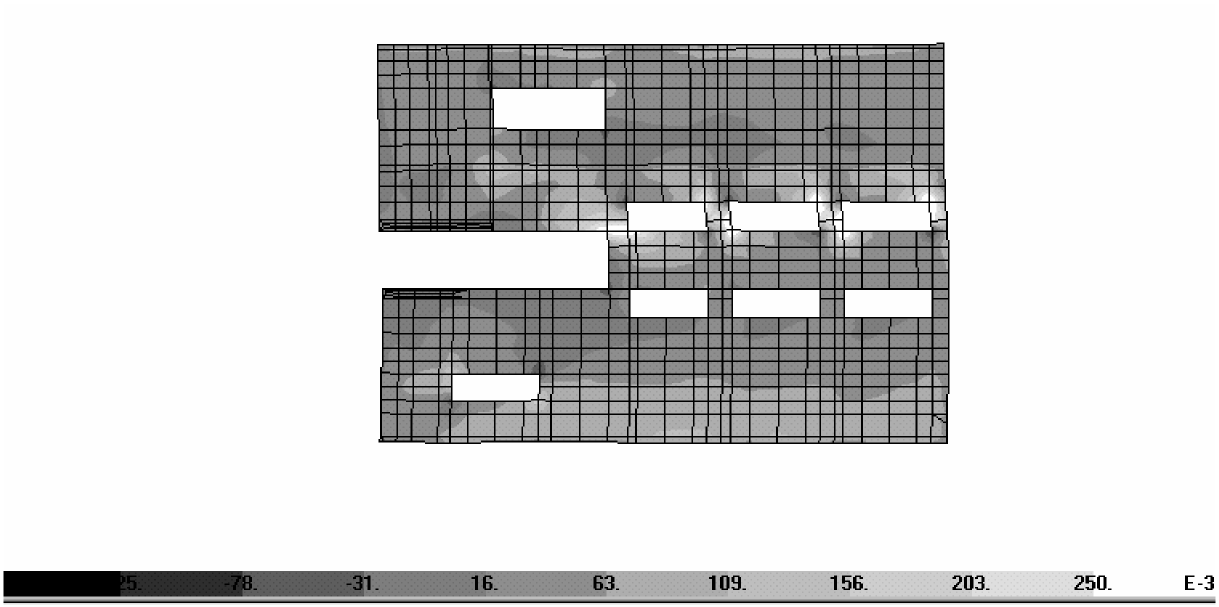

Fig. 4-A2 (a) 1g in the north-south direction

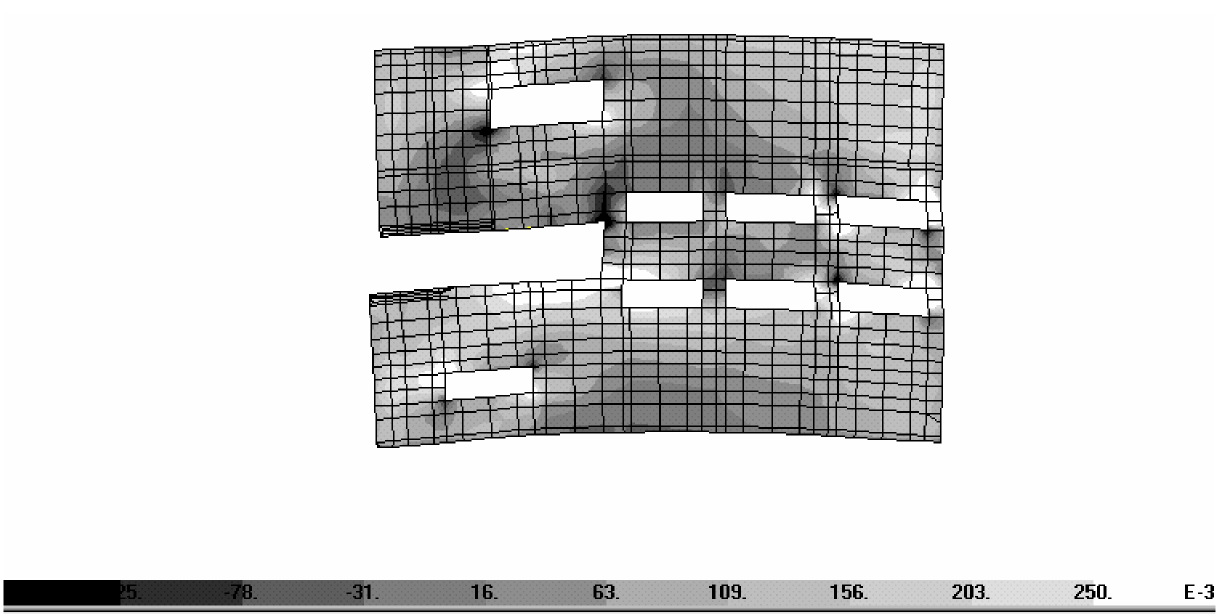

Fig. 4-A2 (b) 1g in the east-west direction

APPENDIX 4-B1 3-D VIEW OF THE FR MODEL

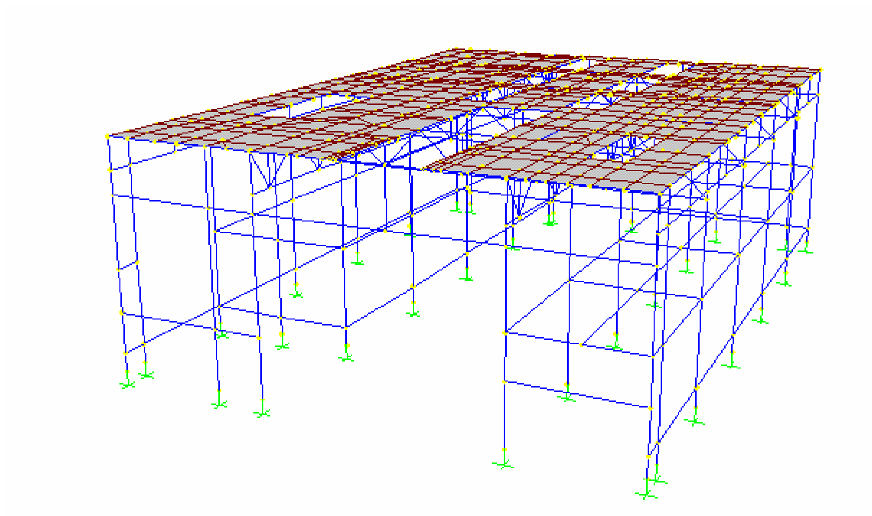

Fig. 4-B1 3-D view of the FR model

‘

APPENDIX 4-B2 MAXIMUM STRESS AT THE ROOF LEVEL FOR THE FR MODEL

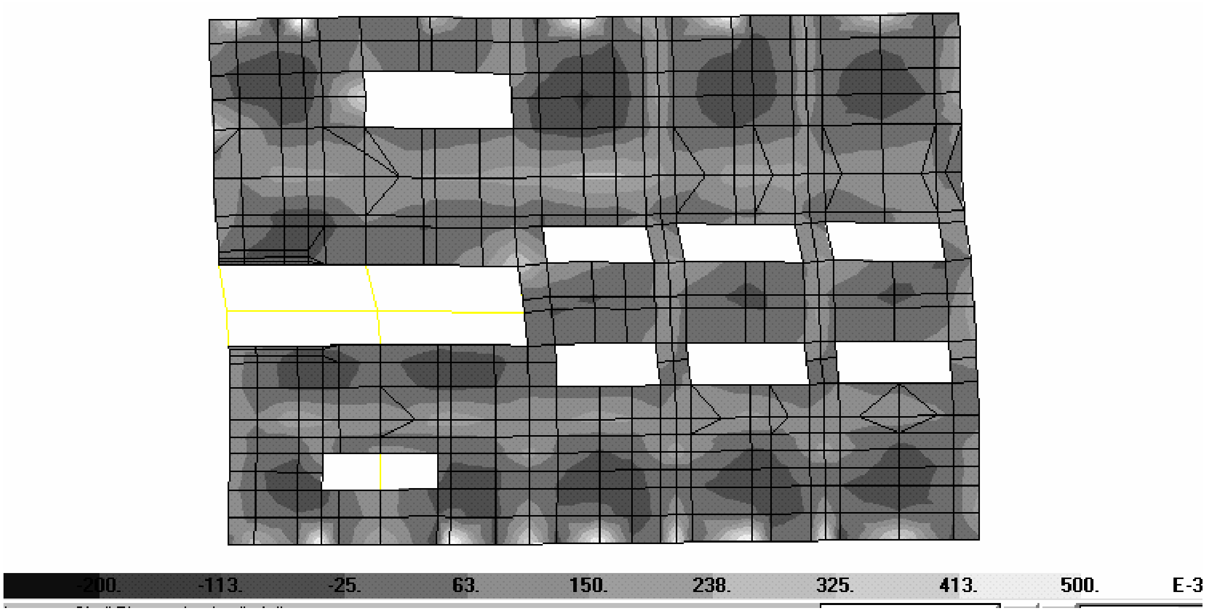

Fig. 4-B2 (a) 1g in the north-south direction

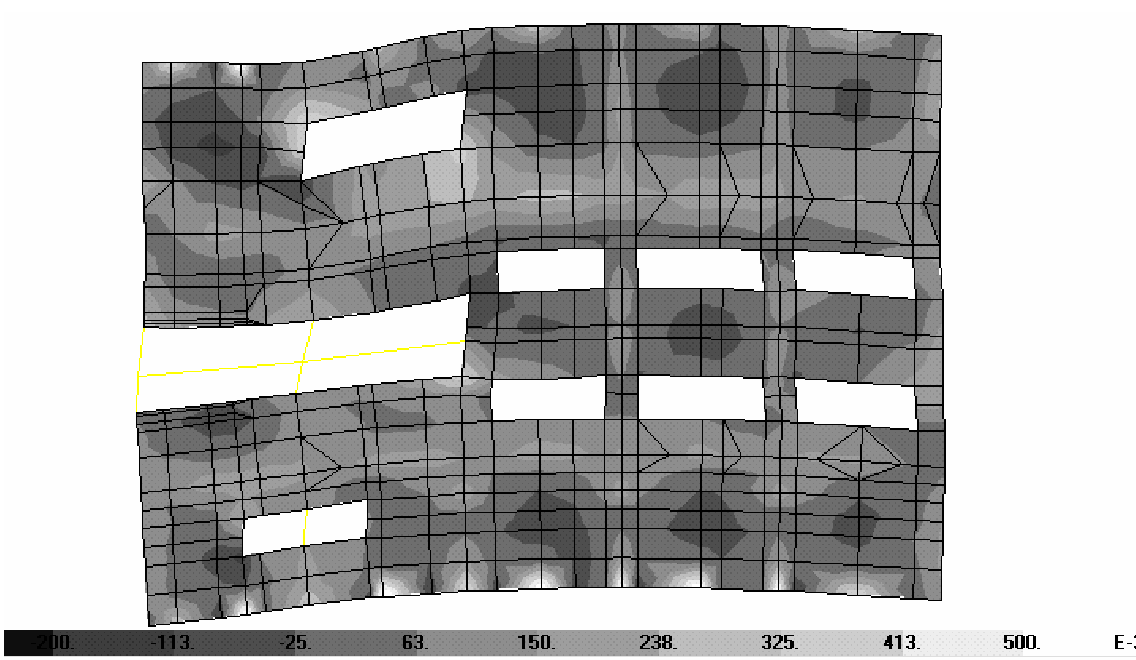

Fig. 4-B2 (b) 1g in the east-west direction

APPENDIX 4-C METHOD TO MODEL THE WALLS FOR THE FR MODEL

The purpose of this study is to compare the response of a simple wall modeled by shell elements and by a superposition of beams and columns. For this purpose, a wall with a length of 1080 in., a thickness of 7 in. and a height of 350 in. was selected. This wall is fixed at the boundaries.

Two different types of model were developed:

Model A: Model using shell elements

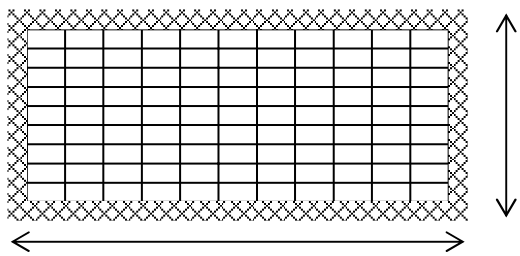

Fig. 4-C1: Shell element model

Several meshes were used to get convergence of the results. The results, presented in Table 4C-1, are the ones obtained with a mesh of 9 x 11 elements.

Model B: Model using frame elements

The same wall was modeled using frame elements as shown below.

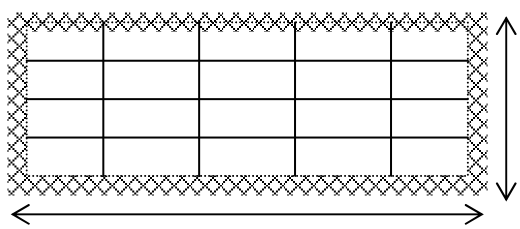

Fig. 4-C2: Frame element model

Model B: the inertia of each element is considered, as stated in the strip method.

For this model, the horizontal members are considered massless, in order not to double the weight of the wall; the purpose of modeling the beams is to represent the actual stiffness of the wall when using a column analogy.

By submitting the three models to a response spectrum (defined by UBC 97), the following results are obtained (Table 4-C1):

Table 4-C1: Mode comparison

Model	A	B
First Mode (sec)	0.13	0.12
Max. Displacement Out of plane (in)	0.6	0.5

Model A is the most accurate for this type of structure; however, as noted in Section 4.2.3, use of shell elements created several difficulties.

Model B produces results that are in good agreement with the finite element model (Model A), and therefore, is appropriate for modeling out-of-plane response of wall panels.

APPENDIX 4-D RESPONSE SPECTRUM PG&E

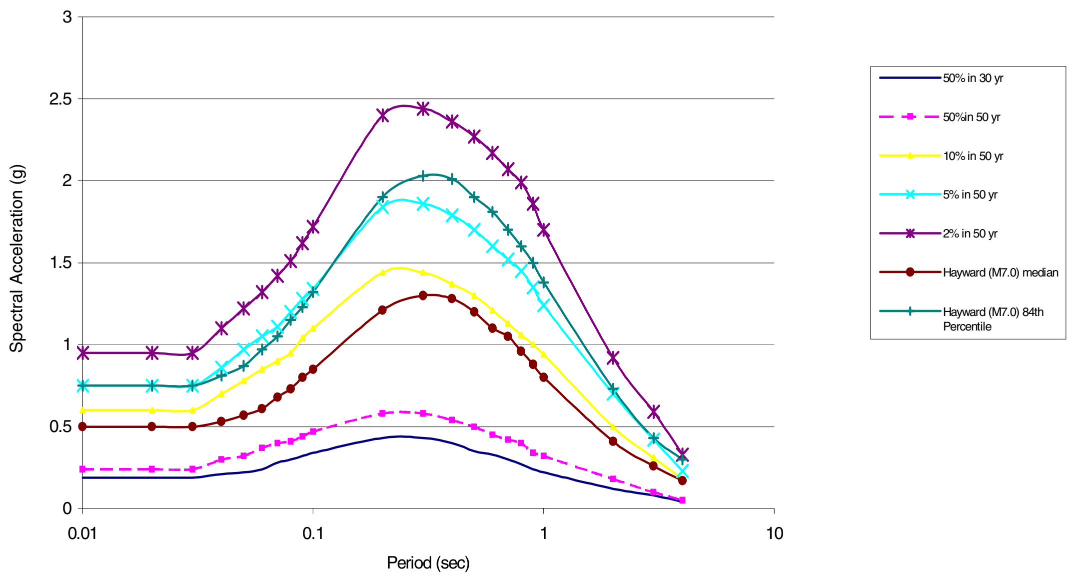

Figure 4-D1: PG&E response spectra

APPENDIX 4-E INFLUENCE OF THE DYNAMIC EFFECTS

The purpose of this study is to compare the out-of-plane response of a simple wall when subjected to static or dynamic force. For this purpose, a wall with a length of 1080 in., a thickness of 7 in. and a height of 350 in. was selected (Fig. 4-E1).

All the analyses are performed in 2-D with SAP 2000. The wall is pinned at the base and two springs are added on top of the structure to model the rotational and translational stiffness of the wall to roof connection. The first spring is a translational spring of 2200 kips/in.; the second is a rotational spring of 25,000 kips in./sec. These two values are somewhat arbitrary; however, varying the spring values did not influence the conclusions of this study.

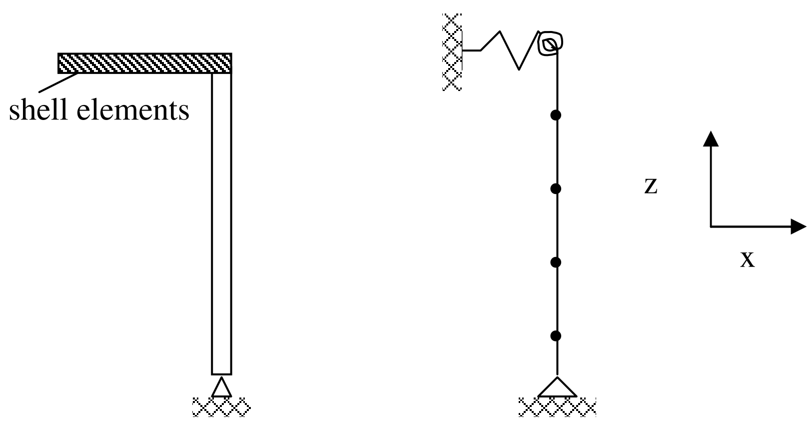

Fig. 4-E1 Model of the wall

The first step is to run a dynamic analysis using the response spectrum given by UBC 94. The displacement and rotation at the top of the wall obtained are shown in Table 4-E1.

Table 4E-1: Dynamic analysis

	Displacement in the X direction	Rotation about the Y direction
Spectrum UBC 94	0.42 in	0.25 rad

Using the same model, a static analysis is performed by imposing the displacement and the rotation values of Table 4-E1 at the top of the wall. The moment diagrams about the Y direction are compared in Fig. 4-E2.

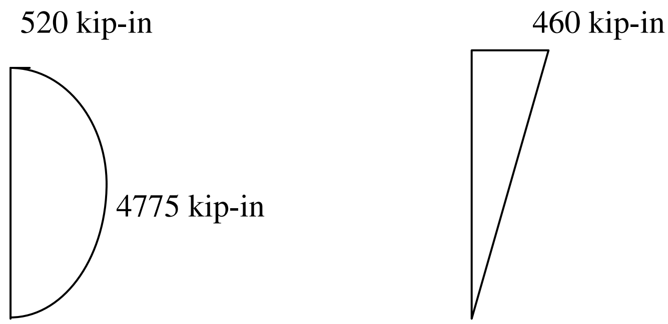

Dynamic analysis

Static analysis

Fig. 4-E2 Moment diagram about the y-axis

Analysis results indicate that the dynamic actions produced out-of-planes moments as much as 10 times greater than those for a static analysis. Moreover, maximum displacements occur at different locations. Thus, for thin wall panels subjected to transverse loads, dynamic response must be considered.

APPENDIX 4-F MODAL MASS PARTICIPATION

Table 4-F1: Modal mass participation for the FE model

MODE	PERIOD IN	INDIVIDUAL MODE (PERCENT)		CUMULATIVE MODE (PERCENT)	
		UX	UY	UX	UY
1	0.132976	0.004	12.9062	0.004	12.9062
2	0.116425	0.0054	0.2615	0.0094	13.1677
3	0.113681	0.0001	13.9018	0.0095	27.0696
4	0.098485	0.0022	1.2022	0.0117	28.2717
5	0.098341	7.2696	0.0171	7.2813	28.2888
6	0.096814	0.0475	1.1886	7.3289	29.4774
7	0.094945	0.1052	0.6683	7.4341	30.1457
8	0.09313	0.0047	0.0361	7.4388	30.1818
9	0.087225	0	0.001	7.4388	30.1828
10	0.084764	0.0016	0.1168	7.4404	30.2996
11	0.082814	0.3492	0.606	7.7896	30.9056
12	0.082596	0.0409	2.8178	7.8305	33.7234
13	0.081426	0.0277	1.7759	7.8582	35.4993
14	0.079931	0.0134	21.8805	7.8716	57.3798
15	0.078371	0.087	0.029	7.9586	57.4088
16	0.077073	0.1246	4.5007	8.0833	61.9096
17	0.075393	0.0002	1.9315	8.0835	63.8411
18	0.073696	0.0154	0.0618	8.0988	63.9028
19	0.070254	0.0001	0.0381	8.0989	63.9409
20	0.069969	1.3622	0.0248	9.4611	63.9657
21	0.069358	0.0165	0.2716	9.4776	64.2373
22	0.068031	0.0961	0.0318	9.5736	64.269
23	0.065641	0.1309	0.002	9.7046	64.271
24	0.064685	0.046	0.2332	9.7506	64.5042
25	0.063181	0.4941	0.0055	10.2447	64.5097
26	0.062096	0.0585	0.0094	10.3032	64.5191
27	0.061241	0.0555	0.1933	10.3587	64.7124
28	0.060439	0.2043	0.0374	10.5629	64.7498
29	0.060174	0.0003	0.05	10.5632	64.7998
30	0.058899	0.9147	0.0038	11.4779	64.8036
31	0.058628	0.7648	0.0071	12.2427	64.8107
32	0.058029	0.1058	1.5166	12.3485	66.3273
33	0.056757	1.7995	0.4466	14.1479	66.7739
34	0.055135	0.5268	0.4484	14.6747	67.2222

35	0.052715	0.5021	0.05	15.1769	67.2723
36	0.052442	1.2858	0.0294	16.4626	67.3017
37	0.051552	1.7284	0.1974	18.191	67.4991
38	0.050259	0.6607	0.0016	18.8517	67.5007
39	0.050151	1.3457	0.822	20.1973	68.3228
40	0.049952	13.5455	0.2341	33.7428	68.5568
41	0.048991	2.5605	0.0237	36.3033	68.5805
42	0.048754	7.5392	0.1622	43.8424	68.7428
43	0.047739	0.0212	0.1432	43.8636	68.8859
44	0.047502	0.0121	0.1985	43.8757	69.0844
45	0.047333	0.0112	0.0547	43.8868	69.1391
46	0.047	0.0003	0.011	43.8872	69.1501
47	0.046365	0.884	0.1566	44.7712	69.3068
48	0.045474	0.0462	0.0244	44.8174	69.3312
49	0.045246	0.0912	0.4277	44.9086	69.7589
50	0.044949	0.5729	0.0681	45.4815	69.827
51	0.04477	0	0.0003	45.4815	69.8273
52	0.044407	2.7091	0.3018	48.1906	70.129
53	0.043642	0.1806	0.2292	48.3712	70.3583
54	0.043147	0.9214	0.0012	49.2926	70.3595
55	0.042719	0.0032	0.0466	49.2958	70.4061
56	0.042244	0.0994	0.0107	49.3952	70.4168
57	0.042205	0.1159	0.024	49.5111	70.4408
58	0.041889	0.0316	0.0213	49.5427	70.4621
59	0.041352	0.1079	1.9409	49.6506	72.403
60	0.041118	0.4355	0.137	50.0861	72.54
61	0.040789	0.0047	0.2113	50.0909	72.7514
62	0.040618	0.5244	0.0105	50.6153	72.7619
63	0.040275	0.0908	0.6517	50.7061	73.4136
64	0.039821	0.1349	0.2141	50.841	73.6276
65	0.039578	0.0285	0.1143	50.8695	73.7419
66	0.039218	0.0077	0.0005	50.8772	73.7424
67	0.038845	0.5231	0.422	51.4003	74.1644
68	0.038631	0.3487	0.012	51.749	74.1764
69	0.038289	0.0193	0.0004	51.7683	74.1769
70	0.037937	0.2146	0.0002	51.9829	74.177
71	0.037814	0.3003	0.1795	52.2832	74.3566
72	0.037605	0.2774	0.0859	52.5606	74.4425
73	0.037083	0.0005	0.2713	52.5611	74.7138
74	0.036981	0.0962	0.1608	52.6573	74.8746
75	0.036718	0.0126	0.0024	52.6699	74.877
76	0.036488	0.0239	0.0373	52.6939	74.9144
77	0.036348	0.1587	0.4056	52.8526	75.3199
78	0.036078	0.2541	0.2473	53.1067	75.5673
79	0.035653	0.0177	0.2176	53.1244	75.7848
80	0.035492	0.0432	0.0111	53.1676	75.7959
81	0.035467	0.0951	0.016	53.2627	75.812
82	0.035214	0.0297	0.1445	53.2923	75.9565

83	0.035033	0.0368	0.001	53.3292	75.9575
84	0.034877	0.0592	0.021	53.3884	75.9785
85	0.03482	0.0051	0.049	53.3934	76.0274
86	0.034589	0.0069	0.0005	53.4003	76.0279
87	0.034544	0.1847	0.0275	53.585	76.0554
88	0.0343	0.0277	0.0931	53.6127	76.1485
89	0.034006	0.0087	0.0024	53.6214	76.1509
90	0.033785	0.0757	0.0028	53.6971	76.1537
91	0.033736	0.9661	0.076	54.6632	76.2298
92	0.033275	1.6709	0.0004	56.334	76.2302
93	0.033229	0.0059	0.0187	56.34	76.2489
94	0.0331	0.1146	0.0419	56.4546	76.2908
95	0.032506	0.0076	0.0215	56.4622	76.3123
96	0.032423	0.038	0.0066	56.5003	76.3189
97	0.032227	0.1335	0.0267	56.6338	76.3456
98	0.032105	0.0123	0.0058	56.646	76.3514
99	0.031912	0.0055	0.033	56.6516	76.3844
100	0.031631	0.0054	0.048	56.6569	76.4324
101	0.031289	0.2675	0.0172	56.9245	76.4497
102	0.030921	0.048	0.0143	56.9725	76.464
103	0.030778	0.2297	0.0741	57.2022	76.5381
104	0.030554	0.2476	0.2122	57.4498	76.7503
105	0.03047	0.1541	0.0314	57.6039	76.7817
106	0.030399	0.0421	0.0031	57.6459	76.7847
107	0.029956	0.0108	0.1988	57.6568	76.9836
108	0.02979	0.0037	0.0109	57.6605	76.9945
109	0.029703	0.4286	0.0084	58.0891	77.0029
110	0.029356	0.0134	0.1306	58.1025	77.1334
111	0.029266	1.4048	0.038	59.5073	77.1714
112	0.029175	0.5449	0.2187	60.0522	77.3901
113	0.028976	0.1814	0.0529	60.2337	77.4431
114	0.028789	2.1288	0.4629	62.3625	77.906
115	0.028497	0.0006	0.1754	62.3631	78.0814
116	0.028283	4.5841	0.8394	66.9472	78.9208
117	0.028267	0.2327	0.6566	67.1799	79.5774
118	0.028039	0.0206	3.814	67.2006	83.3913
119	0.027952	2.368	0.0406	69.5685	83.4319
120	0.027838	0.0982	0.1116	69.6667	83.5435
121	0.027808	0.0203	0.5577	69.687	84.1012
122	0.027506	0.1008	0.1262	69.7877	84.2274
123	0.02741	0.9599	0.0068	70.7476	84.2342
124	0.027321	0.059	0.4391	70.8066	84.6733
125	0.027075	0.7034	0	71.51	84.6733
126	0.026954	0.1301	0.0054	71.6401	84.6788
127	0.026856	0.1967	1.2051	71.8368	85.8839
128	0.026635	0.3201	1.043	72.1569	86.9268
129	0.02639	0.3059	0.001	72.4627	86.9278
130	0.02627	0.0037	0.0047	72.4665	86.9326

131	0.026229	0.4169	0.0005	72.8834	86.9331
132	0.026136	1.126	0.0569	74.0094	86.99
133	0.026112	0.0406	0.3276	74.05	87.3176
134	0.025982	0.0513	0.0058	74.1013	87.3234
135	0.025864	0.1251	0.3791	74.2263	87.7025
136	0.025663	0.001	0.2269	74.2273	87.9294
137	0.025606	0.0416	0.4086	74.2689	88.3381
138	0.025506	0.1323	0.0228	74.4012	88.3608
139	0.025453	0.8242	0.2213	75.2254	88.5821
140	0.025283	0.0243	0.3123	75.2496	88.8945
141	0.025064	0.0285	0.1285	75.2781	89.023
142	0.024964	0.3656	0.056	75.6438	89.079
143	0.024879	0.0022	0.4388	75.6459	89.5178
144	0.024806	0.3799	0.0016	76.0258	89.5195
145	0.024668	0.1737	0.0041	76.1996	89.5235
146	0.024555	0.181	0.0582	76.3806	89.5818
147	0.024379	0.024	0.1308	76.4046	89.7126
148	0.02422	0.0061	0.0005	76.4107	89.7131
149	0.024037	0.0568	0.136	76.4675	89.8491
150	0.023921	0.0185	0.0161	76.486	89.8652
151	0.023849	0.0064	0.019	76.4924	89.8842
152	0.02379	0.0157	0.0034	76.5081	89.8877
153	0.023654	0.0645	0.0693	76.5726	89.9569
154	0.023594	0.0068	0.0099	76.5795	89.9669
155	0.023552	0.1851	0.0166	76.7646	89.9835
156	0.023431	0.0871	0.0035	76.8517	89.9869
157	0.023373	0.0657	0.0515	76.9173	90.0384
158	0.023291	0.0548	0.061	76.9721	90.0994
159	0.02324	0.0069	0.003	76.979	90.1024
160	0.023148	0.0212	0.0019	77.0002	90.1043
161	0.023099	0.1223	0.0367	77.1225	90.141
162	0.023086	0.1517	0.0207	77.2742	90.1617
163	0.022984	0.0509	0.0304	77.3251	90.1921
164	0.022878	0.0335	0.0044	77.3586	90.1964
165	0.02283	0.2774	0.0013	77.636	90.1977
166	0.022813	0.2527	0.004	77.8887	90.2017
167	0.022742	0.0074	0.0092	77.8961	90.211
168	0.02273	0.0159	0.0041	77.912	90.2151
169	0.022595	0.0162	0.0001	77.9282	90.2151
170	0.022586	0.3109	0.0121	78.2391	90.2272
171	0.022433	0.002	0.047	78.2412	90.2743
172	0.022424	0.0119	0.0035	78.253	90.2778
173	0.02234	0.1965	0	78.4495	90.2778
174	0.02228	0.0869	0.0698	78.5364	90.3475
175	0.022161	0.0023	0.0323	78.5387	90.3798
176	0.022067	0.4607	0.088	78.9994	90.4678
177	0.021942	0.0751	0.0424	79.0745	90.5102
178	0.021914	0.1312	0.0587	79.2057	90.5688

179	0.021844	0.0085	0.0171	79.2142	90.5859
180	0.021773	0.2848	0.0024	79.499	90.5883
181	0.021596	0.4265	0.0043	79.9255	90.5926
182	0.021534	0.124	0.0014	80.0495	90.594
183	0.021393	0.4856	0.0064	80.5351	90.6004
184	0.021365	0.0174	0.0519	80.5525	90.6523
185	0.021271	0.0208	0.065	80.5732	90.7173
186	0.021238	0.0027	0.0013	80.5759	90.7186
187	0.021177	0.0941	0.0145	80.67	90.7331
188	0.021109	0.1716	0.0051	80.8416	90.7382
189	0.02108	0.0035	0.015	80.8452	90.7532
190	0.02108	0.0007	0.0047	80.8458	90.7579
191	0.021017	0.0052	0.0089	80.851	90.7669
192	0.02096	0.0177	0.0016	80.8687	90.7685
193	0.020867	0.5813	0.0219	81.45	90.7904
194	0.020766	0.5158	0.0592	81.9658	90.8496
195	0.020637	0.5038	0.0762	82.4695	90.9258
196	0.020499	0.3269	0.0322	82.7964	90.9581
197	0.020205	0.0349	0.0061	82.8313	90.9642
198	0.020136	0.0042	0.0197	82.8356	90.9839
199	0.020056	0.1749	0.0114	83.0105	90.9953
200	0.019984	0.0173	0.1064	83.0278	91.1016
201	0.019969	0.0025	0.0117	83.0303	91.1133
202	0.019813	0.0773	0.0061	83.1076	91.1194
203	0.019782	0.1124	0.0001	83.22	91.1195
204	0.019695	0.0179	0.0136	83.2379	91.1331
205	0.019651	0.1418	0.0031	83.3797	91.1362
206	0.019613	0.0965	0.0092	83.4762	91.1454
207	0.019521	0.0225	0.0059	83.4987	91.1513
208	0.019473	0.0024	0	83.5011	91.1513
209	0.019482	0.1795	0.0669	83.6805	91.2182
210	0.019369	0.0746	0.0128	83.7551	91.231
211	0.019296	0.0699	0.0233	83.825	91.2543
212	0.019258	0.038	0.1366	83.863	91.3909
213	0.019159	0.0114	0.0066	83.8743	91.3976
214	0.019103	0.0933	0.0005	83.9676	91.398
215	0.019089	0.0117	0.0632	83.9793	91.4612
216	0.019032	0.0251	0.0063	84.0044	91.4675
217	0.018966	0.113	0.0011	84.1174	91.4686
218	0.018949	0.1073	0.0045	84.2247	91.4731
219	0.018913	0.0044	0.0148	84.2291	91.4879
220	0.018879	0.0027	0.0017	84.2318	91.4897
221	0.018783	0.5868	0.0035	84.8186	91.4932
222	0.018661	0.2105	0.0007	85.0291	91.4939
223	0.018562	0.2635	0.0012	85.2926	91.4951
224	0.018476	0.0074	0.0534	85.3	91.5485
225	0.018446	0.0971	0.1708	85.3971	91.7193
226	0.018435	0.1518	0.0223	85.5489	91.7416

227	0.018318	0.0102	0.0011	85.5591	91.7427
228	0.01827	0.0332	0.0066	85.5923	91.7493
229	0.018246	0.0026	0.0098	85.5949	91.7591
230	0.01819	0.011	0.0273	85.6059	91.7863
231	0.018152	0.1248	0	85.7307	91.7864
232	0.018112	0.0032	0.0013	85.7339	91.7876
233	0.018069	0.0362	0.0001	85.7701	91.7877
234	0.017955	0.0087	0.0029	85.7788	91.7906
235	0.017937	0.0211	0.0294	85.7999	91.82
236	0.017877	0.0005	0.023	85.8004	91.843
237	0.017814	0.0617	0.0419	85.8621	91.8848
238	0.017721	0.0032	0.0416	85.8652	91.9264
239	0.017685	0.0101	0	85.8753	91.9264
240	0.017631	0.0001	0.027	85.8754	91.9534
241	0.017558	0.0053	0.0355	85.8808	91.9889
242	0.017532	0.013	0.0105	85.8938	91.9994
243	0.017482	0.0002	0.0002	85.894	91.9996
244	0.017469	0.0028	0.0061	85.8968	92.0057
245	0.017398	0.0008	0.0023	85.8976	92.008
246	0.017323	0.0046	0.0041	85.9022	92.0121
247	0.017288	0.0064	0.12	85.9086	92.1321
248	0.017249	0.0026	0.0124	85.9112	92.1445
249	0.01722	0.0389	0.0302	85.9501	92.1747
250	0.017195	0.0085	0.0268	85.9586	92.2015
251	0.017174	0.0016	0.0382	85.9603	92.2397
252	0.017079	0.0048	0.0181	85.9651	92.2578
253	0.017034	0.0401	0.0039	86.0051	92.2617
254	0.016949	0.0137	0.0029	86.0188	92.2645
255	0.016923	0.0045	0.0513	86.0233	92.3159
256	0.016851	0.0037	0.0119	86.027	92.3278
257	0.01682	0.0475	0.0027	86.0745	92.3305
258	0.016786	0.0001	0.0098	86.0745	92.3402
259	0.01673	0.0015	0.0062	86.0761	92.3465
260	0.016684	0.0005	0.0076	86.0766	92.3541
261	0.016681	0.0026	0.0028	86.0792	92.3568
262	0.016662	0.0001	0.0014	86.0793	92.3583
263	0.016584	0.0002	0	86.0794	92.3583
264	0.016524	0.0043	0.0041	86.0837	92.3624
265	0.016466	0.0136	0.0198	86.0973	92.3822
266	0.016444	0.0025	0.0523	86.0998	92.4345
267	0.016333	0.0304	0.0009	86.1302	92.4354
268	0.01629	0.0197	0.0024	86.15	92.4378
269	0.01624	0.0007	0.0208	86.1507	92.4586
270	0.01616	0.0069	0.0006	86.1576	92.4591
271	0.016133	0.0058	0.0001	86.1634	92.4592
272	0.016079	0.0096	0.0004	86.173	92.4596
273	0.016078	0.0039	0	86.177	92.4596
274	0.016029	0.0028	0.0047	86.1798	92.4643

275	0.015992	0.0047	0.0217	86.1846	92.486
276	0.015951	0.0003	0.0174	86.1849	92.5034
277	0.015931	0.0074	0.0068	86.1923	92.5103
278	0.015896	0.0007	0.0459	86.193	92.5561
279	0.015856	0.0013	0.0276	86.1943	92.5837
280	0.015778	0.0248	0.007	86.2191	92.5907
281	0.015759	0.0835	0.0077	86.3026	92.5985
282	0.015706	0.017	0.0028	86.3196	92.6012
283	0.015679	0.0099	0.0131	86.3295	92.6143
284	0.015652	0.0396	0.0046	86.369	92.6188
285	0.015613	0.0157	0.0026	86.3847	92.6214
286	0.015594	0.0296	0.0006	86.4143	92.622
287	0.015548	0.0001	0.019	86.4144	92.641
288	0.015527	0.0005	0.0081	86.4149	92.6492
289	0.015496	0.0284	0.0009	86.4433	92.6501
290	0.01545	0.0117	0.0017	86.455	92.6518
291	0.015432	0.004	0.0012	86.459	92.653
292	0.015381	0.0005	0.0095	86.4595	92.6624
293	0.015328	0.0003	0.0152	86.4598	92.6777
294	0.015311	0.0128	0.0027	86.4726	92.6803
295	0.015303	0.0275	0	86.5002	92.6803
296	0.015181	0.0371	0.0002	86.5373	92.6806
297	0.015192	0.0935	0.0033	86.6308	92.6839
298	0.015144	0.0284	0.0008	86.6592	92.6847
299	0.015084	0.0088	0.0005	86.6679	92.6852
300	0.015035	0.0922	0.0001	86.7601	92.6853

Table 4-F2 Modal mass participation for the FR model

MODE	PERIOD	INDIVIDUAL MODE (PERCENT)		CUMULATIVE MODE (PERCENT)	
		UX	UY	UX	UY
1	0.124295	0.0249	8.8578	0.0249	8.8578
2	0.108882	0.0277	13.2615	0.0526	22.1193
3	0.096655	0.0121	0.0035	0.0647	22.1228
4	0.092594	0.0002	0.0176	0.0649	22.1404
5	0.091344	0.3016	12.9648	0.3664	35.1052
6	0.089801	0.1029	4.7098	0.4694	39.815
7	0.086989	0.3252	0.0808	0.7946	39.8958
8	0.085126	0.6171	0.082	1.4118	39.9778
9	0.083531	4.5541	0.6479	5.9658	40.6256
10	0.080789	6.3043	0.2109	12.2701	40.8366
11	0.075991	0.0078	0.0674	12.2779	40.9039
12	0.074664	0.4856	0.0006	12.7635	40.9045
13	0.072058	3.0242	2.9667	15.7877	43.8712
14	0.070321	0.5044	11.3737	16.2921	55.2449
15	0.068108	7.5019	1.7864	23.794	57.0313
16	0.063447	4.2056	0.1566	27.9996	57.1879
17	0.059853	10.7195	0.0014	38.7191	57.1893
18	0.058349	2.5214	0.2071	41.2405	57.3964
19	0.052339	13.4387	0.5587	54.6792	57.9551
20	0.048207	0.4083	0.7655	55.0876	58.7206
21	0.04378	7.5041	0.0826	62.5917	58.8032
22	0.041552	0.0292	3.4423	62.6209	62.2455
23	0.035888	4.5862	0.2248	67.2071	62.4702
24	0.03331	0.0029	11.0714	67.2099	73.5416
25	0.026646	2.0497	3.5533	69.2596	77.095
26	0.025994	12.8729	1.0102	82.1325	78.1052
27	0.016913	3.1914	2.0702	85.3239	80.1754
28	0.016399	0.8648	6.5069	86.1888	86.6823
29	0.008842	0.0949	9.8067	86.2836	96.489
30	0.008154	9.7991	0.082	96.0828	96.571

APPENDIX 4-G WALLS CAPACITY

- **East wall**

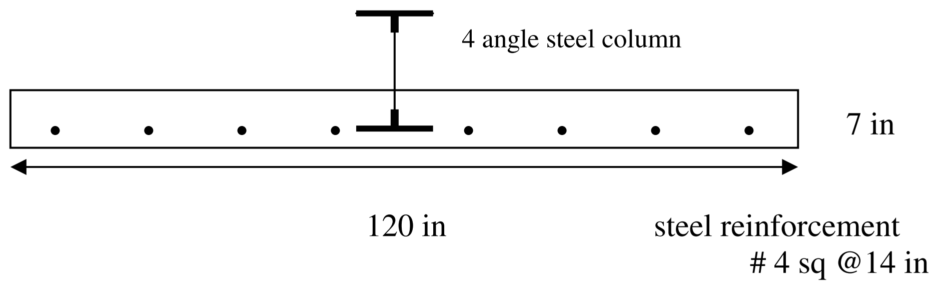

Fig. 4-G1: Walls capacity for the east wall

- **North wall: 1st column**

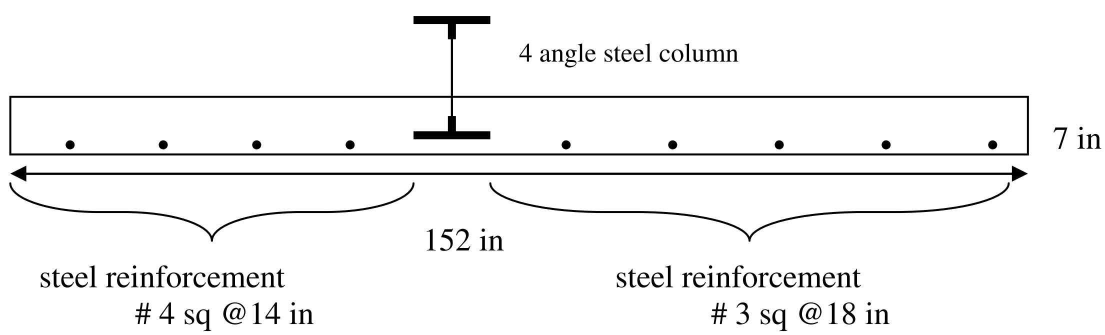

Fig. 4-G2: Walls capacity for the north wall: 1st column

North wall: 2nd column

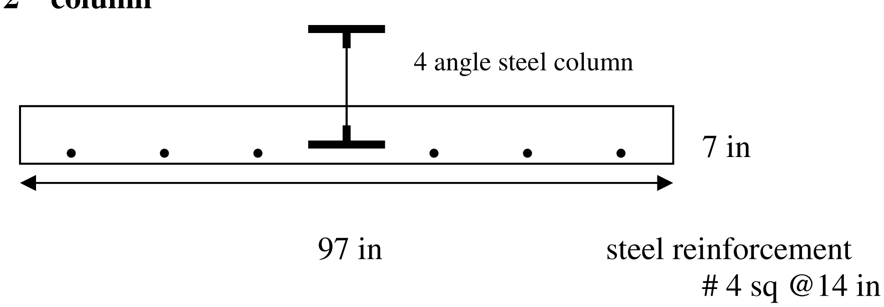

Fig. 4-G3: Walls capacity for the north wall: 2nd column

Note: the reinforcing steel bars are rectangular and placed at 2 in. in the concrete

```
berkeastwallmx
:
SYSTEM:
 T=1      P= 1          E= 0        TOL= 0.0001    :
:
SECTION:
 1    HI=8       HJ=5     N1=8       N2=5      X=56.5  Y=7
 2    HI=120     HJ= 7    N1=120     N2= 7     X=0     Y=0:
:
CONFINED:
 1    F=1,8,5,1,8
STEEL:
  1   X= 4      Y= 2        A= 0.25    T= 1
  4   X=46      Y=2         G=1,4,1
  5   X=56.88   Y=2         A=0.2344
  13  X=63.13   Y=2         G=5,13,1
  14  X=74      Y=2         A=0.25
  17  X=116     Y=2         G=14,17,1
  18  X=60      Y=3.04853   A=0.4
  20  X=60      Y=4.6875    G=18,20,1
  21  X=60      Y=5.5       A=0.36
  27  X=60      Y=7.8       G=21,27,1
  28  X=60      Y=8.31      A=0.2344
  30  X=60      Y=9.9515    G=28,30,1
  31  X=56.88   Y=11        A=0.25
  33  X=63.13   Y=11        G=31,33,1
:
PROPERTY:
  FC=4    E1=0.002  E2=0.0038 FR=0.4:
  FC=0.01 E1=0.002  E2=0.0038 FR=0.01             :
  FY=45 FU=70 FF=65 E1=0.03 E2=0.12 E3=0.20 E=29000 ET=1100
:
DATA:
  EC=0.003   A=0     N=30
:
END
```

Table 4-G1 East wall P-M interaction values

Mxx	P	Myy	curvature	Mxx	P
5.13E+02	-4.18E+02	-6.43E-01		513.3	-417.7
1.19E+03	1.55E-01	-1.38E-01	4.92E-04	-5.81E+02	-3.52E-03
1.20E+03	1.30E+02	-1.30E-01	4.54E-04	-9.18E+02	1.29E+02
1.09E+03	2.59E+02	-6.88E-02	4.35E-04	-1.25E+03	2.58E+02
9.97E+02	3.88E+02	1.24E-02	4.09E-04	-1.60E+03	3.88E+02
8.49E+02	5.18E+02	5.47E-02	3.96E-04	-1.86E+03	5.17E+02
6.97E+02	6.47E+02	9.84E-02	3.82E-04	-2.06E+03	6.47E+02
5.91E+02	7.76E+02	1.58E-01	3.62E-04	-2.26E+03	7.76E+02
3.77E+02	9.06E+02	1.91E-01	3.52E-04	-2.48E+03	9.05E+02
1.60E+02	1.04E+03	2.25E-01	3.41E-04	-2.71E+03	1.04E+03
-5.89E+01	1.16E+03	2.60E-01	3.29E-04	-2.94E+03	1.16E+03
-2.74E+02	1.29E+03	2.98E-01	3.17E-04	-3.19E+03	1.29E+03
-5.73E+02	1.42E+03	3.29E-01	3.08E-04	-3.44E+03	1.42E+03
-8.68E+02	1.55E+03	3.53E-01	2.99E-04	-3.70E+03	1.55E+03
-1.14E+03	1.68E+03	3.81E-01	2.88E-04	-3.97E+03	1.68E+03
-1.53E+03	1.81E+03	4.01E-01	2.80E-04	-4.24E+03	1.81E+03
-1.91E+03	1.94E+03	4.21E-01	2.73E-04	-4.52E+03	1.94E+03
-2.26E+03	2.07E+03	4.45E-01	2.64E-04	-4.80E+03	2.07E+03
-2.73E+03	2.20E+03	4.62E-01	2.57E-04	-5.09E+03	2.20E+03
-3.21E+03	2.33E+03	4.79E-01	2.51E-04	-5.37E+03	2.33E+03
-3.69E+03	2.46E+03	4.98E-01	2.44E-04	-5.67E+03	2.46E+03
-4.17E+03	2.59E+03	5.17E-01	2.37E-04	-5.96E+03	2.59E+03
-4.66E+03	2.72E+03	5.37E-01	2.29E-04	-6.25E+03	2.72E+03
-5.15E+03	2.85E+03	5.59E-01	2.21E-04	-6.55E+03	2.85E+03
-5.64E+03	2.98E+03	5.83E-01	2.12E-04	-6.87E+03	2.98E+03
-6.14E+03	3.10E+03	6.08E-01	2.03E-04	-7.19E+03	3.10E+03
-6.65E+03	3.23E+03	6.37E-01	1.92E-04	-7.53E+03	3.23E+03
-7.17E+03	3.36E+03	6.70E-01	1.80E-04	-7.86E+03	3.36E+03
-7.75E+03	3.49E+03	7.12E-01	1.65E-04	-6.52E+03	2.83E+03
-8.44E+03	3.62E+03	7.67E-01	1.39E-04	-6.52E+03	2.83E+03
-6.52E+03	2.83E+03	7.57E-01	4.44E-19	-6.52E+03	2.83E+03

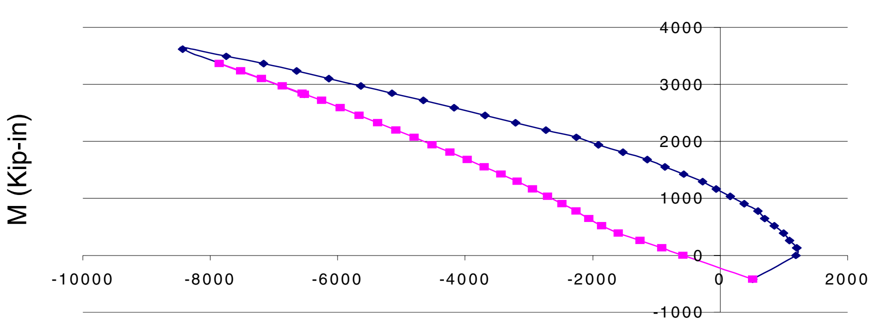

Figure 4-G4: East Wall PM Interaction Diagram
A=0-180

APPENDIX 4-H TRUSSES

The entire truss is composed of simple or double angles. Because they can be in compression or in tension, both have to be checked:

- tension: the structure presents three types of elements:
- type 1: 2L 3.5, 2.5, ¼
- type 2: 2L 2 , 2 , ¼
- type 3: L 2.5, 2 , ¼

These truss members can fail in tension in three different ways:

(a) yield in gross section: $\phi Pn = 0.9 * Ag * Fy$

(b) fracture on net section: $\phi Pn = 0.75 * Ae * Fu$

(c) block shear: $$\phi Pn = \text{Max} \left\{ \begin{array}{l} 0.75*(Ans(0.6Fu) + Atg(Fy) \\ 0.75*(Ant(Fu) + Avg(0.6Fy) \end{array} \right\}$$

with Ag	gross section area		
An	net section area:	$An = Ag - A_{holes}$	
Ae	effective net section area	$Ae = U\ An$ (with U: area reduction coefficient)	
Avg	gross shear area	Atg	gross tension area
Ans	net shear area	Ant	net tension area

The results of these calculations are displayed in the Table 4-H1 & 2.

Table 4-H1 Axial capacity (ΦPn) for yield gross section failure
and fracture on net section

TYPE	Yield Gross Section ΦPn	Fracture on Net Section ΦPn
2L 3.5, 2.5, ¼	93	92
2L 2 , 2 , ¼	61	55
L 2.5, 2 , ¼	34	32

Table 4-H2 Axial capacity (ΦPn) for block shear failure

Number of holes:	2	3	4	5
2L 3.5, 2.5, ¼	60	75	91	106
2L 2 , 2 , ¼	48	62	77	92
L 2.5, 2 , ¼	51	66	81	96

The maximum axial demands acting on the model for both response spectra are displayed in Table 4-H3:

Table 4-H3 Maximum demand acting on the truss elements (kips)

Location	Y=179"	Y=530"	X=249"	X=435"	X=647"	X=837"
Spectra 1	16	16	13	6	8	6
Spectra 2	7	9	8	14	24	17

The maximum demands are lower than the capacity of each element, thus the truss elements are expected to have good performance.

APPENDIX 4-I BUILT-UP STEEL COLUMNS

The interior steel columns are composed by 4 angles (4*3*5/16) and reduced at mid height by almost half of their width. The two parts of the columns are studied as two different columns:

The upper part will be designed as the top column

The lower part as the bottom column;

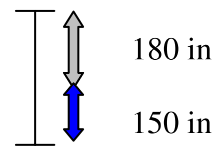

Fig. 4-I1: Model of the built-up columns

The properties of the columns are summarized in Table 4-I1.

Table 4-I1: Properties of the built-up columns

	Bottom column	Top column
Ixx	626	195
Iyy	30	30
A	12	11
K	1.2	1
Q	0.6	1
ΦPn	153	239
Mpx	88	147
Mpy	1 700	965
ΦMx	1 710	1057
ΦMy	417	417
Vn=0.6*fy*Aw	94	55

The demand applied on the columns is summarized in Table 4-I2.

Table 4-I2 Maximal demands

Pu	13	13
Mx	8	9
My	752	257

Units are in Kips, in.

APPENDIX 4-J PINNED BASE FR MODEL

The fundamental period for the pinned-base model is 0.15 sec. Compared to the fundamental period of the fixed-base FR model (0.12 sec.), the building is more flexible. This was expected considering that more degrees of freedom are allowed at the base of the wall. The same elements considered in Chapter 4.3.1 are evaluated in the following sections.

(a) Roof

The displacement at the roof level have been defined from the SAP 2000 model and presented in Table 4-J1.

Table 4-J1: Displacement results at the roof level (*C1*C2*C3)

	Spec 100% X - 30% Y	Spec 30% X - 100% Y
Max Displacement in X dir. (in)	0.03	0.01
Max Displacement in Y dir. (in)	0.06	0.05
Max Drift in X dir. (%)	0.007	0.003
Max Drift in Y dir. (%)	0.018	0.015

The maximum displacements at the roof level are almost the same as the one obtained for the fixed base FR model. The building is very stiff. Therefore, transverse roof level displacements are insignificant and the building is behaving in the elastic range.

(b) Walls

It is important to notice that, as for the fixed-base model:

- The demand values displayed in the following tables have been multiplied by the factor C1*C2*C3 (Section 3.3.2.3.A FEMA 273), and so are fictitious (designed to represent displacements and not forces). These values are appropriate for deformation-controlled elements but they will be divided by the factor C1*C2*C3 for force-controlled elements.
- For the out-of-plane moment, assumed to be deformation-controlled, the element demand modifier, m, has been defined as equal to 4 (Table 6-11 of FEMA 273). The in-plane-moment and the shear are considered force-controlled actions.

East Wall: Wall sections between the large openings were evaluated using standard procedures. Cross-section and material information to define the moment capacity of these panels are presented in Appendix 4-G.

(i) Demand obtained from analysis

Table 4-J2(a) Maximum demand on the east wall panels

Load case	P (k)	Vx (k)	Vy (k)	Mx (kip-in)	My (kip-in)
100% X, 30% Y	29	72	3	191	5 851
30% X, 100% Y	38	74	7	558	4 654

(ii) Capacity

Moment capacity $M_{nx} = 1\ 200$ kip-in

$M_{ny} = 21\ 700$ kip-in

Shear capacity $V_n = 2A_{cv}\sqrt{f_c'} + 0.6 f_y d t_w = 162$ kips

(iii) Evaluation

Table 4-J2(b) Acceptance criteria

Load case	Vu/ΦVn in-plane	Mx/ΦMnx in-plane	My/ΦMny out-of-plane
100% X, 30% Y	0.43	0.16	0.09
30% X, 100% Y	0.45	0.45	0.07

(iv) Discussion

Ratios displayed in Table J-2(b) indicate that demands on the element are significantly less than capacity. Therefore, acceptable performance is expected. It is important to note that allowing free rotation about the weak axis of the wall slightly decreases the moment developed in the wall, but has no noticeable influence on the shear.

North Wall: The three column elements presented in Fig. 4.12 are evaluated.

1st column (north wall)

(i) Demand obtained from analyses

Table 4-J3(a) Maximum demand on the first column of the north wall

Load case	P (k)	Vx (k)	Vy (k)	Mx (kip-in)	My (kip-in)
100% X, 30% Y	24	0.4	45	5 338	26
30% X, 100% Y	11	0.1	124	14 382	9

(ii) Capacity

Moment capacity $M_{nx} = 32\ 800$ kip-in

$M_{ny} = 1\ 160$ kip-in

Shear capacity $V_n = 190$ kips

(iii) Evaluation

Table 4-J3(b) Acceptance criteria

Load case	Vu/ΦVn in-plane	Mx/ΦMnx in-plane	My/ΦMny out-of-plane
100% X, 30% Y	0.24	0.05	0.02
30% X, 100% Y	0.65	0.15	0.01

2nd column (north wall)

(i) Demand obtained from analyses

Table 4-J4(a) Maximum demand on the second column of the north wall

Load case	P (k)	Vx (k)	Vy (k)	Mx (kip-in)	My (kip-in)
100% X, 30% Y	6	0.6	20	2 332	72
30% X, 100% Y	15	0.2	55	6 315	26

(ii) Capacity

Moment capacity $M_{nx} = 15\ 900$ kip-in

$M_{ny} = 2\ 080$ kip-in

Shear capacity $V_n = 86$ kips

(iii) Evaluation

Table 4-J4(b) Acceptance criteria

Load case	Vu/ΦVn in-plane	Mx/ΦMnx in-plane	My/ΦMny out-of-plane
100% X, 30% Y	0.24	0.05	0.03
30% X, 100% Y	0.64	0.13	0.01

<u>*3rd column (north wall)*</u>

(i) Demand obtained from analysis

Table 4-J5(a) Maximum demand on the third column of the north wall

Load case	P (k)	Vx (k)	Vy (k)	Mx (kip-in)	My (kip-in)
100% X, 30% Y	5	1.4	27	2 346	87
30% X, 100% Y	14	1.9	79	6 511	135

(ii) Capacity

Moment capacity $M_{nx} = 15\ 900$ kip-in

$M_{nx} = 2\ 080$ kip-in

Shear capacity $V_n = 86$ kips

(iii) Evaluation

Table 4-J5(b) Acceptance criteria

Load case	Vu/ΦVn in-plane	Mx/ΦMnx in-plane	My/ΦMny out-of-plane
100% X, 30% Y	0.32	0.05	0.04
30% X, 100% Y	0.91	0.13	0.06

The ratios display in Table 4-J3 (b), 4-J4 (b), 4-J5 (b) indicate that the demands on the elements are less than the capacity; therefore, acceptable performance is expected. Note that a factor κ of 0.75 and design material properties, which would lower the demand/ capacity ratios for in-plane actions considerably (concrete strength is likely much higher), have been used. Considering the lack of information, this makes the calculation relatively conservative.

(c) Built-up steel columns

The LRFD Criteria (4-3) and the Acceptance Criteria (4-4) from FEMA 273 are applied as in Chapter 4.3.1 (c). The values of $m_x = 2$ and $m_y = 8$ are obtained from Table 5-8 (FEMA 273/274), for a collapse-prevention limit state. The following results are obtained:

Column between roof and gallery slab:

$$\frac{P_u}{2P_n} + \left[\frac{M_{ux}}{2M_{nx}} + \frac{M_{uy}}{8M_{ny}}\right] = 0.12 < 1$$

Column between gallery slab and base:

$$\frac{P_u}{2P_n} + \left[\frac{M_{ux}}{2M_{nx}} + \frac{M_{uy}}{8M_{ny}}\right] = 0.37 < 1$$

Comparing the ratios obtained from the fixed-base FR model, no trend is apparent. However, these ratios are much lower than one and then acceptable behavior is expected.

(d) Trusses

The properties of the trusses and the calculations for tension are presented in Appendix 4-H. For compression, biaxial bending was considered. The demand, capacity and the evaluation of each element evaluated are summarized in Tables 4-J6 and 4-J7.

Table 4-J6: South–north trusses

Section Angle	Location *	l	λ	ϕPn (kips)	Pu (kips)	Mux (kip-in)	Muy (kip-in)	Pu/ϕPn	(4-8)
2L 3.5, 2 , 1/4	A a	54	0.64	74.2	39.2	0.7	2.6	0.35	0.33
L 2.5, 2 , 1/4	A b	68	1.80	10.3	7.5	0	0	0.58	0.49

* Refer to Fig. 4.13 and 4.15

Table 4-J7: East-west trusses

Section Angle	Location *	l	λ	ϕPn (kips)	Pu (kips)	Mux (kip-in)	Muy (kip-in)	Pu/ϕPn	(4-8)
2L 3.5, 2 , 1/4	III 1	71	0.84	67.1	45.1	9.1	0.1	0.67	0.70
2L 3.5, 2 , 1/4	IV 1	71	0.84	67.1	32.6	6.9	0.1	0.48	0.80
2L 3.5, 2 , 1/4	I 2	122	1.45	36.7	6.5	0.3	1.1	0.18	0.16
2L 3.5, 2 , 1/4	IV2	122	1.45	36.7	22.9	0.9	0.3	0.62	0.55
2L 2.5, 2 , 1/4	III 3	82	1.51	39.8	13.7	0	0	0.34	0.29
2L 2.5, 2 , 1/4	IV 3	82	1.51	39.8	9.4	0	0	0.24	0.20

* Refer to Fig. 4.14 and 4.15

λ is the limiting width-thickness ratios defined by LRFD

All the demands have been multiplied by C1*C2*C3. However, the building is behaving in the elastic range, and the factor C1*C2*C3 is then equal to 1. By using a higher factor, the calculations are more conservative.

The ratios given in Tables 4-J6 and 4-J7 are less than one. Therefore, the acceptance criteria are satisfied. Results for the fixed-base FR model indicate acceptable performance. However, the ratios are higher for the truss elements close to the interior wall at the north end. This is likely due to the fact that the west and interior wall go through higher deformation if their base is pinned. This does not happen at proximity of the east wall because the slab counterbalances the phenomena.

APPENDIX 4-K 3-D VIEW OF THE SFSI MODEL

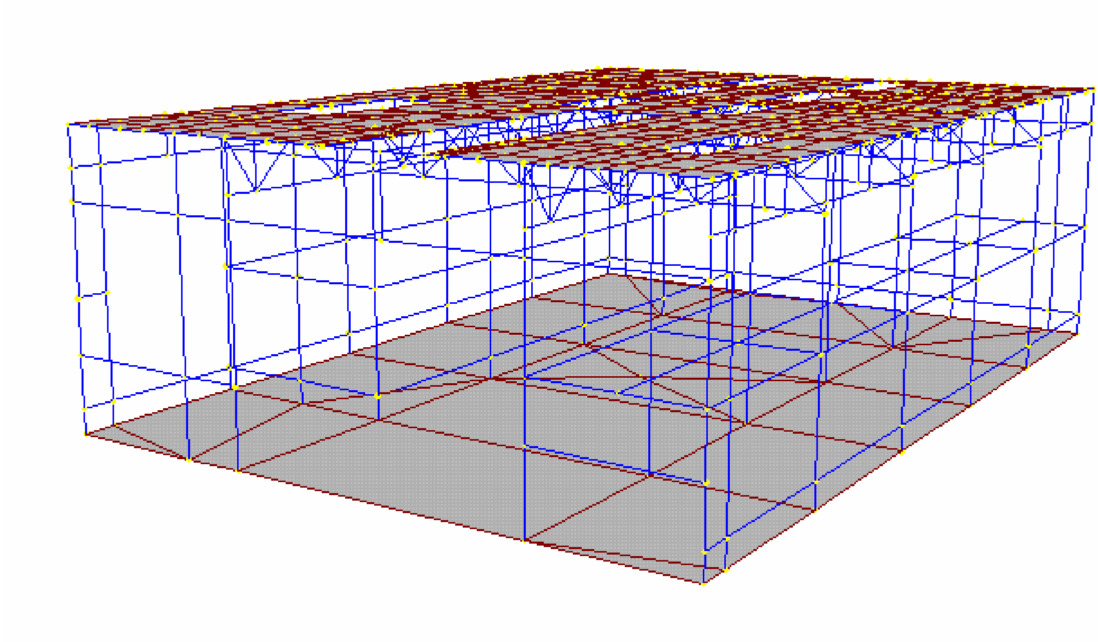

Fig. 4-K1 3-D view of the SFSI model

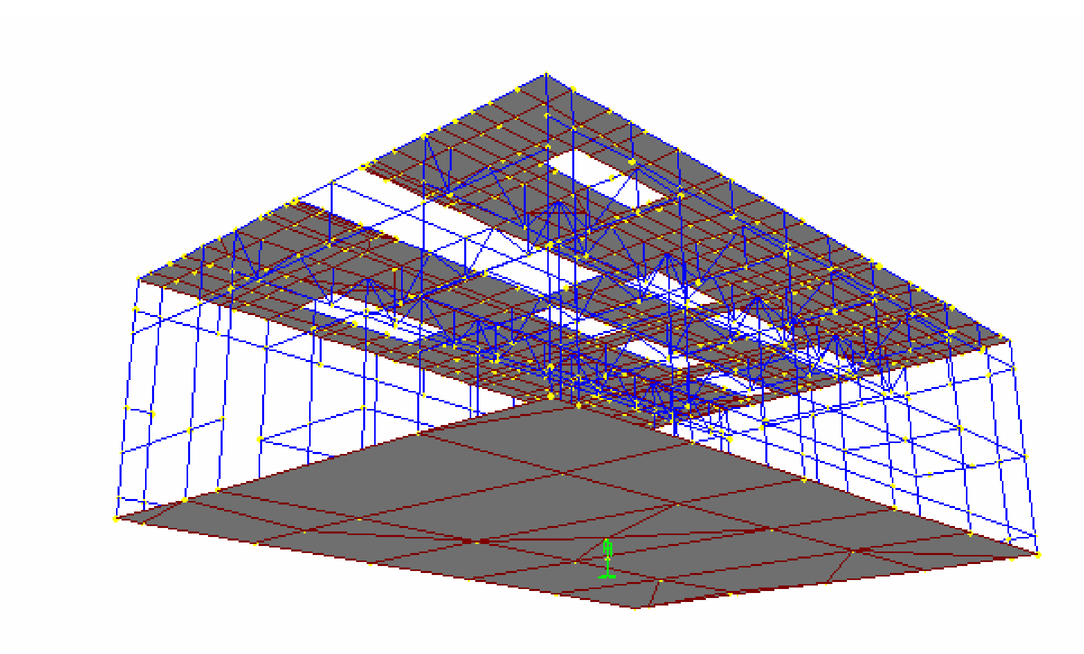

Fig. 4-K2 3-D view of the SFSI model

APPENDIX 4-L BUILT-UP STEEL COLUMNS FOR THE SOIL-FOUNDATION-STRUCTURE INTERACTION MODEL

The interior steel columns are composed by 4 angles (4*3*5/16) and reduced at mid height by almost half of their width. The two parts are studied as two difference columns:

the upper part will be design as the top column

the lower part as the bottom column;

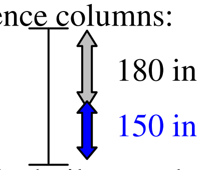

Fig. 4-L1 Model of the built-up columns

The properties of the columns are summarized in Table 4-L1.

Table 4-L1: Properties of the built-up columns

	Bottom column	Top column
Ixx	626	195
Iyy	30	30
A	12	11
K	1.2	1
Q	0.6	1
ΦPn	153	239
Mpx	88	147
Mpy	1 700	965
ΦMx	1 710	1057
ΦMy	417	417
Vn=0.6*fy*Aw	94	55

The demands applied on the columns are summarized in Table 4-L2.

Table 4-L2 Maximal demands

Pu	13	10
Mx	4	6
My	427	87

Units are in Kips, in.

PEER REPORTS

PEER reports are available from the National Information Service for Earthquake Engineering (NISEE). To order PEER reports, please contact the Pacific Earthquake Engineering Research Center, 1301 South 46th Street, Richmond, California 94804-4698. Tel.: (510) 231-9468; Fax: (510) 231-9461.

PEER 2001/12 *Development of Geotechnical Capabilities in OpenSees*. Boris Jeremić. September 2001. $13.00

PEER 2001/10 *Amplification Factors for Spectral Acceleration in Active Regions.* Jonathan P. Stewart, Andrew H. Liu, Yoojoong Choi, and Mehmet B. Baturay. December 2001. $20.00

PEER 2001/09 *Ground Motion Evaluation Procedures for Performance-Based Design.* Jonathan P. Stewart, Shyh-Jeng Chiou, Jonathan D. Bray, Robert W. Graves, Paul G. Somerville, and Norman A. Abrahamson. September 2001. $26.00

PEER 2001/08 *Experimental and Computational Evaluation of Reinforced Concrete Bridge Beam-Column Connections for Seismic Performance*. Clay J. Naito, Jack P. Moehle, and Khalid M. Mosalam. November 2001. $26.00

PEER 2001/07 *The Rocking Spectrum and the Shortcomings of Design Guidelines.* Nicos Makris and Dimitrios Konstantinidis. August 2001. $15.00

PEER 2001/06 *Development of an Electrical Substation Equipment Performance Database for Evaluation of Equipment Fragilities*. Thalia Agnanos. April 1999. $15.00

PEER 2001/05 *Stiffness Analysis of Fiber-Reinforced Elastomeric Isolators.* Hsiang-Chuan Tsai and James M. Kelly. May 2001. $20.00

PEER 2001/04 *Organizational and Societal Considerations for Performance-Based Earthquake Engineering.* Peter J. May. April 2001. $15.00

PEER 2001/03 *A Modal Pushover Analysis Procedure to Estimate Seismic Demands for Buildings: Theory and Preliminary Evaluation.* Anil K. Chopra and Rakesh K. Goel. January 2001. $15.00

PEER 2001/02 *Seismic Response Analysis of Highway Overcrossings Including Soil-Structure Interaction.* Jian Zhang and Nicos Makris. March 2001. $20.00

PEER 2001/01 *Experimental Study of Large Seismic Steel Beam-to-Column Connections.* Egor P. Popov and Shakhzod M. Takhirov. November 2000. $15.00

PEER 2000/10 *The Second U.S.-Japan Workshop on Performance-Based Earthquake Engineering Methodology for Reinforced Concrete Building Structures.* March 2000. $39.00

PEER 2000/09 *Structural Engineering Reconnaissance of the August 17, 1999 Earthquake: Kocaeli (Izmit), Turkey.* Halil Sezen, Kenneth J. Elwood, Andrew S. Whittaker, Khalid Mosalam, John J. Wallace, and John F. Stanton. December 2000. $20.00

PEER 2000/08 *Behavior of Reinforced Concrete Bridge Columns Having Varying Aspect Ratios and Varying Lengths of Confinement.* Anthony J. Calderone, Dawn E. Lehman, and Jack P. Moehle. January 2001. $20.00

PEER 2000/07 *Cover-Plate and Flange-Plate Reinforced Steel Moment-Resisting Connections.* Taejin Kim, Andrew S. Whittaker, Amir S. Gilani, Vitelmo V. Bertero, and Shakhzod M. Takhirov. September 2000. $33.00

PEER 2000/06 *Seismic Evaluation and Analysis of 230-kV Disconnect Switches.* Amir S. J. Gilani, Andrew S. Whittaker, Gregory L. Fenves, Chun-Hao Chen, Henry Ho, and Eric Fujisaki. July 2000. $26.00

PEER 2000/05 *Performance-Based Evaluation of Exterior Reinforced Concrete Building Joints for Seismic Excitation.* Chandra Clyde, Chris P. Pantelides, and Lawrence D. Reaveley. July 2000. $15.00

PEER 2000/04 *An Evaluation of Seismic Energy Demand: An Attenuation Approach.* Chung-Che Chou and Chia-Ming Uang. July 1999. $20.00

PEER 2000/03 *Framing Earthquake Retrofitting Decisions: The Case of Hillside Homes in Los Angeles.* Detlof von Winterfeldt, Nels Roselund, and Alicia Kitsuse. March 2000. $13.00

PEER 2000/02 *U.S.-Japan Workshop on the Effects of Near-Field Earthquake Shaking.* Andrew Whittaker, ed. July 2000. $20.00

PEER 2000/01 *Further Studies on Seismic Interaction in Interconnected Electrical Substation Equipment.* Armen Der Kiureghian, Kee-Jeung Hong, and Jerome L. Sackman. November 1999. $20.00

PEER 1999/14 *Seismic Evaluation and Retrofit of 230-kV Porcelain Transformer Bushings*. Amir S. Gilani, Andrew S. Whittaker, Gregory L. Fenves, and Eric Fujisaki. December 1999. $26.00

PEER 1999/13 *Building Vulnerability Studies: Modeling and Evaluation of Tilt-up and Steel Reinforced Concrete Buildings.* John W. Wallace, Jonathan P. Stewart, and Andrew S. Whittaker, editors. December 1999. $26.00

PEER 1999/12 *Rehabilitation of Nonductile RC Frame Building Using Encasement Plates and Energy-Dissipating Devices.* Mehrdad Sasani, Vitelmo V. Bertero, James C. Anderson. December 1999. $26.00

PEER 1999/11 *Performance Evaluation Database for Concrete Bridge Components and Systems under Simulated Seismic Loads.* Yael D. Hose and Frieder Seible. November 1999. $20.00

PEER 1999/10 *U.S.-Japan Workshop on Performance-Based Earthquake Engineering Methodology for Reinforced Concrete Building Structures.* December 1999. $33.00

PEER 1999/09 *Performance Improvement of Long Period Building Structures Subjected to Severe Pulse-Type Ground Motions*. James C. Anderson, Vitelmo V. Bertero, and Raul Bertero. October 1999. $26.00

PEER 1999/08 *Envelopes for Seismic Response Vectors.* Charles Menun and Armen Der Kiureghian. July 1999. $26.00

PEER 1999/07 *Documentation of Strengths and Weaknesses of Current Computer Analysis Methods for Seismic Performance of Reinforced Concrete Members.* William F. Cofer. November 1999. $15.00

PEER 1999/06 *Rocking Response and Overturning of Anchored Equipment under Seismic Excitations.* Nicos Makris and Jian Zhang. November 1999. $15.00

PEER 1999/05 *Seismic Evaluation of 550 kV Porcelain Transformer Bushings.* Amir S. Gilani, Andrew S. Whittaker, Gregory L. Fenves, and Eric Fujisaki. October 1999. $15.00

PEER 1999/04 *Adoption and Enforcement of Earthquake Risk-Reduction Measures.* Peter J. May, Raymond J. Burby, T. Jens Feeley, and Robert Wood. $15.00

PEER 1999/03 *Task 3 Characterization of Site Response General Site Categories*. Adrian Rodriguez-Marek, Jonathan D. Bray, and Norman Abrahamson. February 1999. $20.00

PEER 1999/02 *Capacity-Demand-Diagram Methods for Estimating Seismic Deformation of Inelastic Structures: SDF Systems*. Anil K. Chopra and Rakesh Goel. April 1999. $15.00

PEER 1999/01 *Interaction in Interconnected Electrical Substation Equipment Subjected to Earthquake Ground Motions.* Armen Der Kiureghian, Jerome L. Sackman, and Kee-Jeung Hong. February 1999. $20.00

PEER 1998/08 *Behavior and Failure Analysis of a Multiple-Frame Highway Bridge in the 1994 Northridge Earthquake.* Gregory L. Fenves and Michael Ellery. December 1998. $20.00

PEER 1998/07 *Empirical Evaluation of Inertial Soil-Structure Interaction Effects.* Jonathan P. Stewart, Raymond B. Seed, and Gregory L. Fenves. November 1998. $26.00

PEER 1998/06 *Effect of Damping Mechanisms on the Response of Seismic Isolated Structures.* Nicos Makris and Shih-Po Chang. November 1998. $15.00

PEER 1998/05 *Rocking Response and Overturning of Equipment under Horizontal Pulse-Type Motions.* Nicos Makris and Yiannis Roussos. October 1998. $15.00

PEER 1998/04 *Pacific Earthquake Engineering Research Invitational Workshop Proceedings, May 14–15, 1998: Defining the Links between Planning, Policy Analysis, Economics and Earthquake Engineering.* Mary Comerio and Peter Gordon. September 1998. $15.00

PEER 1998/03 *Repair/Upgrade Procedures for Welded Beam to Column Connections.* James C. Anderson and Xiaojing Duan. May 1998. $33.00

PEER 1998/02 *Seismic Evaluation of 196 kV Porcelain Transformer Bushings.* Amir S. Gilani, Juan W. Chavez, Gregory L. Fenves, and Andrew S. Whittaker. May 1998. $20.00

PEER 1998/01 *Seismic Performance of Well-Confined Concrete Bridge Columns.* Dawn E. Lehman and Jack P. Moehle. December 2000. $33.00